Technical Report

TR-00-07

Äspö Hard Rock Laboratory

Final report of the first stage of the tracer retention understanding experiments

Anders Winberg
Conterra AB

Peter Andersson
GEOSIGMA AB

Jan Hermanson
Golder Grundteknik

Johan Byegård
Department of Nuclear Chemistry
Chalmers University of Technology, CTH

Vladimir Cvetkovic
Department of Water Resources Engineering
Royal Institute of Technology, KTH

Lars Birgersson
Kemakta Konsult AB

March 2000

Svensk Kärnbränslehantering AB
Swedish Nuclear Fuel
and Waste Management Co
Box 5864
SE-102 40 Stockholm Sweden
Tel 08-459 84 00
+46 8 459 84 00
Fax 08-661 57 19
+46 8 661 57 19

Äspö Hard Rock Laboratory

Final report of the first stage of the tracer retention understanding experiments

Anders Winberg
Conterra AB

Peter Andersson
GEOSIGMA AB

Jan Hermanson
Golder Grundteknik

Johan Byegård
Department of Nuclear Chemistry
Chalmers University of Technology, CTH

Vladimir Cvetkovic
Department of Water Resources Engineering
Royal Institute of Technology, KTH

Lars Birgersson
Kemakta Konsult AB

March 2000

Keywords: aperture, in situ, laboratory tests, model, pore space, retention, single fracture, tracer test, transport, TRUE, Äspö.

Foreword

Important contributions to the realisation of work performed during the First TRUE Stage and the present report have, apart from the authors, been given by the following organisations, groups and individuals:

Paul Bossart, Geotechniches Institut, Bern, Switzerland

Department of Nuclear Chemistry, CTH, Gothenburg
Henrik Johansson
Gunnar Skarnemark
Mats Skålberg

Duke Engineering, Stockholm
Markus Laaksoharju
Christina Skårman

John Gale, Fracflow Consultants, S:t Johns, NF, Canada

GEOSIGMA AB, Uppsala
Agne Bern
Seje Carlsten
Bengt Gentzschein
Kent Hansson
Jan-Erik Ludvigsson
Rune Nordqvist
John Olausson
Margareta Smellie
Allan Stråhle
Eva Wass

Eva Hakami, Itasca Consultants, Stockholm
Hua Cheng, Dept of Water Resources Engineering, KTH, Stockholm
Martin Mazurek, RWIG, University of Bern, Switzerland
Ann-Chatrin Nilsson, Dept of Inorganic Chemistry, Stockholm
Randall Roberts, SANDIA National Laboratory, Albuquerque, NM, U.S.A.
Jan-Olof Selroos, SKB, Stockholm
Eva-Lena Tullborg, Terralogica AB, Gråbo

SKB Äspö Hard Rock Laboratory
Lars Andersson
Ebbe Eriksson
Patrik Hagman
Johannes Heikkilä
Katinka Klingberg
Mansueto Morosini, On-site coordinator
Per Nilsson
Gunnar Ramqvist
Olle Olsson, Head of Division of Repository Technology
Leif Stenberg, On-site coordinator
Anna Säfvestad

Äspö Task Force on groundwater modelling and transport of solutes

TRUE-1 Review group
Professor Ivars Neretnieks, Royal Instituite of Technology (KTH), Stockholm
Dr. Scott Altmann, ANDRA, France
Dr. Russell Alexander, NAGRA, Switzerland

Abstract

The first stage of the Tracer Retention Understanding Experiments (TRUE) was performed as a SKB funded project. The overall objectives of TRUE are to develop the understanding of radionuclide migration and retention in fractured rock, to evaluate the realism in applied model concepts, and to assess whether the necessary input data to the models can be collected from site characterisation. Further, to evaluate the usefulness and feasibility of different model approaches, and finally to provide *in situ* data on radionuclide migration and retention. The strive for address with multiple approaches is facilitated through a close collaboration with the Äspö Task Force on Modelling of Groundwater Flow and Transport of Solutes. The TRUE programme is a staged programme which addresses various scales from laboratory (< 0.5 m), detailed scale (< 10 m) and block scale (10–50 m). The First TRUE Stage was performed in the detailed scale with the specific objectives of providing data and conceptualising the investigated feature using conservative and sorbing tracers. Further, to improve methodologies for performing tracer tests, and to develop and test a methodology for obtaining pore volume/aperture data from epoxy resin injection, excavation and subsequent analyses.

The experimental site is located at approximately 400 m depth in the northeastern part of the Äspö Hard Rock Laboratory. The identification of conductive fractures and the target feature has benefited from the use of BIPS borehole TV imaging combined with detailed flow logging. The assessment of the conductive geometry has been further sustained by cross-hole pressure interference data. The investigated target feature (Feature A) is a reactivated mylonite which has later undergone brittle deformation. The feature is oriented northwest, along the principal horizontal stress orientation, and is a typical conductor for Äspö conditions. Hydraulic characterisation shows that the feature is relatively well isolated from its surrounding. The near proximity of the experimental array to the tunnel (10–15 m) implies a strong gradient (approximately 10%) in the structure, which has to be overcome and controlled during the experiments.

A methodology for characterising fracture pore space using resin injection, excavation using large diameter coring and subsequent analysis with photo-microscopic and image analysis techniques was developed and tested at a separate site. The results show that epoxy resin can be injected over several hours, and that the estimated areal spread is in the order of square metres. The mean apertures of the two investigated samples were 239 and 266 microns, respectively. Assessment of spatial correlation show practical ranges in the order of a few millimetres.

Performed tracer tests with conservative tracers in Feature A show that the feature is connected between its interpreted intercepts in the array. The parameters evaluated from the conservative tests; flow porosity, dispersivity and fracture conductivity are similar, indicating a relative homogeneity.

Previous work has identified cationic tracers, featured by sorption through ion exchange, as the most suitable tracers for sorbing tracer experiments at ambient Äspö conditions. Laboratory experiments on generic Äspö material and site-specific material

included batch sorption experiments on various size fractions of the geological material, and through diffusion experiments on core samples of variable length on a centimetre length scale. The sorbtivity was found to be strongly affected by the biotite content and the sorption was also found to increase with contact time. The sorbtivity was found to follow the relative order; $^{22}Na^{+} < {}^{47}Ca^{2+} \approx {}^{85}Sr^{2+} << {}^{86}Rb^{+} \approx {}^{133}Ba^{2+} < {}^{137}Cs^{+}$.

The field tracer tests, using essentially the same cocktail of sorbing tracers as in the laboratory, were found to show the same relative sorbtivity as seen in the laboratory. A test using ^{137}Cs showed that after termination of the test, some 63% of the injected activity remained sorbed in the rock.

The interpretation of the *in situ* tests with sorbing tracers was performed using the LaSAR approach, developed as a part of the TRUE project. In this approach the studied flow path is viewed as a part of an open fracture. Key processes are spatially variable advection and mass transfer. The evaluation shows that laboratory diffusion data are not representative for in situ conditions, and that a close fit between field and modelled breakthrough is obtained only when a parameter group which includes diffusion is enhanced with a factor varying between 32–50 for all tracers and experiments (except for Cs) and 137 for Cs. Our interpretation is that the enhancement is mainly due to higher diffusivity/porosity and higher sorption in the part of the altered rim zone of the feature which is accessible over the time scales of the *in situ* experiments, compared to data obtained from core samples in the laboratory. Estimates of *in situ* values of the important transport parameters are provided under an assumption of a valid range of porosity in the accessible part of the rim zone in the order of 2–2.4%.

Unlimited diffusion/sorption in the matrix rock was interpreted as the dominant retention mechanism on the time scales of the TRUE-1 *in situ* experiments. This is particularly true for the more strongly sorbing tracers, e.g. Cs. The effects on tracer retention by equilibrium surface sorption and limited sorption in gouge material were found to be observable, but of secondary importance. Similarly, the effect of sorption into stagnant water zones was found to be limited.

Sammanfattning

Den första fasen av "Tracer Retention Understanding Experiments (TRUE) har genomförts som ett av SKB helfinansierat projekt vid Äspölaboratoriet. De övergripande målen med TRUE är att utveckla förståelsen av fördröjande processer som påverkar transport av radionuklider, utvärdera realismen i utnyttjande matematiska modellkoncept, samt huruvida nödvändiga indata till modellerna kan erhållas från platsundersökningar. Vidare att utvärdera användbarheten av olika modellansatser, och slutligen att tillhandahålla fältdata på fördröjning och transport av radionuklider i kristallin berggrund. Ambitionen att utvärdera olika modellkoncept har uppfyllts genom ett nära samarbete med "Äspö Task Force on Modelling of Groundwater Flow and Transport of Solutes", en arbetsgrupp inom internationella Äspösamarbetet. TRUE-programmet innefattar studier i laboratorieskala (< 0.5 m), detaljskala (enskilda sprickor) (< 10 m) och blockskala (10–50 m). Den första fasen av TRUE (TRUE-1) har utförts i detaljskala med de specifika målen att generera data och beskriva den undersökta strukturen med konservativa (icke-reaktiva) och sorberande (reaktiva) spårämnen. Vidare att förbättra metoder för att genomföra spårförsök mellan borrhål, och att utveckla och utvärdera en metodik för att erhålla information om storlek och variation i sprickvidd med hjälp av injektion av epoxyharts, efterföljande borrning och analyser.

Experimentplatsen är belägen på ett djup av 400 m i den nordvästra delen av Äspölaboratoriet. Identifiering av vattenförande sprickor, inklusive den spricka som valts ut för fältförsöken, har möjliggjorts genom borrhåls-TV (BIPS) kombinerad med detaljerad flödesloggning. Bestämning av konnektiviteten hos de sprickor som identifierats i de fem borrhålen har möjliggjorts genom hydrauliska mellanhåls-mätningar (interferenstester). Den undersökta strukturen (Feature A) är en reaktiverad mylonitisk zon, som senare undergått spröd deformation. Strukturen har en nordvästlig riktning, parallell med huvudspänningsriktningen, och är en typisk konduktiv spricka för Äspöförhållanden. Den hydrauliska karakteriseringen har visat att strukturen är väl isolerad från sin omgivning. Dess läge i tunnelns omedelbara närhet (10–15 m) innebär en stor hydraulisk gradient (c. 10%) i strukturen, som måste överkommas och kontrolleras i samband med experimenten.

En metodik för att karakterisera porvolymen (sprickvidden) hos en sprick med hjälp av injicering av epoxyharts, provtagning med hjälp av kärnborrning med stor diameter, och efterföljande analys med fotomikroskopisk och bildbehandlingsteknik har utvecklats och utprovats på en separat plats i laboratoriet. Resultaten visar att epoxyharts kan injiceras under flera timmar, och att utbredningen är i storleksordnbingen av ett par kvadratmeter. Medelsprickvidden hos två kärnprover var 239 respektive 266 mikrometer. Utvärdering av den rumsliga korrelationen visar korrelationslängder på upp till ett par millimeter.

Genomförda spårförsök med konservativa färgspårämnen i Feature A visar att strukturen är hydrauliskt och transportmässigt sammanbunden över den undersökta delen av sprickan (< 10m). Transportparametrar utvärderade från dessa försök,

ex. flödesporositet, dispersivitet och sprickkonduktivitet är likartade för olika försöksuppställningar, vilket pekar på en relativ homogenitet inom sprickplanet.

Tidigare studier har visat att en- och två-värda katjoner, som kännetecknas av sorbtion genom jonbytesprocesser, som de mest lämpliga spårämnena för kemiska förhållanden liknade de som råder vid Äspölaboratoriet. Laboratorieexperiment på oomvandlat gologiskt material från Äspö och plats-specifikt material från den undersökta Feature A omfattade batch-försök på olika storleksfraktioner av det geologiska materialet samt genomdiffusionsförsök på kärnprover i centimeterskala. Sorptionen befanns öka med större biotit-innehåll och ökade också med längre kontakttid. Sorptionen i laboratoriet befanns följa följande relative ordning, $^{22}Na^{+} < {}^{47}Ca^{2+} \approx {}^{85}Sr^{2+} << {}^{86}Rb^{+} \approx {}^{133}Ba^{2+} < {}^{137}Cs^{+}$.

Spårförsöken i fält, som genomfördes med samma cocktail av sorberande spårämnen som utnyttjats i labororatoriet, påvisade samma realtiva sorbtionsstyrka som i laboratoriet. Ett försök med ^{137}Cs visade efter avslutningen att ungefär 63% av den injicerade aktiviteten satt kvar sorberad på sprickans och injiceringssektionens väggar.

Utvärderingen av *in situ* försöken med radioaktiva sorberande spårämnen utfördes med LaSAR-konceptet som utvecklats som en del av TRUE-projektet. I detta koncept betraktas den aktuella flödesvägen som en del av en öppen spricka. De huvudsakliga retentionsprocesserna är rumsligt varierad advektion och massöverföring (diffusion och sorption). Resultatet av utvärderingen visar att laboratoriedata, främst kopplat till porositet och diffusivitet, inte är representativa för *in situ* förhållanden, och att en god överensstämmelse mellan modellerade genombrottskurvor och motsvarande fältdata kan erhållas om den parametergrupp som bestämmer diffusion/sorption är förhöjd med en faktor 32–50 för samtliga spårämnen och utförda experiment (exklusive Cs) och 137 för Cs. Vår tolkning är att denna förhöjning till största del beror på en högre diffusivitet/porositet och sorption i den omvandlade randzonen till Feature A, jämförbart med utnyttjade transportparametrar från laboratorieförsök på kärnprover. Skattningar av *in situ* värden på viktiga transportparametrar har erhållits under antagande att porositeten i den del av randzonen som är tillgänglig över tidsskalor relevanta för de utförda spårförsöken ligger i intervallet 2–2.4%.

Oändlig diffusion/sorption i bergmatrisen är tolkad som den huvudsakliga retentions-mekanismen över tidsskalor relevanta för TRUE-1 försöken. Detta gäller speciellt de mer starkt sorberande spårämnena, exempelvis Cs. Effekten på retentionen av jämviktsytsorption och ändlig sorption i sprickfyllnadsmaterial (gouge) kan observeras, men är av underordnad betydelse. På samma sätt är effekten av diffusion in i stagnanta vattenzoner begränsad.

Executive summary

Background

SKB's concept on deep geological disposal of spent nuclear fuel is based on a multi-barrier system for isolation of the spent fuel from the biosphere. The barriers are a low-solubility waste form, encapsulation of the fuel in a copper canister, a bentonite buffer surrounding the canister, and the host rock. The host rock should provide a stable mechanical and chemical environment for the engineered barriers and it should reduce and retard transport of radionuclides released from the engineered barriers. In case of an early canister damage, the retention capacity of the host rock for the short lived radionuclides such as Cs and Sr is important. Actinides become important in the longer time perspective.

In planning the experiments to be performed during the Operating Phase of the Äspö Hard Rock Laboratory the need for a better understanding of radionuclide transport and retention processes was recognised. The needs of performance assessment included an urge to increase confidence in models to be used for quantifying transport of sorbing radionuclides. It was also considered important from the performance assessment perspective to be able to show that pertinent transport data and parameters (distribution coefficients, diffusivity, parameters corresponding to the "flow wetted surface area", etc.) could be obtained from site characterisation or field experiments, and that laboratory results could be related to retention parameters obtained *in situ*. To answer up to these needs, SKB initiated a tracer test programme named the Tracer Retention Understanding Experiments (TRUE).

General objectives and scope

The overall objectives of TRUE are to:

- Develop the understanding of radionuclide migration and retention in fractured rock,
- Evaluate to what extent concepts used in models are based on realistic descriptions of fractured rock and if adequate data can be collected in site characterisation,
- Evaluate the usefulness and feasibility of different approaches to model radionuclide migration and retention,
- Provide *in situ* data on radionuclide migration and retention.

The TRUE programme constitutes a staged approach where data for conceptual and numerical modelling should be provided at intervals. Periodic evaluation of test results and a close integration of experimental and modelling work should provide the basis for detailed planning of subsequent test cycles and the successive improvement of models.

The planned duration of each stage is approximately 4 years and total duration of the programme is nearly 10 years, beginning in 1994 and ending in 2003.

The basic idea behind TRUE is to perform a series of tracer experiments with successively increasing complexity. In principle, each tracer experiment will consist of a cycle of activities beginning with geological characterisation of the site, design modelling, followed by a set of hydraulic and tracer tests, possibly followed by epoxy resin injection, excavation, and analysis for flow path geometry and tracer concentration. The first test cycle (TRUE-1) described in this report is detailed scale (< 10 m), of limited time duration, and primarily aimed at technology development. TRUE Block Scale (Winberg, 1997, 1999), currently in its final stages, addresses tracer transport and retention in a network of fractures over a 10–50 m length scale. In progress is also an in situ matrix diffusion experiment, the so-called Long-Term Diffusion Experiment (LTDE). Plans are also under way for detailed scale tracer tests of longer time duration (TRUE-2), which will allow further tests of retention mechanisms. The integrated results of the TRUE experiments are expected to form a basis for understanding scaling relationships of flow and transport phenomena in fractured rocks.

The Äspö Task Force on Modelling of Groundwater Flow and Transport of Solutes has been engaged for providing advice on experimental design, predictive modelling, and evaluation (Elert, 1999) of experimental data from TRUE. The close interaction between TRUE and the Task Force constitutes an important element in the evaluation of different conceptual models and approaches to radionuclide transport.

Specific objectives and workscope

The First TRUE Stage (TRUE-1) is aimed at understanding tracer transport in a single fracture, which could e.g. be viewed to represent a fracture intersecting a canister deposition hole. TRUE-1 was initially aimed at testing of equipment, adaptation of tracer test methodology to Äspö conditions, and the understanding of conservative tracer transport. The programme was later expanded to also include field tests with sorbing tracers. In addition, a technology for obtaining the internal structure of pore space in the fracture from injection of epoxy resin was to be developed.

Initial characterisation and experimental array

The experimental phase was preceded by an elaborate site selection programme. It was identified that sites for the planned experiments had to be sited using hard data from pilot boreholes. It was also identified that the experimental volumes should be located outside the tunnel spiral, partly to avoid complicated boundary conditions, but also because of the noted enhanced hydraulic connectivity in the rock volume bounded by the spiral access tunnel at Äspö HRL. The defined site selection programme, called SELECT, involved drilling of eight 56 mm cored boreholes, 15–70 m long, with the objective of finding suitable locations for the TRUE-1 experiments. The boreholes/cores were subject to various types of characterisation methods including i.a. borehole TV imaging (BIPS). The collected characterisation data were used to assess whether

suitable target features for the experiments were available, and to what extent the identified experimental volumes and target features were likely to be affected by activities in neighbouring rock blocks. Three features were identified as suitable for further study within the so-called TRUE-1 rock block. To investigate these features further, a new niche was developed from which an additional four cored 56 mm boreholes were drilled to intercept all three features located some 10–15 m into the rock, cf. Figure EX-1.

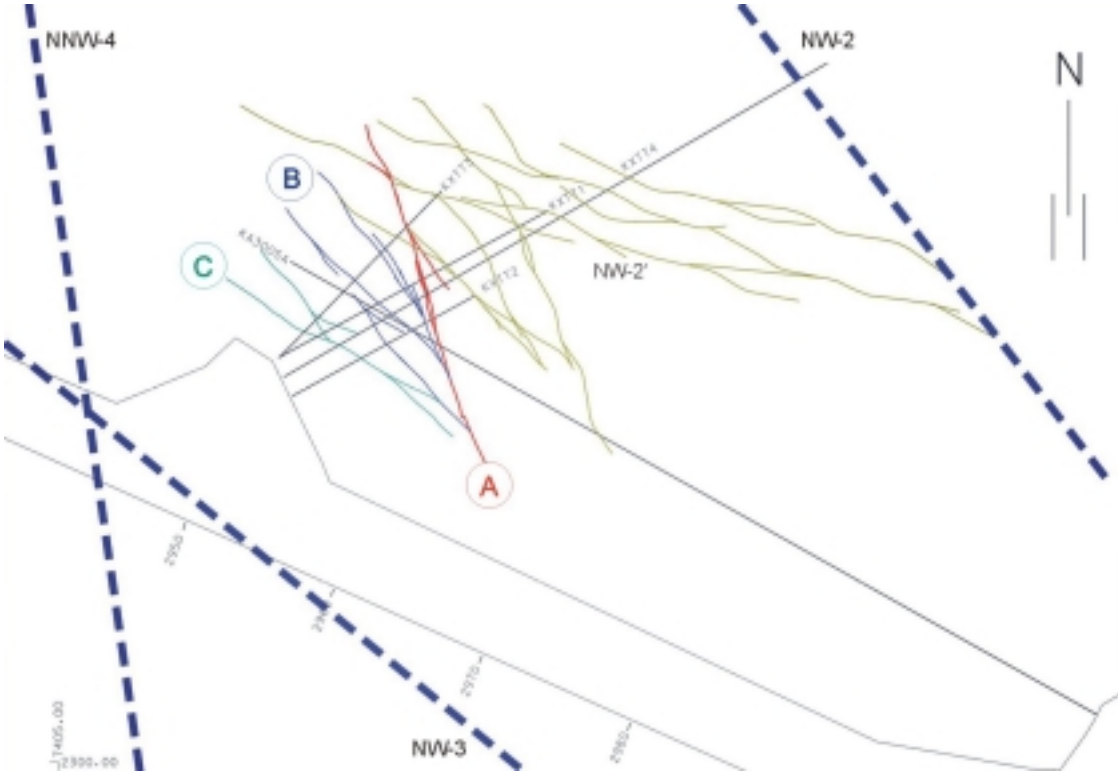

Figure EX-1. *Horizontal section at Z=–400 masl showing structural model based on identified conductive geological structures in the TRUE-1 rock volume.*

Results

Detailed characterisation and descriptive models

Pressure responses in the instrumented borehole KA3005A and temporary downhole installations in the new boreholes were used for preliminary assessments of connectivity and preliminary structural inference. The most important characterisation methods used were detailed core logging, BIPS imaging, and single packer flow logging. Following the basic characterisation, the boreholes were equipped with multi-packer systems with up to five test sections followed by an elaborate cross-hole interference test programme. Response matrices based on defined response measures were utilised in interpreting the response patterns. Four features, A, B, C and D were identified within the array,

cf. Figure EX-1. Feature A was selected for further study on the basis of its relative simplicity (single fracture), relative hydraulic isolation and suitable transmissivity range.

Geological and structural setting

The experimental volume is located in medium-grained Äspö diorite. A steep penetrative foliation oriented NW exists throughout the investigated rock volume. Fracturing is dominated by a NW fracture set with a less prominent set oriented NE. The investigated volume is bounded by a group of site scale structures; NW-2, NNW-4 and NW-3, cf. Figure EX-1.

A detailed conceptual cross section model of Feature A includes the main fracture, which is partially following a reactivated mylonite, cf. Figure EX-2. The latter has acted as a brittle precursor for the main fracture. The feature is centred on an altered rim zone consisting of altered Äspö Diorite and the mylonite. The undulation of the main fracture in relation to the mylonitic precursor allow water to be in contact with both altered Äspö diorite and mylonite, the latter with a lower porosity and diffusivity. The total thickness of the feature including the altered rim zone is varying between 0.05–0.09 m. Evidence of gouge on fracture surfaces has been noted in detailed mineralogical investigations (Winberg, 1996). Gouge material, mainly made up of macroscopic pieces of altered Äspö diorite and a fine fraction including clay, has been collected in other structures of the same kind, i.a. in the TRUE Block Scale rock volume. Consequently, gouge material is included in the conceptual model.

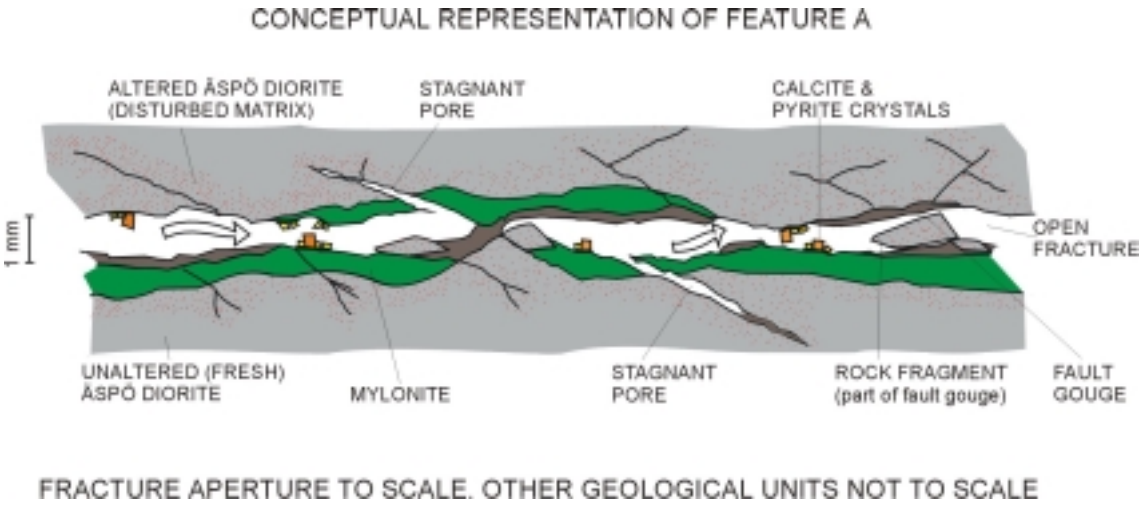

Figure EX-2. *Schematic conceptual representation of Feature A in cross section. Note that the fracture aperture is to approximate scale. The thickness of the remainder of the constituents is not to scale. The total thickness of Feature A including altered Äspö diorite is varying between 0.05 and 0.09 m.*

Hydrogeology and hydrogeochemistry

The investigated Feature A is a representative conductor at Äspö with a transmissivity in the order of $0.08–4 \cdot 10^{-7}$ m^2/s as observed from the hydraulic tests. The hydraulic tests indicate pseudo-spherical flow dimension throughout the array, indicating three-dimensional connectivity. However, monitoring of steady state pressure indicates that Feature A is relatively well isolated from neighbouring hydraulic conductors. Hence, the high flow dimensionality has been interpreted as Feature A being part of a leaky aquifer system, possibly in combination with a constant head boundary.

The water sampled in the investigated feature is of Na-Ca-K:Cl-SO4-HCO3 character with a chloride concentration in excess of 5000 mg/l. The chemical data support the relative isolation of Feature A from its surrounding. Stable isotope data indicate that the sampled waters plot close to the meteoric water line, indicating water derived from post-glacial environments.

Laboratory investigations

Batch sorption and through diffusion experiments on generic Äspö material and site-specific TRUE-1 material indicate a relative sorbtivity amongst the tested radioactive sorbing tracers according to; $^{22}Na^{+} < {}^{47}Ca^{2+} \approx {}^{85}Sr^{2+} << {}^{86}Rb^{+} \approx {}^{133}Ba^{2+} < {}^{137}Cs^{+}$, ranging from $(4–30) \cdot 10^{-6}$ m^3/kg for Na^{+} to $(1–400) \cdot 10^{-3}$ m^3/kg for Cs^{+}, (Byegård et al., 1998). The sorption in the batch laboratory experiments is observed to be time dependent, i.e. the evaluated K_d increases with increasing contact time. Diffusivities for the sorbing tracers relative to site-specific material from Feature A (one single diffusion cell dominated by mylonite) are in the order of $1.3–3 \cdot 10^{-14}$ m^2/s. The porosity of generic Äspö diorite is estimated to 0.4% whereas the porosity of the site-specific diffusion cell (dominated by mylonite) is estimated to 0.1%.

Mineralogically, the mylonites are characterised by very fine-grained epidote, quartz, K-feldspar/albite, and in some cases chlorite, some minerals found as idiomorphic crystals. The Äspö diorite wall rock show evidence of replacement of biotite with chlorite and epidote. Plagioclase is strongly altered to albite, sericite and epidote. Red-staining seen in the altered Äspö diorite is attributed to minute grains of Fe-oxide/ oxyhydroxides. Detailed analysis reveal the presence of clay minerals as an outer rim on the fracture coating, suggesting the presence of fault gouge in Feature A, the latter also assumed in part to be made up of fragments of altered Äspö diorite.

Tests with conservative tracers

A series of 18 tracer tests have been performed at the TRUE-1 site. The majority of these tests were conservative tests with dye tracers or metal complexes in a radially converging flow configuration, or (unequal strength) dipole configuration. Of these, three setups were employed for tests with radioactive sorbing tracers. The equipment for field tracer tests was originally constructed for injection of a small concentrated volume of tracer, required to be instantly homogenised in the injection section. Both the

injection and the sampling systems utilise a circulating system which connect the borehole collar and the test section. It was soon realised that the injection procedure introduced a large tailing, thus potentially masking important transport processes. For the tests with sorbing tracers measures were taken to eliminate this tailing through an exchange procedure through which the water in the circulation system was replaced with non-traced water. This resulted in a sharper termination of the injection pulse.

The results of the conservative tests identified a triangle of the interpreted intercepts with Feature A, with an approximate 5 m mutual separation, as the most suitable combination of sink-source sections for subsequent tests with sorbing tracers, on the basis of distance/transport times and mass recovery. For a pumping flow rate $Q \geq 0.2$ l/min the two flow paths yielded a mass recovery in excess of 85%. The evaluation of the conservative tracer tests using a 1D advection-dispersion model shows similar transport parameters in terms of dispersivities, fracture conductivities and flow porosity. Flow porosities are in the order of $0.5–4 \cdot 10^{-3}$. Dispersivities are in the range 0.34–2.0 m, for the most part about 10% of the flow path length. The evaluated dispersivities of one of the flow paths are markedly higher, suggesting possible activation of multiple flow paths.

Tests with sorbing tracers

In the case of the tests with sorbing tracers (STT-1, STT-1b and STT-2), Uranine, tritiated water (HTO) and $^{82}Br^-$ and $^{131}I^-$ were used as conservative reference tracers. The radioactive sorbing tracers included those used in the laboratory and some additional short-lived tracers. The activity of the gamma-emitting tracers was monitored on site using a HPGe detector with a multi-channel analyser. A similar stationary detector was used in the laboratory for analysis of collected samples. The injection signal of Uranine was analysed in line using a portable fluorometer. The concentrations of HTO and Uranine in the injection water were analysed in the laboratory with a liquid scintillometer and a stationary fluorometer, respectively. Breakthrough in the *in situ* experiments has been observed for the sorbing tracers Na^+, Ca^{2+}, Sr^{2+}, Rb^+, Ba^{2+}, Cs^+, K^+, Co^{2+}.

The preliminary evaluation included plotting of the injection concentrations (activities). Similarly, the breakthroughs of the different tracers were co-plotted in various ways. The breakthrough curves show a relative breakthrough equitable to that observed in the laboratory results, reflecting the relative sorbtivity of the tracers. One of the tested flow paths shows slow reversibility, and may even indicate irreversible sorption in the ^{137}Cs breakthrough. After 10870 hours (15 months), some 63% of the Cs activity still remained sorbed on the surfaces of the injection section and the fracture. Reduction of the flow rate with 50% resulted in dual peaks in the breakthrough. However, despite the fact that the lower flow rate had been used at previous occasions, the noted dual peak had been masked. The separation of transport in the two paths as seen in the STT-2 dual peak breakthrough curve is attributed to a subtle change in boundary conditions during this last test.

Evaluation of tests with sorbing tracers

Evaluation of the tests has been performed using what is here referred to as the Lagrangian Stochastic Advection Reaction model (LaSAR) (Cvetkovic et al, 1999). In this approach the flow path is viewed as part of an open fracture. The key processes are spatially variable advection and mass transfer, the latter assumed linear, and the coupled effect of multiple processes is obtained by convolution. To account for dispersive effects, the convoluted result for the flow path is integrated over different stream lines, described by a distribution of τ and β. The parameter β [T/L] is flow-dependent, integrating the inverse of the velocity-weighted aperture along the a flow path, and τ is the water residence time. The product $q\beta$ [L^2] provides an estimate of the area over which the tracer is in contact with the rock matrix ("flow-wetted surface"), where q [L^3/T] is the volumetric flow rate carrying the tracer. The parameters β and τ have been shown to be significantly correlated for generic conditions and also for Feature A specific conditions, such that an approximate linear (deterministic) relationship $\beta = k \cdot \tau$ is applicable. Using Monte Carlo simulations of flow and particle transport in Feature A, $k_0 \approx 3400$ m^{-1} is estimated as an ensemble average. Input data to these simulations include measured transmissivity data and boundary conditions extrapolated from measured hydraulic head and transient drawdown data. For the strict assumption of linear relation between β and τ, k is equivalent to the "flow wetted surface per volume of water" (a_w) as defined and used in the recently concluded safety analysis SR-97 (SKB, 1999). The sorption parameters for the fracture are the distribution coefficients for surface sorption K_a and sorption in gouge K_d^g. The key parameter group controlling sorption/diffusion into the rock matrix is $\beta\kappa$ $[T]^{1/2}$ where $\kappa = \theta[D(1+K_d^m)]^{1/2} = \theta(DR_m)^{1/2} = (\theta D_w F R_m)^{1/2}$, θ is the porosity and F is the formation factor, respectively of the matrix (note that no distinction is made between the "total porosity" and the "diffusion porosity"), D is the pore diffusivity in the rock matrix (θD is the effective diffusion coefficient in the rock matrix), D_w is the water diffusivity, and K_d^m is the sorption coefficient in the rock matrix. The evaluation includes determination of the water residence time distribution $g(\tau)$ by deconvoluting breakthrough curves for HTO. The reactive breakthroughs are evaluated using $g(\tau)$. One of the stated hypotheses is that the laboratory-derived value of κ may not be representative of the corresponding value in the field.

Evaluation modelling has been performed where different transport processes successively have been included. The evaluation shows that a close fit with the data is obtained if the product $\beta\kappa$ is enhanced as $f\beta\kappa$, where the enhancement factor is 137 for Cs, in the range f=32–50 for all other tracers and tests of TRUE-1. The observed range of factors f indicates that the reasons for the enhancement are both physical as well as chemical (i.e., diffusion and sorption). In particular, we find that higher values of matrix porosity and/or pore diffusivity, and matrix sorption are applicable in the field compared to the values measured in the laboratory scale, and that the flow-dependent parameter k in the relationship $\beta = k\tau$ is larger in the field than has been estimated from simulations. Detailed analysis has shown that a factor 3 of the enhancement factor 137 for Cs can be attributed to k, whereas the remaining factor 46 (3*46=138) is attributed to enhanced diffusion/sorption in the matrix rock. The above interpretation is consistent with the fact that a significant portion of the flow path is assumed being in contact with portions of a rim zone made up of altered Äspö diorite, featured by a porosity higher

than the unaltered diorite and that estimated from a site-specific rock sample dominated by mylonite, and also with the fact that individual realisations exhibited considerable deviations in k from the ensemble average $k_0 \approx 3400$ m^{-1}. The kinetic effects associated with sorption in gouge material are more evident in the breakthrough of the weakly sorbing Na and Sr, as opposed to the more strongly sorbing Cs, since diffusion/sorption has a much stronger impact on Cs than on Na and Sr.

Understanding of transport processes

Unlimited diffusion/sorption in the rock matrix is interpreted as the dominant retention mechanism at the time scales of the TRUE-1 *in situ* experiments. The observed mass transfer rates are highest for the more strongly sorbing tracers, eg. Cs. The observed dependence on tracer sorption properties also entails that the effect of diffusion into stagnant water zones is small. The effects on tracer retention by equilibrium surface sorption and limited sorption onto gouge material are observable, but of secondary importance. Variability in fracture aperture has significant effect on the breakthrough of sorbing tracers, due to its impact on surface sorption and diffusion/sorption. In fact, the observed breakthroughs for all tracers and tests cannot be interpreted in a consistent manner if this variability is not accounted for.

Provision of data for evaluation model

The framework used in the evaluation, cf. Section 8.4, requires parameters which define the diffusion/sorption in the matrix (κ), surface sorption (K_a), volumetric distribution coefficient (K_d^g) and a rate coefficient (α) associated with gouge material. The former two of these parameters are obtained from selected laboratory data based on through-diffusion experiments on generic Äspö diorite, the so called "Modelling Input Data Set" (MIDS). The parameters related to sorption onto gouge are presently not available from the laboratory, and are calibrated using *in situ* tracer test results. Further, a statistical relation between β and τ is required. This is obtained from a combination of a residence time distribution calibrated using conservative tracer (HTO) breakthrough and Monte Carlo simulations of particle transport in the modelled feature.

Estimation of *in situ* transport parameters

The analysis of the experiments has indicated the importance of the rim zone of altered rock along the studied fracture. Site-specific Feature A related data are presently scarce. However, using independent information from ia. Äspö, it is hypothesised based on results from Äspö that a representative range of porosity for the part of the altered rim zone which is accessible for mass transfer over the time scales of the *in situ* experiments is θ=2–3%. Using this estimate, Archie's law (which empirically relate porosity and the formation factor) and the calibrated parameter group which governs diffusion/sorption, $k_q f \kappa$, estimates of the D_e and K_d^m are obtained and compared to available laboratory diffusivity and sorption data, the latter on different size fractions. Typically,

the K_d^m values obtained in the laboratory from longer time (36 days) tests on the 1–2 mm size fraction agree with estimated *in situ* K_d^m values, suggesting that these batch tests capture the variability in sorption representative of the flow paths and the time scales used in the *in situ* tests. Estimated *in situ* D_e values are approximately a factor 30 higher than diffusivities of the MIDS data set.

Predictive capability of developed model

Laboratory data of diffusion/sorption parameters constitute a basis for robust and relatively accurate predictions of reactive tracer breakthrough. This provided that the water residence time distribution $g(\tau)$ is known and that variability in the β parameter is accounted for. Using laboratory data for diffusion/sorption (κ) the first arrival is predicted accurately (in particular that of the strongly sorbing Cs), or is somewhat underestimated. The peak concentration of Cs is however overestimated with up to one order of magnitude. The latter deviations can be considered conservative from a performance assessment perspective.

Analysis of pore space

A methodology for injection of epoxy resin has been demonstrated for a near tunnel situation at an auxiliary pilot test site. Epoxy resin has been injected over a period of an hour, and the estimated spread is in the order of a square metre/-s. The excavation has been performed using large diameter coring (146–200 mm). Subsequent analysis of the resin-impregnated fractures have been performed using "photo microscopic" and an "image analysis" techniques. The results show mean apertures of the analysed fracture planes in the order of 266 and 239 microns, respectively. The analysis of spatial continuity reveal very little structure, with a practical range in the order of a few millimetres.

Conclusions

Available tracer test methodology has been successfully adapted and applied in the detailed scale at the prevailing conditions (high pressures (P >30 bars) and high salinity ([Cl] > 5000 mg/l)). In this context the use of tracer dilution tests in combination with pumping has proven to be a good tool for tracer test design. The existing natural gradient which controls the background flow makes it difficult to perform high-recovery tracer tests over longer distances (> 5 m) and at low pumping flow rates (< 0.2 l/min). Two flow paths in Feature A which qualify for tests with radioactive sorbing tracers have been identified and successfully used.

The proposed cationic tracers featured by sorption by ion exchange have been successfully applied in laboratory experiments and in *in situ* experiments. The sorbtivity of the exposed geological material is shown to depend on the concentration of biotite. The sorbtivity of the tracers used in the laboratory experiments on geological material

from Äspö, show the following relative order; $Na^+ < Ca^{2+} \approx Sr^{2+} << Rb^+ \approx Ba^{2+} < Cs^+$. The observed relationship is also consistently observed in the *in situ* test results. Laboratory results indicate that the sorption of the more sorbing species, Rb, Ba and Cs, are affected by slowly reversible, or even irreversible processes. Similarly, the performed *in situ* experiments show a similar behaviour for Co, Ba and Cs. The tracer test methodology developed and used in this work is applicable to characterisation work in various phases of repository development.

The developed modelling framework is found appropriate for evaluating the dominant effects of reactive transport in a single fracture. A key result is the derivation of flow-dependent parameter β which integrates the inverse of the velocity-weighted aperture along the flow path, accounts for aperture variability and controls surface sorption and diffusion/sorption into the matrix rock. Assuming a linear relation between β and τ, as $\beta = k \cdot \tau$, the proportionality factor k is equivalent to the "flow wetted surface" per volume of water (a_w). We established the coefficient $k_0 \approx 3400$ m^{-1} as the most representative value. The estimated value of k is within bounds of a_w reported in the literature. Sorption in gouge material has been found to be dominant for the breakthrough of weakly sorbing species (Na and Sr).

Unlimited diffusion/sorption in the rock matrix has been interpreted as the dominant retention mechanism on the time scales of the TRUE-1 *in situ* experiments and the observed diffusion rates are found to be strongly dependent on the sorption properties of the individual tracers. The effects on tracer retention by equilibrium surface sorption and limited sorption in gouge material are observable, but of secondary importance. Similarly, the effect of sorption into stagnant water zones is small.

Values on parameters for the main retention processes included in evaluation concept (LaSAR) have been obtained either directly from laboratory data, or indirectly through calibration using *in situ* data. The evaluation shows that the *in situ* parameter group which governs diffusion/sorption in matrix rock is enhanced in relation to the selected MIDS data set, the latter derived from *in situ* through diffusion experiments on generic Äspö diorite. Given the observed range of the calibrated enhancement factor f, the "enhancement" is attributed both to physical effects (i.e. a higher value of matrix porosity and/or diffusivity) as well as higher matrix sorption, which is applicable in the field compared to the MIDS data set. This indicates the importance of the accessible part of the altered rim zone along the fracture which is assumed to be featured by increased, albeit variable, porosity/diffusivity in relation to unaltered matrix rock. A minor contribution to the interpreted enhancement is attributed to the flow dependent parameter k (in the $\beta = k \cdot \tau$ relationship), being higher in the field than the ensemble average obtained from numerical simulations. The use of laboratory data on diffusion/sorption parameters are shown to constitute a basis for robust and relatively accurate predictions of reactive tracer breakthrough, particularly of the first arrival. Performed post-estimation of *in situ* values of important transport parameters, eg. D_e and K_d^m, are regarded as important contributions to predictive modelling of future and ongoing TRUE experiments performed on similar time scales.

A workable technology and procedure for obtaining pore space/aperture data from *in situ* epoxy resin injection and subsequent excavation and analysis has been developed and applied in a Pilot Resin Experiment (at a different location than the TRUE-1 experiment)

The performed characterisation provide a powerful set of tools for assessment of conductive geometry and connectivity in future preliminary site characterisation, and in particular during future detailed site characterisation. The use of borehole TV imaging in combination with detailed flow logging identifies the conductive features in a borehole. Cross-hole pressure interference testing, including observations during drilling of a new borehole, provide information on how the conductive features connect.

The performed transport experiments in the laboratory combined with detailed mineralogical and geochemical characterisation provides a platform for export of generic transport characteristics to sites with similar geological and chemical conditions.

The close interaction with the Äspö Task Force on Modelling of Groundwater Flow and Transport of Solutes has provided a very important support in initial experimental design. Further, by performing blind model predictions, a basis for a scientific test of our understanding and predictive capability is obtained. The ongoing evaluation of the predictions of the performed tests with sorbing tracers will provide further insight in our understanding of flow and retention in a single fracture.

Contents

List of Figures

Figure 4-1. *The location of mylonites (red) and every fifth recorded brittle (open) fracture (hatched blue) in the TRUE-1 boreholes (after Bossart et al., in prep.). The 2D section is oriented parallel to the KXTT-boreholes at an orientation of 060/40 and the coloured lines illustrate the location where the structures intersect this plane, extrapolated from their respective intercept in the boreholes . Note that the mapping here is based solely on BIPS imaging, whereas the lithology presented in Figure 3-2 is based on a detailed mapping of the core.*

Figure 4-2. *Structural model based on identified conductive geological structures in the TRUE-1 volume.*

Figure 4-3. *Three-dimensional perspective view of structural model of identified conductive features in the TRUE-1 rock volume. Planes represent the simplest solution of planar extrapolation between intercepts in boreholes. Cylinders represent packer locations in the final multi-packer array.*

Figure 4-4. *Detailed description of Feature A in borehole KXTT1 (partly after Möri and Bossart, 1997).*

Figure 4-5. *Detailed description of Feature A in borehole KXTT2 (partly after Möri and Bossart, 1997).*

Figure 4-6. *Detailed description of Feature A in borehole KXTT3 (partly after Möri and Bossart, 1997).*

Figure 4-7. *Detailed description of Feature A in borehole KXTT4 (partly after Möri and Bossart, 1997).*

Figure 4-8. *Detailed description of Feature A in borehole KA3005A (partly after Möri and Bossart, 1997)*

Figure 5-1. *Results of single packer flow logging with 0.5–1 m section length in boreholes KXTT1 through KXTT4 and KA3005A.*

Figure 5-2. *Hydraulic responses from disturbance in KXTTT1 showing responses to interference test no. 8 with a sink in KXTT4:P2 (NW-2'). Section KXTT1:R1 (red) includes NW-2' and section KXTT1:R2 (green) includes Feature A, cf. Appendix B.*

Figure 5-3. *Pump flow as a function of drawdown as inferred from pumping in KXTT3:R2 in Feature A, TRUE-1 site.*

Figure 5-4. *Pump flow as a function of drawdown as inferred from pumping in KXTT3:R2 in Feature A, TRUE-1 site (blow up of part of Figure 5-3).*

Figure 5-5. *Hydraulic head in sections containing Feature A during the period June 1995 through December 1998.*

Figure 5-6. *Hydraulic head in five sections of borehole KXTT4 during June 1995 to December 1998.*

Figure 5-7. *Hydraulic head in Feature A immediately before performance of tracer test PDT-3, cf. table 7-1, performed in June, 1997. Interpolated point data (SURFER™).*

Figure 5-8. *Inflow to tunnel section 2/840–2/944 m during June 1995 through December 1998.*

Figure 5-9. *$\delta^{18}O$ versus $\delta^{2}H$ for Äspö site groundwater. Evolution trends associated with influx of brine water (Trend #1), glacial water (Trend #2), marine water (Trend #3) and meteoric water (Trend #4).*

Figure 5-10. *Principal Component Analysis (PCA) plot showing the non-saline, brackish and saline groundwaters of the Äspö HRL site in comparison to the TRUE-1 data. The principal component plot is based on the major components, stable isotopes and tritium. The most extreme groundwaters which are considered well sampled, and which have an analytically established composition, are by definition called reference waters. An end-member is a modelled water composition which is believed to be the original groundwater composition of the reference water (rectangular boxes). A line is drawn between the reference waters such that a polygon is formed. The polygon can be used as a "phase" diagram to calculate the mixing ratios and the mass balance for the different samples. The relative weights for the different elements included in the analysis are shown in the equations for the first and second principal components, respectively.*

Figure 6-1. *Concentration profiles of Cs^{+} in Äspö diorite. Diffusion time 472 days.*

Figure 6-2. *Thin section of fresh samples (Äspö diorite and Fine-grained granite) and altered and mylonitised samples from the Feature A fracture (see text for details). Two samples from Feature A KXTT1:15.77 m are shown. One represents the sample used for diffusion experiment and the other show the same fracture and the adjacent wall rock. The black dots on the picture of the KXTT4 samples are residues from the SEM/EDS studies. The size of the images is approximately 40x25 mm.*

Figure 7-1. *Borehole intersection pattern with Feature A (as seen in the plane of the feature) and test geometries used for the TRUE-1 tracer tests.*

Figure 7-2. *Schematic drawing of the injection system for the TRUE-1 tracer tests with sorbing tracers.*

Figure 7-3. *Schematic drawing of the sampling system for the TRUE-1 tracer tests with sorbing tracers.*

Figure 7-4. *Tracer injection concentrations (activities) normalised to maximum measured concentration (activity) in the injection section KXTT4:R3 during the first 10 hours of injection of STT-1.*

Figure 7-5. *Tracer injection concentration (lnC) versus elapsed time, t (h), for Uranine in the injection section KXTT1:R2 during the first 160 hours of injection in STT-1b.*

Figure 7-6. *Electrical conductivity (green) and flow rate (red) of water pumped from KXTT3:R2 during STT-1, STT-1b and STT-2, June 1997 to October 1998.*

Figure 7-7. *Tracer breakthrough after 100 hours in the pumping section KXTT3:R2 during STT-1b. Concentrations are normalised to concentrations in the injection section at t=2hours.*

Figure 7-8. *Tracer breakthrough after 100 hours in the pumping section KXTT3:R2 during STT-1. Tracer concentrations are normalised to concentration in injection section at t=4 hours.*

Figure 7-9. *Tracer breakthrough after 100 hours in the pumping section KXTT3:R2 during STT-2. Tracer concentrations are normalised to concentration in injection section at t=2 hrs.*

Figure 7-10. *Detailed conceptual model of geometry of flow path between sections KXTT4:R3 and KXTT3:R2.*

Figure 7-11. *Example from STT-1b showing masking of late time breakthrough by the injection function.*

Figure 8-1. *Schematic of a cross section perpendicular to the plane of Feature A.*

Figure 8-2. *Example of evaluation graph for Cs obtained from test STT-1. Curves 1,2,3 and 4 are obtained using the LaSAR model (all equations are given in the Appendix G); Curve 1 is obtained by assuming that surface (equilibrium) sorption with constant (effective) β is the only retention mechanism, Curve 2 is obtained by assuming that surface (equilibrium) sorption with variable β is the only retention mechanism, Curve 3 is obtained by assuming that surface (equilibrium) sorption, matrix diffusion and matrix sorption with variable β are the retention mechanisms, and Curve 4 is the same as Curve 3 where in addition non-equilibrium sorption in the gouge is accounted for.*

Figure 8-3. *Example of evaluation graph for Ba obtained from test STT-1. The various curves are explained in the figure caption of Figure 8-2a.*

Figure 8-4. *Example of evaluation graph for Sr obtained from test STT-1b. The various curves are explained in the figure caption of Figure 8-2a.*

Figure 9-1. *Cross-section of the Pilot Resin site seen from the east. The intersection with the target structure for the nine KXTP-boreholes used for the site characterisation and three larger holes drilled prior to provide material for laboratory tests are illustrated.*

Figure 9-2. *View of the pilot resin site showing the KXTP-boreholes, fracture planes of main hydraulic importance (blue) and the initial target structure (green).*

Figure 9-3. *Resin sampling holes KXTE1 and KXTE3 (vertical section seen from west) The indicated discs illustrate the location of the fracture planes used for resin thickness analysis.*

Figure 9-4. *Image examples. a) Typical section from Sample 1b. Fairly constant aperture. Fairly rough fracture surfaces. b) Typical section from sample 3b in area without contacts. Fairly constant aperture between contacts. Smooth surfaces.*

Figure 9-5. *Example of a histograms showing aperture (μm) distribution of Sample 1b (integration of all four quadrants). Contact areas are included in the analysis.*

Figure 9-6. *Sample 3b. Semivariograms for X- and Y-directions based on all four quadrants.*

Figure 10-1. *Schematic conceptual breakdown of structures and conductive elements at different scales in the TRUE-1 block (after Bossart et al., in prep.).*

Figure 10-2. *Schematic conceptual representation of Feature A. Note that the fracture aperture is to approximate scale. The thickness of the remainder of the constituents is not to scale. The total thickness of Feature A including altered Äspö diorite is varying between 0.05 and 0.09 m.*

Figure 11-1. *Example of interpretation of the breakthrough of the more strongly sorbing sorbing tracer Cs, exemplifying predictive capability and effect of variability in β.*

List of Tables

Table 5-7. Specific storage derived for Feature A from evaluation of flow and pressure build-up tests using the GRF method (Winberg, 1996) and using the GTFM evaluation code (Roberts, 1998). The evaluated corresponding transmissivities are reported in Section 5.6.4.

Table 5-8. Hydraulic head (masl) in sections containing Feature A prior to start of the TRUE-1 tracer tests (Preliminary tracer tests (PTT), Radially converging tracer tests (RC-1) and Dipole Tracer Tests (DP-1 - DP-4), and preliminary design tests PDT-1, PDT-2 and PDT-3). Tests STT-1, STT-1b and STT-2 were made in direct succession to the test PDT-3, cf. Table 7-1.

Table 5-9. Natural groundwater flow. Comparison between tracer dilution tests performed in October 1995 and April 1997, cf. Appendix B. *) = not measured.

Table 5-10. TRUE-l – Groundwater chemical analyses, cf. Appendix E.

Table 5-11. Major characteristics of the brackish and saline groundwaters sampled at the TRUE-1 site and in adjacent borehole sections.

Table 6-1. Sorption coefficients, K_d (m^3/kg) obtained for the generic Äspö material experiment using Äspö diorite and Fine-grained granite as solid phases. The values given are based on a contact time of 14 days. When uncertainties are given, they are based on the standard deviation of 2–4 samples (2 σ confidence interval).

Table 6-2. Porosity and the diffusivity determined for the generic Äspö rock material by the through-diffusion experiment. The uncertainties are based on the standard deviation of the results of 5 different samples.

Table 6-3. Distribution coefficients determined for the generic Äspö rock material by through-diffusion experiments. In the calculations, the tritiated water tracer has been considered as a non-sorbing tracer.

Table 6-4. Comparison of porosity measured with different techniques: water saturation, through diffusion measurements and the ^{14}C-PMMA method.

Table 6-5. Summary of parameters derived from fitting of the two pathways model to the experimental results. The porosities are based on the through diffusion experiments with HTO in the same diffusion cells. Through diffusion data for $^{133}Ba^{2+}$ and $^{137}Cs^{+}$ from the 1 cm cells number 19 and 22 are presented for comparison.

Table 6-6. Average mineralogical composition (weight %) of the mylonites, the altered material, Fine-grained granite (FGG), Äspö diorite (ÄD) from Äspö Hard Rock Laboratory (Sample label corresponds to KXT-hole and depth in metres).

Table 6-7. Chemical analyses of the 1-2 mm size fractions of Äspö diorite (ÄD) and Fine-grained granite (FGG) from Äspö Hard Rock Laboratory. Rb, Ba, Cs, U, Th, Hf and the REEs are analysed using INAA (Studsvik Nuclear, Radiometry, Nyköping) . All other elements are analysed with ICP-MS (Svensk Grundämnes-analys AB, Luleå). All concentrations refer to single samples.

Table 6-8. Sorption coefficients, K_d (m^3/kg) obtained using the Feature A site specific rock material as solid phase. The values given are based on a contact time of 9 days.

Table 6-9. Evaluation of breakthrough data by a least square fitting of the data to the one-dimensional solution of the diffusion equation. $D_{w,i}$ is the free water diffusivity of ion i at infinite dilution.

Table 6-10. Chemical analyses of site specific material from the TRUE-1 site. The drill cores are KXTT2, KXTT3 and KXTT4. Rb, Ba, Cs, U, Th, Hf and the rare earth elements are analysed using INAA (Studsvik Nuclear, Radiometry, Nyköping). All other elements are analysed with ICP-MS (SGAB, Luleå). All concentrations refer to single samples.

Table 6-11. Matrix sorption and diffusion data obtained from through diffusion experiments in rock cylinders of Äspö diorite and TRUE-1 Feature A site specific material.

Table 6-12. Selected surface sorption coefficients (K_a) for Äspö diorite and TRUE-1 Feature A site specific material.

Table 6-13. Sorption K_d for the tracers contacted with Äspö diorite, mylonite and altered granite, using TRUE-1 Feature A site-specific conditions.

Table 7-1. Summary of tracer tests performed within the TRUE-1 Project.

Table 7-2. Compilation of data on volumes of injection sections and injection flow rates for tests STT-1, STT-1b and STT-2.

Table 7-3. Sampling system used in TRUE-1 tracer experiments, advantages and weaknesses.

Table 7-4. Conservative tracers used during the TRUE-1 tracer experiments.

Table 7-5. Sorbing tracers used during TRUE-1 tracer tests.

Table 7-6. Summary of flow and transport parameters determined for the flow path KXTT1:R2 → KXTT3:R2 (distance 5.03 m).

Table 7-7. Summary of flow and transport parameters determined for the flow path KXTT4:R3 → KXTT3:R2 (distance 4.68 m).

Table 7-8. Summary of flow and transport parameters determined for the five less tested flow paths (distances varying between 2.59 to 9.57 m).

Table 7-9. Tracer travel times, t_{peak} and $t_{50\%}$, and corresponding retardation ratios, R_{peak} and $R_{50\%}$,, in STT-1 and STT-1b. In STT-2, $t_{5\%}$ was used instead of t_{peak} to calculate the retardation ratio, $R_{5\%}$, due to the double peaks observed in this experiment (from Johansson et al., in press).

Table 7-10. Tracer mass recoveries, R_i, in the STT-1, STT-1b and STT-2 experiments, based on integration of injection and breakthrough curves multiplied by injection flow rate and pumping flow rate, respectively. Time given in parenthesis is the integration time (from Johansson et al., in press).

Table 8-1. Calibrated parameters for HTO and sorbing tracers of the TRUE-1 tests. Note that only the tracers for which laboratory data are available within the TRUE programme are included. The slope of the linear relationship $\beta = k\,\tau$ is $k \approx 3400\ m^{-1}$.

Table 9-1. Boreholes drilled at the Pilot Resin site.

Table 9-2. Water inflow rates and calculated transmissivities.

Table 9-3. Summary of performed resin injections at the Pilot Resin Injection Experiment site.

Table 9-4. Compilation of resin occurrence in the KXTE cores.

Table 9-5. Summary statistics of data from complete samples and sample quadrants.

1 Introduction

This report presents the results from the First Stage of the Tracer Retention Understanding Experiments, commonly denoted the TRUE-1 experiment. The associated experiments were carried out at the Äspö Hard Rock Laboratory (Äspö HRL) between November 1994 and December 1998. The current report presents and discusses the characterisation, experiments and evaluation performed and summarises the results obtained and experiences made. The basic objective of TRUE-1 was to perform and analyse transport experiments with non-sorbing and sorbing tracers in a discrete singular fracture in crystalline rock in the detailed scale over distances up to 10 m.

1.1 Background

The SKB disposal concept comprise three barriers; a Cu-Fe canister, a buffer made up of compacted bentonite and the crystalline bedrock. The former two barriers constitute the man-made engineered barriers, whereas the latter constitute the natural barrier. The latter is expected to provide the necessary retention to transport of radionuclides, such that a release from the engineered barriers yield dose rates which are harmful to the habitants of the Biosphere.

Transport of radionuclides in crystalline bedrock is governed by the flowing groundwater in the available fracture system. However, in addition processes of physical (diffusion) and chemical (sorption) nature, provide additional retention of radionuclide transport in relation to the velocity of the flowing water. The TRUE series of experiments have as their overall objective to increase the understanding of the processes which govern radionuclide transport. Experimental work is conducted on various scales, including Laboratory Scale (<0.5m), Detailed Scale (0.5–10 m), and Block Scale (10–50 m).

Experiments on transport of solutes in Swedish crystalline have previously been performed as part of the Stripa Experiments (Abelin et al., 1985) and the Finnsjön Experiment (Gustafsson, et al., 1984, Andersson et al., 1993). However, there is a general lack of *in situ* sorption data. An opportunity to collect additional transport data has opened up with the SKB Äspö Hard Rock Laboratory (Äspö HRL) near Oskarshamn, SE Sweden, cf. Figures 1-1 and 1-2. This underground facility provide an opportunity for research, development and demonstration in a realistic and relatively undisturbed underground crystalline rock environment down to depths planned for a future deep repository. The studies, planned or ongoing, include research and supporting studies in the fields of excavation damage, groundwater flow, transport of solutes and demonstration of techniques for repository construction.

Figure 1-1. *Location of the Äspö Hard Rock Laboratory.*

Äspö HRL provides SKB and other national radioactive waste management agencies with the opportunity to test equipment and methods under actual conditions before applying the techniques to their own research facilities and planned repositories. An additional component of the international cooperation, which is highly relevant to TRUE programme, is the work performed within the Äspö Task Force on groundwater flow and solute transport. In the case of the TRUE-1 experiments the contributions of the Äspö Task Force include experimental design calculations, blind predictions and evaluation of *in situ* tracer experiments.

1.2 Objectives

The overall objectives of the Tracer Retention Understanding Experiments (TRUE) are to (Bäckblom and Olsson, 1994):

- develop the understanding of radionuclide migration and retention in fractured rock.

- evaluate to what extent concepts used in models are based on realistic descriptions of fractured rock and if adequate data can be collected in site characterisation.

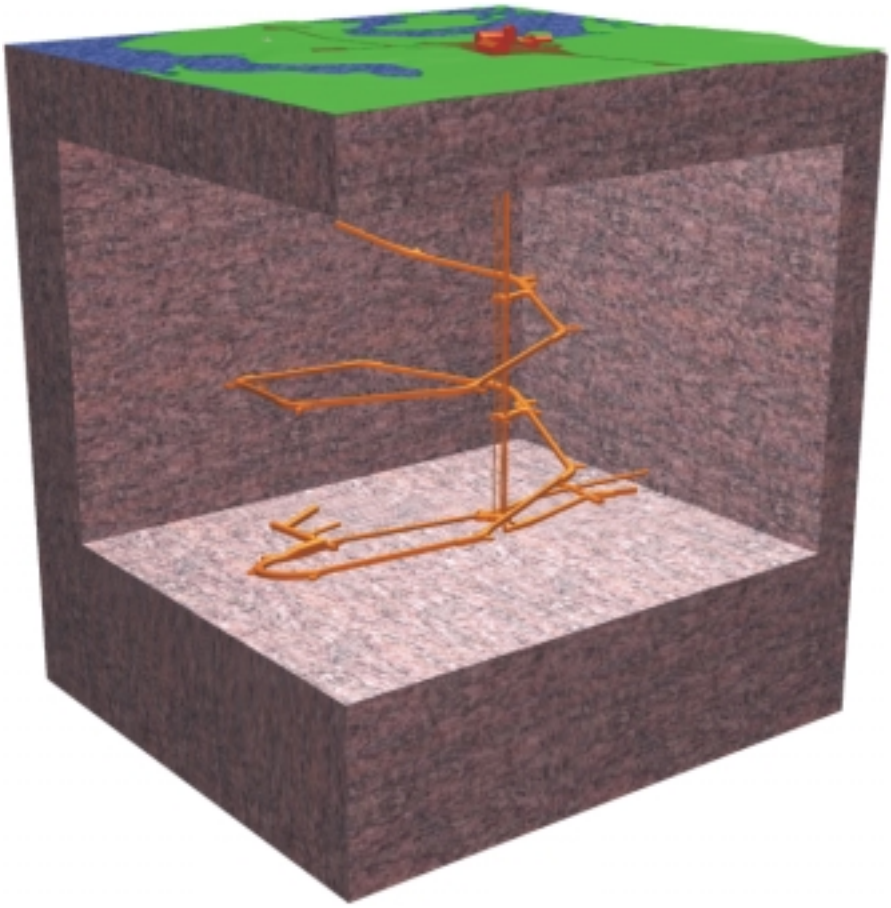

Figure 1-2. *Outline of the Äspö hard Rock Laboratory.*

- evaluate the usefulness and feasibility of different approaches to model radionuclide migration and retention.

- provide *in situ* data on radionuclide migration and retention.

To answer up to the complexity of the issues addressed, the work is performed in stages. Plans for each experimental stage will be detailed successively including stage goals and scope. The specific objectives of the First TRUE Stage (TRUE-1) were to (Winberg, 1994):

- conceptualise and parameterise an experimental site on a detailed scale (L=0.5–10 m) using tracer tests with conservative and sorbing tracers in a simple test geometry,

- improve tracer test methodologies for conservative tracer tests in a detailed scale,

- develop and test a technology for injection of epoxy resin on a detailed scale and to develop and test techniques for excavation (drilling) of injected volumes and subsequent analysis,

- test sampling- and analysis technologies to be employed in the analysis of matrix diffusion.

The First TRUE Stage was expected to constitute a training exercise for tracer test technology on a detailed scale using conservative and sorbing tracers. In addition, to provide supporting technology development for sampling and analysis of detailed aperture distributions obtained through resin injection and subsequent drilling. The First TRUE Stage was also expected to contribute the technology adaptation and development, data and experience which would constitute the necessary platform for subsequent more elaborate experiments within TRUE.

The original plan did not contain planned usage of sorbing tracers. The need to include sorbing tracers was identified by SKB late 1995, and the use of sorbing tracers was amended accordingly. The test of techniques for sampling and analysis of matrix diffusion were aborted early on. The address of the latter issue is presently the focus for the planned Long-Term Diffusion Experiment (LTDE) which constitute a part of TRUE.

1.3 Rationale

The safety of a Swedish KBS-3 type repository relies heavily on the engineered barrier system that contains the waste. The barrier system is made up of the Cu-Fe-canister and the buffer material (bentonite clay) in which the canister is embedded. The buffer material, with self-sealing ability when exposed to groundwater, should prevent any corroding species from reaching the canister and should provide primary containment in case of canister breach and subsequent radionuclide release. In the case that the engineered barrier fails, the geosphere provides the remaining retention potential which should ideally allow radionuclides to reach the biosphere only at harmless radioactive levels. Realistic estimates/predictions of the geosphere retention capacity are thus critical for any safety assessment. Of particular interest in this regard is the near-field adjacent to the canister holes and storage tunnels. The near-field rock should provide a stable mechanical and chemical environment for the engineered barrier. It should prevent corroding species from reaching the engineered barrier, but primarily it should retard migration of radionuclides released from the engineered barriers. The amount of radionuclides reaching the biosphere depends to a large extent on their fate in the near-field, i.e. the local interaction between the groundwater, the host rock and the radionuclides.

In the near-field, transport of radionuclides is envisioned to take place in single permeable fractures. The primary processes which govern radionuclide transport in a single fracture are fluid advection and applicable retardation mechanisms. The

retardation implies that the transport of radionuclides is slower than the average groundwater velocity in the fractures. The primary retardation mechanisms are sorption of radionuclides on fracture surfaces and diffusion of radionuclides into the rock matrix, with associated sorption on inner surfaces. The retardation due to sorption (and related processes) depends primarily on the type of radionuclide, distribution of flow across the fracture surfaces and the chemical composition of the groundwater and host rock fracture minerals, the capacity of radionuclides to diffuse into the rock matrix, and sorption within the matrix.

The key issue in safety and performance assessment is thus the local mass transfer (due to sorption and diffusion) from the dominant flow paths (mainly single fractures or groups of fractures) to the host rock in the vicinity of the waste packages. This local mass transfer is likely be the focus for future site investigations and detailed characterisations during construction of a repository since the relevant field data are sparse. In addition these mass transfer processes will be described/predicted by flow and transport models. In the assessment of the performance of the host rock as a natural barrier to radionuclide release to the biosphere, it is essential to show that the models used adequately describe the essential aspects of radionuclide transport in the near-field host rock and that relevant and realistic input data are used in the models. The TRUE-1 experiments will serve to establish the methodology which will provide the necessary data through integrated laboratory/field experiments and modelling.

The TRUE-1 experiment will also provide important insight into the scaling of transport parameters from laboratory to detailed (near-field) scale. From the ongoing Block Scale Experiment, Winberg (1997, 1999), which addresses a 10–50 m length scale, additional knowledge into the scaling of transport parameters will be gained. The outlined sequence of tests; Laboratory, Detailed and Block scale tests, will serve as an important basis for extrapolation of descriptions of local transport phenomena and transport parameters also to a (limited) far-field scale.

1.4 Previous transport experiments in fractures

During the last two decades several tracer experiments have been performed to study the transport properties of fractured crystalline rock (e.g. Landström *et al.*, 1983, Abelin *et al.*, 1985, Andersson and Klockars, 1985, Abelin *et al.*, 1987, Gustafsson and Andersson, 1991, Birgersson *et al.*, 1992, Andersson *et al.*, 1992, and Cady et al 1993). These experiments have generally been performed with conservative tracers, i.e. non-sorbing (non-reactive) tracers which follow the water movement, and have provided data on flow porosity, dispersion, and the heterogeneity of the flow system. Many experiments have shown that flow within fractures is heterogeneous and may in some instances occur within relatively narrow channels. In some cases, results indicate that flow occurs over a relatively large fraction of the fracture surface. Some of the studies of flow heterogeneity have been performed within the disturbed zone around drifts and it is not clear how representative these results are for flow and transport through fractures in undisturbed rock. To resolve these issues, additional data are required to quantify

heterogeneity and flow distribution within fracture planes, and ideally for different types of fractures. Adequate understanding of the distribution of flow within fractures is also required to estimate the surface area that is available to sorption and diffusion.

There are only a few *in situ* experiments where transport of sorbing tracers have been investigated. In the first phase of the International Stripa Project sorbing tracers were injected in a fracture above a drift (Abelin *et al.*, 1985). The fracture was subsequently excavated, samples taken of the fracture surface and analysed for tracer contents.

Between the years 1985 through 1996 a comprehensive tracer experiment, the Radionuclide Migration Experiment, was conducted at the Grimsel Test Site in Switzerland (Frick *et al.*, 1992, Haderman and Heer, 1996, Heer and Smith, 1998. In this experiment (GTS-MI), several boreholes were drilled through a small shear zone and tracer tests were performed under different hydraulic boundary conditions, in various combinations of sources and sinks, and over varying transport distances. Various non-sorbing (Uranine, ^{3}He, ^{4}He, $^{82}Br^{-}$, $^{123}I^{-}$) weakly sorbing ($^{22}Na^{+}$, $^{24}Na^{+}$) and more strongly sorbing tracers ($^{85}Sr^{2+}$, $^{86}Rb^{+}$, $^{134}Cs^{+}$, $^{137}Cs^{+}$) were used. The relative breakthrough was investigated for cocktails of tracers injected as a pulse in a dipole flow field. Fixing some independently derived parameters and calibrating additional transport parameters using conservative tracers, predictions were subsequently made for sorbing tracer transport, including predictions for other flow paths. The work done has included interaction between experimentalists, modellers and repository performance assessors. The GTS-MI included an elaborate laboratory program with the objective to compare field and laboratory K_d values and detailed structural and mineralogical characterisation and conceptualisation of the flow paths. Modelling showed a consistent picture with regard to sorption data from the laboratory and the field experiments.

The existence, manifestation and effect of matrix diffusion (Neretnieks, 1980) have been addressed in various circumstances. The excavation and analysis of the surfaces of the fracture subject to the single fracture experiment at Stripa (Abelin *et al.*, 1985) indicated penetration of tracer into the rock matrix. Recent investigations at Stripa in a small divergent flow field using two conservative tracers with different diffusivities showed no effect of matrix diffusion (Andersson *et al.*, 1992).

In the evaluation of both the GTS-MI experiments (Haderman and Heer, 1996) and tracer tests performed in the Culebra Dolomite at the WIPP site (Beauheim, et al. 1996, Meigs et al. 1996) inclusion of matrix diffusion was necessary to explain and model the obtained tracer breakthrough curves. The performed tracer tests at the WIPP site constitutes a first unique example of how well-designed tracer tests can be used to improve understanding of the acting transport processes and hence improve the safety case for licensing of an actual repository site.

1.5 Tested hypotheses

The TRUE-1 experiment is a multi-task project which includes laboratory and *in situ* experimentation. In addition, technology and methodology adaptation and development has been carried out with regards to performance of *in situ* tracer tests and pore space characterisation using *in situ* resin injection and subsequent excavation. Furthermore, a substantial contribution has been made in the development of a workable evaluation framework for tracer tests with sorbing (reactive) tracers.

The specific hypotheses tested in the First TRUE Stage are;

- Current available *in situ* tracer test methodology can with minor adaptations be made applicable to the specific ambient conditions met at Äspö HRL,

- The cationic tracers proposed by Byegård (1993), subsequently subject to laboratory through diffusion and batch sorption tests using Äspö rock materials, are also usable in *in situ* experiments,

- It is possible to develop a workable technology and procedure for obtaining pore space/aperture data from *in situ* resin injection and subsequent excavation and analysis,

- Tracer transport processes are understood sufficiently well to enable prediction of tracer breakthrough based on a combination of laboratory and *in situ* characterisation data,

- Due to heterogeneity in rock and fracture mineralogical and physical properties, the parameter values for mass transfer reactions (sorption and diffusion) determined in the laboratory may differ from the corresponding parameters values derived from *in situ* experiments,

It should in honesty be stated that the above hypotheses were not stated explicitly in the original planning documents, but have been formulated during the course of the project. The stated hypotheses are however in full accord with the objectives of the experiment.

1.6 Location and configuration of the main experiment

A set of physical and logistical requirements were listed as a guide for locating the TRUE-1 experiment (Winberg, 1994). These included requirements related to hydraulic isolation (risk for disturbance), hydraulic gradient, transmissivity, rock stress situation, lithological homogeneity, fracture frequency, etc. It was decided that a selection of a suitable target volume necessitated drilling of a number of pilot boreholes, distributed near the experimental level at depths ranging from

350–450 m below sea level. The performed site selection programme, SELECT, is reported by Winberg, et al. (1996).

The outcome of the SELECT project showed a suitable target volume between length coordinates 2/945 and 3/005 metres in the main access tunnel, as observed in borehole KA3005A, drilled from length coordinate 3/005 m, cf. Figures 1-3 and 4-2. In this borehole a series of suitable fractures oriented northwest were identified between 35 and 50 metres with a suitable transmissivity. To access the identified rock volume, a new experimental niche was excavated at about 2/945 m providing access to the identified structures beyond 10 metres. In order to characterise and evaluate the identified fractures a series of four additional boreholes were drilled in a northeasterly direction with the intention of providing a near circular pattern of intersection in the individual target fractures. An overview of the drilled 56 mm boreholes and relevant data are provided in Table 1-1, cf. Figures 4-2 and 4-3.

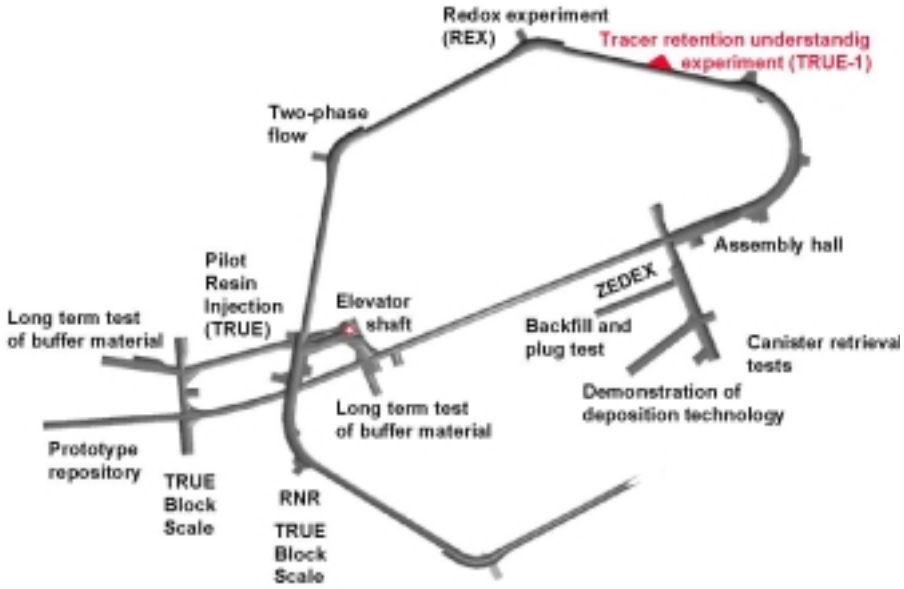

Figure 1-3. *Plane view of main experimental level at the Äspö HRL showing location of the TRUE-1 experiment.*

Table 1-1. Geometrical data on the boreholes at the TRUE-1 site. All boreholes have a diameter of 56 mm.

Borehole Id code	Easting (m)	Northing (m)	Elevation (masl)	Bearing (deg)	Inclination (deg)	Length (m)
KA3005A	2363.82	7408.09	–399.86	299.11	–4.50	58.11
KA3010A	2369.59	7405.33	–399.87	99.54	–4.70	60.66
KXTT1	2313.56	7430.00	–392.12	61.53	–45.64	28.76
KXTT2	2314.38	7427.63	–392.42	61.21	–44.52	18.30
KXTT3	2313.55	7429.95	–391.07	44.42	–36.98	17.43
KXTT4	2313.86	7428.80	–391.14	60.02	–36.48	49.31

1.7 Outline of experimental programme

The basic idea of a TRUE experimental stage is to carry out a cycle of activities beginning with geological characterisation of the site, followed by hydraulic and tracer tests, and finally epoxy resin is injected, the tested rock volume excavated, and analysed for flow path geometry and tracer concentration. As indicated previously, this first stage of TRUE was primarily aimed at adaptation and development of technology and methodology. A specific address of retention mechanism was not included in the original plans, but was amended by including tests with sorbing tracers as of late 1995.

1.7.1 Quantified parameters

The TRUE-1 experimental, analysis and evaluation programmes have included quantification of the following parameters:

Host rock characteristics
- Lithology
- Alteration
- Transmissivity (evaluated)
- Storativity (evaluated)

Fracture characteristics

Geometry
- Frequency and intensity
- Mineralogy and geochemistry
- Transmissivity (evaluated)
- Connectivity
- Groundwater chemistry

Transport characteristics

Matrix rock
- Diffusivity D_e (evaluated from laboratory experiments)
- Volumetric distribution coefficients for rock K_d (on defined size fractions) (evaluated from laboratory experiments)
- Porosity (evaluated from laboratory experiments)

Fracture
- Residence time distributions (measured)
- Flow velocity (ambient and induced)
- Flow porosity (evaluated)
- Disperisivity (evaluated)
- Aperture (measured (resin) and evaluated)
- Spatial variability of aperture (measured (resin) and evaluated)

Model-specific parameters

- Parameter β (integrated flow velocity-averaged aperture along flow path), cf. Section 8.3 (derived)
- Residence time for conservative tracer τ (measured)
- Coefficient k, in $\beta=k\cdot\tau$, cf. Section 8.3 (derived)
- Enhancement factor for diffusion *f* (calibrated)
- Parameter κ (composite parameter for diffusion/sorption derived from measured laboratory data)
- Surface distribution coefficient K_a (derived from measured laboratory data)
- Rate coefficients α (calibrated)
- Distribution coefficient for gouge material K_d^g (calibrated)

1.7.2 Characterisation techniques used

The following techniques were employed in the characterisation of the target volume including identification of the most suitable of the identified potential target features (Winberg, 1996):

1) Drilling of 56 mm boreholes with careful monitoring of inflow between uptakes and observation of pressure responses in already existing boreholes with provisional packer systems. First assessment of location of target structures and their mutual connectivity.

2) Borehole deviation measurements have been made with the MAXIBOR and FOTOBOR techniques. This information serves to provide accurate borehole geometry and also to obtain absolute geometries of mapped fractures.

3) Core logging has been performed using the PETROCORE system and provide basic geological classification and identification of fractures.

4) Borehole TV imaging using the RAAX BIPS system was employed for the first time in production at Äspö. In combination with the core log and flow log results, the borehole TV images constitute a very powerful tool for identification of conductive fractures.

5) Single hole directional borehole radar surveys using the RAMAC system were employed to obtain fracture and structure geometry and extent beyond the borehole walls.

6) Acoustic flow logging using the UCM probe was used to verify and improve the identification of conductive structures.

7) Transient flow and pressure build-up tests were employed to quantify the transmissivity of the boreholes in consecutive 3 m test sections.

8) Single packer flow logging in 0.5 and 1 metre steps were employed to improve further the identification of conductive structures.

9) Multi-packer systems with up to 5 test sections were used to isolate the selected target feature and adjacent structures in the boreholes.

10) Chemical analyses were performed of the groundwater sampled in the packed of sections in the boreholes.

11) Cross-hole hydraulic interference tests were carried out within the established array to verify the connectivity obtained from the drilling and to assess reciprocity in observed hydraulic responses.

12) Repeated tracer dilution tests were performed to quantify the background flow and changes in the flow field over the duration of the tracer test programme.

13) Multiple hole injection tracer tests with conservative tracers were performed in different flow geometries and in different combinations of sources and sinks in the borehole array.

Table 1-2. Summary of investigation methods applied in the First TRUE Stage.

Method/activity	Purpose	Parameters determined
Drilling	Localisation and characterisation of target features	Penetration rate Drill-water pressure Inflow between uptakes
Collection and sampling of drilling water	Relevance of water samples and retention properties	Drilling water content, drilling debris balance
Pressure monitoring during drilling	Identification of structures Connectivity	Pressure responses as a function of drilling depth
Borehole deviation	Geometry of boreholes and structures. Geometry of experiment	Orientation of drill core, Borehole coordinates, Core losses
Core logging	Geological classification, identification of fractures	Lithology, fractures, fracture minerals, alteration, veins, crushed zones
Borehole TV imaging	Structure identification, classification and geometry	Lithology, width, absolute orientation
Borehole radar (directional)	Fracture geometry and extent	Fracture geometry
Flow and pressure build-up tests	Hydraulic properties of fractures	Transmissivity, specific storage, flow dimension
Water sampling	Hydrogeochemical characteristics of identified structures. Relative isolation	Concentration of major trace elements, stable isotopes, microbes
Interference test	Geohydrological characterisation, hydraulic boundaries, connectivity	Transmissivity Storativity
Multiple-hole tracer tests	Flow and transport properties of studied feature	Groundwater flow, resi-dence times, transport parameters.
Dilution tests (single-hole tracer tests)	Ambient groundwater flow, flow heterogeneity	Groundwater flux, local hydraulic gradient

14) Tracer tests in radially converging flow geometry with radioactive sorbing tracers in flow paths selected on the basis of previously performed tracer tests with conservative tracers.

15) Resin injection, excavation and analysis of pore space (Pilot Resin Experiment performed in the F-tunnel, cf. Figure 1-3).

A summary of the characterisation methods employed is shown in Table 1-2.

2 Geological setting

2.1 Regional setting

The regional setting of Äspö has been established from an interpretation of geological field investigations and geophysical survey data, on a 25 x 25 kilometre scale. The Äspö area is mainly of a granitic composition with different types of Småland granite belonging to the Transscandinavian Igneous Belt. The presence of some E-W elongated massifs of basic rocks have been inferred by positive magnetic and gravity anomalies (Gustafson *et al*., 1988).

Information from all geological and geophysical investigations corroborates a tectonic picture of the Äspö area dominated by an almost orthogonal system of 1st order lineaments (N-S and E-W). These lineaments are in the order of 20 to 50 kilometres in length and often coincide with magnetic low zones (some hundred metres wide) with a central fracture zone up to some tens of metres wide. In addition to the system of 1st order lineaments, there are also 2nd order lineaments trending NW and NE and forming another, almost orthogonal, system. The 2nd order lineaments are mostly in the order of 100 to 200 metres wide and extend from 1 to 20 kilometres in length. Lineaments trending NNW and NNE (3rd order lineaments) are interpreted as being a conjugate shear set to the tensional fracture zones trending N-S. The location of the main lineaments in the neighbourhood of Äspö are shown in Figure 2-1 (Rhén *et al*., 1997).

2.2 Geological setting of the Äspö HRL site

2.2.1 Lithology and alteration

The dominant rocks at Äspö belong to the 1700–1800 M year old Småland granite suite, with mafic inclusions and dykes probably formed in a continuous magma-mingling and magma-mixing process (Gustafson *et al.,* 1988). The result of these processes is a very inhomogeneous rock mass, ranging in mineralogical composition from granites to dioritic or gabbroic rocks. Rather large, irregular, bodies of diorite/gabbro have been located in boreholes at great depth in the site area. Fine grained granite and pegmatite also occur frequently at Äspö as more or less well defined dykes or veins intersecting the older rocks. Aplite, pegmatite and dolerite have only been observed as very narrow dykes, seldom more than a few centimetres wide.

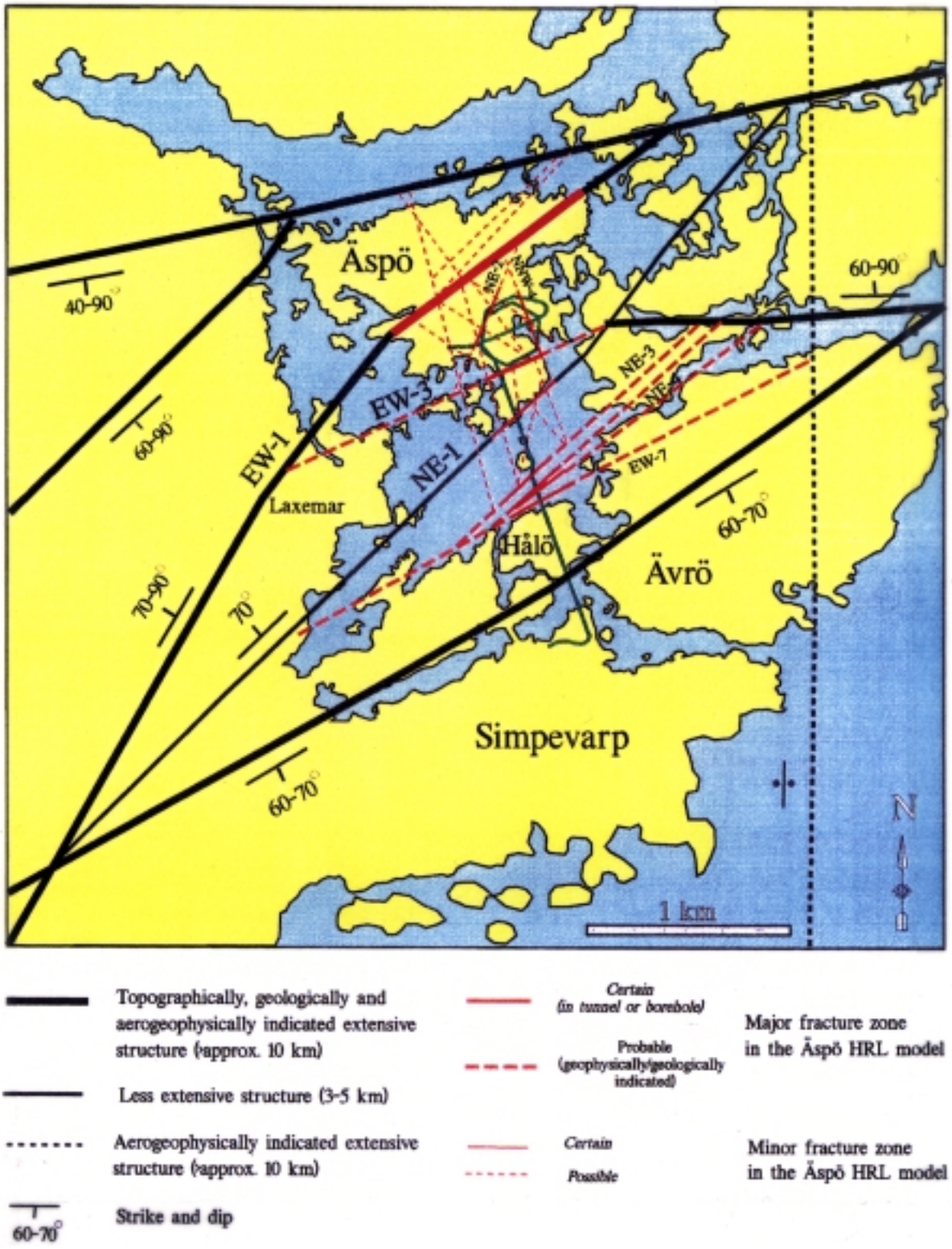

Figure 2-1. *Fracture zones in the Äspö HRL (red) fit in the pattern of regional structures (black).*

Minor inclusions of mafic rock types (greenstones) are common within the granite. Narrow shear zones, resulting from different deformation intensities, are present at all scales. Mylonite zones up to several metres wide occur in places.

The classification of the rocks of Äspö are divided into four units (Wikberg *et al*., 1991):

- The typical Småland granite is dominant down to a depth of 100–150 metres in the Äspö drift south of the Äspö Island. Macroscopically, the unaltered Småland granite is grey to reddish grey, medium to coarse grained and somewhat porphyritic, with a generally massive texture.

- The Småland granite grades into the more mafic Äspö diorite at depth in the Äspö drift. The grey-reddish grey, medium grained porphyritic Äspö diorite contains less quartz and microcline balanced by a higher plagioclase and biotite content compared to the Småland granite. Petrographically, the Äspö diorite is a quartz-monzodiorite, granodiorite or quartz monzonite.

- Fine grained, red to greyish red granite occurs very frequently on the Äspö island as well defined dykes intersecting the older rocks but also as irregular veins and sheets. The dykes usually vary in width between 0.1 metres and up to 5 metres. They are generally orientated NE-SW. Most of the typical fine grained granite dykes are strongly deformed, which has resulted in brittle deformation.

The most common rock type in the greenstone group is a greyish to black, fine grained, often rather homogeneous, mafic rock probably of volcanic origin which is always strongly altered.

2.2.2 Fracture zones

A NE-ENE trending, steep, penetrating foliation is the most dominant structural element in the 1700–1800 M year old Äspö granitoids and seems to be the oldest sign of ductile deformation related to a sub-horizontal NNW-SSE compression.

Intensified strain associated with amphibolite-facies metamorphism is evident as gneissic zones trending NE-ENE, dipping to the NNW. Elevated to a higher structural level between 1700–1400 M years ago, these old gneissic zones were reactivated as mylonitic NE trending shear zones, especially in the central parts of Äspö, in a ductile-semiductile deformation phase.

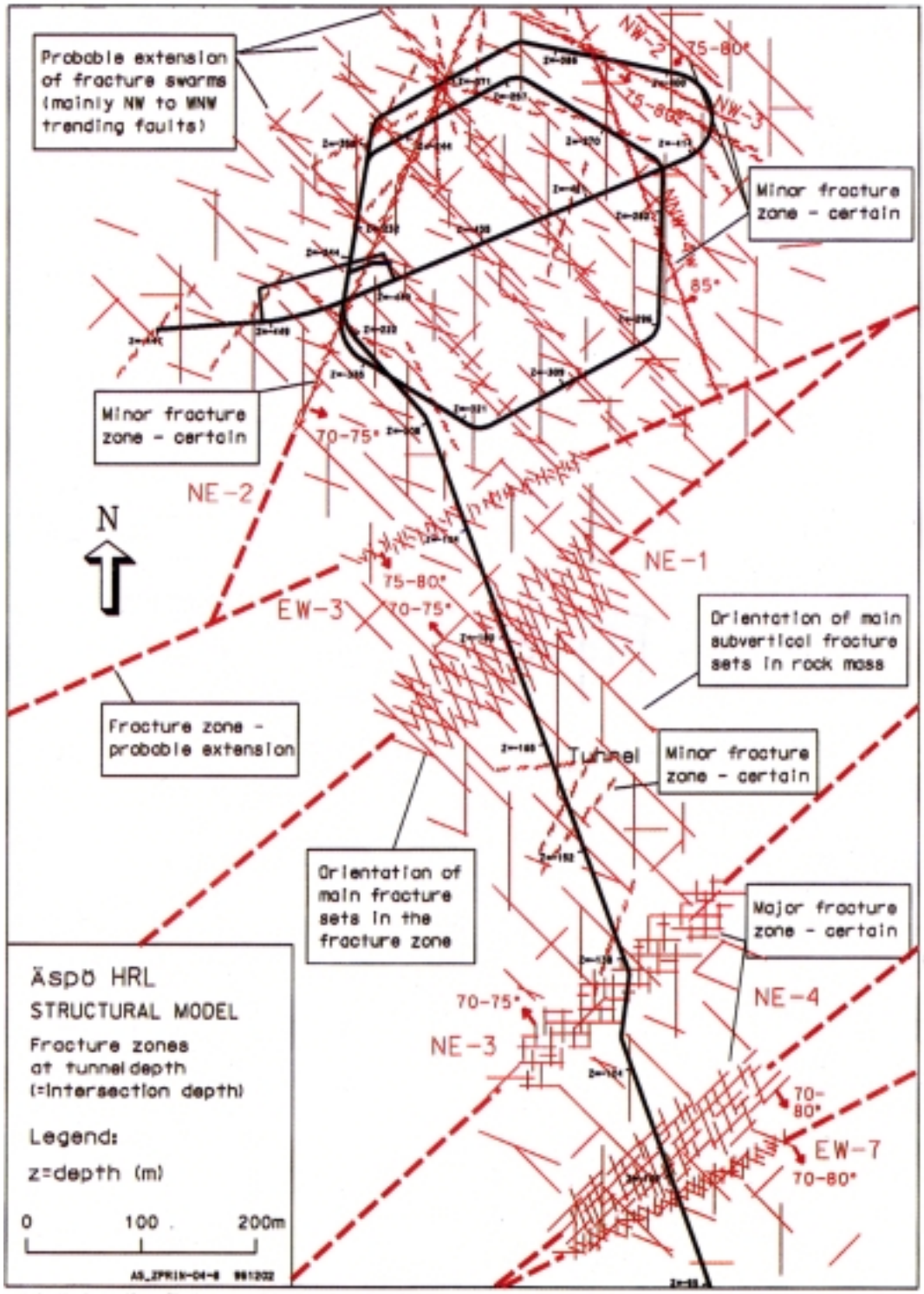

Figure 2-2. *Structural model of the Äspö site area (Rhén et al., 1997).*

Strong foliation and mylonites are common in the Äspö shear-zone, EW-1 (Figure 2-1), where more than 10 metre long bodies of mylonite occur, trending E-W and dipping steeply to the north. Regional evidence suggests that the E-W trending mylonites are older than those trending NE. Small scale mylonitic shear planes less than about 1 centimetre wide and up to a few metres long, with a wide range of orientations, are found in many parts of the island.

The first brittle faults probably developed in the region in response to the emplacement of younger granites. These faults and older ductile zones were reactivated several times. The rock mass became increasingly brittle as it was uplifted and exposed about 1000 M years ago. Parts of the epidotic vein system reactivated and its fractures were later filled by chlorite, zeolites and calcite.

Fracture zones at Äspö have a wide range of orientations and styles and most of them result from the reactivation of older structures. The style of each fracture zone tends to depend on the nature of the older structure being reactivated, such as E-W gneissic zones, NE or E-W trending mylonites and gently dipping alteration zones. Fracture zones with N, NE or E-W trends, on Äspö normally had ductile precursors whereas those trending NW apparently did not.

Except for the fracture zone which reactivated the NE trending Äspö shear zone EW-1 (Figure 2-1), there is no fracture zone of a regional extent crossing the island. Fracture zones trending ENE and NE which bound Äspö to the north and south have been interpreted from geophysical data.

On a more local scale, outside the Äspö shear zone EW-1, fracture zones are mainly orientated in an E-W direction (Figure 2-2). Whilst the outcrop mapping of fractures performed on the Äspö island showed a dominant set of fractures orientated NW with dips 70^{o}–90^{o}. In addition, narrow fracture zones trending approximately N-S to NW are common and found to be hydraulically important, with most of the fracture zones and fractures orientated in a N-S direction forming an en-echelon pattern. A few gently SW dipping fracture zones have also been mapped underground in the Äspö-Hålö area.

2.2.3 Stress field

Stress measurements have been performed at the experimental level in boreholes in the vicinity of the performed ZEDEX experiment (Myrvang, 1997) and in the vicinity of the site of the planned Prototype Repository Experiment (Ljunggren and Bergsten, 1998). The measurements have been performed using the CSIRO and the Borre probe developed by the Swedish State Power Board, respectively. The results. The magnitudes of measured stresses are presented in a tentative format in Table 2-1. The orientation of measured maximum horizontal stress σ_H at the two sites is shown in Figure 2-3.

Table 2-1. Summary of rock stress measurements in KXZSD8HR and KXZSD8HL (ZEDEX site) and KA3579G (Prototype Repository site). Results given as maximum (σ_H), minimum (σ_h) and vertical (σ_v) horizontal stress (MPa).

Site	σ_H	σ_h	σ_v
ZEDEX	15–24	4–13	7–15
Prototype	22–36	13–20	19–24

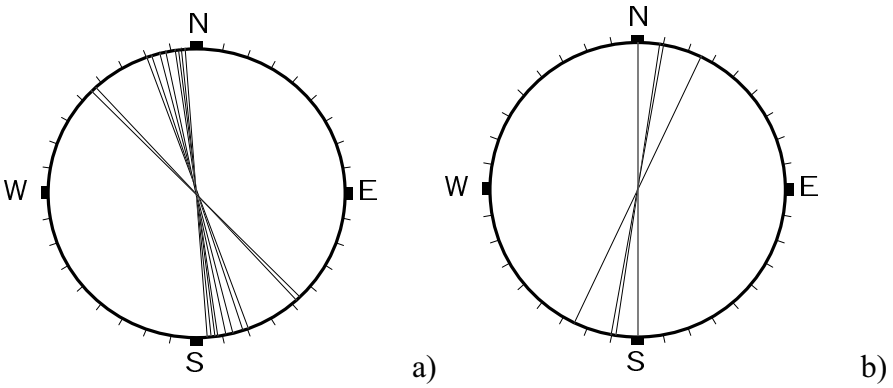

Figure 2-3. *Orientations of measured maximum horizontal stress (σ_H) in relation to local Äspö north at a) the ZEDEX site and b) the Prototype Repository site.*

3 Geologic characterisation

3.1 Introduction

This chapter provides an overview of the geologic characterisation of the TRUE-1 rock block. The geology has been documented through a number of detailed investigations of the TRUE-1 boreholes and the tunnel section adjacent to the experimental site. The analysis of the discontinuities in the TRUE-1 Block, visual inspection of tunnel outcrops, core samples and digital images of borehole walls provides the background material for the construction of a 3D structural model using a CAD system.

The primary data collection and geological characterisation involves the following methods:

- BIPS (Borehole Image Processing System) logging of all TRUE-1 boreholes
- Detailed geological and structural core mapping in combination with BIPS images
- Standard tunnel trace maps of the tunnel section 2/944–3/004 m
- Detailed tunnel trace maps of the tunnel section 2/944–3/004 m performed by Bossart and Mazurek and reported by Winberg (1996)
- General geological information from the HRL site scale structural model by Rhén et al (1997) and from the SKB site characterisation database SICADA.

3.1.1 Methodology of geological characterisation; boreholes and tunnel

The development of the structural conceptual model for the TRUE-1 site has been systematically performed by analysing both cores and tunnel data. The general procedure is shown in Figure 3-1.

The detailed core mapping covers the following quantified parameters:

- Fracture location (borehole length)
- Fracture orientation (Strike/dip, Äspö Local North)
- Foliation orientation (Strike/dip, Äspö Local North)
- Fracture mineralisation
- Ductile deformation (subjective scale 0–3), cf. Section 3.3.1
- Cataclastic deformation (subjective scale 0–3), cf. Section 3.3.2.

- Alteration (subjective scale 0–3), cf. Section 3.3.3.
- Open or sealed fractures (as observed from the BIPS log)
- Rock type
- Rock contacts (borehole length, m)
- Rock texture

The fracture traces on the north tunnel wall in conjunction to the TRUE-1 site (2/944–3/004 m) have been mapped by Mazurek and Bossart and are included as an tunnel trace map in Winberg (1996). The mapped parameters are:

- Fracture trace length
- Fracture location
- Rock types
- Fracture mineralogy

A summary table based on the detailed trace map of the TRUE-1 tunnel section (2/944–3/004 m) is shown in Table 3-1. The actual trace map can be found in Winberg (1996).

Table 3-1. Statistics for the tunnel section 2/944–3/004 m (after Bossart et al., in prep.).

	Trace map of tunnel wall Winberg (1996)	**Scan line mapping data (Bossart et al., in prep.)**
Section	2944 – 3004 m	2950 – 2980 m
Total mapped section	60 m trace map	30 m scan line
Approximate mapped perimeter	4 m	–
Total trace length	304.8 m	31.20 m
Number of fracture traces	229	49
Mean trace length	1.33 m	0.64 m
Std Dev of trace length	1.21 m	0.67 m
Approx. mapped tunnel surface area	240 m^2	–
Approximate fracture intensity P_{21} or P_{10}, cf. Section 3.5.3	P_{21} = 1.27 m^{-1}	P_{10} = 1.63 m^{-1}

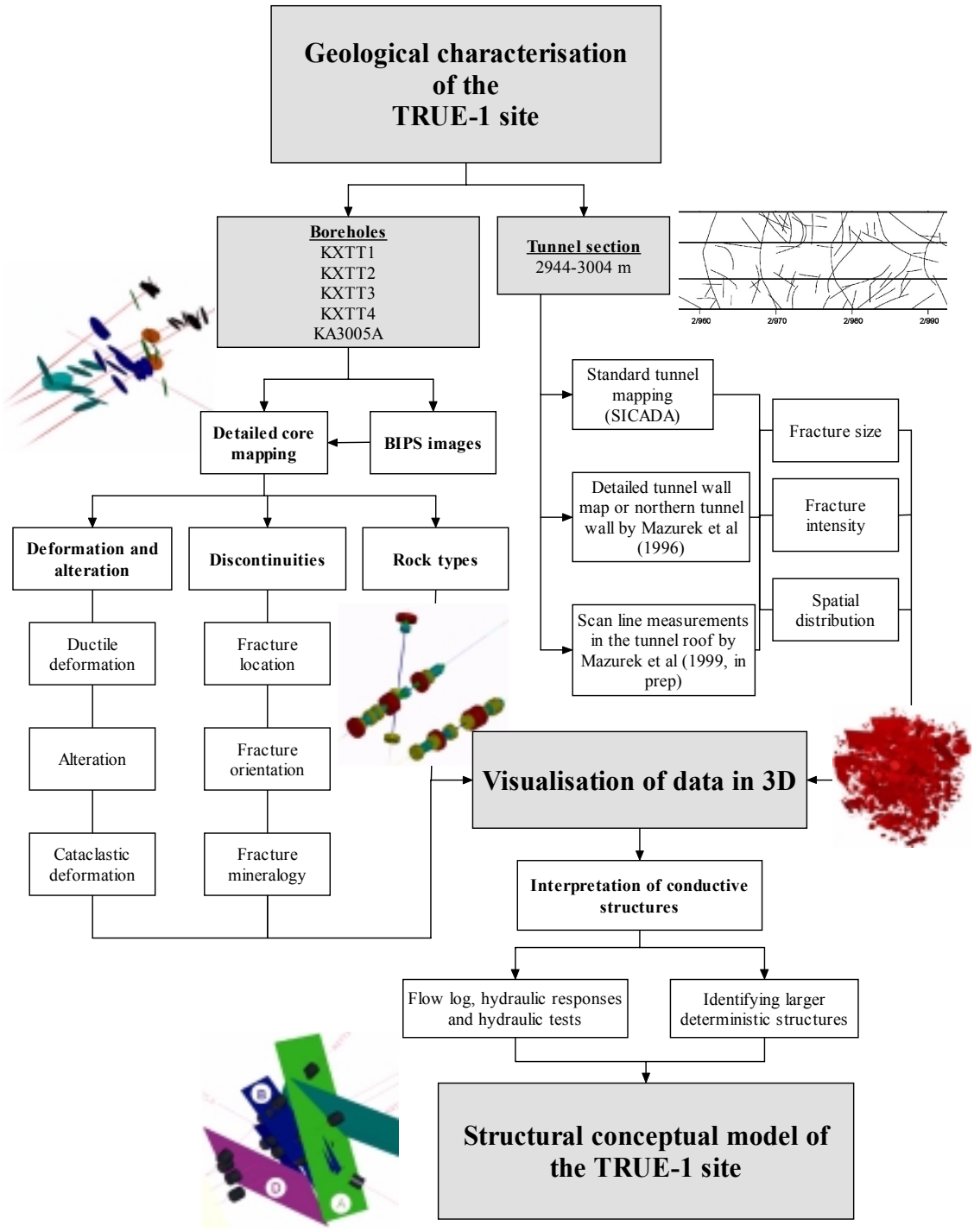

Figure 3-1. *Flow chart illustrating the methodology to establish the structural conceptual model of the TRUE-1 block.*

3.2 Lithology of the TRUE-1 site

The initial 10–15 m of all cores is made up of rather homogeneous diorite, sometimes transitioning into granite, cf. Figure 3-2. The diorite changes character towards NE, where it becomes fine-grained and dark, containing felsic phenocrysts at approximately 10 m depth. There are two varieties of this phenocryst-bearing Äspö diorite; one where the phenocrysts are small and. The other variety contain larger phenocrysts, sometimes transitioning into a coarse diorite.

In the core of KA3005A the diorite is generally more massive than in the core of KXTT1 through KXTT4. The diorite is often rich in epidote. Sometimes it is heavily impregnated with hematite which can make it hard to distinguish it from Småland granite, which is commonly the case in fractured areas. Parts of the phenocryst-bearing diorite in KXTT4, between L=18 and L=19.5 m, is different from phenocryst-bearing diorite found in the other cores. The contrast between the dark, fine grained matrix and the light coloured, fractured and fragmented phenocrysts is more pronounced, giving it the appearance of a star-speckled sky. This type of diorite is not notably more fractured than the common diorite.

Mylonites are observed in all cores and are characterised as being rich in epidote and impregnated with hematite. Aplite or red porphyric veins occasionally cut through the diorite.

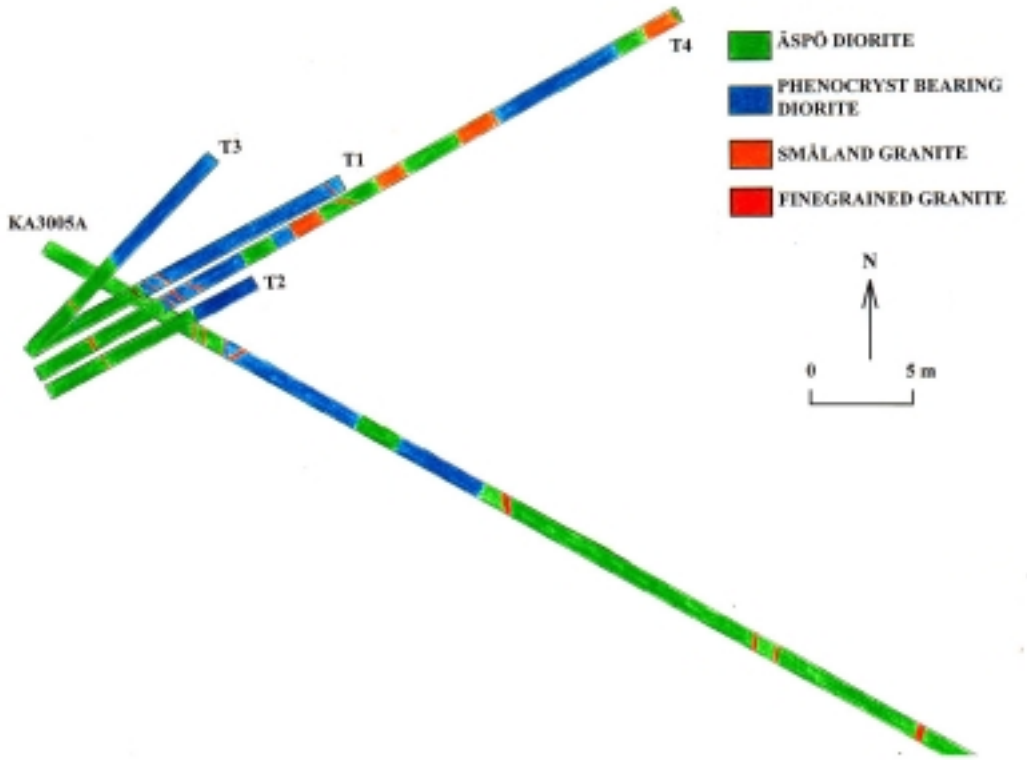

Figure 3-2. *Detailed lithology of the cores of the TRUE-1 site, cf. Figure 4-1.*

3.3 Structural properties

The characteristics of conductive fractures suitable for experiments such as the TRUE-1 experiment need to be quantified and characterised in spatial terms. The detailed geological database provides information not only of the target fracture itself, but also of the character of the host rock in its proximity. The complex geology next to, and within the fracture is described in a simplified fashion in terms of two basic components; deformation and alteration.

The definitions used in the subjective rating of deformation are based on a classification diagram of fault rocks (Sibson 1977), which separates tectonic deformation in two subclasses defined by the fact that an extremely deformed ductile structure, i.e. a mylonite, has an organised foliation fabric whereas a cataclasite exhibits a random fabric. When deformation is cataclastic, the cohesive rock contains fragments of randomly oriented, grains and brecciated rock. Ductile and cataclastic deformation are thus treated as separate parameters.

Alteration is defined as the summed up visual impression of the colour of the rock, grain size and epidotisation/chloritisation adjacent to discontinuities.

3.3.1 Ductile deformation

There exists a general penetrative steep foliation throughout the investigated rock oriented NW. Sections along the boreholes that have a more pronounced foliation fabric are classified as being structures with a varying degree of ductile deformation. Sections with a high degree of ductile deformation, i.e. sections with mylonites or other highly strained sections, are oriented NW with a steep inclination as shown in Figure 3-3. The orientation of mylonites without any brittle fractures does not differ from fractured mylonites. However, the proportion of reactivated mylonites is higher than mylonites without fractures, implying that the history of deformation in the rock has in parts been preferentially located to previous zones of weakness.

3.3.2 Cataclastic deformation

In the general deformation history of a typical crystalline rock, cataclastic deformation tends to occur well after the early ductile movements in the high temperature plastic rock. Cataclastic structures contain fragments of the host rock but are still cohesive. In the TRUE-1 block cataclastic deformation occur mainly in structures that are oriented NW with a steep dip, c.f. Figure 3-3. The cataclastic structures are often reactivating older planes of weakness in the rock such as mylonites. Approximately 1/3 all observed

cataclastic structures are located in, or adjacent to mylonites. The proportion of cataclastic structures with open fractures is higher than cohesive cataclasites. However, the orientation of cohesive and reactivated cataclasites are similar and does not indicate that specific cataclasites are more easily reactivated than others.

3.3.3 Alteration adjacent to fractures

The definition of the term alteration is in our investigation constrained to a combination of changes in colour, grain shape, grain size and chloritisation/epidotisation of plagioclase and biotite close to the fracture. The transformation of plagioclase and biotite to albite, sericite, epidote and chlorite also increases the porosity in the matrix around the fractures. The characteristics of alteration described above are all assumed to be an effect of the fractures being exposed to hydrothermal fluids sometime during the Proterozoic (2500–570 Myrs) and indicates previous conductive structures. Sections with highly altered host rock contain fractures with a predominant NW strike and steep dip, c.f. Figure 3-3. Approximately 1/3 of the altered structure coincide with mylonites. The proportion of altered sections with open fractures is higher than sections without, indicating that brittle reactivation tends to occur in previously altered rock.

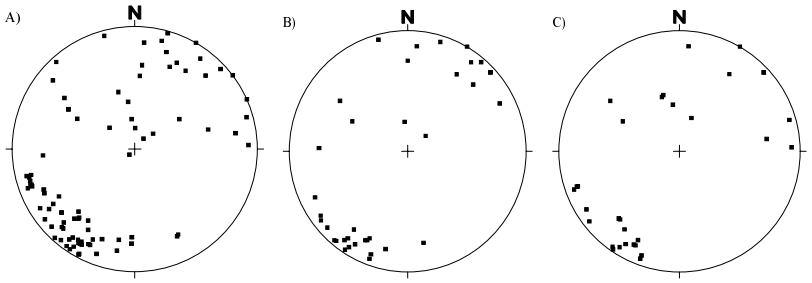

Figure 3-3. *Stereo plots of poles of fracture planes in sections showing A) high ductile deformation, B) cataclastic deformation and C) alteration (lower hemisphere projection).*

3.4 Fracture mineralogy

The dominant fracture filling minerals are chlorite (38%), calcite and chlorite (32%), calcite (12%), epidote and/or chlorite and calcite (7%) and other combinations, together with or without quartz, Fe-oxyhydroxide and other accessories (11%).

The longest fractures are often filled with quartz, epidote and/or mylonite and often show evidence of having been reactivated during faulting to form gouge or breccia. These fractures were later filled with calcite and Fe-oxyhydroxides as a result of the

circulation of water. The shortest fractures are filled with chlorite, calcite or a combination of both.

Fault gouge sometimes occurs in faults and fracture zones, often with multiple deformation phases (ductile-cataclasis-alteration etc). Thin section analyses of fault gouge show a mixed content with fragments of quartz, feldspar, plagioclase, chlorite and a component of mixed layer clays with a high proportion of illite. Secondary growth of calcite and pyrite is also common.

3.5 Fracturing

Fractures in the TRUE-1 volume have been mapped both in cores and from TV images of the borehole wall (BIPS). The latter method gives an image that is largely free of engineered fractures, commonly observed in the core material, and sometimes difficult to distinguish from the natural ones. It is also possible to visually observe fractures that have an appreciable aperture, i.e. fractures that are potentially very conductive. In total 1481 fractures where mapped in the TRUE-1 boreholes. At least 220 of those fractures where interpreted to be open based on BIPS images. With a total mapped borehole length of 171.9 m, this yields an estimate of the conductive fracture frequency of 1.3 fractures/m.

Below follows a summary of fracture characteristics observed in the investigated TRUE-1 rock volume.

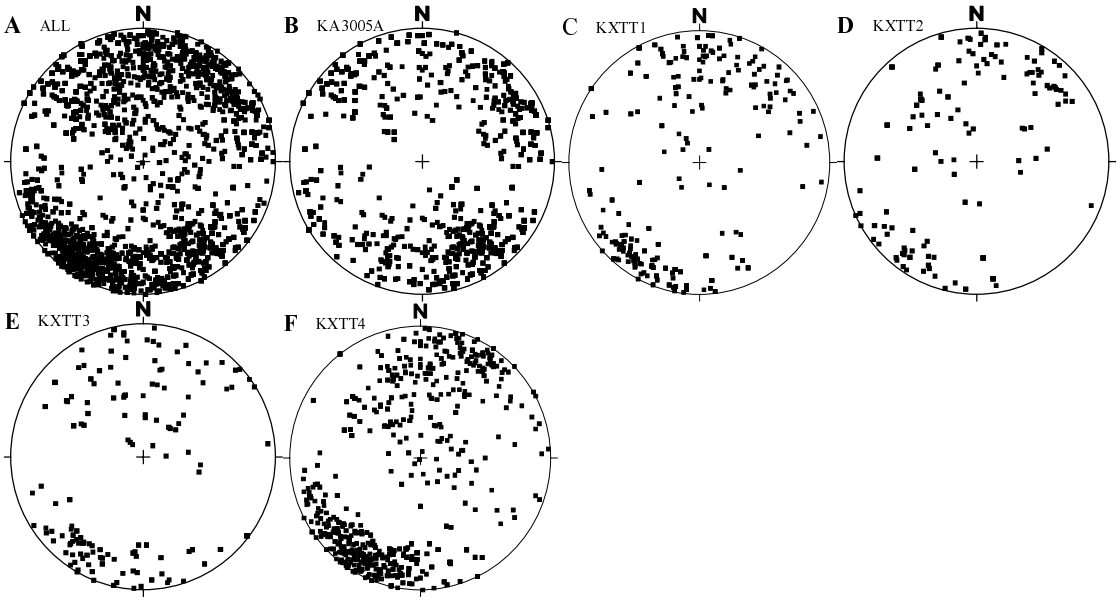

Figure 3-4. *Stereo plots of poles of fracture planes sampling the TRUE-1 rock volume.*

3.5.1 Orientation

The TRUE-1 volume is dominated by steeply dipping NW trending fractures. There also is a weak N-S fracture set. However, the often observed subhorizontal fracture set is virtually non-existent, c.f. Figure 3-4. The apparent difference in fracture orientations in KA3005A compared to the other boreholes is attributed to the different orientation of this borehole, cf. Table 1-1, Figures 3-4 and 3-5.

Fracture orientations, when plotted for defined regions of the investigated volume, show similar trends in the different KXTT-boreholes, although zone NW-2 appears to influence the inner part of borehole KXTT4, cf. Figure 3-5.

Open fractures tend to be more clustered towards the NW than sealed fractures which form a N-S to NE-SW set. It should be noted that the measured direction of maximum horizontal stress in the vicinity of the area is trending NW, cf. Section 2.2.3, and may well explain that open fractures are more commonly subparallel to this direction.

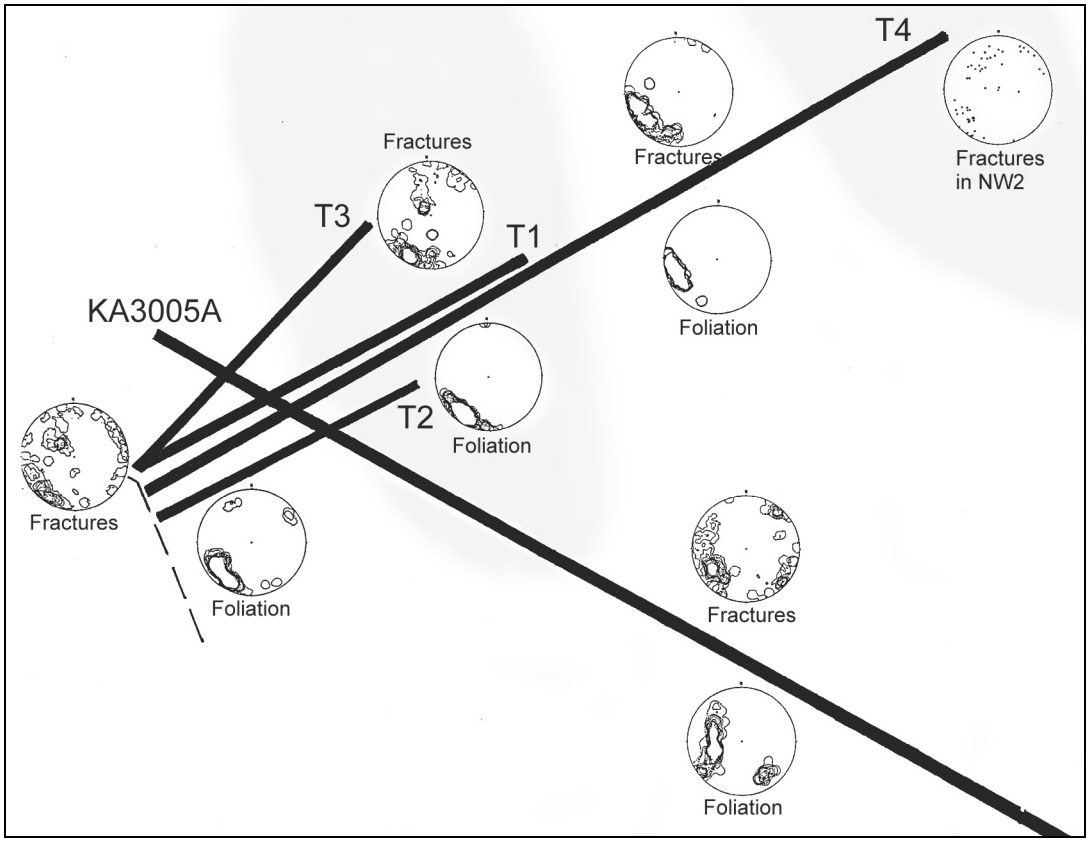

Figure 3-5. *Orientation of fractures and foliation in different regions of the TRUE-1 rock volume, cf. Figures 4-2 and 4-3. The orientation of fractures and foliation is generally constant throughout the volume. The apparent difference in orientation and foliation in KA3005A is due to its very different orientation compared to the other boreholes. No correction made for orientation bias.*

However, relating sections of high groundwater inflow in all boreholes with the structural properties discussed above reveal a positive correlation to fractures in sections with a high degree of alteration (Bossart et al., in prep.). This implies that conductive fractures are not only controlled by stress but do show signs of a previous history of circulation of hydrothermal fluids.

3.5.2 Size

Fracture size has been estimated by Dershowitz et al (1996) from data of water-bearing fractures from tunnel legs E–F (2/207–3/384 m), F–G (3/384–3/527 m), and G–H (2/527–2/722 m). The analysed data only include fractures identified as conductive and exclude data in identified fracture zones. LaPointe et al. (1995) evaluated these trace lengths to derive a fracture size (effective radius) distribution. Based upon the LaPointe et al. analysis, the effective radius of conductive fractures can be described by a lognormal distribution with mean radius varying between 6 and 14 metres, and a standard deviation between 2 and 13 metres. It should also be noted that traces shorter than 1 m were not mapped in the standard mapping campaigns performed by the site geologists at Äspö.

A detailed fracture size analysis of trace data was performed on the tunnel wall map of the tunnel section next to the TRUE-1 site as presented in Winberg (1996). This investigation focused on all visible fractures rather than only water-bearing fractures. Traces shorter than 0.2 m have not been mapped on the tunnel wall according to Mazurek & Bossart (pers. comm.). The effective radius of fractures in the mapped population can be described by either a lognormal or power law distribution with a mean size of approximately 0.5 m.

Two different size estimates thus exist, where the larger estimate reflects conductive faults most often intersecting the whole tunnel perimeter, and the smaller population reflects the network visible on a detailed scale on the tunnel wall, not necessarily conductive.

3.5.3 Intensity

The fracture frequency of the TRUE-1 volume was calculated using two different approaches; one based on conductive fractures mapped in the boreholes and the other from observable fractures on the tunnel wall.

Winberg (1996) presents a conductive fracture frequency per unit length, P_{10c}, of 1.55 m^{-1} based on both Oxfilet analyses (Dershowitz et al., 1995, Osnes et al., 1988) and geologically identified conductive fractures in the boreholes.

Fracture trace length per unit area, P_{21}, has been calculated from the detailed map of the TRUE-1 tunnel section where $P_{21} = 1.17$ m/m^2.

The relationship between P_{21} and P_{10} depends on the orientation distribution of the features relative to the line along which P_{10} is estimated, as well as on the orientation of the plane on which P_{21} is evaluated (Dershowitz and Herda, 1992). Rather than using the measures P_{10} or P_{21}, fracture intensity is best described by P_{32}, i.e. a measure of fracture area per unit volume of rock, which is invariant to the distributions of fracture size and orientation. P_{32} can be derived from either P_{10} or P_{21} through simulated sampling of a network model such that

$$P_{32}=P_{32,sim}(P_{10,obs}/P_{10,sim}) \quad \text{or} \quad P_{32}=P_{32,sim}(P_{21,obs}/P_{21,sim}) \tag{3-1}$$

By using simulated sampling, the equivalent P_{10} of a borehole parallel to the tunnel wall map is estimated to 0.8 m^{-1}. This frequency is less than the frequency of open fractures observed by Bossart et al (in prep.) in the TRUE-1 boreholes, $P_{10} = 1.28$ m^{-1}. The reasons for this difference may be many, for example engineered fractures in the borehole data, change of rock quality close to the tunnel, redistribution of stress around the tunnel or different mapping techniques. With regards to the conductive fracture intensity in the TRUE-1 block, inflow is only recorded in the boreholes and the intensity has to be derived from borehole data.

The conductive fracture frequency reported by Bossart et al (in prep.) is equivalent to a conductive fracture intensity $P_{32c} = 3.11$ m^{-1}. Winberg (1996) reports a $P_{10c}=1.55$ m^{-1} based on flow log analysis and identified conductive structures. This value corresponds to $P_{32c}=3.17$ m^{-1}. The difference between the two estimates of P_{32} is less than 3%.

3.5.4 Location

The location of fractures intersecting the KXTT-borehole array can be established deterministically based on the drill cores and the BIPS borehole TV logs. However, the location of fractures within the TRUE-1 Block which do not intersect the TRUE-1 boreholes can only be derived statistically. The location of fractures within the TRUE-1 Block was estimated by a variety of increasingly sophisticated approaches where the primary assumption was a Poisson distributed fracture population. The model for location of fractures in the network was improved in a stepwise manner through conditioning to match the observed conductive fracture intersections in the TRUE-1 boreholes as reported by Winberg (1996).

3.6 Summary of main results

The geological characterisation of the TRUE-1 rock volume provides a wide spectrum of information which in parts will form the basis of the establishment of the conceptual structural model, but can also be directly used as input to stochastic numerical models. Tables 3-2 and 3-3 summarise the results described in previous sections regarding the geological and structural properties of the investigated rock.

Table 3-4 summarises the fracture network parameters for both the conductive fractures as observed in the TRUE-1 cores as well as for the network as observed on the tunnel wall next to the site.

Table 3-2. Summary of the geological characteristics of the TRUE-1 rock block related to orientation of fractures and fabric of the rock.

Parameter	Orientation	Character
Open fractures	Dominating NW orientation	Fairly homogeneous clustering. Steep inclination
Tight fractures	NW-SE, N-S and NE-SW fracture sets. Dominating NW orientation	Wider spread in the fracture orientation compared to open fractures. Three identifiable sets.
Rock types	No preferred orientation of rock contacts with FGG	There is no difference in orientation between open and tight fractures in different rock types.
Ductile deformation	Follows the prevailing NW orientation of the fracturing	Orientation of open fractures do not differ from that of sealed fractures. The proportion of open fractures is higher in sections with a high degree of ductile deformation.
Cataclastic deformation	Follows the NW trend of dominating fracturing	Often reactivates sections of highly deformed ductile structures. Approx. 1/3 of the cataclastic sections have ductile precursors. Open fracture orientations do not differ from tight fractures. The proportion of open fractures is higher in sections with a high degree of cataclastic deformation.
Alteration	Occurs in NW-SE, N-S and in NE-SW directions. Dominating NW trend	Approx. 1/3 of the highly altered sections have ductile precursors. Open fracture orientations do not differ from tight fractures. The proportion of open fractures is higher in highly altered sections.

Parameter	Orientation	Character
Foliation	NW trending foliation in KXTT1–T4	Orientation of foliation tends to change towards NW in the western part of the TRUE-1 block. Influence from larger zones NW-2 and its off springs (eg. NW2').
Inflow	NW trending fractures with a high degree of alteration in sections of increased flow ($\Delta Q >$ 2.4 l/min).	The maximum inflows occur for the most part through fractures that have undergone a previous history of hydrothermal events, i.e. sections with a high degree of alteration tend to be the most conductive sections .

Table 3-3. Summary of correlation of geological characteristics to fracture frequency and flow in the rock.

Parameter	Fracture frequency	Character
Open fractures	Varies between 1.3 to 2 m^{-1} in the KXTT-boreholes. In KA3005A it is equal to 0.3 m^{-1}.	Variable between boreholes. Highest frequency in KXTT4 which intercepts NW-2 or some of its offspring's. KA3005A is drilled in a different orientation in an apparently "dry" part of the rock domain.
Sealed fractures	Varies between 6.5 to 10.5 m^{-1}	Highest frequency in KXTT4 Lowest frequency in KXTT1 and KXTT2.
Rock types	No correlation	No apparent difference in fracture frequency between rock types
Ductile deformation	No correlation	Coupled to cataclasis and alteration
Cataclastic deformation	No correlation	Coupled to ductile deformation and alteration
Alteration	Positive correlation	Coupled to ductile deformation and cataclasis
Inflow	Weakly correlated to open fractures in KXTT1–T3.	No coupling to geological deformation or rock type

Table 3-4. Summary of the fracture network parameters partly derived by Dershowitz et al (1996) and reported by Winberg (1996).

Parameter	Conductive fracture network as described in Winberg (1996)		Geometric fracture network based on the tunnel wall trace map reported by Winberg (1996)
Location model	Baecher Model	from Winberg et al (1996) trace map	
Orientation distribution	Bootstrap	from BIPS measurements in KXTT1–4 and KA3005A	
Size distribution	Lognormal, Mean = 6 m and Std Dev = 2 m	from 890 conductive fractures in the Äspö HRL	Lognormal, Mean = 0.5 m, Std Dev = 0.5
Fracture intensity	$P_{32c} = 2.45\ m^{-1}$ $T_{min} = 5x10^{-9}\ m^2/s$	Oxfilet analysis of flow logs and from geological mapping	$P_{32} = 2.1\ m^{-1}$

4 Structural model

4.1 Introduction

A three-dimensional structural-geological model of the TRUE-1 Block has been constructed. In this process the intercepts of various structures have been visualised and interpolated. The Äspö local grid system has been used throughout the building of the model. The model contains both site scale fracture zones, an intermediate group of structures, and the minor deterministic structures. Specifically, the target structure for the tracer experiments, is described and visualised in detail.

4.2 Bounding deterministic fracture zones

The TRUE-1 site is bounded by a group if site scale structures; NW-2, NNW-4 and a third zone, NW-3, located west of NNW-4, c.f. Figure 4-2. An offspring to NW-2, denoted NW-2', is interpreted to intersect the eastern part of the experimental volume. Despite its weak structural characteristics, the observed hydraulic connectivity sustain the interpretation of this zone, which falls in a mid category between fracture zones identified on a site scale and the minor deterministic features identified within the studied block.

Table 4-1 presents the main geometrical properties of these fracture zones. The bounding zones influence the local fracture orientation distribution such that there is a higher proportion of more NNW trending fractures close to zone NNW-4. However, the preferential orientation of water bearing fractures seems to be fairly constant due NW, which is also the orientation of the principal horizontal stress.

Table 4-1. Characteristics of bounding fracture zones in the tunnel section 2/900–3/005 m and associated boreholes (after Winberg 1996).

Zone	Intercept/-s	Orientation	Width at intercept	Remarks
NNW-4	Tunnel	355/90	5 m	No flow
NW-2	KA3010A	130/77	10 m	Flow
NW-2'	KXTT1,T2&T4	306/89	5 m	Flow
NW-3	Tunnel,bh	300/75–90	10 m	Flow

4.3 Deterministic structural modelling

The multiphase deformation history of the TRUE-1 block shows a consistent pattern of reactivated ductile precursors which are interpreted to be associated with most of the hydraulic pathways in the investigated block. Connectivity is accomplished partly by related discontinuities, such as splay fractures, interconnecting the major faults. Multiphase deformation structures in the experimental volume are shown in Figure 4-1 and illustrates the locations which are considered most likely to be involved in establishing hydraulic connectivity within the studied rock volume.

Conductive features have been identified and correlated between boreholes by means of observations of inflow during drilling and associated hydraulic pressure responses, detailed single packer flow logging, and cross-hole interference tests. If there exist several possible fractures in packed off sections, structures with similar geological character are preferentially selected and extrapolated between the boreholes to form a 3D structural geological model only containing features of primary experimental interest.

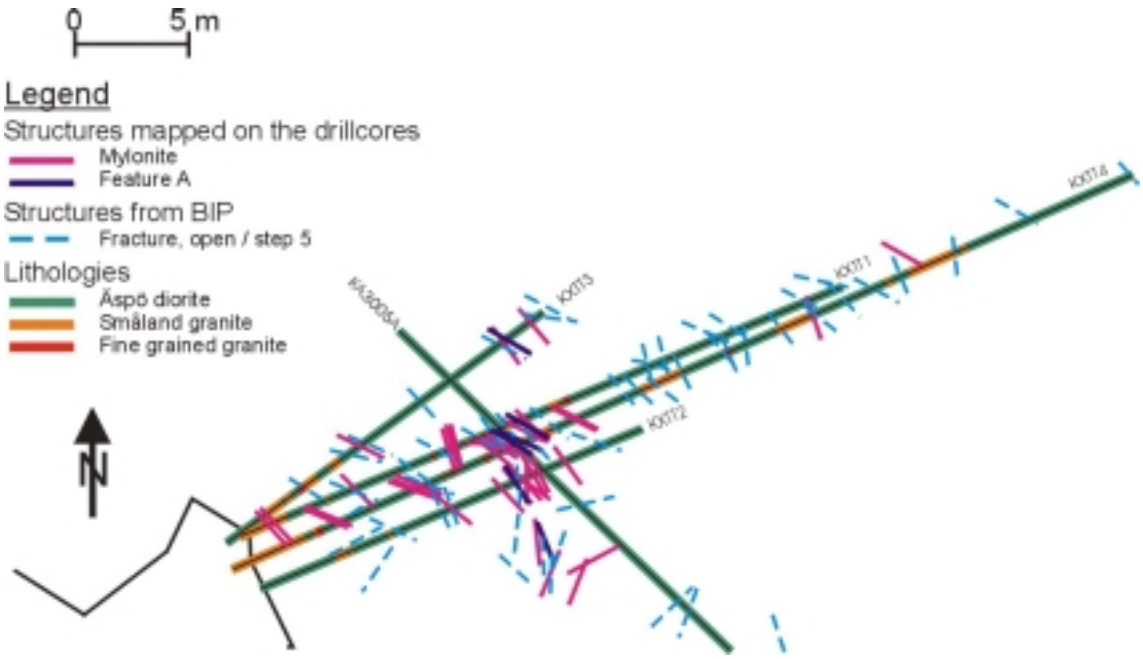

Figure 4-1. *The location of mylonites (red) and every fifth recorded brittle (open) fracture (hatched blue) in the TRUE-1 boreholes (after Bossart et al., in prep.). The 2D section is oriented parallel to the KXTT- boreholes at an orientation of 060/40 and the coloured lines illustrate the location where the structures intersect this plane, extrapolated from their respective intercept in the boreholes . Note that the mapping here is based solely on BIPS imaging, whereas the lithology presented in Figure 3-2 is based on a detailed mapping of the core.*

The connected features do not necessarily constitute ideal planar structures. Tectonic structures in the 1.8 Ga old bedrock have undergone several deformations, including brecciation, mineralisation, faulting etc. and are commonly complex with a variable width and number of connected fractures along its extension. An intercept in a borehole of one interpreted hydraulic feature can therefore involve more than one discontinuity.

The output of the analysis is a conceptual structural-geological model with possible water bearing features and bounding structures. This model is subsequently used as a basis for numerical model predictions of flow and transport in the identified features and the rock mass.

4.3.1 Identified features in the TRUE-1 volume

A purely structural interpretation of the most prominent geological features in the TRUE-1 volume has been performed by Bossart et al (in prep.). This model illustrates the geological system based on geologic data and not necessarily on conductive structures. In our work this analysis has been extended to also incorporate information on conductive fractures and results from hydraulic tests.

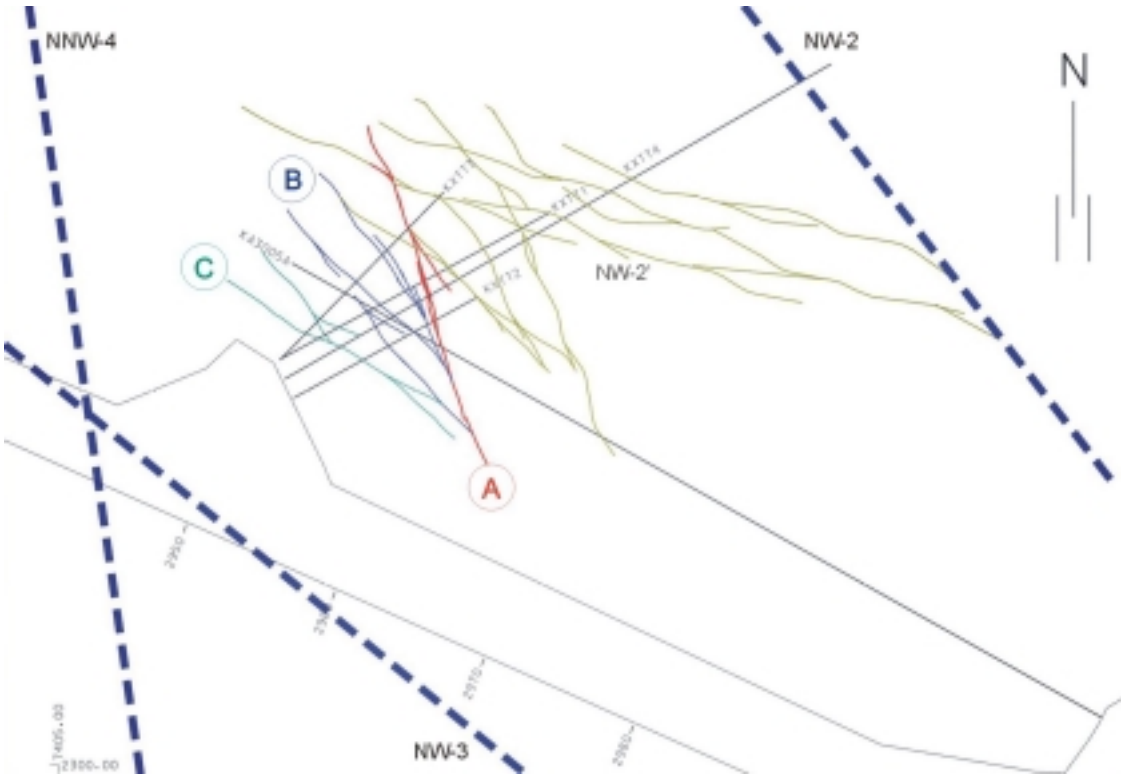

Figure 4-2. *Horizontal section at Z=–400 masl showing structural model based on identified conductive geological structures in the TRUE-1 volume. Note difference in reference planes between Figure 4-1 and Figure 4-2.*

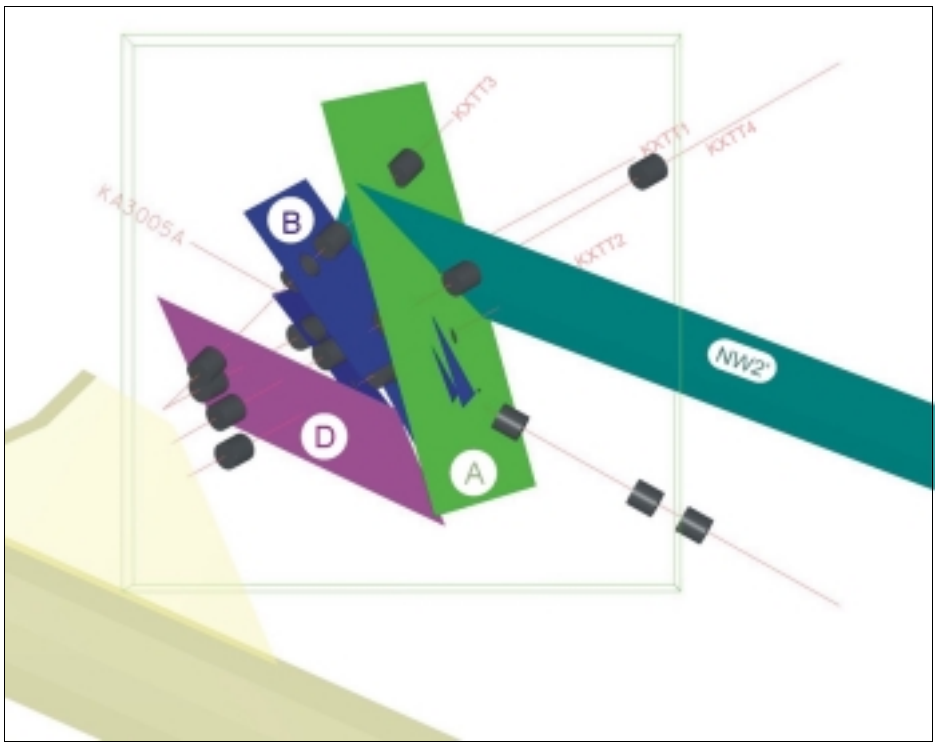

Figure 4-3. *Three-dimensional perspective view of structural model of identified conductive features in the TRUE-1 rock volume. Planes represent the simplest solution of planar extrapolation between intercepts in boreholes. Cylinders represent packer locations in the final multi-packer array.*

Five hydraulic features extending between two or more boreholes have been defined with the information from inflow during drilling, hydraulic tests and responses measured during drilling and testing. The identified features are denoted A, B, C, D and NW-2' and are illustrated in Figure 4-2 and in a simplified form in a 3D perspective view in Figure 4-3. The geological character of each feature is described in detail in the following sections.

4.3.2 Feature A

Feature A is intersected by all five boreholes sampling the TRUE-1 Block and can, for modelling reasons, be approximated by one single, steeply dipping NW trending plane, c.f. Figure 4-3. The planar structure fitted to the five interpreted borehole intercepts has an orientation of 331/79 (N29W/79E). In general the fitted plane is subparallel to the geometries at the individual intercepts, cf. Appendix A. The calculated misfit at any intercept from a five-point least-square fit plane is less than 0.07 m, implying a relatively planar fault plane within the area covered by the borehole array. However, any extrapolation beyond tens of metres is considered uncertain. The borehole intercepts are characterised by the presence of a reactivated mylonitic structure along one, or alternatively two sub-parallel fault planes. There are also indications of mylonitic structures in the tunnel between L=3/950–3/970 m with very much of the same

appearance as in the KXTT-cores. The mylonitic structures in the tunnel exhibit a large variability in dip (from 35–60°) along a given mylonitic structure. This is in distinct contrast to the well-defined steep dip (79°) inferred from within the borehole array. It has at this point been substantiated that Feature A does not intercept the tunnel. However, it cannot be ruled out that one of the mylonitic seams observed in the tunnel may be an extension of Feature A. It should be pointed out that available hydraulic information support the fact that Feature A is not in hydraulic contact with the tunnel. North of the borehole array Feature A intersects the interpreted features of the hydraulically interconnected Zone NW-2', c.f. Figure 4-2.

4.3.3 Feature B

This feature is structurally complex, consisting of minor open fractures intersected by the boreholes in the KXTT-array at lengths varying between 4 to 8 m, c.f. Figure 4-2. The complexity of the feature does not allow any planar interpolation through all intercepts. The feature is rather interpreted as being made up of a number of different planar fractures, as presented in Appendix A. Geometrically, Feature B intersects Feature A south of the borehole array.

4.3.4 Feature C

Feature C, not shown in Figure 4-3, is interpreted as a single gently dipping fracture intersecting boreholes KXTT1 and KXTT2. Since it is found only in two boreholes it is the least defined of the identified features within the TRUE-1 Block. Using the two intercepts, Feature C can be approximated by a subhorizontal fracture plane oriented 76/38 (N76E/38W), c.f. Appendix A. There are only minor findings of mineral coatings, mainly calcite and chlorite. There are a few splay fractures found in the core of KXTT2, possibly associated with this feature. The orientation of Feature C implies no intersection with any of the other boreholes in the TRUE-1 borehole array. However, this feature could potentially facilitate hydraulic connection between Features A and B.

4.3.5 Feature D

This feature is intersected by the KXTT-array at borehole lengths varying between 4 to 7 m and consists of nine interpreted fractures of widely dispersed orientations, c.f. Appendix A. The general structural expression of this feature is similar to that of Feature B, which it intersects and to which it is connected hydraulically. The mineralogical and kinematic imprint on the fractures making up Feature D is characterised by calcite and chlorite coatings with no or very little indications of fault movements. The geometry of the feature is very complex, c.f. Figure 4-2, and does not allow any planar representation and should rather be interpreted as a complex NW trending composite feature with a wide spread in both orientation and location.

Geometrical 3D modelling reveals that the feature can be regarded as being made up of a group of fractures in a complex and variable geometry dipping steeply to the NW and being oriented subparallel to the orientation of borehole KA3005A, c.f. Figure 4-3.

4.3.6 Feature NW-2'

Cross-hole interferen ce and single hole hydraulic tests have revealed a conductive zone immediately east of the interpreted Feature A which internally is well connected hydraulically, and also to the adjacent Feature A. Structural analysis of the hydraulically indicated parts of boreholes KXTT1, KXTT3 and KXTT4 shows that no singular feature can be identified which explains the noted hydraulic characteristics. Instead one primary feature observed in all three boreholes plus two features observed only in two boreholes can be identified. The geometries of the intercepts of the three features making up NW-2' are listed in Appendix A. The complex geometry of NW-2' is illustrated in Figure 4-2. The primary feature (306/89) show idiomorphic calcite crystals, whereas the other two (340/90 and 323/84) show variable characteristics. The resolution in the hydraulic measurements does not permit further refinement in identification of the structural element(-s) responsible for the hydraulic responses. All three identified features are considered to be different structures that make up the hydraulically interconnected zone denoted NW-2'. It is not possible to assign a definite width to Zone NW-2'.

4.4 Detailed description of Feature A

Feature A is intersected by all five boreholes sampling the TRUE-1 Block and has been approximated by one single fracture plane oriented NW with steep easterly dip.

Feature A is a reactivated mylonite, i.e. a ductile mylonite which has later experienced brittle deformation. The brittle reactivation is associated with one major fault plane which is also assumed to represent the water conducting part of Feature A. The main fault associated with the reactivation has not stringently followed the mylonite, resulting in lenses of wall rock contained in the feature, cf. Figures 4-4 through Figure 4-8. A few subparallel fractures, possibly splay fractures, occur associated with the main fault.

The mineralogical analyses of the five samples collected from the interpreted Feature A, support the fact that these samples belong to the same type of structure, i.e. a thin mylonite. The term mylonite is used here in a broad sense and includes epidote rich samples with a considerable reduction in grain size and veins with recrystalised quartz. However, in a few samples grains of K-feldspar remain as residues in the fine-grained matrix.

Mineralogically, the mylonites are characterised by very fine-grained epidote, quartz, K-feldspar/albite and in some cases chlorite. Calcite, fluorite, quartz and K-feldspar are found as idiomorphic crystals in voids and microfractures.

The altered wall rock (altered Äspö diorite) adjacent to the mylonite show replacement of biotite with chlorite and epidote, and plagioclase is strongly altered to "saussurite" (albite, sericite and epidote). Red staining of the wall rock is common and is probably due to minute grains of Fe(III) oxide/oxyhydroxides as a result of oxidation of magnetite originally present. The basic mineralogy of the mylonite, altered Äspö diorite and unaltered Äspö diorite (Byegård, et al., 1998), cf. Table 6-6.

Scanning Electron Microscopy (SEM) combined with Energy Dispersive Spectroscopy (EDS) were applied for identification of minute grains of zeolite/feldspar and are reported in Winberg (1996). The analysis show that only K-feldspar was found and no zeolites are indicated in Feature A. The planes of the major fault are coated with calcite and chlorite. In addition, SEM/EDS analyses reveal the presence of clay minerals as an outer rim of the coating which indicates presence of fault gouge in Feature A, which possibly has been flushed away during the drilling process. It should be noted that analyses of gouge material from other structures, e.g. within the TRUE Block Scale Project, indicate that the gouge material partly is made up of mm-cm sized irregular specimens of the altered wall rock.

Winberg (1996) also reports that analyses of $\delta^{18}O$ and $\delta^{13}C$ of calcites from Feature A indicate presence of at least two generations of calcite. One of these generations is possibly recent and seems to be related to biogenic activity resulting in bicarbonate with low $\delta^{13}C$-values. This production may either be *in situ* or due to influx of biogenic bicarbonate into the fracture.

The thickness of Feature A (including the mylonite and the ductile deformation zone) as inferred from core inspection and inspection of detailed BIPS borehole TV images is varying between 0.05m (KXTT2) and 0.09m (KXTT3). The geometry inferred from the five borehole intercepts and the geological synthesis indicate that Feature A may be either undulating on a larger scale or is made up of several interconnected fractures as illustrated in Figure 4-2. The physical aperture of the fracture itself is variable and is, on the basis of the available intercepts, estimated to be in the order of 1–3 mm.

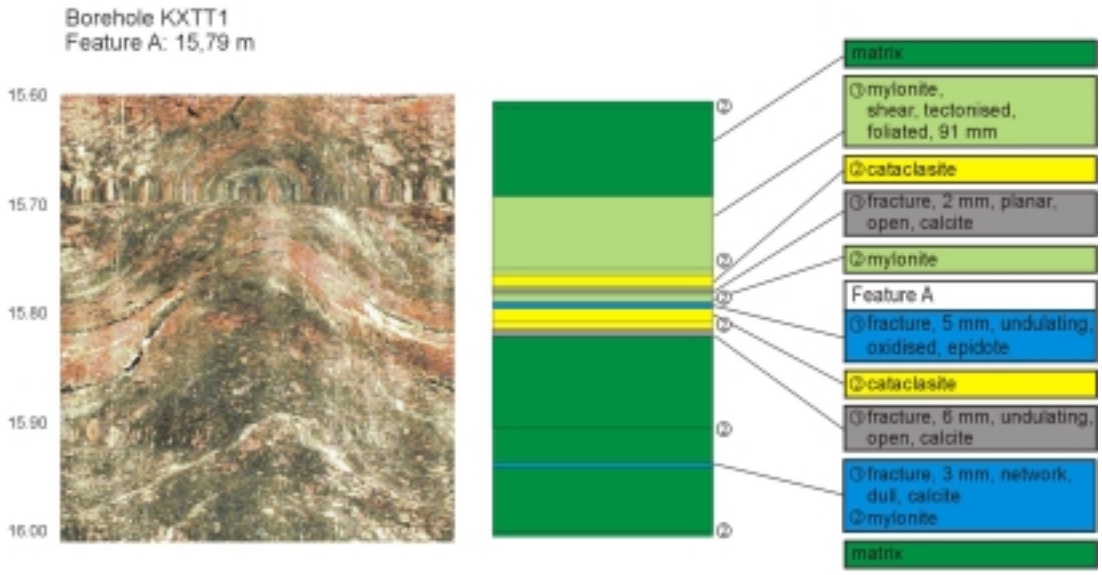

Figure 4-4. *Detailed description of Feature A in borehole KXTT1 (partly after Möri and Bossart, 1997).*

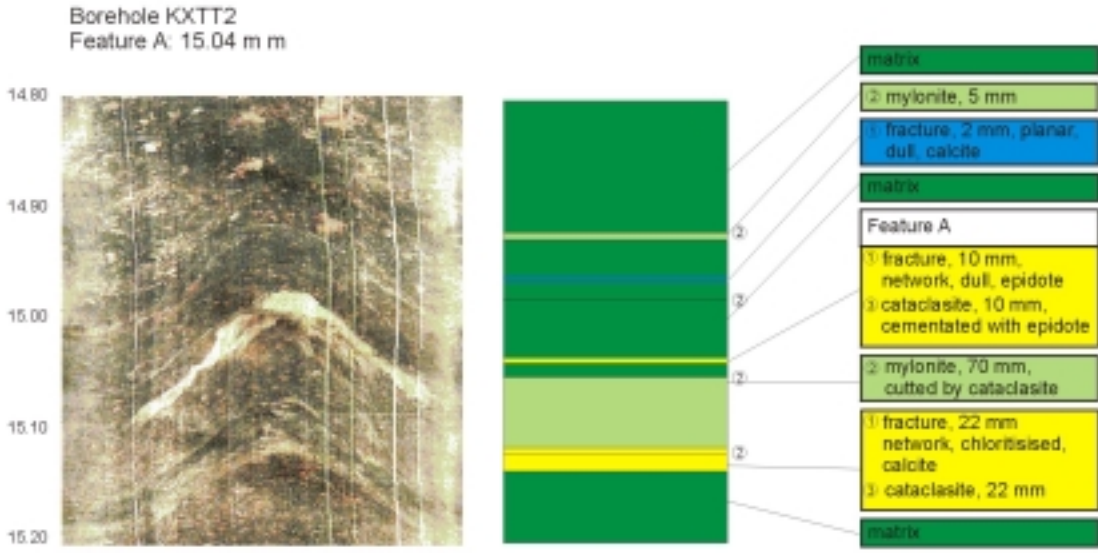

Figure 4-5. *Detailed description of Feature A in borehole KXTT2 (partly after Möri and Bossart, 1997).*

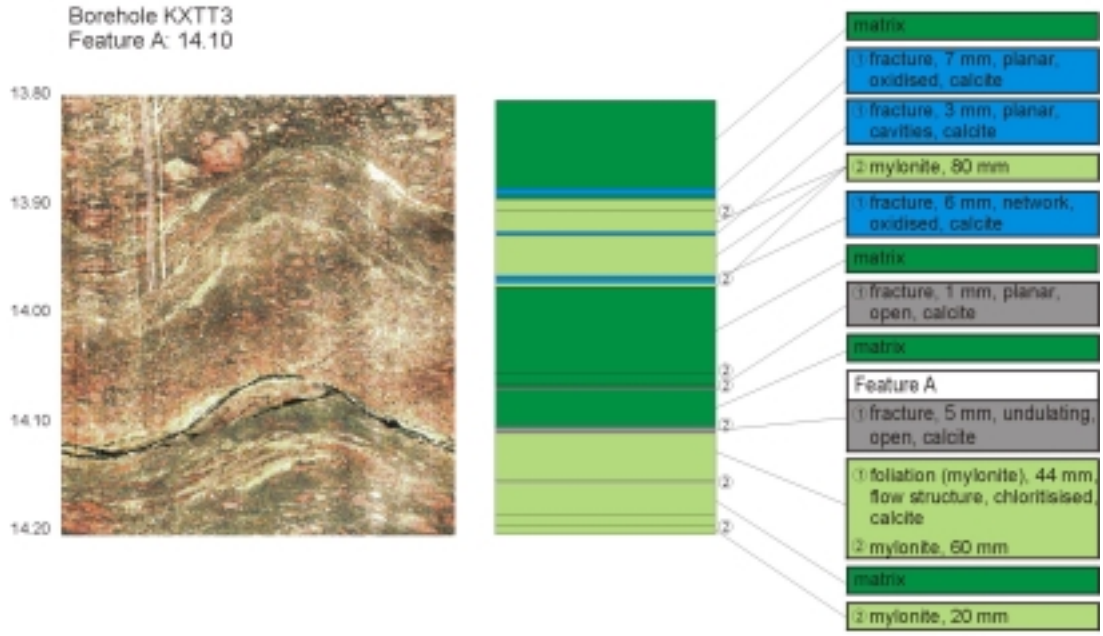

Figure 4-6. *Detailed description of Feature A in borehole KXTT3 (partly after Möri and Bossart, 1997).*

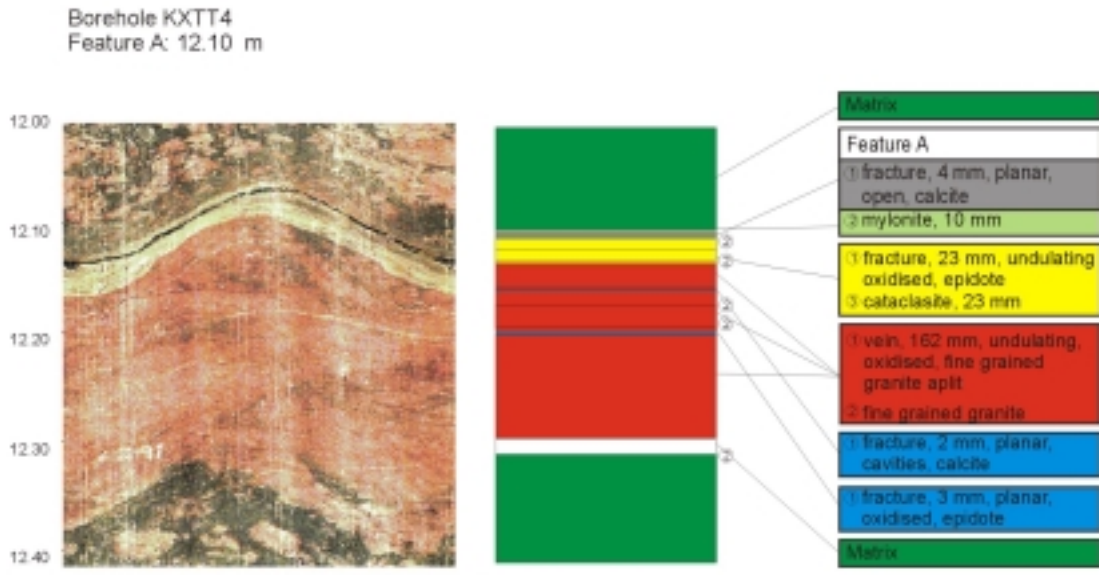

Figure 4-7. *Detailed description of Feature A in borehole KXTT4 (partly after Möri and Bossart, 1997).*

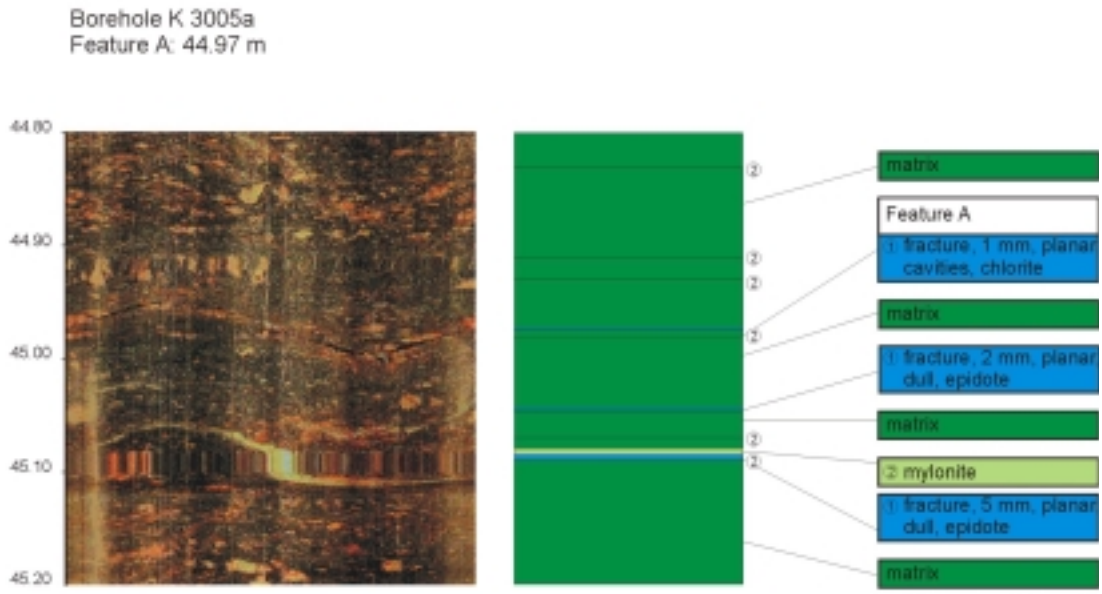

Figure 4-8. *Detailed description of Feature A in borehole KA3005A (partly after Möri and Bossart, 1997).*

5 Results of hydraulic characterisation

5.1 Introduction

This chapter presents the results of the hydraulic characterisation performed in the TRUE-1 block and in the identified target structure. The basic results of the hydraulic characterisation is presented in Winberg (1996). The hydraulic investigations have been conducted with two different focuses which have shifted with time during the experimental work. The initial work had a relatively wide focus, primarily directed towards identifying conductive structures, assessing their connectivity within the studied block, quantifying the transmissivity of the structures, and finally to provide the basis for selecting a target structure in the investigated rock volume. The second focus was more on the identified target structure and its interaction with its immediate surroundings.

The techniques used for the initial investigation of the block included recording of the observed inflows and pressure responses observed during the drilling. The specific hydraulic tests include flow and pressure build up tests, high resolution single packer flow logging and cross-hole interference tests. In addition continuous measurements of hydraulic pressure have been made in the borehole sections which are connected to the Äspö HRL Hydro Monitoring System (HMS) (Almén and Stenberg, in prep). Furthermore, tracer dilution tests have been conducted in selected sections in the array in order to quantify natural groundwater flow, and any imposed changes over the duration of the experiment.

The tracer tests performed in the identified target structure, have as their main objective to collect information on the transport characteristics and information of transport connectivity of the studied feature, cf. Chapter 7. Moreover, the tracer tests also imply collection of cross-hole interference data as a result of the pumpings made.

5.2 Identified points of inflow

Fractures which carry water were identified in a tentative way during the drilling of the boreholes. The careful measurements of the inflow between uptakes allows identification of conductive sections with a resolution of approximately three metres, which corresponds to the length of the used core barrel. The accuracy of the measurements, which are made using graded plastic vessels, is about ± 5% (0.1 l/min). In the case of the characterisation at the TRUE-1 block the best way to identify and quantify conductive fractures is the single packer flow logging technique, cf. Section 1.8. These measurements were made with a spatial resolution of 0.5 m. The results

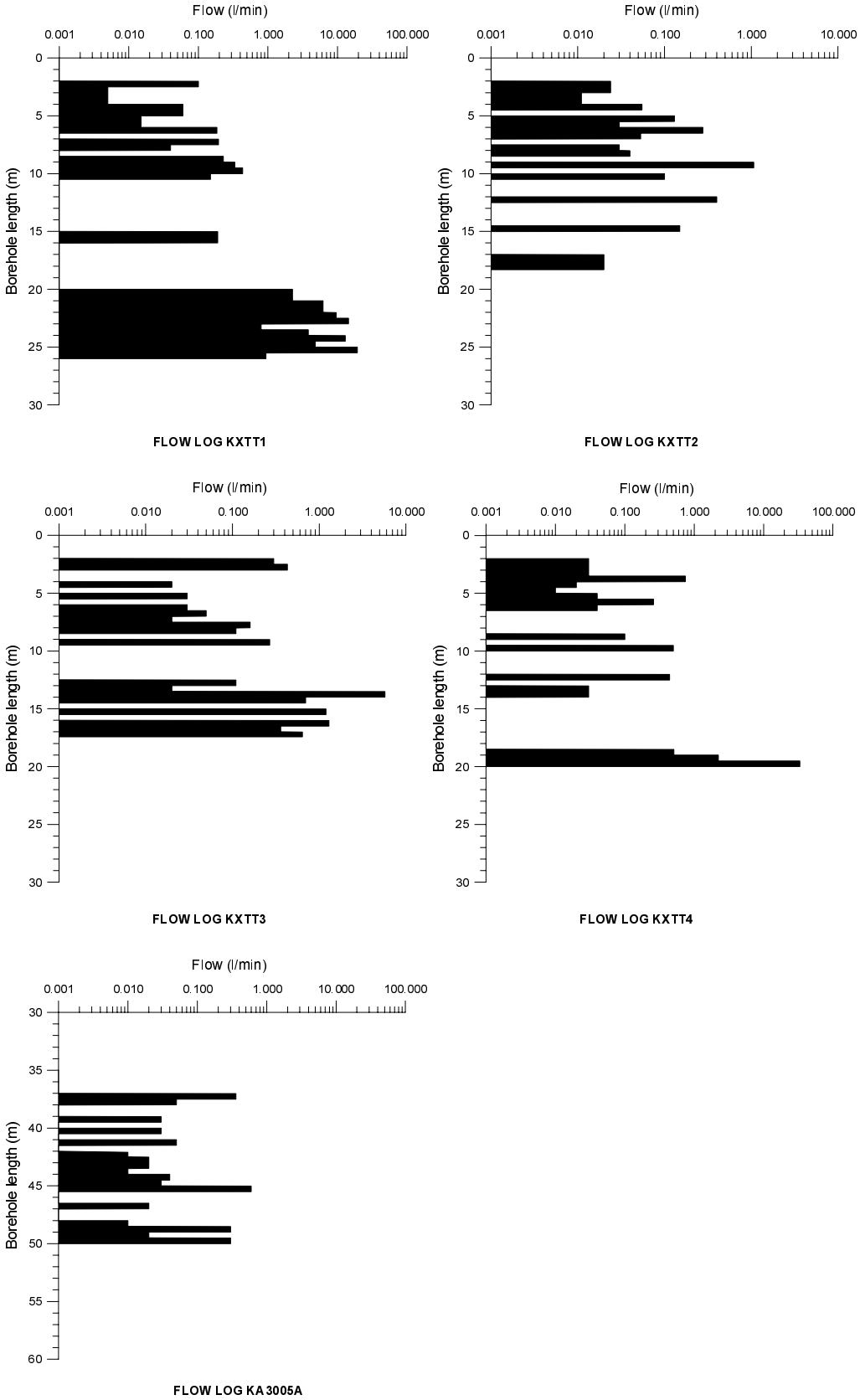

Figure 5-1*. Results of single packer flow logging with 0.5–1 m section length in boreholes KXTT1 through KXTT4 and KA3005A, cf. Winberg (1996). Truncated logs excluding long measurement sections in the bottom of KXTT1, KXTT4 and KA3005A.*

the flow logging are presented in Figure 5-1. Obvious from the figure is a general pattern in boreholes KXTT1 through KXTT4, where three to four distinct anomalies are located between 10–20 m. The minimum detectable flow difference is about 0.01 l/min.

5.3 Connectivity

The hydraulic connectivity, as obtained from pressure responses in instrumented boreholes during drilling supplied the first set of data by which a tentative hydraulic model of the TRUE-1 block was constructed. Assuming that the investigated block is intersected by planar structures, and that the general structural model of Äspö HRL is applicable it was possible to also construct tentative structural models after completion of each borehole, independent of the ongoing structural modelling. This stepwise initial updating of a naive structural-hydraulic model was very important for the successive positioning and orientation of the sequence of boreholes KXTT2 through KXTT4. These data and the results of the single packer flow logging, cf. Section 5.6.1., and the results of the flow and pressure build-up tests, cf. Section 5.6.2, and the results of the core logging and BIPS, cf. Chapter 3, were used to position the multi-packer systems in the boreholes, cf. Appendix B.

However the main body of information about connectivity within the block resulted from the cross-hole interference test programme which was performed in the instrumented array. The objectives of these tests were to assess connectivity within identified structures, between different structures, and also to assess the sensitivity to disturbance from activities elsewhere in the laboratory. In total, 14 tests were performed where the tested sections were allowed to flow between 30 to 319 minutes, and flows varied between 0.14 to 52.2 l/min, cf. Table 5-1. Pressure responses were recorded by the HMS system or by using portable data loggers.

5.3.1 Response matrices

In order to visualise the pattern of mutual connectivity the responses were compiled in a response matrix. In devising these matrices two response measures have been calculated and indexed;

I) normalised response time ratio: $t_r(s=0.1\ m)/R^2$

II) normalised drawdown ratio: $\log (s/Q)$

where

Table 5-1. Compilation of data on performed cross-hole interference tests performed in the TRUE-1 block.

Test #	Borehole	Section id code **)	Flow (l/min)*	Flow period (min)	Feature
1	KXTT1	P2	0.28	78	A
2	KXTT1	P3	1.70	248	B
3	KXTT2	P1	0.14	73	A
4	KXTT2	P3	0.95	248	B
5	KXTT2	P2	0.34	70	B
6	KXTT3	P2	4.12	319	A
7	KXTT3	P3	0.40	70	B
8	KXTT4	P2	7.30	268	NW-2’
9	KXTT4	P4	0.40	61	B
10	KA3010A	P1+P2	25.40	218	NW-2
11	KA3005A	P4	0.65	67	A?
12	KA3005A	P2	0.90	188	A
13	KXTT1	P1–P4	52.20	232	NW-2
14	KXTT4	P3	0.48	30	A

*) Flow at the end of flow period

**) The section id code is explained in Appendix B

t_r = time in minutes at which drawdown s in a given observation section is 0.1 m

s = drawdown in a given observation section due to pumping (m)

Q= measured flow from sink section at the end of the flow period (m^3/s)

R= shortest distance between mid points of sink and observation section (m)

The defined indexing is presented in Appendix C and the constructed response matrices are presented in Appendix D.

Measure I is a proportional to the inverse of diffusivity T/S, whereas the Measure II is proportional to the inverse of transmissivity T. The matrices, cf. Appendix D, show almost ubiquitous responses to tests performed in NNW-2 and NW-2' (Tests #8, #10 and #13), including sections containing Feature A. NW-2' has proven to be internally well connected , cf. Figure 5-2, which is also supported by the fact that sections containing the zone in KXTT1, KXTT3 and KXTT4 all show near identical hydraulic head. A support for hydraulic separation with respect to Zone NW-2 is given by the fact that the head in sections in KXTT4 and KA3010A, assumed to contain Zone NW-2, is significantly higher.

Tests performed in Feature A, in contrast, show preferred responses in section containing Feature A, or in some cases adjoining sections to the section containing Feature A. This reflects the relative hydraulic isolation of Feature A. Tests in Feature B show a more complex pattern with responses also in sections containing Feature D, showing the more complex nature of the latter two structures.

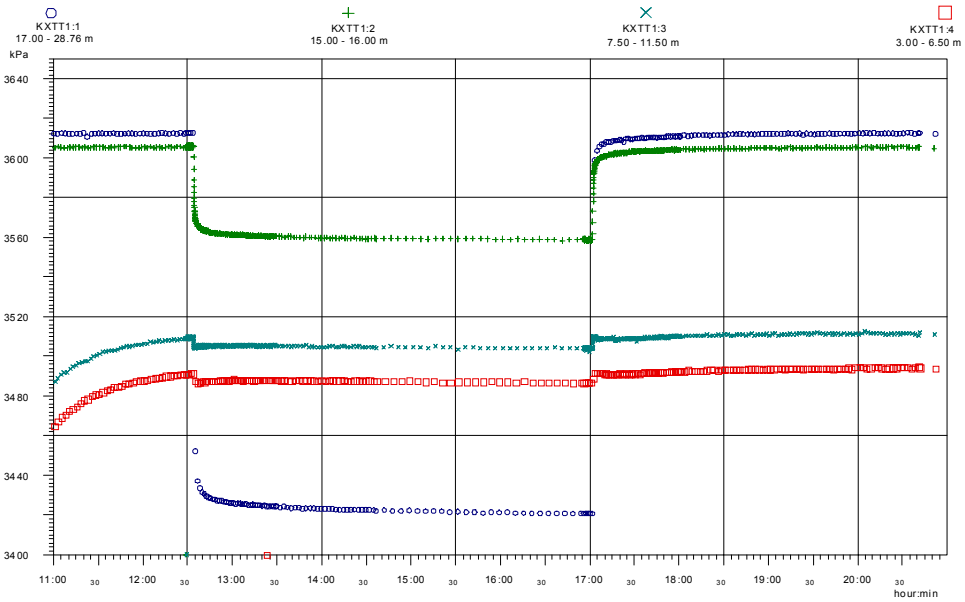

Figure 5-2. *Hydraulic responses from disturbance in KXTTT1 showing responses to interference test no. 8 with a sink in KXTT4:P2 (NW-2'). Section KXTT1:R1 (red) includes NW-2' and section KXTT1:R2 (green) includes Feature A, cf. Appendix B.*

5.4 Flow dimension

The flow dimension constitutes a measure on the dimensionality of the flow during a transient hydraulic test. The flow dimension can in principle vary in space and time as the test progresses, eg. a transition from early time one-dimensional pipe flow to two-dimensional (radial) flow and finally to a late time flow in a three-dimensional network of fractures.

By plotting the derivative of the pressure drawdown or recovery (in semi-log space) versus time in a log-log plot it is possible to identify the flow dimension from the slope of the pressure derivative. According to Mishra (1992), in a plot of the drawdown or pressure recovery (semi-log space) derivatives should have the slope 1-n/2 in a log-log graph for a constant flow tests in a porous medium. The following cases can be distinguished;

n=3 (spherical flow):	slope = –0.5 in log-log graph
n=2 (radial flow):	slope = 0
n=1 (linear flow):	slope = 0.5
n=0 (wellbore storage)	slope = 1

The analysis of the performed cross-hole interference tests (Winberg, 1996) indicates initial signs of wellbore storage. Later time data generally indicate pseudo-spherical (leaky) flow, indicated by the negative slope in the derivative plots. Very few sections show portions of the curves with a constant derivative, indicative of radial flow. This is also true for positive slopes.

The analysis of the single hole flow and pressure build up tests supports the above observations. Winberg (1996) presents flow dimensions from analysis using the Generalised Radial Flow model (GRF), cf. Section 5.5, with dimensions varying from 2.4 to 3, i.e. pseudo-spherical flow. The resolution in the determination of the flow dimension is estimated to be ± 0.2.

In subsequent analysis of flow and pressure build-up test data from Feature A using the interpretation code GTFM (Roberts, 1998), cf. Section 5.5, the flow dimension has, if required, been allowed to vary spatially, to obtain a better fit to the data. The resulting flow dimensions applicable to Feature A are all above 2, with values between 2.3–3.2 for KXTT1, KA3005A and KXTT2. The tests in KXTT3 and KXTT4 show flow dimensions between 3.3 and 3.9. These values are generally higher than the ones presented in Winberg (1996), cf. Table 5-2. In the case of the test in KXTT2 a variable flow dimension model including two flow dimensions; n1 and n2, was used in the analysis. The values of n1 and n2 were estimated to 2.6 and 7.6 respectively. The

uncertainty of these latter two values was also found to be high. In addition the estimate of the flow dimension is seen to be inversely correlated with the estimate of the hydraulic conductivity K.

Given that a linear constant-pressure boundary condition will result in a semi-log pressure derivative with a late time slope of –1 (i.e. n=4), a flow dimension of 4 can be explained by a constant pressure boundary at some distance from the borehole. Leaky systems can show even higher flow dimensions. A flow dimension higher than 3 can in this context be explained by a either a leaky aquifer or a constant head boundary.

Table 5-2. Comparison of flow dimension between results from GTFM analysis and GRF analysis of flow and pressure build up tests in Feature A. Evaluated transmissivities are presented in Table 5-5.

Borehole	Section (m)	Flow dimension (Winberg 1996)	Flow dimension (Roberts, 1998)
KXTT1	13–16	2.6	2.4 – 2.6
KXTT2	12.5–15.5	2.6	2
KXTT2	12.5–15.5	2.6	3.8 – 11
KXTT3	12–15	2.6	3.9
KXTT4	9.5–12.5	2.6	3.3 – 3.5
KA3005A	44.5–45.5	2	2.3 – 3.2

5.5 Flow models and evaluation

A variety of flow models have been applied in the interpretation of the hydraulic tests performed in the TRUE-1 block. They range from relatively simple approximations, made in conjunction with steady state evaluations, to more complex transient evaluations. The transient state evaluation allows use of alternative flow models. The identification of flow dimension, cf. Section 5.4, provides input to this selection. Below, the flow models applied to different types of hydraulic tests are tentatively described.

5.5.1 Single packer flow logging

On the basis of a flow measurement made for the whole hole, a steady state transmissivity for complete borehole length was estimated using the Moye's formula (Moye, 1967). This formula assumes an initial radial flow regime which at a certain distance is transformed to a spherical flow regime. This distance is assumed to be approximately half the section length. The transmissivity can be evaluated as;

$$T = (Q/\Delta h)\cdot((1+\ln L/2r_w)/2\pi) \qquad (5\text{-}1)$$

where T (m^2/s) is the transmissivity of the packed-off section, Q (m^3/s) is the mean pumping rate, r_w is the borehole radius (m), Δh is head difference (m) and L (m) is the length of the packed-off section. The evaluation is made assuming steady state.

The flow logs results in a dQ differentiated for each test section from cumulative flow measurements. By multiplying the proportion of the flow for the given section with the total transmissivity of the hole, an estimate of the transmissivity of each section is obtained at each measurement station (step=0.5 m) (Winberg, 1996).

5.5.2 Flow and pressure build-up tests

In accordance with the flow dimension analysis which shows dominating pseudo-spherical flow, the transmissivity was first estimated assuming steady state conditions and using Moye's formula, cf. Equation 5-1, applied to the flow and recovery phases of the tests.

For comparison, evaluation of the tests was also made with an approximate GRF-analysis (Generalised Radial Flow) of the flow phase using type curves developed by Doe and Geier (1991).

The tests performed in sections containing the target Feature A have later been subject to extended evaluation using the numerical well-test analysis code GTFM (Pickens et al., 1997). Estimates of fitting parameters were obtained by non-linear regression using flow-rate, pressure and pressure-derivative data from each test section (Roberts, 1998). For the most part the radial-leaky flow model has been used. The analysis provide estimates of the hydraulic conductivity, specific storage, flow dimension, wellbore storage and static formation pressure. The analysis also include address of quantification of fitting parameter uncertainty resulting from conceptual model uncertainty and correlation between fitting parameters. In addition, the problem of non-uniqueness in well-test analysis is discussed for the case when the flow geometry is unknown.

The lack of information regarding the spatial variability of hydraulic conductivity, specific storage, and flow geometry results, for a given well-test problem, in an infinite

number of solutions. In the case of the performed analysis the hydraulic conductivity and specific storage have been assumed constant.

5.5.3 Cross-hole interference tests

A leaky aquifer model was employed to evaluate the hydraulic parameters for the observation sections. This model is a simplification of the more general theory for leaky aquifer systems presented by Hantush (1967), cf. Winberg (1996). Using the flow model, the transmissivity T and storativity S of the observation section can be estimated. Furthermore, the leakage coefficient k'/b' can be estimated. The leakage coefficient in this case represents the flow occurring in an idealised leaky aquifer, over – or underlain by a confining layer through which leakage occurs from an upper (or lower) aquifer. In the case of the TRUE-1 block, the identified target feature can be said to represent the leaky aquifer, whereas the confining layer is represented by the rock in between the structures. Thus the hydraulic conductivity K' of the rock mass can in principle be estimated if the thickness b is known, or can be estimated.

In the sink sections, a very fast drawdown generally occurred, rapidly approaching almost steady-state conditions resulting in very flat drawdown curves in the log-log representation. The same pattern is also observed in some of the observation sections located close to the sink section. For these sections, the Thiem's steady state equation was used to estimate the transmissivity.

5.6 Transmissivity

Transmissivity data from different hydraulic tests performed in the TRUE-1 array and from alternative types of evaluation are presented in this section. The types of tests performed include single packer flow logging, flow and pressure build-up tests and cross-hole interference tests.

5.6.1 Single packer flow logging

Calculated transmissivities for 0.5 or 1 m sections reported by Winberg (1996) vary between no-flow up to $6.6 \cdot 10^{-7}$ m^2/s. The lowest measurable flow rates equates to a transmissivity of about $6.2 \cdot 10^{-10}$ m^2/s. Table 5-3 presents summed up transmissivities compatible with the 3 m sections tested using flow and pressure build-up tests, cf. Section 5.6.2. The summed up transmissivities range from values < 10^{-9} m^2/s to values in excess of $2.2 \cdot 10^{-6}$ m^2/s.

A comparison between summed up consecutive 0.5 and/or 1 m sections corresponding to the sections measured by flow and pressure build-up tests, show a very good correspondence, cf. Table 5-3. Generally, the transmissivity from the flow logging is on the average a factor 2.6 lower than that coming from the steady state analysis of the flow and pressure build-up tests.

5.6.2 Flow and pressure build-up tests

The transmissivities calculated using Moye's formula are presented in Table 5-3. The lower measurement limit for these tests is about $T_{lim}= 5 \cdot 10^{-10}$ m^2/s. The highest evaluated transmissivity is about $2.8 \cdot 10^{-6}$ m^2/s. A comparison with the results of the double packer flow logging is presented in Section 5.6.1.

Calculated transmissivities obtained from the GRF analysis of the sections focused on Feature A are reported in Section 5.6.4.

Table 5-3. Comparison between transmissivities evaluated from single flow logging and from flow and pressure build-up tests. Evaluation is made using the so-called Moye's formula, (from Winberg, 1996).

Borehole	Test section (m)	L (m)	T_M (m^2/s)	T_F (m^2/s)	Comments
KXTT1	2.0–4.0	2.0	–	6.1 E-9	Casing 0–2.0 m
	4.0–7.0	3.0	8.1 E-8	1.5 E-8	D
	7.0–10.0	3.0	1.5 E-7	7.2 E-8	B, D
	10.0–13.0	3.0	2.0 E-7	8.7 E-9	
	13.0–16.0	3.0	1.0 E-8	1.1 E-8	A, C
	16.0–20.0	4.0	–	< E-9	
	20.0–23.0	3.0	3.0 E-6	1.9 E-6	NW-2'
	23.0–26.0	3.0	2.0 E-6	2.5 E-6	NW-2'
	26.0–28.8	2.8	–	3.5 E-9	
KXTT2	2.0–3.5	1.5	–	2.0 E-9	Casing 0–2.0 m
	3.5–6.5	3.0	7.2 E-8	2.8 E-8	D
	6.5–9.5	3.0	8.4 E-8	6.8 E-8	B, D
	9.5–12.5	3.0	2.0 E-8	2.8 E-8	B
	12.5–15.5	3.0	1.0 E-8	8.5 E-9	A, C
	15.5–18.3	3.2	–	1.1 E-9	

Borehole	Test section (m)	L (m)	T_M (m^2/s)	T_F (m^2/s)	Comments
KXTT3	2.0–4.0	2.0	–	4.0 E-8	Casing 0–2.0 m
	4.0–7.0	3.0	5.1 E-9	7.1 E-9	Below measurement limit, test was interrupted. D
	7.0–10.0	3.0	5.9 E-8	3.1 E-8	B
	10.0–12.0	2.0	–	< E-9	
	12.0–15.0	3.0	3.3 E-7	3.6 E-7	A
	15.0–17.4	2.4	3.1 E-7	1.9 E-7	Possibly flow around packers. NW-2’
KXTT4	2.0–3.5	1.5	–	1.8 E-9	Casing 0–2.0 m
	3.5–6.5	3.0	2.1 E-7	6.9 E-8	D
	6.5–9.5	3.0	2.0 E-8	6.1 E-9	B
	9.5–12.5	3.0	6.6 E-8	5.8 E-8	A, B
	12.5–15.5	3.0	< 5 E-9?	>3.7 E-9	No flow.
	15.5–18.5	3.0	–	< E-9	
	18.5–21.5	3.0	2.8 E-6	>2.2 E-6	NW-2’
	21.5–27.5	6.0	–	2.2 E-7	NW-2’, T_F=20.5–28.5 m
	27.5–30.5	3.0	8.7 E-7	>7.6 E-7	
	30.5–33.5	3.0	1.3 E-6	1.3 E-6	
	33.5–49.8	16.3	–	5.7 E-7	NW-2
KA3005A	2.0–37.0	35.0	–	< E-9	Casing 0-2.0 m
	36.9–37.9	1.0	2.5 E-8	2.4 E-8	Main flow at 36.9-37.4m
KA3005A	37.4–43.5	6.1	–	1.4 E-8	
	43.5–44.5	1.0	5.0 E-11	3.3 E-9	
	44.5–45.5	1.0	4.2 E-8	4.2 E-8	Main flow at 45.0–45.25m. A
	45.5–46.5	1.0	6.1 E-11	< E-09	
	46.5–48.4	1.9	–	2.0 E-9	
	48.4–49.4	1.0	2.8 E-8	2.1 E-8	B
	49.4–58.1	8.7	–	2.0 E-8	

Table 5-4. TRUE-1 Interference tests. Calculated hydraulic parameters for the source sections and observations sections containing Feature A (Tests #1, #3, #6, #12 and #14). Evaluation for observation sections made assuming flow in a leaky aquifer (from Winberg, 1996) (S=sink section).

Test#	Section	T (m^2/s)	S	K'/b' (s^{-1})	T_F (m^2/s)
1	KXTT1:P2 (S)	$1.3\cdot10^{-8}$	–	–	$1.2\cdot10^{-8}$
	KXTT2:P1	$5.8\cdot10^{-7}$	$5.9\cdot10^{-6}$	$3.2\cdot10^{-8}$	$9.7\cdot10^{-9}$
	KXTT3:P2	$3.4\cdot10^{-7}$	$2.0\cdot10^{-7}$	$1.1\cdot10^{-8}$	$3.6\cdot10^{-7}$
	KXTT4:P3	$1.3\cdot10^{-6}$	$1.6\cdot10^{-6}$	$5.6\cdot10^{-8}$	$3.1\cdot10^{-8}$
	KA3005A:P2	$6.2\cdot10^{-6}$	$1.4\cdot10^{-5}$	$8.1\cdot10^{-9}$	$5.0\cdot10^{-8}$
3	KXTT1:P2	$1.5\cdot10^{-6}$	$7.0\cdot10^{-6}$	$9.0\cdot10^{-9}$	$1.2\cdot10^{-8}$
	KXTT2:P1 (S)	$6.6\cdot10^{-9}$	–	–	$9.7\cdot10^{-9}$
	KXTT3:P2	$2.7\cdot10^{-7}$	$3.8\cdot10^{-7}$	$1.7\cdot10^{-9}$	$3.6\cdot10^{-7}$
	KXTT4:P3	$6.8\cdot10^{-7}$	$6.8\cdot10^{-7}$	$3.5\cdot10^{-9}$	$3.1\cdot10^{-8}$
	KA3005A:P2	$2.3A10^{-7}$	$4.8\cdot10^{-6}$	$3.4\cdot10^{-9}$	$5.0\cdot10^{-8}$
6	KXTT1:P2	$4.5\cdot10^{-7}$	$5.7\cdot10^{-8}$	$3.7\cdot10^{-9}$	$1.2\cdot10^{-8}$
	KXTT2:P1	$6.4\cdot10^{-8}$	$9.6\cdot10^{-8}$	$4.0\cdot10^{-10}$	$9.7\cdot10^{-9}$
	KXTT3:P2 (S)	$3.4\cdot10^{-7}$	–	–	$3.6\cdot10^{-7}$
	KXTT4:P3	$1.1\cdot10^{-7}$	$2.1\cdot10^{-7}$	$6.3\cdot10^{-10}$	$3.1\cdot10^{-8}$
	KA3005A:P2	$1.6\cdot10^{-6}$	$3.6\cdot10^{-6}$	$1.6\cdot10^{-9}$	$5.0\cdot10^{-8}$
12	KXTT1:P2	$4.4\cdot10^{-6}$	$2.4\cdot10^{-5}$	$1.3\cdot10^{-8}$	$1.2\cdot10^{-8}$
	KXTT2:P1	$9.9\cdot10^{-8}$	$2.9\cdot10^{-6}$	$2.3\cdot10^{-9}$	$9.7\cdot10^{-9}$
	KXTT3:P2	$2.0\cdot10^{-6}$	$5.5\cdot10^{-6}$	$3.4\cdot10^{-9}$	$3.6\cdot10^{-7}$
	KXTT4:P3	$2.6\cdot10^{-6}$	$1.3\cdot10^{-5}$	$9.4\cdot10^{-9}$	$3.1\cdot10^{-8}$
	KA3005A:P2 (S)	$4.8\cdot10^{-8}$	–	–	$5.0\cdot10^{-8}$
14	KXTT1:P2	$5.7\cdot10^{-6}$	$1.3\cdot10^{-6}$	$9.9\cdot10^{-9}$	$1.2\cdot10^{-8}$
	KXTT2:P1	$1.9\cdot10^{-6}$	$8.0\cdot10^{-7}$	$1.3\cdot10^{-9}$	$9.7\cdot10^{-9}$
	KXTT3:P2	$3.3\cdot10^{-6}$	$1.4\cdot10^{-6}$	$8.6\cdot10^{-9}$	$3.6\cdot10^{-7}$
	KXTT4:P3 (S)	$2.2\cdot10^{-8}$	–	–	$3.1\cdot10^{-8}$
	KA3005A:P2	$4.5\cdot10^{-7}$	$2.3\cdot10^{-6}$	$4.1\cdot10^{-10}$	$5.0\cdot10^{-8}$

5.6.3 Cross-hole interference tests

The evaluation was concentrated on the tests performed in Feature A (Tests #1, #3, #6, #12 and #14), cf. Table 5-4, and tests performed in zone NW-2 (Tests #10 and #13) and in zone NW-2' (Test #8). Of the pressure responses, only the most distinct ones were used for evaluation of hydraulic properties.

Since sections containing Zone NW-2' have been found to be highly conductive, the zone is interpreted as an important hydraulic feature, which may in part explain the pseudo-spherical (leaky) flow behaviour seen both in single and cross-hole tests in the TRUE-1 rock block.

Table 5-5. Compilation of values of transmissivity derived for Feature A from different types of hydraulic tests and evaluation methods.

Borehole	Single packer flow logging in 0.5 m sections	Flow and pressure build-up tests	Flow and pressure build-up tests	Flow and pressure build-up tests	Cross-hole interference tests **)
Evaluation method	Moye's formula	Moye's formula	GRF-analysis	GTFM analysis	Thiem's equation
KXTT1	$1.1 \cdot 10^{-8}$	$1.0 \cdot 10^{-8}$	$3.0 \cdot 10^{-8}$	$(2.7–4.2) \cdot 10^{-8}$	$1.3 \cdot 10^{-8}$
KXTT2	$8.5 \cdot 10^{-9}$	$1.0 \cdot 10^{-8}$	$3.3 \cdot 10^{-8}$	$(2.4–4.8) \cdot 10^{-9}$ *)	$6.6 \cdot 10^{-9}$
KXTT3	$3.1 \cdot 10^{-7}$	$3.3 \cdot 10^{-7}$	$1.0 \cdot 10^{-6}$	$3.3 \cdot 10^{-8}$	$3.4 \cdot 10^{-7}$
KXTT4	$2.7 \cdot 10^{-8}$	$6.6 \cdot 10^{-8}$	$1.9 \cdot 10^{-7}$	$(7.5–8.7) \cdot 10^{-9}$	$2.2 \cdot 10^{-8}$
KA3005A	$3.9 \cdot 10^{-8}$	$4.2 \cdot 10^{-8}$	$4.9 \cdot 10^{-8}$	$2.0 \cdot 10^{-8} – 1.0 \cdot 10^{-7}$	$4.8 \cdot 10^{-8}$

*) Results from results evaluated using a leaky model

**) Evaluated from data from the pumped (sink) section

5.6.4 Transmissivity of Feature A

The Feature A has been tested with different types of hydraulic tests which in turn has been subject to alternative evaluation concepts. Table 5-5 shows a compilation of the transmissivity data from the various sources. A comparison between the results obtained from the double packer flow logging and the flow and pressure build-up tests evaluated using Moye's formula show a very good correspondence. Normalising the results shows that the GRF results generally are a factor three higher than the single packer flow logging results and the Moye's formula evaluation of the flow and pressure build-up tests, while the GTFM results are about one order of magnitude lower. Overall the evaluated transmissivities for Feature A from the respective five boreholes are within one order of magnitude.

A typical range of transmissivity for Feature A is $8 \cdot 10^{-9} – 4 \cdot 10^{-7}$ m^2/s.

5.6.5 Assessment of non-linear effects

During the tracer test programme, cf. Chapter 7, additional flow and drawdown data have been collected in conjunction with the different tracer tests, which provide additional information on the hydraulic parameters, evaluated on the basis of the associated interference pressure data. In all, six new data points are available for the preferred pump section, KXTT3:R2, used during TRUE-1. Table 5-6, Figures 5-3 and 5-4 report the pump flows and inferred specific capacities at the respective employed drawdown.

Table 5-6. Pump flows and specific capacities for different induced drawdown observed for different hydraulic and tracer tests.

Drawdown s (m)	Pump flow Q (l/min)	Specific capacity Q/s (m^2/s)	Comment
1.3	0.1	$1.28 \cdot 10^{-6}$	PDT-1, pump start
3.1	0.2	$1.07 \cdot 10^{-6}$	PDT-2, pump start
8	0.4	$8.33 \cdot 10^{-7}$	PDT-3, pump start
8.9	0.42	$7.86 \cdot 10^{-7}$	Pre-test to PTT, pump start
17.3	0.606	$5.83 \cdot 10^{-7}$	After PDT-1, test of max flow, pump start
24	0.835	$5.79 \cdot 10^{-7}$	PTT, 1995
261.7	4.12	$2.62 \cdot 10^{-7}$	Interference test #6, $H_o – H_p$

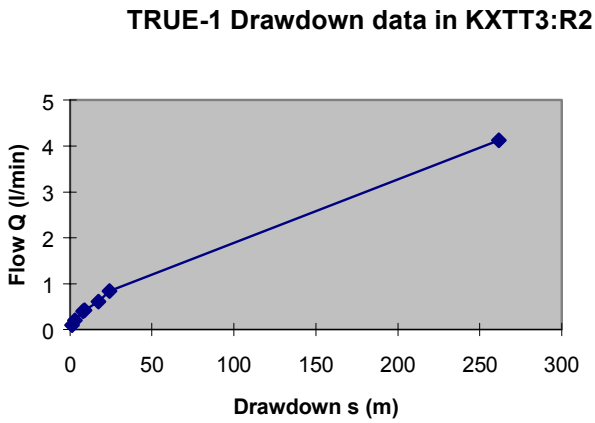

Figure 5-3. *Pump flow as a function of drawdown as inferred from pumping in KXTT3:R2 in Feature A, TRUE-1 site.*

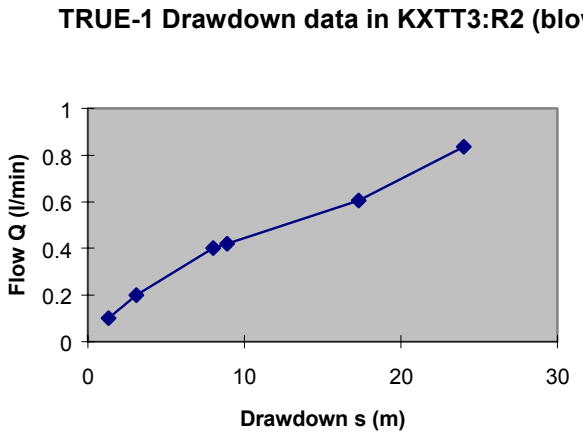

Figure 5-4. *Pump flow as a function of drawdown as inferred from pumping in KXTT3:R2 in Feature A, TRUE-1 site (blow up of part of Figure 5-3).*

The results indicate that the pump flow rates at high drawdown (s > 10 m), are significantly reduced compared to the ones at lower drawdown. This is also reflected in the specific capacities reported in Table 5-6. The observed reduction is attributed either to boundary effects, or more likely, increased flow resistance due to turbulence in the fracture in the immediate vicinity of the borehole intercept.

The results presented above suggests that the reported transmissivity evaluated on the basis of the performed interference tests in Feature A, may be underestimated with up to a factor 5, as inferred from the analysis of data from KXTT3:R2, cf. Table 5-6, and particularly for the high-transmissive intercept in KXTT3. This underestimation is attributed to turbulence in the fracture during the interference test at the highest drawdown, s=261.7 m.

5.7 Specific storage and storativity

Values of specific storage have been obtained from the evaluation of the flow and pressure build-up tests in Feature A using the GRF and GTFM models, cf. Table 5-7. No unique correlation between the two sets of evaluated values can be observed. In the majority of cases, the GTFM-derived specific storage is somewhat higher. In the case of KXTT1 and KA3005A, however, the GTFM values are associated with a high uncertainty and are significantly lower than those obtained from GRF.

A typical specific storage value from the GRF analysis for Feature A is in the range $1 \cdot 10^{-6} – 2 \cdot 10^{-5}$ s^{-1}.

Table 5-7. Specific storage derived for Feature A from evaluation of flow and pressure build-up tests using the GRF method (Winberg, 1996) and using the GTFM evaluation code (Roberts, 1998). The evaluated corresponding transmissivities are reported in Section 5.6.4.

Borehole	Section (m)	S_s (m^{-1}) (Winberg, 1996)	S_s (m^{-1}) (Roberts, 1998)
KXTT1	13 – 16	$1.1 \cdot 10^{-6}$	$1.3 \cdot 10^{-12} – 3.5 \cdot 10^{-10}$
KXTT2	12.5 – 15.5	$1.2 \cdot 10^{-6}$	$1.2 \cdot 10^{-5} – 3.3 \cdot 10^{-5}$
KXTT2	12.5 – 15.5	$1.2 \cdot 10^{-6}$	$2 \cdot 10^{-4} – 4.3 \cdot 10^{-4}$
KXTT3	12 – 15	$1.5 \cdot 10^{-5}$	$2 \cdot 10^{-5}$
KXTT4	9.5 – 12.5	$6.4 \cdot 10^{-6}$	$4.1 \cdot 10^{-7} – 9.4 \cdot 10^{-7}$
KA3005A	44.5 – 45.5	$2.8 \cdot 10^{-5}$	$1 \cdot 10^{-12} – 1 \cdot 10^{-9}$

As opposed to specific storage, storativity can only be derived from analysis of pressure responses in observation boreholes. Values on storativity relevant fracture zones NW-2 and NW-2’ are in the range $3 \cdot 10^{-7} – 2 \cdot 10^{-5}$. Storativity values derived for Feature A are in the range $6 \cdot 10^{-8} – 2 \cdot 10^{-5}$, Table 5-4.

5.8 Hydraulic head and gradients

The hydraulic pressure in the TRUE-1 rock block and its immediate environment has been monitored in approximately 30 test sections, the specific number of sections varying, depending on the type of activity performed in the TRUE-1 block. All sections except two constitute sections connected to the Äspö HRL Hydro Monitoring System (HMS) (Almén and Stenberg, in prep), whereas the remaining sections are equipped with individual pressure transducers connected to portable data loggers. The logging systems have predefined scan rates and trigging values which enable capture of unexpected hydraulic events. In case of special pre-defined activities, the scanning sequence is often set in advance.

The measured pressure values have for certain applications been recalculated to a hydraulic (point water) head using the following formula;

$$HH = K1 + K2 \times MV \qquad (5\text{-}2)$$

HH = Hydraulic Head (m.a.s.l.)
MV = Measured value (kPa)

$$K1 = (\rho_s \times g \times (Z_{tr} - Z_{mid}) - P_0) / (\rho_0 \times g) + Z_{mid} \qquad (5\text{-}3)$$

ρ_s = Density in tube between the pressure gauge and the section midpoint (kg/m;)
g = 9.81 = Acceleration due to gravity (m/s5)
Z_{tr} = Elevation of pressure gauge (m.a.s.l.)
Z_{mid} = Elevation of section mid point (m.a.s.l.)
P_0 = 101325 = Normal barometric pressure on ground surface (Pa)
ρ_0 = Density of "fresh water" (kg/m;)

$$K2 = 1000 / (\rho_0 \times g) \qquad (5\text{-}4)$$

5.8.1 General trends

During the period June 1996 through December 1998 the hydraulic pressure in the TRUE-1 borehole array has been in decline. This trend is general and affect the individual sections with an equal strength until July 1997, cf. Figure 5-5. After this time pressures starts to deviate during the pumping for tracer tests STT-1, STT-1b and STT-2. In the figure one can identify an annual variation which is superimposed on this general decrease in hydraulic pressure. The lowered hydraulic pressure is attributed to the successive development of underground tunnels and drifts. During 1996 the effect in

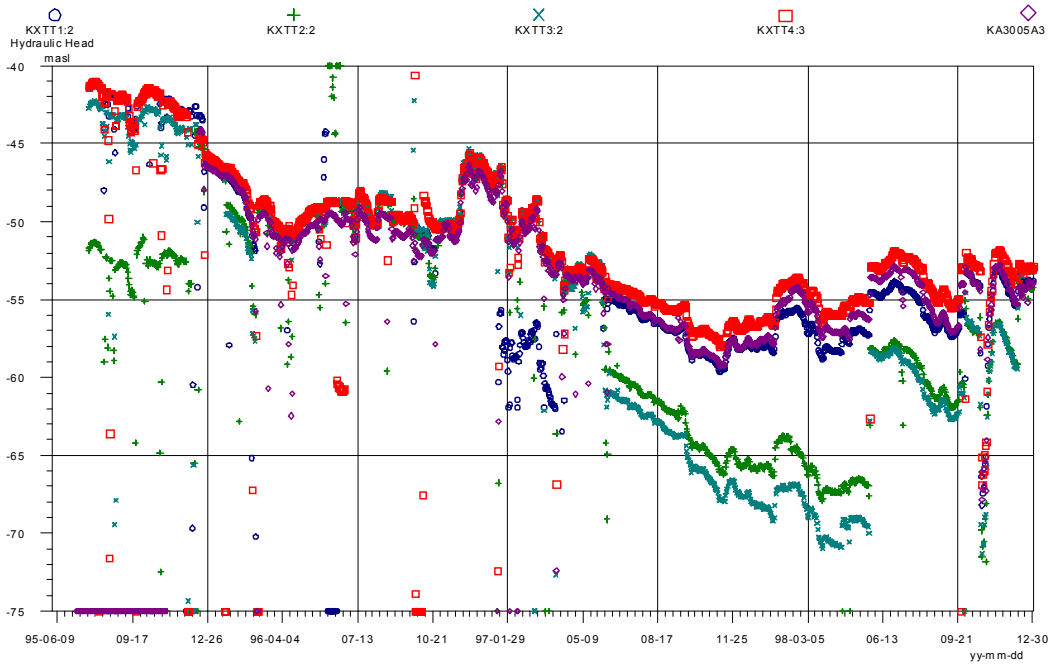

Figure 5-5. *Hydraulic head in sections containing Feature A during the period June 1995 through December 1998.*

the TRUE-1 block is limited, less than 20 kPa (2 metres) whereas the decrease during 1997 is a as high as 150 kPa (15 metres).

5.8.2 Hydraulic head and gradients in the TRUE-1 Block

The hydraulic head has lowered during the course of the project. The lowering is significantly larger closer to the tunnel. This is illustrated in Figure 5-6 for borehole KXTT4 where sections in the interior of the TRUE-1 rock block (sections 1 and 2) has reduced with approximately 10m, while sections close to the tunnel (sections 4 and 5) have reduced with approximately 15–20 m. This uneven reduction in of the head also implies that the hydraulic gradient towards the tunnel increased during the project from about 0.6 to 1.0 m/m.

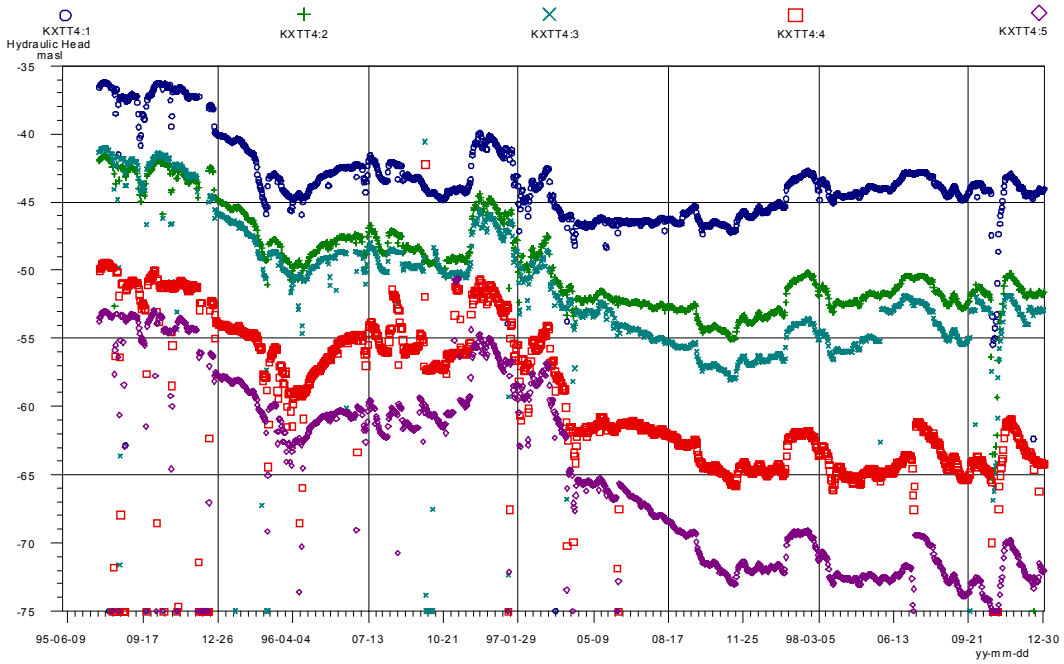

Figure 5-6. *Hydraulic head in five sections of borehole KXTT4 during June 1995 to December 1998.*

5.8.3 Hydraulic head and gradient in Feature A

The general direction of groundwater flow, inferred from measurements of hydraulic head in Feature A, is from KXTT3 towards KA3005A, i.e. towards (in direction of) the lower parts of the tunnel, possibly influenced by the leakage of Zone NNW-4 in the Assembly Hall at tunnel length 3/100 m. Table 5-8 shows the hydraulic head in the sections containing Feature A in conjunction with performed tracers tests. Figure 5-7 shows an interpolation of the hydraulic head measured in the five sections containing Feature A, immediately before test PDT-3 in June 1997, cf. Table 7-1.

On the basis of the measurements of hydraulic head shown in Table 5-8, the hydraulic gradient has been evaluated within Feature A. The hydraulic gradient has for the most part of the test period been about 10%. The period prior to reinstrumentation of the boreholes in December 1995 shows a completely different pressure distribution but a similar gradient. The head measurement prior to test PDT-1, cf. Table 7-1, shows a somewhat lower gradient, approximately 5%.

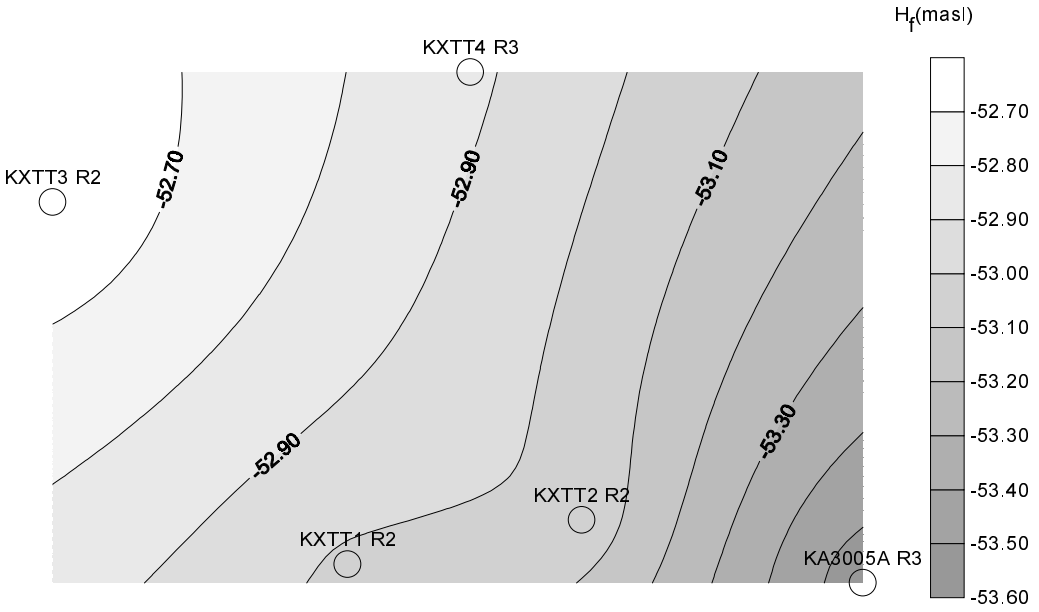

Figure 5-7. *Hydraulic head in Feature A immediately before performance of tracer test PDT-3, cf. table 7-1, performed in June, 1997. Interpolated point data (SURFER™).*

Table 5-8. Hydraulic head (masl) in sections containing Feature A prior to start of the TRUE-1 tracer tests (Preliminary tracer tests (PTT), Radially converging tracer tests (RC-1) and Dipole Tracer Tests (DP-1–DP-4), and preliminary design tests PDT-1, PDT-2 and PDT-3). Tests STT-1, STT-1b and STT-2 were made in direct succession to the test PDT-3, cf. Table 7-1.

Borehole section	PTT *)	RC-1	DP1–DP4	RC-2, DP5–DP6	PDT-1	PDT-2	PDT-3
Date	1/9 1995	17/1 1996	28/5 1996	25/9 1996	17/4 1997	5/8 1997	6/6 1997
KXTT1 R2	–41.8	–46.50	–49.09	–50.20	–53.15	–53.23	–53.02
KXTT2 R2	–42.3	–46.85	–49.36	–50.38	–52.95	–53.13	–53.03
KXTT3 R2	–43.2	–46.50	–48.97	–50.00	–52.78	–52.82	–52.62
KXTT4 R3	–41.8	–46.40	–49.04	–50.12	–52.90	–53.05	–52.88
KA3005A	–42.3	–46.95	–49.90	–50.93	–53.33	–53.68	–53.57

*) Readings taken prior to reinstrumentation of the TRUE-1 boreholes in December 1996, cf. Appendix B.

5.9 Natural groundwater flow

Measurements of the natural groundwater flow have been performed in Features A and B at two occasions during the TRUE-1 tracer test programme, in October 1995 and in April 1997. The measurements have been performed in a selection of test sections using the tracer dilution technique. The main objective of the repeated measurements has been to check whether any changes in the natural groundwater flow have occurred during the TRUE-1 tracer test programme. Possible causes for such changes may eg. be the excavation performed during the period October 1996–February 1997 or chemical changes in the fracture (clogging). The results of the two measurement campaigns are presented in Table 5-9.

Table 5-9. Natural groundwater flow. Comparison between tracer dilution tests performed in October 1995 and April 1997. The section id code is explained in Appendix B. *) = not measured.

Borehole	Section Id code	Volume (ml)	$Flow_{1997}$ (ml/min)	$Flow_{1995}$ (ml/min)	Comments
KXTT1	R2	1560	0.08	0.1	
	R3	8275	1.10	1.8	section increased 2.0 m
KXTT2	R2	1548	0.01	*)	
	R3	4299	0.33	0.3	moved 0.25 m
KXTT3	R2	1915	1.67	1.4	section decreased 1.5 m
	R3	5252	0.11	0.1	section increased 1.5 m
KXTT4	R3	1898	0.01	*)	
	R4	5210	2.81	5.0	section increased 0.5 m
KA3005A	R2	7945	0.40	*)	
	R3	2285	0.18	0.2	moved 0.35 m

A straight comparison between the results of the October 1995 and April 1997 tracer dilution measurements is to some extent limited by the fact that the packer positions were changed in December 1996. With regards to Feature A, section KXTT1:R2 has not been changed and shows the same flow in April 1997 as in October 1995. On the other hand section KXTT3:R2 has been shortened by 1.5 m and the flow rate has increased

slightly. The sections KXTT2:R3, KXTT3:R3 and KA3005A:R3 have been moved or decreased in length, but the measured flows in these sections have not changed. Two sections which have been increased in length, KXTT1:R3 and KXTT4:R4, and the flow is found to have been decreased in both cases. In summary, the observed changes in flow are small, and the magnitude of the flow rates are consistent with the evaluated local transmissivities and the hydraulic gradients in Features A and B. The old and new packer positions are given in Appendix B.

5.10 Inflow to tunnel section

Inflow to the measurement weirs distributed in the Äspö Tunnel is monitored on a continuous basis. The average inflow to the tunnel section 2/840 – 2/944 m has gradually decreased since 1995 from about 100 m^3/day down to 85 m^3/day in December 1998. cf. Figure 5-8. This decreasing trend may be an effect of water storage close to the tunnel being emptied. This is also consistent with the lowering of pressure observed in the sections close to the tunnel, cf. Section 5.9.

For the year 1998, however, a shorter period of further enhanced reduction of inflow can be noted in October, after which a trend of increased inflow back to normal levels is noted. The reduction is attributed to development of new underground facilities affecting the leakage from Zone NNW-4 in the TBM assembly hall area.

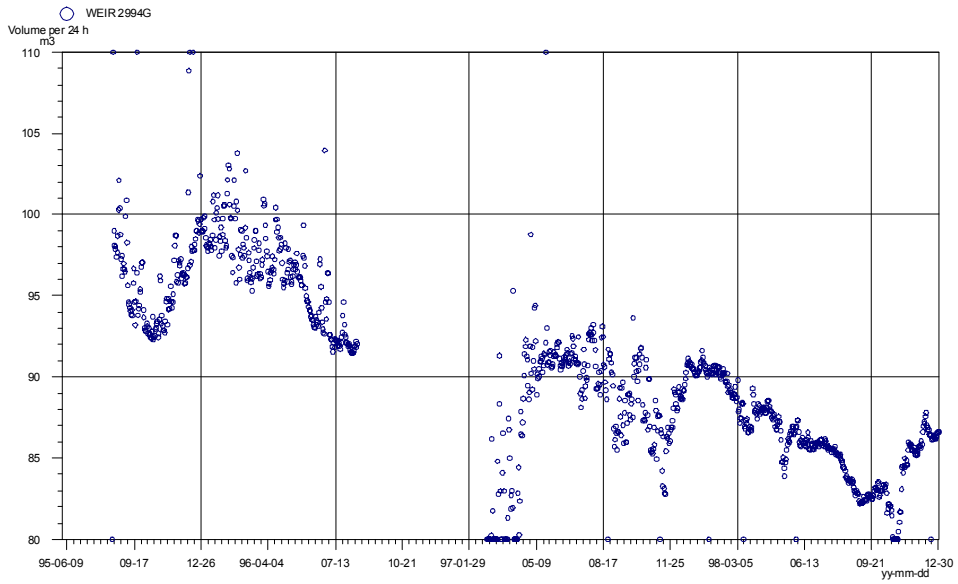

Figure 5-8. *Inflow (m^3/24 h) to tunnel section 2/840–2/944 m during June 1995 through December 1998.*

5.11 Hydrogeochemical characterisation

5.11.1 Water analyses

Collection and analyses of groundwater samples have primarily been used to assess the hydrogeochemical characteristics of the investigated target Feature A. Towards the end of 1995 the TRUE-1 borehole array was reconfigured to optimise the isolation of identified structures and add dummy bodies to some of the sections. In this context, results of analyses of samples collected before the reinstrumentation compared to results following the reinstrumentation proved that the isolation of Feature A was affirmative. The analysis results for the main elements are listed in Table 5-10 and the full tabulation of the data for Feature A is provided in Appendix E. The uncertainty in the chemical analyses is discussed in a general context by Sävestad and Nilsson (1999).

The data in Table 5-10 show some important characteristics. First, the analyses results from Feature A stand out with an elevated concentration of chloride, and a reduced carbonate concentration. Sections containing NW-2' show a chemical signature which is similar to Feature A. The data related to Feature B on the other hand show distinctly lower chloride and high carbonate concentrations. Similar trends can be observed in the stable isotope data. Hence, independent support for the hydraulic connection between Feature A and Structure NW-2' and the relative isolation between Features A and B is provided, cf. Sections 5.3.

Water quality during tracer tests reported in Chapter 7.

5.11.2 Classification of sampled groundwater

The Äspö site groundwater system has been classified into three different groups: non-saline, brackish and saline groundwaters, on the basis of the site specific chloride distribution. The chloride concentration for the groups is as follows:

Non-saline groundwater	<1000 Cl (mg/l)
Brackish groundwater	1000–5000 Cl (mg/l)
Saline groundwater	>5000 Cl (mg/l)

The samples from the TRUE-1 site belong to the saline and brackish groundwater types according to the classification presented in Table 5-11.

Table 5-10. TRUE-1 – Selected groundwater chemical analyses from the experimental period, see also Appendix E, N.D. = No data.

TRUE label	Section	Feature	Sample	Date	Na (mg/l)	K (mg/l)	Ca (mg/l)	Mg (mg/l)	HCO_3 (mg/l)	Cl (mg/l)	SO_4 (mg/l)	^{2}H ‰ (SMOW)	^{18}O ‰ (SMOW)
KXTT1:R2	L=15.00–16.00	A	2341	960410	1769	14.1	1286	81.4	91	5084	343	–76.9	–10.2
KXTT2:R2	L=14.55–15.55	A	2348	960412	1754	13.8	1263	80.8	91	5119	358	–78.4	–10.2
KXTT3:R2	L=12.42–14.42	A	2343	960410	1776	14.3	1301	82.3	92	5091	347	–78.4	–10.2
KXTT4:R3	L=11.92–13.92	A	2345	960411	1764	14.2	1254	81.5	98	5013	343	–78.6	–10.1
KXTT4:R3	L=11.92–13.92	A	2385	970306	1880	13.1	1510	80.5	72	5520	362	N.D.	N.D.
KXTT4:R3	L=11.92–13.92	A	2404	970702	1890	15.4	1680	67.9	55	5840	336	N.D.	N.D.
KXTT4:R3	L=11.92–13.92	A	2457	971003	1940	13.4	1709	69.8	43	6090	356	–86.8	–11.1
KXTT4:R3	L=11.92–13.92	A	2473	971202	1870	13.8	1610	70.8	50	5960	358	–85.6	–11.0
KXTT4:R3	L=11.92–13.92	A	2491	980304	1730	12.2	1310	71.5	88	5150	332	–81.4	–10.3
KXTT4:R3	L=11.92–13.92	A	2525	980603	1710	14.8	1120	72.6	115	4490	328	–77.2	–9.8
KXTT4:R3	L=11.92–13.92	A	2649	980930	1670	14.4	1030	71.9	119	4240	322	–83.0	–9.4
KXTT4:R3	L=11.92–13.92	A	2896	990413	1530	11.5	873	69.3	145	4030	N.D.	–74.3	–9.2
KA3005A:R3	L=44.78–45.78	A	2344	960411	1730	13.6	1191	82.5	93	4878	351	–75.5	–10.0
KXTT2:R3	L=11.55–13.55	B	2347	960411	1632	11.6	964	79.7	124	4389	327	–68.4	–9.3
KXTT3:R3	L=8.92–11.42	B	2346	960411	1621	12.1	947	79.9	130	4297	295	–73.4	–9.3
KXTT4:R2	L=14.92–23.42	NW-2’	2340	960409	1732	14.1	1192	83.2	106	4921	330	–77.0	–9.9
KA3067A:P4	L=6.55–27.05	NW-3	2342	960410	2374	12.7	2706	49.3	10	8585	426	–95.2	–13.0
SA2880A	L=11.92–13.92	NNW-4	2349	960422	3157	13.6	4378	41.1	22	12956	625	–87.7	–12.3

Table 5-11. Major characteristics of the brackish and saline groundwaters sampled at the TRUE-1 site and in adjacent borehole sections.

TRUE-1 label	Feature	Water type	Major Ions	[Cl] (mg/l)
KA3005A:R3	A	Brackish	Na-Ca-K:Cl-SO4-HCO3	1000–5000
KXTT4:R3	A	Saline	Na-Ca-K:Cl-SO4-HCO3	>5000
KXTT1:R2	A	Saline	Na-Ca-K:Cl-SO4-HCO3	>5000
KXTT3:R2	A	Saline	Na-Ca-K:Cl-SO4-HCO3	>5000
KXTT2:R2	A	Saline	Na-Ca-K:Cl-SO4-HCO3	>5000
KXTT3:R3	B	Brackish	Na-Ca-K:Cl-SO4-HCO3	1000–5000
KXTT2:R3	B	Brackish	Na-Ca-K:Cl-SO4-HCO3	1000–5000
KXTT4:R2	NW-2’	Brackish	Na-Ca-K:Cl-SO4-HCO3	1000–5000
KA3067A:P4	NW-3	Saline	Ca-Na-K:Cl-SO4-HCO3	>5000
SA2880A	NNW-4	Saline	Ca-Na-K:Cl-SO4-HCO3	>5000

5.11.3 Stable isotope data

The stable isotope data are generally used to detect if the sampled groundwaters have a meteoric component. The range of the data from the TRUE-1 site are $\delta^{18}O = -10.4$ to -8.9 ‰ and $\delta^{2}H = -60.2$ to -44.9 ‰. In Figure 5-9 the samples from Äspö HRL are plotted in relation to the standard meteoric water line. The indicated Trend #1 shows a distinct brine characteristic along a slope greater than 8. This is in accordance with the deep Canadian brines (Frape et al., 1984; Frape and Fritz, 1987) which show similar characteristics to low temperature Precambrian granitic shield areas. The trend can reflect a greater dependency on water-rock reactions (Alley, 1993) in combination with minimal influence from past marine and glacial melt fluctuations at large depths. The other evolution trends seen are believed to be associated with influx of glacial water (Trend #2), marine water (Trend #3) and meteoric water (Trend #4). The TRUE-1 data plot close to the meteoric water line (Trend #4) which shows that these waters are derived from post-glacial environments.

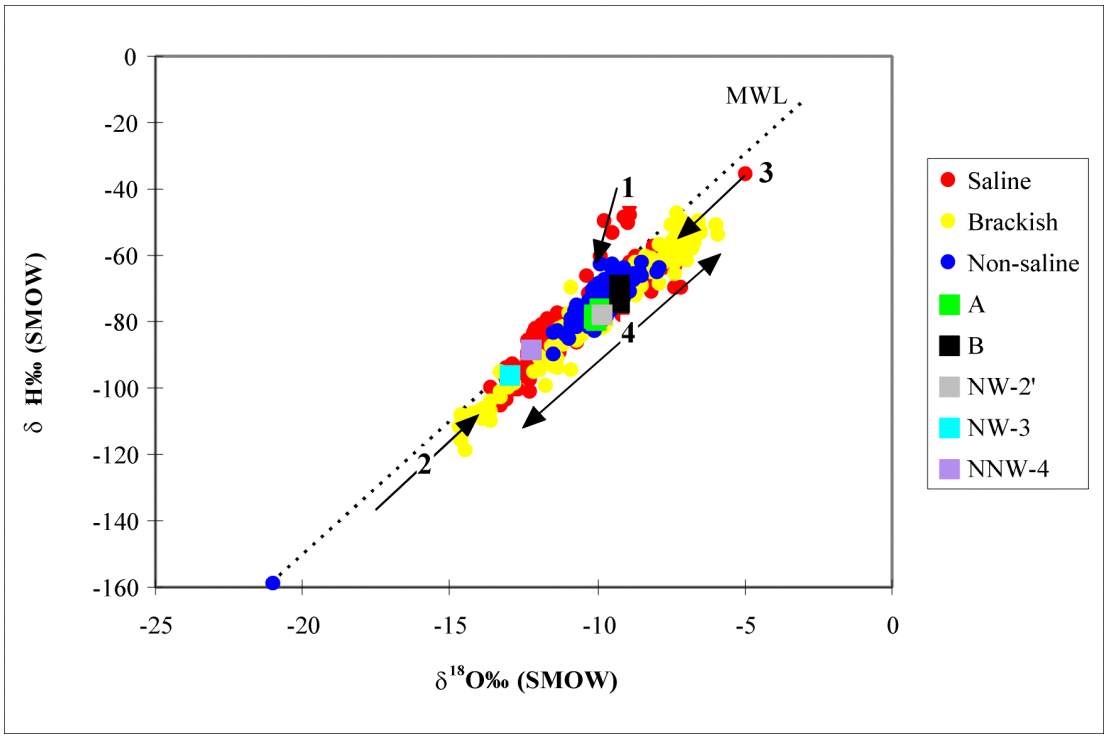

Figure 5-9. *$\delta^{18}O$ versus $\delta^{2}H$ for Äspö site groundwater. Evolution trends associated with influx of brine water (Trend #1), glacial water (Trend #2), marine water (Trend #3) and meteoric water (Trend #4).*

5.11.4 Mixing calculations

With the use of a combination of multivariate techniques (principal component analyses, mixing calculations and mass balance calculations) an attempt has been made to relate the groundwaters sampled at the TRUE-1 site to the overall chemical conditions at the Äspö HRL. The details of the methodology will not be given here, but is described in detail by Laaksoharju et al. (1995) and Laaksoharju and Skårman, 1995).

The results of the PCA analysis of sampled groundwaters from the TRUE-1 site, superimposed on data from Äspö HRL are shown in Figure 5-10. The plot has also been used to define end members from a groundwater composition point of view. The relative weights of the component elements are shown on the respective axis.

Features A, B and NW-2' show similar and stable mixing portions where the water is a result of a mixture of glacial, marine and meteoric groundwaters. Features NW-3 and NNW-4 have compositions which are a result of a mixture between brine, glacial and meteoric groundwaters.

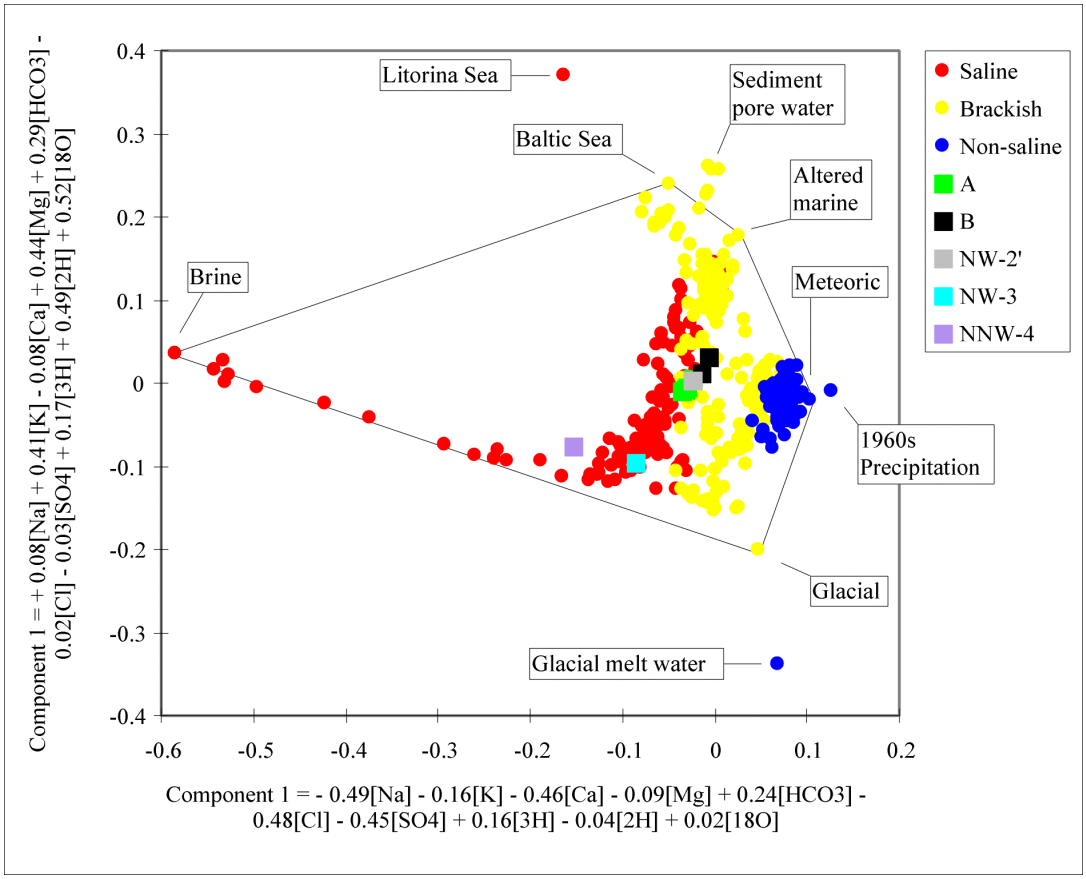

Figure 5-10. *Principal Component Analysis (PCA) plot showing the non-saline, brackish and saline groundwaters of the Äspö HRL site in comparison to the TRUE-1 data. The principal component plot is based on the major components, stable isotopes and tritium. The most extreme groundwaters which are considered well sampled, and which have an analytically established composition, are by definition called reference waters. An end-member is a modelled water composition which is believed to be the original groundwater composition of the reference water (rectangular boxes). A line is drawn between the reference waters such that a polygon is formed. The polygon can be used as a "phase" diagram to calculate the mixing ratios and the mass balance for the different samples. The relative weights for the different elements included in the analysis are shown in the equations for the first and second principal components, respectively.*

5.12 Main results from hydraulic and hydrochemical characterisation

The main results from the performed hydraulic characterisation may be summarised as follows;

- Points of inflow have been tentatively identified using inflow measurements between drilling uptakes. This identification has been made more refined using single packer flow logging with 0.5 or 1 m resolution.

- An initial pattern of connectivity has been obtained from pressure responses due to drilling advance. This pattern was improved by the subsequent interference test programme.

- Feature A is connected to Zone NW-2' as supported by measurements of hydraulic head, but is found to be relatively well isolated from adjacent structures, including Feature B.

- Flow dimension is generally found to be greater than two, and in some cases higher than three, indicating pseudo-spherical flow conditions, which can be explained by a leaky aquifer model, possibly in combination with a constant pressure boundary.

- Various hydraulic test methods and evaluation techniques have been used to estimate the transmissivity of Feature A. Transmissivities are found to be compatible as obtained from the various sources, with the exception of the estimates from evaluation using GTFM which generally is about an order of magnitude lower than the other estimates.

- The typical transmissivity of Feature A varies from about $8 \cdot 10^{-9}$ to $4 \cdot 10^{-7}$ m^2/s. A typical specific storage value for Feature A based on the GRF evaluation is in the range $1 \cdot 10^{-6} – 2 \cdot 10^{-5}$ s^{-1}.

- The general trend in hydraulic gradient across the block is increasing over the duration of the tracer test programme from about 0.6 m/m in 1995 to about 1 m/m in 1998. The hydraulic gradient in Feature A has remained relatively stable at 10% throughout the duration of the project.

- No significant changes in natural flow rate has been observed in repeated tracer dilution tests, and the magnitude of the flow rates are consistent with the evaluated local transmissivities and the hydraulic gradients in features A and B.

Hydrogeochemical analyses show that the Feature A ground water is saline with a chloride concentration in excess of 5000 mg/l. The chemical data support the interpretation of relative isolation of Feature A in relation to adjacent structures. Stable isotope data indicate that the waters are derived from post-glacial environments.

6 Results from laboratory programme

6.1 Introduction

One of the aims with the TRUE-1 project (Winberg 1994), is to study and model tracer retention using information from the different experimental scales, *i.e.* coupling of results obtained both in field experiments and laboratory experiments. From the breakthrough results of the sorbing tracers used in *in situ* experiments, information about the interaction of the groundwater and the rock matrix can be obtained. It may thus be possible to understand and quantify flow and retention entities and processes like matrix diffusion, sorption capacity of fractures, and the "flow wetted surface". To be able to interpret and model the *in situ* sorption results, supporting laboratory experiments are essential.

The experimental techniques that have been applied in this experimental laboratory programme are:

- Static batch experiments, investigating the sorption and desorption of the tracers on crushed and sieved geologic materials.

- Through-diffusion experiments, using intact geologic material obtained form different drill cores.

The experiments were conducted at Dept of Nuclear Chemistry, Chalmers University of Technology, Gothenburg. Elaborate descriptions of the experimental methods and the terminology used in this experimental programme are given in Byegård *et al.* (1998).

6.2 Generic rock material

6.2.1 Batch Sorption Experiment

The sorption coefficients for the contact of the cationic tracers with generic Äspö rock material, Äspö diorite and Fine-grained granite, were obtained by batch experiments. In these experiments, the sorption of radioactive tracers were studied in a mixture of 1–2 g of crushed and sieved rock and 8 ml of synthetic Äspö groundwater. Further details on the materials used and the experiments are given in Byegård *et al*. (1998)

The sorption coefficients determined from the batch experiments on the generic Äspö material are given in Table 6-1. For the more strongly sorbing species, *e.g.,*

Table 6-1. Sorption coefficients, K_d (m^3/kg) obtained for the generic Äspö material experiment using Äspö diorite and Fine-grained granite as solid phases. The values given are based on a contact time of 14 days. When uncertainties are given, they are based on the standard deviation of 2–4 samples (2 σ confidence interval).

Fraction size (mm)	Na^+	Ca^{2+}	Rb^+	Sr^{2+}	Cs^+	Ba^{2+}
Äspö diorite						
0.045–0.090	$10\cdot10^{-6}$	$63\cdot10^{-6}$	$8.1\pm1.4\cdot10^{-3}$	$100\cdot10^{-6}$	$290\pm1\cdot10^{-3}$	$4.3\pm0.03\cdot10^{-3}$
0.090–0.25	$9\cdot10^{-6}$		$6.7\cdot10^{-3}$	$77\cdot10^{-6}$	$110\cdot10^{-3}$	$3.1\cdot10^{-3}$
0.25–0.5	$10\cdot10^{-6}$	$55\cdot10^{-6}$	$4.9\pm0.1\cdot10^{-3}$	$73\cdot10^{-6}$	$150\pm1\cdot10^{-3}$	$2.1\pm0.02\cdot10^{-3}$
0.5–1	$8\cdot10^{-6}$		$3.3\cdot10^{-3}$	$50\cdot10^{-6}$	$38\cdot10^{-3}$	$1.5\cdot10^{-3}$
1.0–2.0	$7\cdot10^{-6}$	$37\cdot10^{-6}$	$1.9\pm0.4\cdot10^{-3}$	$36\cdot10^{-6}$	$30\pm4\cdot10^{-3}$	$0.90\pm0.03\cdot10^{-3}$
2.0–4.0	$7\cdot10^{-6}$		$1.4\cdot10^{-3}$	$29\cdot10^{-6}$	$8.2\cdot10^{-3}$	$0.74\cdot10^{-3}$
Fine-grained Granite						
0.045–0.090	$27\cdot10^{-6}$	$30\cdot10^{-6}$	$2.8\pm0.1\cdot10^{-3}$	$84\cdot10^{-6}$	$57\pm1\cdot10^{-3}$	$2.7\pm0.06\cdot10^{-3}$
0.090–0.25	$13\cdot10^{-6}$			$45\cdot10^{-6}$	$30\cdot10^{-3}$	
0.25–0.5	$13\cdot10^{-6}$	$13\cdot10^{-6}$	$1.2\pm0.06\cdot10^{-3}$	$31\cdot10^{-6}$	$19\pm2\cdot10^{-3}$	$1.1\pm0.1\cdot10^{-3}$
0.5–1	$4\cdot10^{-6}$			$21\cdot10^{-6}$	$10\cdot10^{-3}$	
1.0–2.0	$5\cdot10^{-6}$	$13\cdot10^{-6}$	$1.4\pm0.02\cdot10^{-3}$	$18\cdot10^{-6}$	$8.3\pm0.3\cdot10^{-3}$	$0.60\pm0.04\cdot10^{-3}$
2.0–4.0	$4\cdot10^{-6}$			$14\cdot10^{-6}$	$6.7\cdot10^{-3}$	

Rb^+, Cs^+ and Ba^{2+}, the sorption coefficients have been estimated from the loss of radioactive tracer in the water phase. For Na^+ and Sr^{2+} the sorption coefficients have been determined from measurements of the content of radioactive tracers in the solid phase after the separation of the solid phase from the original aqueous phase. For Ca^{2+} desorption was performed after the sorption experiment. The sorption coefficients are given assuming fully reversible sorption.

6.2.2 Diffusion

The diffusivity of the cationic tracers were studied in through diffusion experiments. The samples, which have a diameter of 46 mm, varied in length between 10 and 40 mm. The experimental design and the through diffusion theory applied in the interpretation of the results have been described by Byegård *et al*. (1998) and Johansson *et al.* (1997). The porosity and diffusion results are summarised in Table 6-2. In Table 6-3, the distribution coefficients obtained from the diffusion experiments are given. The rock capacity factor α is given by Equation 6-1. In the case of a non-sorbing tracer, say HTO, then $\alpha = \varepsilon_T$, equivalent to the total porosity, cf. Tables 6-2 and 6-5.

$$\alpha = \varepsilon_T + K_d \cdot \rho \qquad (6\text{-}1)$$

Table 6-2. Porosity and the diffusivity determined for the generic Äspö rock material by the through-diffusion experiment. The uncertainties are based on the standard deviation of the results of 5 different samples.

Rock Type Cell length (cm)	Porosity $\alpha_{HTO} \equiv \varepsilon$	Effective diffusivity, D_e, (m^2/s) $D_{e\,(HTO)}$	$D_{e\,(Na)}$	$D_{e\,(Ca)}$	$D_{e\,(Sr)}$	$D_{e\,(Cs)}$	$D_{e\,(Ba)}$
Äspö diorite							
1	$5.5\pm2.8\cdot10^{-3}$	$1.2\pm0.6\cdot10^{-13}$	$7.8\cdot10^{-14}$	$4.3\cdot10^{-14}$	$6.3\cdot10^{-14}$		$5\cdot10^{-16}$
2	$3.4\pm1.4\cdot10^{-3}$	$1.1\pm0.2\cdot10^{-13}$	$7.3\cdot10^{-14}$	$3.2\cdot10^{-14}$	$2.8\cdot10^{-14}$		
4	$8.6\cdot10^{-4}$	$3.2\pm0.2\cdot10^{-14}$	$1.5\cdot10^{-14}$				
Fine-grained granite							
1	$4.5\pm2.4\cdot10^{-3}$	$1.6\pm1.2\cdot10^{-13}$	$6.4\cdot10^{-14}$	$1.4\cdot10^{-13}$	$3.5\cdot10^{-14}$	$1.8\cdot10^{-14}$	
2	$2.8\pm2.0\cdot10^{-3}$	$5.1\pm2.0\cdot10^{-14}$	$6.0\cdot10^{-14}$	$7.3\cdot10^{-14}$	$7.9\cdot10^{-14}$		
4			$6.2\cdot10^{-14}$				

Table 6-3. Distribution coefficients determined for the generic Äspö rock material by through-diffusion experiments. In the calculations, the tritiated water tracer (HTO) has been considered as a non-sorbing tracer.

Rock Type Cell length (cm)	Distribution Coefficients, K_d (m^3/kg) Na	Ca	Sr	Cs
Äspö diorite				
1	$1.5\cdot10^{-6}$	$5.5\cdot10^{-6}$	$6.9\cdot10^{-6}$	
2	$2.3\cdot10^{-6}$	$4.9\cdot10^{-6}$	$2.5\cdot10^{-6}$	
Fine-grained granite				
1	$2.6\cdot10^{-6}$	$3.6\cdot10^{-6}$	$8.2\cdot10^{-6}$	$2\cdot10^{-5}$
2	$3.2\cdot10^{-6}$	$3.5\cdot10^{-6}$	$7.5\cdot10^{-7}$	

where

α = rock capacity factor (–)
K_d = volumetric distribution coefficient (m^3/kg)
ρ = density of the rock (kg/m^3)

6.2.3 Porosity

The porosity of the generic rock material has been studied by water saturation, by through diffusion studies and by the ^{14}C-PMMA method. Full description of the

Table 6-4. Comparison of porosity measured with different techniques: water saturation, through diffusion measurements and the ^{14}C-PMMA method.

Rock type	Water saturation [a] (% ±1 σ between samples)	Through diffusion [b] (% ±1σ between samples)	^{14}C-PMMA method [c] (% ±1 σ)
ÄD	0.55 ± 0.06	0.35 ± 0.15	0.4 ± 0.1
FGG	0.25 ± 0.01	0.3 ± 0.2	0.2 ± 0.1

[a] Measured on 1,2 and 4 cm thick drill core slices, Äspö diorite 6 samples, Fine-grained granite 10 samples.
[b] From HTO through diffusion in 5 samples of 2 cm thickness for each rock type.
[c] Measured on 4 cm thick drill core samples.

methods and the results are given in Byegård et al. (1998). A summary of the results are presented in Table 6-4.

6.2.4 Depth of penetration

In the through diffusion studies no, or only an extremely low, breakthrough was obtained for the stronger sorbing tracers used, *i.e.*, Rb^+, Cs^+ and Ba^{2+}. The short half-life of the $^{86}Rb^+$ tracer (18.6 days) made further diffusion studies of this tracer impossible. However, for $^{137}Cs^+$ and $^{133}Ba^{2+}$, studies of the penetration depth of the tracers were performed by cutting the rock slab in the diffusion cell and measuring the concentration as a function of the depth. An example of the diffusion of Cs^+ in Äspö diorite is given in Figure 6-1. The penetration profiles have been fitted using a double porosity.

Table 6-5. Summary of parameters derived from fitting of the two pathways model to the experimental results. The porosities are based on the through diffusion experiments with HTO in the same diffusion cells. Through diffusion data for $^{133}Ba^{2+}$ and $^{137}Cs^+$ from the 1 cm cells number 19 and 22 are presented for comparison.

				Slow process (short penetration)				Fast process (deep penetration)			
Cell no	Ele-ment	Rock Type	ε	D_e (m^2/s)	α (1)	K_d (m^3/kg)	D_a (m^2/s)	D_e (m^2/s)	α (1)	K_d (m^3/kg)	D_a (m^2/s)
20	Ba^{2+}	FGG	$9\cdot10^{-4}$	$7\cdot10^{-15}$	0.16	$6\cdot10^{-5}$	$4\cdot10^{-14}$	$3\cdot10^{-16}$	$2\cdot10^{-3}$	$4\cdot10^{-7}$	$1.5\cdot10^{-13}$
21	Ba^{2+}	ÄD	$2.2\cdot10^{-3}$	$1.6\cdot10^{-14}$	0.65	$2\cdot10^{-4}$	$2\cdot10^{-14}$	$4\cdot10^{-15}$	$4.5\cdot10^{-3}$	$2\cdot10^{-5}$	$9\cdot10^{-14}$
24	Cs^+	FGG	$1.1\cdot10^{-3}$	$2\cdot10^{-14}$	0.69	$3\cdot10^{-4}$	$3\cdot10^{-14}$	$1\cdot10^{-15}$	$6.7\cdot10^{-3}$	$2\cdot10^{-6}$	$1.5\cdot10^{-13}$
25	Cs^+	ÄD	$3.2\cdot10^{-3}$	$6.5\cdot10^{-14}$	2.2	$8\cdot10^{-4}$	$3\cdot10^{-14}$	$2\cdot10^{-15}$	0.13	$4\cdot10^{-6}$	$1.5\cdot10^{-13}$
				Through diffusion measurement							
				D_e (m^2/s)	α (1)	K_d (m^3/kg)	D_a (m^2/s)				
19	Ba^{2+}	ÄD	$3.5\cdot10^{-3}$	$5\cdot10^{-16}$	$2\cdot10^{-3}$	–	$2.5\cdot10^{-13}$				
22	Cs^+	FGG	$4.1\cdot10^{-3}$	$1.8\cdot10^{-14}$	0.06	$2\cdot10^{-5}$	$3\cdot10^{-13}$				

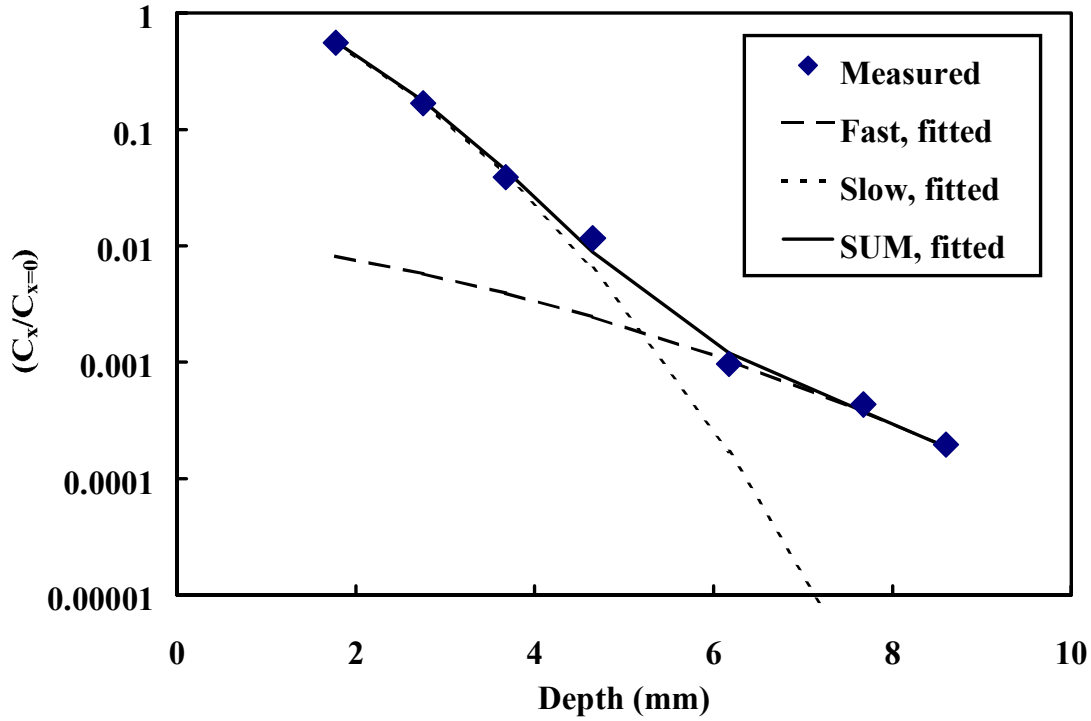

Figure 6-1. Concentration profiles of Cs^+ in Äspö diorite. Diffusion time 472 days.

diffusivity model and the results are presented in Table 6-5. A full description of the experimental methods and the theory applied is given by Byegård *et al*. (1998) and by Johansson *et al*. (1998).

6.2.5 Geological characterisation

Äspö diorite

Äspö diorite is the dominating rock type in the Äspö area. It is a medium-grained and porphyritic quartz monzodiorite/granodiorite which contains K-feldspar phenocrysts, 1–2 cm in size. It is slightly foliated and the porosity is generally in the interval of 0.5±0.2% (Stanfors *et al*. 1993a, Stanfors *et al*. 1993b).

The mineralogical composition has been determined from studies of thin section using transmissive light microscope. Plagioclase, K-feldspar, quartz, biotite and calcite were observed. Accessory minerals were muscovite, titanite, apatite, fluorite, zircon and opaque phases (mostly magnetite). The plagioclase showed partly weak sausuritisation (plagioclase → albite+sericite+epidote) In the thin section analysis, the biotite showed a green colour, indicative of a slight alteration. Chlorite was not present in the thin sections studied. Some microfractures sealed by calcite were observed.

The results of the mineralogical and chemical analyses of the Äspö diorite are given in Table 6-6 and 6-7, respectively.

Fine-grained granite

The trace element analysis and a general mineralogical composition of the Fine-grained granite are given in Tables 6-6 and 6-7, respectively. Generally, the differences between the different size fractions are much lower for the Fine-grained granite than for the Äspö diorite. This observation is in accordance with the texture of the two rock types, *i.e.*, the Fine-grained granite is fine-grained and relatively homogeneous, while the Äspö diorite is characterised by its heterogeneity both in mineral content and sizes of the grains. However, the two smaller fractions contain a slightly higher content of quartz, muscovite, magnetite and perhaps also chlorite. This is accompanied by a lower content of K-feldspar and plagioclase. The Fine-grained granite has a somewhat lower porosity than the Äspö diorite, 0.3±0.2% (Stanfors *et al*. 1993a, Stanfors *et al*. 1993b).

Table 6-6. Average mineralogical composition (weight %) of the mylonites, the altered material, Fine-grained granite (FGG), Äspö diorite (ÄD) from Äspö Hard Rock Laboratory (Sample label corresponds to KXT-hole and depth in metres).

Mineral Sample label	ÄD	Alt.ÄD T2:15.10	Mylonite T2:15.10	Alt.ÄD T3:14.10	FGG	Alt.FGG T4:12.10	Mylonite T4:12.10
Biotite	18	9	2	–	1	–	–
Plagioclase	47	–	–	–	23	–	–
Albite	–	40	40	38	–	30	10
K-feldspar	10	12	10	10	38	20	8
Quartz	14	14	14	15	30	35	22
Epidote	5	7	20	15	1	5	42
Chlorite	–	8	6	15	1	3	7
Sericite	–	2	4	2	3	3	5
Ass*	6	8	4	5	3	4	6

6.3 Feature A site-specific material

6.3.1 Batch experiments

The sorption coefficients for the contacting of cationic tracers with Feature A site-specific rock material were obtained from batch experiments. In these experiments, the sorption of radioactive tracers was studied in a mixture of 2g of crushed and sieved rock (1–2 mm fraction) and 8 ml of synthetic Feature A groundwater. Further details of the experiments are given by Byegård *et al*. (1998).

Table 6-7. Chemical analyses of the 1–2 mm size fractions of Äspö diorite (ÄD) and Fine-grained granite (FGG) from Äspö Hard Rock Laboratory. Rb, Ba, Cs, U, Th, Hf and the REEs are analysed using INAA (Studsvik Nuclear, Radiometry, Nyköping) . All other elements are analysed with ICP-MS (Svensk Grundämnes-analys AB, Luleå). All concentrations refer to single samples.

Main Elements (%)	ÄD	FGG	Trace Elements (mg/kg)	ÄD	FGG
SiO_2	60.1	73.3	Rb	89	207
Al_2O_3	18.1	13.5	Cs	2.4	1.7
CaO	4.4	1.3	Sr	1300	225
Fe_2O_3	5.1	2.1	Ba	1770	865
K_2O	3.2	6.1	Zr	256	280
MgO	2.2	0.5	Hf	6.1	7.3
MnO	0.1	0.05	Nb		20.5
Na_2O	4.7	2.7	Th	5.2	24.1
P_2O_5	0.3	0.11	U	2.1	3.0
TiO_2	0.8	0.36	La	47	84
LOI	1.0	0.3	Ce	104	164
			Nd	46	59
			Sm	8.4	9.7
			Eu	1.6	1.2
			Tb	1.0	1.1
			Yb	2.0	2.3
			Lu	0.3	0.3
			Y	18.1	22.0

The sorption coefficients determined from the batch experiments on the generic Äspö material are given in Table 6-8. For the more strongly sorbing species, eg. Rb^+, Cs^+ and Ba^{2+}, the sorption coefficients have been estimated from the loss of radioactive tracer in the water phase. For Na^+ Ca^{2+} and Sr^{2+}desorption was performed after the sorption experiment and the sorption coefficients are given assuming fully reversible sorption.

6.3.2 Diffusion

A through-diffusion experiment has been performed using site-specific rock material from Feature A. The rock sample was a piece of rock making up the intersection of borehole KXTT1 with Feature A, and consisted of altered and partly mylonitised Äspö diorite limited by two natural fracture surfaces coated with chlorite, both of which have been in contact with groundwater. The uneven fracture surfaces were nearly parallel, and the thickness of the sample in the diffusion direction varied between approximately 16 to 20 mm. A part (~10%) of the start side had a depression, with 10 mm thickness at the thinnest point between the two sides. For further information about the experimental procedures, see Byegård *et al.* (1998).

Table 6-8. Sorption coefficients, K_d (m^3/kg) obtained using the Feature A site specific rock material as solid phase. The values given are based on a contact time of 9 days.

Material	Na^+	Ca^{2+}	Rb^+	Sr^{2+}	Cs^+	Ba^{2+}
Mylonite KXTT2	$6.8\cdot10^{-6}$	$27\cdot10^{-6}$	$2.0\cdot10^{-3}$	$50\cdot10^{-6}$	$8.0\cdot10^{-3}$	$1.3\cdot10^{-3}$
Mylonite KXTT4	$2.6\cdot10^{-6}$	$17\cdot10^{-6}$	$<0.5\cdot10^{-3}$	$26\cdot10^{-6}$	$1.2\cdot10^{-3}$	$0.4\cdot10^{-3}$
Altered ÄD KXTT2	$2.9\cdot10^{-6}$	$27\cdot10^{-6}$	$0.9\cdot10^{-3}$	$41\cdot10^{-6}$	$11\cdot10^{-3}$	$1.2\cdot10^{-3}$
Altered ÄD KXTT3	$4.4\cdot10^{-6}$	$<50\cdot10^{-6}$	$<0.7\cdot10^{-3}$	$90\cdot10^{-6}$	$3.1\cdot10^{-3}$	$1.8\cdot10^{-3}$
Altered FGG KXTT4	$1.1\cdot10^{-6}$	$<20\cdot10^{-6}$	$<0.5\cdot10^{-3}$	$10\cdot10^{-6}$	$1.5\cdot10^{-3}$	$0.4\cdot10^{-3}$
Äspö Diorite	$3.8\cdot10^{-6}$	$54\cdot10^{-6}$	$1.4\cdot10^{-3}$	$110\cdot10^{-6}$	$14\cdot10^{-3}$	$1.2\cdot10^{-3}$
Fine Grained Granite	$6.0\cdot10^{-6}$	$<20\cdot10^{-6}$	$<0.6\cdot10^{-3}$	$31\cdot10^{-6}$	$1.6\cdot10^{-3}$	$0.6\cdot10^{-3}$

All tracers used except ^{86}Rb (decayed) were detected in the measurement container within 3 months. An attempt was made to evaluate the breakthrough curves using the one-dimensional solution to the diffusion equation (Crank, 1975), assuming that the length of the sample is 18 mm. Obviously, this is an oversimplification, but the evaluation gives an indication of the range in diffusivities. The results of the evaluation are presented in Table 6-9. Compared to the results obtained for generic rock material, the site-specific material has a lower porosity ($=\alpha_{HTO}$) and it is indicated that the diffusivities are also lower. The noted lower porosity is attributed to the site-specific sample being mylonitised, cf. Section 6.3.3.

Table 6-9. Evaluation of breakthrough data by a least square fitting of the data to the one-dimensional solution of the diffusion equation. $D_{w,i}$ is the free water diffusivity of ion i at infinite dilution.

Tracer	D_e exp. (m^2/s)	α (1)
HTO	$4\cdot10^{-14}$	$1.5\cdot10^{-3}$
$^{137}Cs^+$	n.e.	n.e.
$^{131}I^-$	$4\cdot10^{-15}$	$1\cdot10^{-3}$
$^{82}Br^-$	n.e.	n.e.
$^{22}Na^+$	$1\cdot10^{-14}$	$< \alpha_{HTO}$
$^{186}ReO_4^-$	n.e.	n.e.
$^{133}Ba^{2+}$	n.e.	n.e.
$^{85}Sr^{2+}$	$7\cdot10^{-15}$	$< \alpha_{HTO}$
$^{47}Ca^{2+}$	$7\cdot10^{-15}$	$< \alpha_{HTO}$
^{169}Yb-DTPA	n.e.	n.e.
^{160}Tb-EDTA	$1\cdot10^{-15}$–$2\cdot10^{-15}$	$< \alpha_{HTO}$
^{177}Lu-DOTA	n.e.	n.e.

6.3.3 Geological characterisation of the site-specific material

Feature A is a reactivated mylonite hosted in Äspö diorite. Wall rock samples of the intersection of the fracture in different boreholes were obtained (Fig. 6-2). This site specific material from Feature A has been analysed chemically, cf. Table 6-10. From the analysis results, the estimated mineralogical composition (Table 6-6) and thin sections of the material (Byegård *et al.* 1998), some general observations can be made.

The altered geologic material from the KXTT2 drill core is an altered Äspö diorite containing epidote and chlorite and also some traces of biotite. This sample is the only one of the site specific samples which contains biotite. Compared to fresh Äspö diorite, an albitisation (breakdown of plagioclase to form albite) has occurred which has resulted in a mobilisation of Ca. This can probably explain the increased concentration of Ca in the adjacent mylonite. A rough estimation of the mineralogy indicates that there are similarities to the mineralogy of non-altered Äspö diorite, except for a higher content of chlorite and epidote. It is also possible that the water content of the biotite residue is higher than for biotite in the non-altered Äspö diorite.

The mylonite from the KXTT2 drill core contains mainly epidote, K- and Na-feldspars and quartz. No biotite is present and formation of fine grained muscovite has occurred. The sample contains approximately 50% epidote, which is associated with high concentration of Sr.

Due to calcite impurities in the mylonite layer of the KXTT3 sample, only an altered geologic material was isolated for the sorption experiment. The altered geologic material located inside the mylonite was found to originate from Äspö diorite. This sample has the same composition as the altered granite from the KXTT2 drill core, except for that the biotite has been completely altered to chlorite.

The altered material from the KXTT4 drill core deviates from the other altered materials; it is an altered Fine-grained granite. Compared to a non-altered sample of the same rock type, the content of muscovite, chlorite and epidote is higher.

The mylonite from the KXTTT4 drill core is extremely fine grained and has a high concentration of epidote. The muscovite content is rather low and the dominating minerals are epidote, quartz, albite and K-feldspar.

For the diffusion experiment on site specific material, sample KXTT1:L=15.77 m was chosen. This sample consist of altered and partly mylonitised Äspö diorite bounded by two natural fracture surfaces coated with chlorite. These natural fracture surfaces are the ones exposed to fluid in the diffusion experiment described in Section 6.3.2. The foliation and the bands of mylonite are orientated parallel with the fracture surfaces which means perpendicular to the measured diffusion paths. The mineralogical composition of the entire sample can be summarised as an altered and fractured Äspö diorite with all biotite replaced with chlorite (similar to KXTT3:L=14.10m) interlayered with millimetre thick shear bands of mylonite (epidote, sericite some chlorite, and quartz) and recrystallised quartz. Also a recrystallisation of magnetite

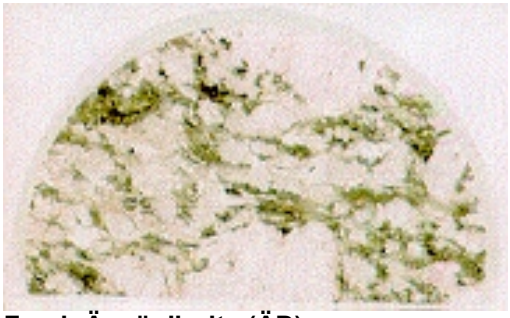

Fresh Äspö diorite (ÄD)

Fresh Fine-grained granite (FGG)

KXTT2, L=15.10 m
Mylonite (top)
Altered ÄD (bottom)

KXTT3, L=14.10 m
Mylonite, not in the experiment (top)
Altered ÄD (bottom)

KXTT4, L=12.10 m
Mylonite (top)
Altered FGG (bottom)

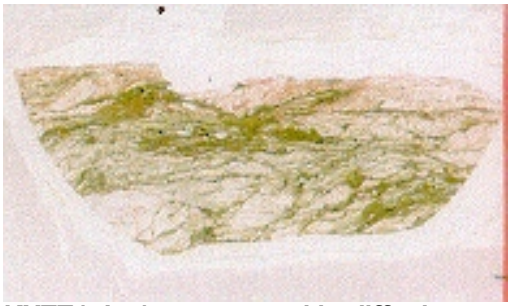

KXTT1, L=15.77 m, used in diffusion test

KXTT1, L=15.77 m

Figure 6-2. *Thin section of fresh samples (Äspö diorite and Fine-grained granite) and altered and mylonitised samples from the Feature A fracture (see text for details). Two samples from Feature A KXTT1:15.77 m are shown. One represents the sample used for diffusion experiment and the other show the same fracture and the adjacent wall rock. The black dots on the picture of the KXTT4 samples are residues from the SEM/EDS studies. The size of the images is approximately 40x25 mm.*

Table 6-10. Chemical analyses of site specific material from the TRUE-1 site. The drill cores are KXTT2, KXTT3 and KXTT4. Rb, Ba, Cs, U, Th, Hf and the rare earth elements are analysed using INAA (Studsvik Nuclear, Radio-metry, Nyköping). All other elements are analysed with ICP-MS (SGAB, Luleå). All concentrations refer to single samples.

Sample	T2:15.10 m Altered ÄD	T2:15.10 m Mylonite	T3:14.10 m Altered ÄD	T4:12.10 m Altered FGG	T4 :12.10 m Mylonite
Main elements (%)					
SiO_2	63.8	61.6	62.6	76.0	62.6
Al_2O_3	16.6	16.1	16.3	13.3	13.0
CaO	3.5	7.2	4.4	1.1	11.1
Fe_2O_3	4.1	5.9	5.4	0.85	7.6
K_2O	2.2	2.2	1.8	3.6	0.7
MgO	1.8	1.6	1.9	0.3	0.9
MnO	0.08	0.11	0.09	0.02	0.13
Na_2O	5.6	3.4	5.3	4.6	0.9
P_2O_5	0.28	0.31	0.36	0.04	0.26
TiO_2	0.7	0.74	0.85	0.13	0.72
LOI	2.4	1.4	1.8	0.8	2.0
Trace elements (ppm)					
Rb	85	89	78	72	32
Cs	2.0	1.7	0.64	0.4	0.2
Sr	785	1760	1260	441	2950
Ba	926	1359	691	1528	308
Zr	228	229	314	82	217
Hf	6.2	5.7	7.3	2.3	5.5
Nb	15.3	15.8	14.7	6.2	14.5
Th	10.3	11.8	8.2	26.3	10.2
U	3.7	5.0	3.0	4.4	3.6
La	43	57	91	29	82
Ce	98	124	172	59	157
Nd	47	58	68	26	62
Sm	8.2	10.0	10.7	6.3	10.6
Eu	1.5	2.0	1.9	0.5	1.9
Tb	1.0	1.2	1.3	1.6	1.3
Yb	2.4	2.8	2.4	2.4	2.6
Lu	0.3	0.4	0.35	0.25	0.36
Y	19.8	24.5	22.4	31.3	24.2

is observed. A few sealed microfractures cross cut the foliation and the mylonites. It is difficult to identify the minerals in these microfractures but it appears to be epidote, chlorite and probably also some FeOOH.

Altered Äspö diorite has a higher porosity than the fresh, 1.0% compared with 0.45% (Eliasson 1993), whereas the mylonitic parts are extremely fine grained and has a lower porosity (probably in the order of 0.25%).

6.4 Integrated results and conclusions

Some general observations from the laboratory experiments are outlined in the report by Byegård *et al.* (1998), can be summarised by the following paragraphs:

- The sorptivity of the geologic material is indicated to depend on the concentration of biotite. Alteration of biotite to chlorite (found in some of the Feature A site specific material) is indicated to decrease the sorptivity.

- The sorption observed in the batch experiments is found to be time-dependent, *i.e.*, K_d increase with increasing contact time. It is indicated that diffusion of the tracers in the crushed particles can explain this behaviour.

- The sorbtivity of the tracers used in the laboratory experiments using geological material from Äspö, show the following relative order; $Na^+ < Ca^{2+} \approx Sr^{2+} < Rb^+ \approx Ba^{2+} < Cs^+$.

- It is observed that the sorption obtained from the through-diffusion experiments is much lower than the sorption obtained from the batch experiment. It is likely that crushing of the rock material causes exposure of new fresh surfaces that are not representative for the intact material. Differences in sorption coefficients are also observed for the stronger sorbing tracers as seen in the results obtained from the through-diffusion experiment and the penetration studies. It is indicated that the heterogeneity of the geologic material, e.g., heterogeneous distribution of the porosity, causes the observed differences.

- It is indicated that the sorption of the more strongly sorbing species, *i.e.*, Rb^+, Cs^+, and Ba^{2+}, is influenced by some non- or slowly reversible processes.

- The study of the sorption as a function of the surface area (BET-surface and geometrical surface) gives a complicated dependence which is not easily explained by a surface sorption/matrix diffusion model

Although the outcome of the laboratory experiment is more complex than what can be explained by simple sorption/diffusion models, attempts to estimate the transport parameters for the TRUE-1 experiments with sorbing tracers have been performed. These are primarily based on the laboratory experiments with Äspö diorite (batch and through diffusion experiments) using anoxic conditions, ambient temperature (20–25^{o}C) and a saline synthetic "Äspö-like" groundwater with an ionic strength I ~ 0.2 and pH 7.5. Data are also available for the batch experiments with crushed site specific material taken from drill core intersections with Feature A. For the latter experiments, a synthetic groundwater with an ionic strength I ~ 0.17, representing the site specific conditions, was used.

6.4.1 Diffusivity

The effective diffusivities for the different tracers are based on mean values from through diffusion measurements in rock cylinders of Äspö diorite of the 1 and 2 cm lengths. It is observed that D_e decreases with increasing cell lengths used in the experiments, but since the porosity is largest in the vicinity of a natural fracture, the 1 and 2 cm samples may be the most representative (which is a qualified guess, since the Äspö diorite used in the laboratory experiments was fresh and unaltered, which is not the case for the fracture material).

The diffusivity and porosity results from the KXTT1 Feature A site specific diffusion cell show four times lower diffusivity and porosity than for the Äspö diorite, i.e. ($D_e^{HTO} \approx 4 \cdot 10^{-14}$, $\varepsilon \approx 0.001$) and ($D_e^{HTO} \approx 1.2 \cdot 10^{-13}$, $\varepsilon \approx 0.004$) for the site specific material and the Äspö diorite, respectively. An estimation of effective diffusivities based on this single sample would therefore be to reduce the diffusivities for the tracers obtained for Äspö diorite with a factor of three in order to obtain the effective diffusivities of the Feature A site specific material.

D_e for the sorbing tracers have been calculated from the relation

$$D_e^{sorb} = D_w^{sorb} \cdot F \tag{6-2}$$

where the formation factor for Äspö diorite has been calculated according to:

$$F = \frac{D_e^{HTO}}{D_w^{HTO}} = \frac{1.2 \cdot 10^{-13}}{2.4 \cdot 10^{-9}} = 5 \cdot 10^{-5} \tag{6-3}$$

and the formation factor for the TRUE-1 Feature A site specific material has been calculated according to:

$$F = \frac{D_e^{HTO}}{D_w^{HTO}} = \frac{4 \cdot 10^{-13}}{2.4 \cdot 10^{-9}} = 1.7 \cdot 10^{-5} \tag{6-4}$$

where D_w is the diffusivity of the tracer in the water phase (Gray 1972). The estimated diffusivities are presented in Table 6-11.

The diffusivities are valid for water with an ionic strength I < 0.5 and a temperature of 20–25°C. A lowering of the temperature with 10°C would theoretically give approximately 25% lower diffusivities.

Table 6-11. Matrix sorption and diffusion data obtained from through diffusion experiments in rock cylinders of Äspö diorite and TRUE-1 Feature A site specific material.

Tracer	K_d (m^3/kg)	D_w (m^2/s)**	ÄD D_e (m^2/s)***	Feature A D_e (m^2/s)***
HTO	–	$2.4 \cdot 10^{-9}$	$1.2 \cdot 10^{-13}$	$4 \cdot 10^{-14}$
Na^+	$1.4 \cdot 10^{-6}$	$1.33 \cdot 10^{-9}$	$6.7 \cdot 10^{-14}$	$2.2 \cdot 10^{-14}$
Rb^+	$4 \cdot 10^{-4}$*	$2.03 \cdot 10^{-9}$	$1.0 \cdot 10^{-13}$	$3 \cdot 10^{-14}$
Cs^+	$8 \cdot 10^{-4}$****	$2.02 \cdot 10^{-9}$	$1.0 \cdot 10^{-13}$	$3 \cdot 10^{-14}$
Ca^{2+}	$5.2 \cdot 10^{-6}$	$0.79 \cdot 10^{-9}$	$4.0 \cdot 10^{-14}$	$1.3 \cdot 10^{-14}$
Sr^{2+}	$4.7 \cdot 10^{-6}$	$0.79 \cdot 10^{-9}$	$4.0 \cdot 10^{-14}$	$1.3 \cdot 10^{-14}$
Ba^{2+}	$2 \cdot 10^{-4}$****	$0.83 \cdot 10^{-9}$	$4.2 \cdot 10^{-14}$	$1.4 \cdot 10^{-14}$

Data valid for 20–25°C (K_d for 10–30°C), I=0.25 (I=0.17 for TRUE-1 diff. cell) and pH=7.5.
* From $K_{d(2-4mm)}/5$, other K_d are mean values from diffusion experiments.
** Calculated water diffusivities at infinite dilution (Gray 1972)
*** $D_e = F \cdot D_w$, $F = 5 \cdot 10^{-5}$ for the Äspö diorite and $F = 1.7 \cdot 10^{-5}$ for the Feature A site specific material.
**** From penetration depth studies

6.4.2 Distribution coefficients

The results of the batch experiments with crushed site specific material show that the sorption strength is similar to that of the Äspö diorite, cf. Table 6-8. Therefore, the estimations of K_d are based on laboratory experiments on Äspö diorite. Sorption coefficients are dependent on ionic strength and pH. The presented sorption data are reasonably valid for a saline groundwater with I = 0.1–0.4, pH = 7–9 and a temperature of 10–30°C .

K_d for sorption within the rock matrix (related to matrix diffusion), is based on K_d evaluated from through diffusion experiments in rock cylinders of Äspö diorite (Na, Ca and Sr) and the penetration studies of Äspö diorite (Cs and Ba). Since no "diffusion K_d" for Rb is available, the K_d for this elements has been estimated from the K_d measured for the largest particle fraction (2–4 mm) in the batch experiments. These batch K_d values have been divided by a factor of 5, which was the observed relation between the diffusion K_d and batch K_d for Na, Ca and Sr. The estimated K_d values are presented in Table 6-11.

An attempt to estimate surface related sorption coefficients, K_a, has been made. As a base the geometrical area and the BET-surface area of the largest particle size and the geometrical surface area of the injection side of the diffusion cells have been used. However, in a real fracture, the size of the surfaces may vary drastically depending on whether the fracture contains crushed particles, clay minerals etc. K_a values determined from experiments with crushed material often tend to overestimate the surface areas.

Assuming spherical shape of the particles of the solid phase used in the batch experiments, K_d can be described as:

$$K_d = K_{di} + K_a \cdot \frac{6}{\rho \cdot d_p} \qquad (6\text{-}5)$$

where K_{di} is the sorption onto inner surfaces and K_a is the sorption onto the outer surfaces. K_a evaluated from Eq. 6-5 (the slope of a plot of K_d vs. $1/d_p$) and from initial sorption onto the injection side of a diffusion cell (Cs sorption) and the Feature A diffusion cell (Cs, Rb) are presented in Table 6-12. K_a has also been calculated from K_d data for the 2–4 mm fraction after the shortest sorption time (1 d), when the penetration into the rock matrix is small. However, a slight diffusion into the pores may lead to an overestimation of K_a even after this contact time. K_a has also been calculated related to the measured BET-surfaces of the 2–4 mm fractions (Kr-gas adsorption).

A comparison of K_d for the 1–2 mm particle size fraction of Feature A site specific material (mylonite and altered granite) and Äspö diorite is presented in Table 6-13. The 1–2 mm fraction was used for this experiment. The synthetic groundwater that was used had the same composition as the Feature A groundwater. A volume of 8.5 ml of synthetic groundwater was contacted to 2 g of solid material. The K_d-values are obtained from measurements of the losses of tracers in the liquid phase and calculating the K_d from the mass balance. The values presented are given for a contact time of 9 days.

Table 6-12. Selected surface sorption coefficients (K_a) for Äspö diorite and TRUE-1 Feature A site specific material.

Tracer	Crushed material, Geom. surf. 14 days[1] K_a (m)	Diff.cell, geom.surf. 10 days[2] K_a (m)	TRUE-1 diff.-cell, geom.surf. 5 days[2] K_a (m)	Crushed material, geom.surf. 1 day[3] K_a (m)	Crushed material, BET-surf. 14 days[4] K_a (m)
Na^+	$7 \cdot 10^{-7}$			$5 \cdot 10^{-6}$	$2 \cdot 10^{-7}$
Rb^+	$5 \cdot 10^{-4}$		$4 \cdot 10^{-3}$	$1 \cdot 10^{-3}$	$6 \cdot 10^{-5}$
Cs^+	$8 \cdot 10^{-3}$	$9 \cdot 10^{-3}$	$1 \cdot 10^{-2}$	$8 \cdot 10^{-3}$	$5 \cdot 10^{-4}$
Ca^{2+}	$4 \cdot 10^{-6}$			$3 \cdot 10^{-5}$	$3 \cdot 10^{-6}$
Sr^{2+}	$8 \cdot 10^{-6}$			$2 \cdot 10^{-5}$	$4 \cdot 10^{-6}$
Ba^{2+}	$2 \cdot 10^{-4}$			$6 \cdot 10^{-4}$	$4 \cdot 10^{-5}$

Data valid for 10–30°C, I=0.25. (I=0.17 for TRUE-1 diff.cell), and pH=7.5

1) From Eq.6-4, plot of K_d vs. $1/d_p$ for the four largest particle fractions. For Na^+, Ca^{2+} and Sr^{2+} the desorption coefficient has been used while for the other tracers, sorption K_d has been used (see Byegård *et al.* 1998).

2) Initial sorption onto the surface of the injection side of the diffusion cell.

3) From K_d/A_{geom} 2–4 mm particle size. A_{geom}=0.67 m^2/kg.

4) From K_d/A_{BET} 2–4mm particle size. A_{BET}=26 m^2/kg.

In those cases where no value is given the sorption was below the detection limit.

The ion exchange is assumed to be in instantaneous equilibrium, since generally, ion exchange reactions are considered as a kinetically fast reaction. If the transport of the sorbing tracer from the bulk of the groundwater to the fracture surface is slow, this may be interpreted as non-equilibrium in the sorption.

6.4.3 Porosity

The mean porosity for the 1 and 2 cm diffusion cells of Äspö diorite ($\varepsilon = 0.4 \pm 0.1\%$) was evaluated from the experiments with tritiated water, for which the rock capacity factor equals the total porosity. The "diffusion" porosity of the single diffusion cell with site specific material is 0.1%.

Table 6-13. Sorption K_d for the tracers contacted with Äspö diorite, mylonite and altered granite, using TRUE-1 Feature A site-specific conditions. Contact time of 9 days.

Tracer	Äspö-Diorite K_d (m^3/kg)	+/–	Mylonite KXTT2 K_d (m^3/kg)	+/–	Alt. Diorite KXTT3 K_d (m^3/kg)	+/–
Na^+	$< 2.8 \cdot 10^{-5}$		$< 2.2 \cdot 10^{-4}$		$< 6.0 \cdot 10^{-5}$	
Ca^{2+}	$< 4.4 \cdot 10^{-5}$		$< 5.3 \cdot 10^{-4}$		$< 6.3 \cdot 10^{-4}$	
Rb^+	$1.4 \cdot 10^{-3}$	$3.5 \cdot 10^{-4}$	$2.1 \cdot 10^{-3}$	$4.3 \cdot 10^{-4}$	$3.8 \cdot 10^{-4}$	$3.1 \cdot 10^{-4}$
Sr^{2+}	$< 2.3 \cdot 10^{-4}$		$< 2.6 \cdot 10^{-4}$		$< 9.4 \cdot 10^{-5}$	
Cs^+	$1.4 \cdot 10^{-2}$	$1.2 \cdot 10^{-3}$	$8.0 \cdot 10^{-3}$	$5.6 \cdot 10^{-4}$	$3.1 \cdot 10^{-3}$	$2.3 \cdot 10^{-4}$
Ba^{2+}	$1.2 \cdot 10^{-3}$	$1.2 \cdot 10^{-4}$	$1.3 \cdot 10^{-3}$	$1.3 \cdot 10^{-4}$	$1.8 \cdot 10^{-3}$	$1.4 \cdot 10^{-4}$

6.4.4 Recommeded input data for modelling

The selection of a recommended Modelling Input Data Set (MIDS) has been done with due consideration to the increased disturbances in crushed rock used in batch tests, compared to the rock discs used in the through-diffusion experiments. K_d values obtained from diffusion experiments, or alternatively large particle size fractions, should be the most representative for the *in situ* rock matrix, at least for time scales of the TRUE-1 experiments. The results presented in this chapter show that the K_d values evaluated from diffusion experiments using the generic Äspö diorite rock gave the lowest values, even though the generic rock was found to be the most sorptive rock type in the batch tests. The K_d values obtained from the diffusion experiments were selected as the best initial estimate of K_d for modeling purposes. No actual measurements of K_a have been performed. However, for modelling purposes, the estimated K_a values for the various tracers for a 14 day contact time and geometrical surfaces is recommended for modelling purposes, cf. Section 6.4.2 and Table 6-12.

Similarly, a porosity of 0.4% obtained from the through-diffusion experimements on generic Äspö diorite material was selected as a representative porosity for the modelling, cf. Section 6.4.3. These values and associated water diffusivities D_w for relevant tracers are compiled as the MIDS data set presented in Table G-1 in Appendix G.

7 Tracer tests

7.1 Introduction

The original plan for TRUE-1 was to conduct a series of tracer tests with the primary purpose of testing methodology and equipment for later stages of the TRUE Project. The objectives of the TRUE-1 tests were later rephrased to also include tests of sorbing tracers and determination of retention parameters. The original plan included one preliminary tracer test (PTT-1), a series of tracer dilution tests, one radially converging, two dipole tracer tests and a combined diverging-converging test. However, due to the changed objectives, the TRUE-1 tracer tests programme finally came to include 18 different test set-ups, either in radially converging or dipole flow geometry, performed during the time period 1995-1998.

A summary of the performed tests, including flow geometry, flow paths tested and the principal literature references is given in Table 7-1. In total seven flow paths in Feature A and one in Feature B have been tested over distances ranging from 2.6 to 9.6 m between injection and withdrawal points, cf. Figure 7-1.

This chapter includes a description of the tests performed, their objectives, performance and evaluation. A summary of the main results is presented in Section 7.6.

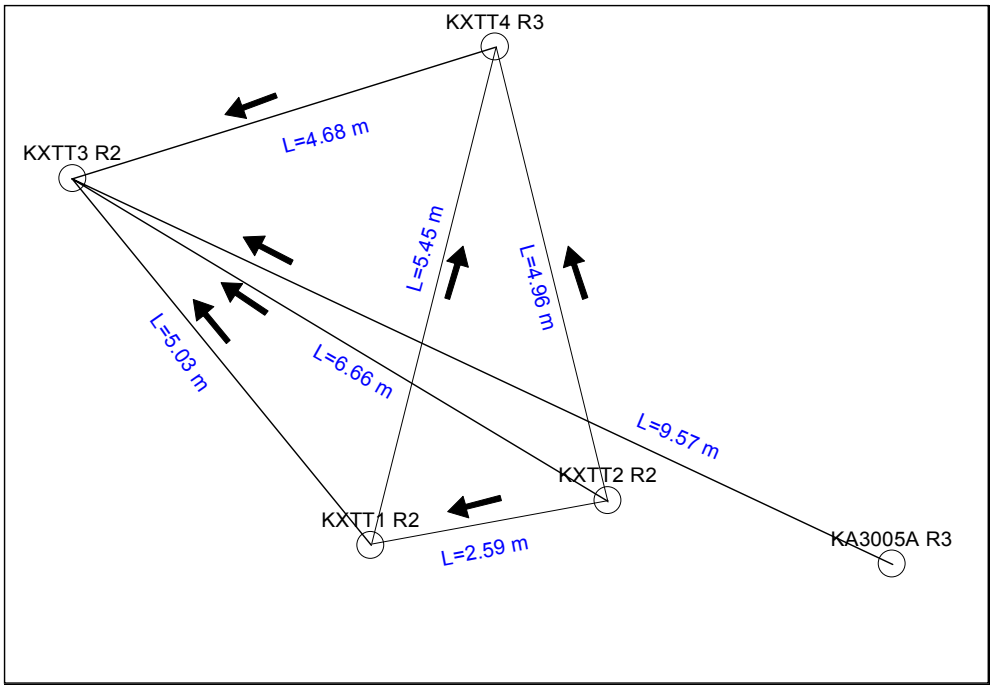

Figure 7-1. *Borehole intersection pattern with Feature A (as seen in the plane of the feature) and test geometries used for the TRUE-1 tracer tests.*

Table 7-1. Summary of tracer tests performed within the TRUE-1 Project.

Test	Flow geometry	Flow path	Mass recovery	Reference
PTT-1	Rad. Conv	T1→ T3 *)	95%	Winberg, 1996
		T3→ T4 **)	92%	
RC-1	Rad. Conv	T1→ T3	93%	Andersson, 1996
		T2→ T3	0	
		T4→ T3	100%	
		KA3005A→ T3	0	
DP-1	Dipole	T1→ T3	88%	Andersson et al., 1997
DP-2	Dipole	T2→ T1	56%	Andersson et al., 1997
DP-3	Dipole	T2→ T1	45%	Andersson et al., 1997
DP-4	Dipole	T2→ T4	30%	Andersson et al., 1997
RC-2	Rad. Conv	T1→ T4	5%	Andersson & Jönsson, 1997
DP-5	Dipole	T4→ T3	28%	Andersson & Jönsson, 1997
DP-6	Dipole	T4→ T3	70%	Andersson & Jönsson, 1997
PDT-1	Rad. Conv	T1→ T3	44%	Andersson and Wass, 1998
		T4→ T3	74%	
PDT-2	Rad. Conv	T1→ T3	52%	Andersson and Wass, 1998
		T4→ T3	99%	
PDT-3	Rad. Conv	T4→ T3	95%	Andersson and Wass, 1998
STT-1	Rad. Conv	T4→ T3	100%	Andersson et al., in press
PDT-4	Rad. Conv	T1→ T3	100%	Andersson et al., 1999a
STT-1b	Rad. Conv	T1→ T3	100%	Andersson et al., 1999a
RC-3	Rad. Conv	T2→ T3	13%	
STT-2	Rad. Conv	T4→ T3	88%	Andersson et al., 1999b

*) Test in Feature A (KXTT4:P3 → KXTT3:P2), cf. Appendix B
**) Test in Feature B (KXTT3:P3 → KXTT4:P4), cf. Appendix B

7.2 Experimental set-ups

7.2.1 Experimental strategy

The basic strategy behind the choice of methodology and equipment for the tracer tests has been to achieve a well-controlled flow field with a minimum of disturbance from the installations and the tracer injection/retrieval procedures. This also includes a minimisation of the volumes in the packed-off borehole intervals by minimising the length of the intervals and by installation of volume reducers (dummies) to reduce the water volume.

The use of radioactive sorbing tracers has further enhanced the need for choosing equipment materials which do not interact with the tracers. Therefore, a special test was done to check possible interactions between tracers and equipment materials (Ittner and Byegård, 1997). The choice of materials used in the injection/retrieval systems has been of particularly great importance for the sorbing tracer tests.

Each borehole in the TRUE-1 array is instrumented with 4–5 inflatable packers such that 4–5 borehole sections are isolated. All isolated borehole sections are connected to the Äspö HRL Hydro Monitoring System (HMS) (Almén and Stenberg, in prep) through data loggers. Each of the sections used as injection or sampling section are equipped with three nylon hoses, two with an inner diameter of 4 mm and one with an inner diameter of 2 mm. The two 4 mm hoses are used for injection, sampling and circulation of fluid in the borehole section, whereas the 2 mm hose is used for pressure monitoring.

The borehole sections in Feature A are also equipped with volume reducers (dummies) and a perforated tube, cf. Andersson (1996). The perforated tube and dummies are important prerequisites to achieve a complete and fast homogenisation of the tracer solution once added to the system. The volume reduction of the system, including tubing, due to the dummies is about 40% for a 1 m section length and 60% for a 2 m section.

7.2.2 Injection equipment and methodology

The equipment for injection of tracers was originally constructed for injection of a small concentrated volume of tracer required to be instantly homogenised in the borehole section. The tracer should subsequently be introduced into the fracture by the flow induced by pumping in the withdrawal borehole. After performing the first major test, RC-1 (Andersson, 1996), it stood clear that this procedure introduced a large tailing in the breakthrough curve due to the low flow rates in the injection sections. This tailing has two major disadvantages, that the time of the experiment become very long and that the tailing potentially can mask important transport processes. It was

therefore decided to include a means of ending the injection and creating a finite pulse injection for the planned tests with sorbing tracers.

A schematic drawing of the tracer injection equipment used in the tracer tests with sorbing tracers is shown in Figure 7-2. The basic idea is to create an internal circulation of the borehole fluid in the injection borehole. The circulation makes it possible to obtain homogeneous tracer concentration inside the borehole and to sample the tracer concentration outside the borehole in order to monitor the dilution of the tracer with time. The configuration of packers, dummy materials and infiltration tubes in a section equipped for circulation is shown in Appendix F.

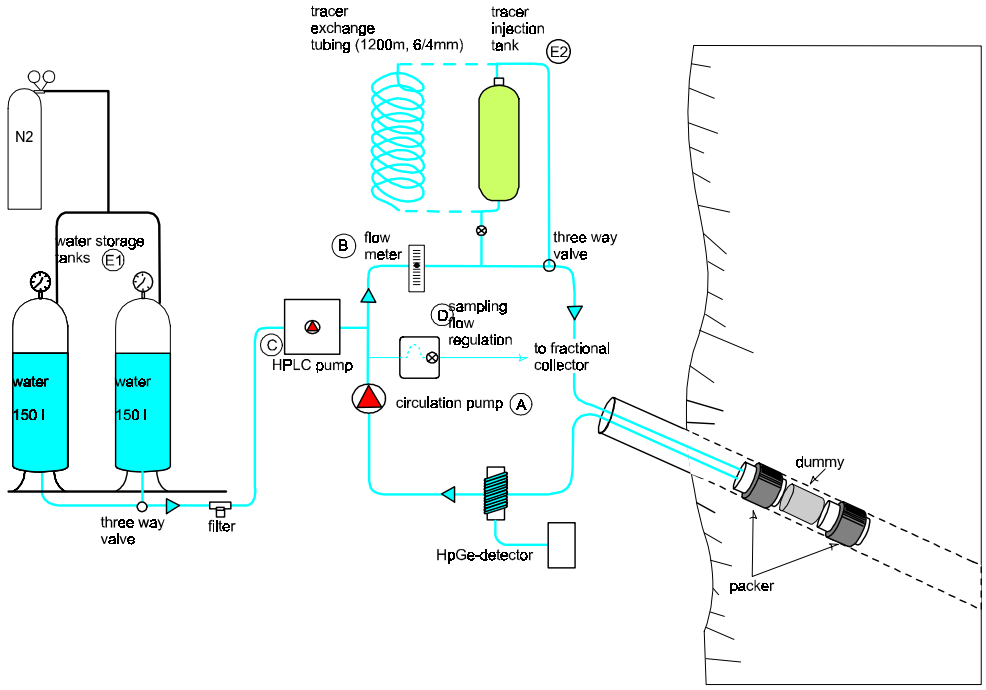

Figure 7-2. *Schematic drawing of the injection system for the TRUE-1 tracer tests with sorbing tracers.*

Circulation is controlled by a pump with variable speed (A) and measured by a flow meter (B). Tracer injections are made either directly into the circulating loop with a HPLC plunger pump (C) or by switching a three-way valve so that the circulating water passes through a stainless steel vessel (E2) filled with tracer solution. Thus, unlabelled water from the circulation loop enters the bottom of the vessel and tracer labelled water enters the circulation loop from the top of the vessel. The three-way valve is then switched back again after replacing the volume of the vessel. The tracer solution in the circulation loop can also be replaced with unlabelled water by switching the three-way valve so that the circulating water passes through a long (1200 m) tube filled with unlabelled water. Tracer solution then enters from one side of the tube and unlabelled water enters the circulation loop from the other side of the tube, thus completing the exchange.

The tracer concentration in the injection loop is measured both *in situ* (radioactive tracers) and by sampling and subsequent analysis. The sampling is made by continuously extracting a small volume of water from the system through a flow controller (constant leak) to a fractional sampler (D). The *in situ* monitoring of the radioactive tracer content (activity) in the injection system is made by using a HPGe-detector measuring in line on the tubing.

Water from Feature A is used for injection of water in the dipole tests and for the tracer exchange is stored in a separate pressurised vessel (E2) under nitrogen atmosphere. Further details about the equipment is given in Andersson, (1996).

Table 7-2 compiles the data on injection flow rates and injections volumes relevant to the three injection sections employed for the TRUE-1 tests with sorbing tracers, ie. STT-1, STT-1b and STT-2.

Table 7-2. Compilation of data on volumes of injection sections and injection flow rates for tests STT-1, STT-1b and STT-2.

Test	Borehole section, cf. Appendix B	Volume including injection loop (ml)	Injection time interval (hrs)	Injection flow rate for Uranine (ml/h)
STT-1	KXTT4:R3	2154	0–4	36.0
			10–70	42.3
			70–200	33.0
STT-1b	KXTT2:R2	1999	0–4	41.9
			20–151	58.1
STT-2	KXTT4:R3	2154	0–4	86.2
			25–310	28.8

7.2.3 Conclusions regarding injection methodology

The main advantage of the injection methodology applied in TRUE-1 is that no excess pressure is created during the injection that may force tracer out into the fracture in an unknown geometry creating a fictive dispersion in the system. Another advantage is that the circulating system allows continuous measurement of the input concentration (source term). It could be argued that it would have been even better to measure the input concentration within the borehole section, as close as possible to the fracture intersection, but it is difficult and expensive to construct a system that allows down-hole measurements of 10 different tracers as used in eg. in STT-1b. The high pressures and salinity of the Äspö water also limit the possibility to use down-hole equipment, especially over longer time scales (months-years).

The injection equipment has generally worked well. The main problem has been associated with the exchange procedure where tracer solution is replaced with unlabelled water. The exchange generally seemed to be efficient directly after

completion (>99% reduction) but after a few minutes the tracer concentration started to increase again creating a second "hump" in the injection curve, cf. Figures 7-4 and 7-5. The injection system was constructed to achieve a fast and good homogenisation of the tracer solution in the borehole section through the dummies and perforated tube described above, cf. Appendix F. However, the perforations of the tube was made by drilling holes with sizes varying according to the pressure drop in the tube at a certain rate of circulation. Some of these holes were very narrow and given the long duration of the tests it is likely that mineral precipitates may have been formed around the holes limiting the flow. Thus, "pockets" of more or less stagnant water are assumed to have occurred in the borehole section from which concentrated tracer solution has diffused back into the unlabelled water volume.

The time schedule of the project did not allow a modification of the design of the down-hole system that could improve the exchange procedure for the final tests with sorbing tracers. For the next stage of detailed experiments, TRUE-2, the down-hole mixing has to be adapted to allow a more efficient exchange of the tracer solution where excessive tailing caused by the input function is avoided.

7.2.4 Sampling equipment and methodology

The sampling system is based on the same principle as the injection system, namely a circulating system with a circulation pump and a flow meter, cf. Figure 7-3. In this case however, water is withdrawn from the borehole with a constant flow rate by means of a flow regulation unit. This unit consists of a mass flow meter coupled to a motorised valve enabling a fast and accurate flow regulation.

The sampling is made with two independent systems, a "constant leak" system producing samples (same as in the injection loop) integrated over a given time interval (typically 5–100 minutes) and a 24-valve sampling unit producing discrete samples.

After sampling, the pumped water is led through a nylon vessel where the water is degassed. The reason for this is that measurements of dye tracer content is made by an in line field fluorometer. As fluorometry is an optical method, gas bubbles have to be removed in advance, otherwise they will create a fictive background content of the dye tracer. The degassed water is pumped from the degassing vessel through the field fluorometer and further through an electrical conductivity probe and a redox probe.

The sampling methodology and equipment has been improved in steps throughout the experimental sequence. The first experiments did not include in line measurements and the redox probe was added at a later stage. In the last of the TRUE-1 experiments, STT-2, in line measurements of the input function of radioactive tracers was also included.

7.2.5 Conclusions regarding the sampling methodology

The sampling methodology with three separate systems, discrete samples, time averaged samples and in line detection has been shown to work well with minor modifications along the chain of experiments. All three systems have their advantages and weaknesses, listed in Table 7-3, but if possible, it is recommended that all three are used simultaneously.

7.3 Tracers and analysis methods used

7.3.1 Conservative tracers

The TRUE-1 Project has not included any specific development of new conservative tracers, although the first major experiment, RC-1, included a test of different tracers to assess whether they are truly conservative or not. The choice of candidate tracers relied

Table 7-3. Sampling system used in TRUE-1 tracer experiments, advantages and weaknesses.

System	Advantages	Weaknesses
Discrete sampling	Correct time, any size of sample possible	Leakage in sampling valve may destroy samples, sensitive to bacterial growth and precipitates
Time averaged sampling (Constant leak)	Very reliable	Delay in tubing, smoothing of concentration peaks
In line detection	Direct control *in situ* or at remote place through data modem.	Long term drift, discrete samples still needed for check and calibration

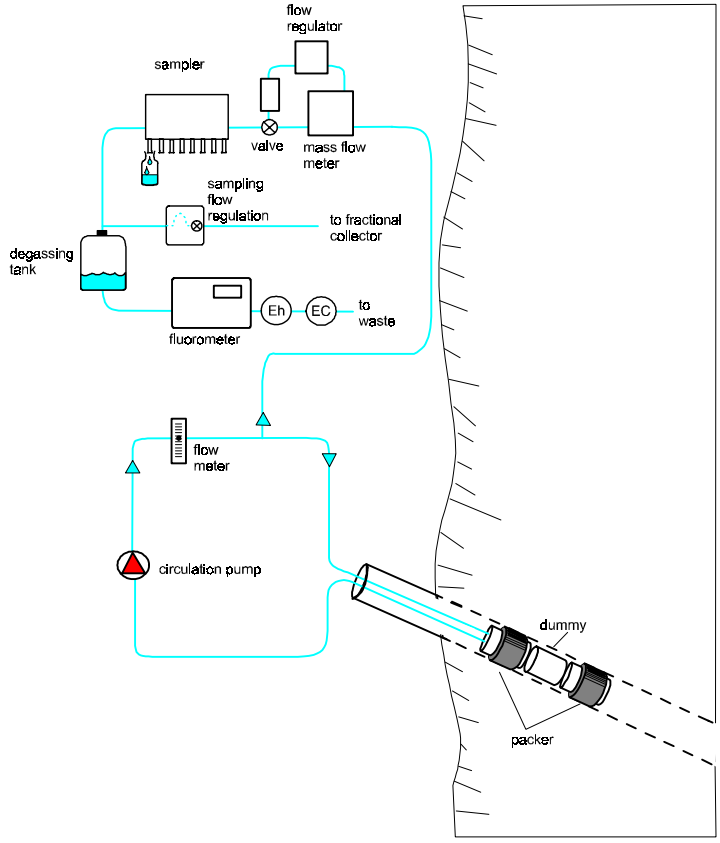

Figure 7-3. *Schematic drawing of the sampling system for the TRUE-1 tracer tests with sorbing tracers.*

on experience from previously performed tracer tests in Swedish crystalline bedrock such as the Stripa Project, the Fracture Zone Project in Finnsjön and the LPT-2 experiment at Äspö HRL. A literature compilation made by Andersson (1995) also helped to identify possible tracers.

The eleven different conservative tracers used (Table 7-4) included a variety of different types; dyes, metal complexes, ions, where the latter also are radioactive. The fluorescent dye Uranine has been used in almost all of the tests and can be viewed as a reference conservative tracer. The main reason for choosing Uranine is the good dynamic range, defined as the span between the maximum possible concentration (solubility in water) and minimum detectability. Other good qualities of Uranine are low price, low analysis costs and possibility to use in line detection. In cases were more than one conservative tracer has been injected in the same flow path (RC-1, STT-1, STT-1b and STT-2), Uranine has given the highest mass recovery among the conservative tracers, although the difference in most cases has been small.

The fluorescent dyes were analysed both in line, using a field fluorometer, and in discrete samples at the laboratory. Samples containing radioactive tracers were

Table 7-4. Conservative tracers used during the TRUE-1 tracer experiments.

Tracer	Type	Experiments (cf. Table 7-1)
Uranine	Fluorescent dye	All except DP-2, DP-4, DP-5
Amino G Acid	Fluorescent dye	RC-1, DP-2, DP-4, DP-5, PDT-1, PDT-2
Rhodamine WT	Fluorescent dye	RC-1
Eosin Y	Fluorescent dye	RC-1
Gd-DTPA	Metal complex	RC-1, DP-1
Eu-DTPA	Metal complex	RC-1
Ho-DTPA	Metal complex	RC-1
Tb-DTPA	Metal complex	RC-1
HTO (Tritium)	Radioactive	PDT-3, STT-1, STT-1b, STT-2
Br-82	Radioactive ion	PDT-3, STT-1b, STT-2
I-131	Radioactive ion	STT-1b, STT-2

analysed on a laboratory fluorometer at the SKB operated radiochemical laboratory BASLAB, while non-radioactive samples were analysed at GEOSIGMA, Uppsala, on a spectrofluorometer. The laboratory analyses are regarded as very accurate, whereas the in line measurements are somewhat disturbed by degassing and iron precipitation. As fluorometry is an optical method, the water should preferably be free from gas bubbles and particles but, in practise, this is very difficult with the Äspö water. Degassing and iron precipitation inevitably occurs on the low pressure side of the pumping. These problems can be partly solved by installation of a degassing tank and filters, but a small drift in the measurement could still be detected possibly due to precipitates forming in the flow-through measurement cell.

The metal complexes were analysed at the SGAB laboratory in Luleå using ICP-MS (Induced Coupled Plasma Mass Spectrometry). The analysis method normally allows measurements of very low concentrations (ppt level), but the samples needed to be diluted, due to the high salinity of the Äspö waters, which increased the detection limit with an order of magnitude. The metal complexes injected during RC-1 showed significantly lower mass recovery than the fluorescent dyes. This can be explained by precipitation of Fe in the sampling bottles. A second injection of Gd-DTPA during DP-1 showed no significant difference from Uranine after acidification of the samples.

Table 7-5. Sorbing tracers used during TRUE-1 tracer tests.

Tracer	Isotope, half life	Experiments (cf. Table 7-1)
Na^+	^{22}Na, $t_{½}$ = 2.6 y	STT-1, STT-1b, STT-2
	^{24}Na, $t_{½}$ = 15 h	PDT-3
K^+	^{42}K, $t_{½}$ = 12.4 h	STT-1b
Rb^+	^{86}Rb, $t_{½}$ = 18.7 d	STT-1, STT-1b, STT-2
Cs^+	^{134}Cs, $t_{½}$ = 2.1 y	STT-2
	^{137}Cs, $t_{½}$ = 30 y	STT-1
Ca^{2+}	^{47}Ca, $t_{½}$ = 4.5 d	STT-1, STT-2
Co^{2+}	^{58}Co, $t_{½}$ = 71.3 d	STT-1b
Sr^{2+}	^{85}Sr, $t_{½}$ = 65 d	STT-1, STT-1b, STT-2
Ba^{2+}	^{131}Ba, $t_{½}$ = 11.7 d	STT-2
	^{133}Ba, $t_{½}$ = 10.4 y	STT-1, STT-2
TcO_4^-	^{99m}Tc, $t_{½}$ = 6.01 h	STT-1b

In the later stages of TRUE-1, a mix of radioactive tracers was used, where three conservative tracers were injected (Table 7-4). All three gave similar breakthrough curves as Uranine although slightly lower recovery. For HTO a small delay compared to Uranine could be noticed in all tests. The analysis methods are described in Section 7.3.2.

7.3.2 Sorbing tracers

The selection of sorbing tracers for TRUE-1 is based on a literature survey by Byegård (1993). He concluded that the best concept to study the sorption capacity of fractures in dynamic experiments would be to use tracers that will sorb by cation exchange. Thus, a number of monovalent and divalent cations were selected, cf. Table 7-5. In addition, the anion TcO_4^- was injected in STT-1b. The main reason for this was to confirm earlier field results (Andersson et al., 1993) that the mobile oxidised form of Tc (TcO_4^-) is reduced to TcO_2, which is believed to be strongly sorbing.

The handling of the radioactive tracers required special arrangements at the TRUE-1 site in order to minimise the risk for radioactive contamination of personnel and equipment. The site was fenced in and the injection equipment (exposed to high radiation) was separated from the sampling equipment (exposed to low radiation) by using two separate steel containers. The containers were specially designed to enable easy sanitation in case of a leak or a spill.

The activity of the different gamma emitting radioactive tracers were measured both by in line measurements using a HPGe detector with a Multi-Channel Analyser (MCA) to enable simultaneous measurement of all tracers and with a similar stationary HPGe detector and MCA at BASLAB. The accuracy of the measurements is governed by the counting time for each sample and the half-life of the tracer. Therefore, short-lived tracers like ^{24}Na, ^{42}K and ^{99m}Tc show relatively high analysis errors even for the fast flow path tested in Feature A.

The HTO samples were measured by Liquid Scintillation at BASLAB. The method gives high accuracy.

7.4 Tracer breakthrough interpretation

7.4.1 Qualitative interpretation

The first step in the interpretation of tracer breakthrough data during TRUE-1 was to examine the data qualitatively by plotting the breakthrough curves, cf. Section 7.6. The plot usually revealed measurement errors that led to an immediate removal of erroneous data points. The plot may also reveal influence of a varying injection function, or variations in the pumping rate in the withdrawal borehole, which need to be accounted for in the evaluation.

Co-plotting of both tracer injection and tracer breakthrough vs. time, respectively, has been found to be especially valuable in interpreting the data. In order to directly compare the data, they need to be normalised either by dividing with the total injected amount of tracer, or by dividing with the maximum concentration during injection (Figure 7-4). These co-plots together with the removal of erroneous data points help identifying experimental problems that need to be checked before doing any deeper analysis of the data, including numerical modelling. Thus, this check is an important part of the quality assurance before releasing the data to different modelling groups.

Another important part of the qualitative interpretation is to check and list events in the vicinity of the experimental site that may influence the transport of tracer such as changes in the hydraulic pressure, or in the water chemistry. This part of the interpretation also includes determination of tracer mass recovery, which also serves as an important quality check of the data. This is further discussed in Section 7.4.5.

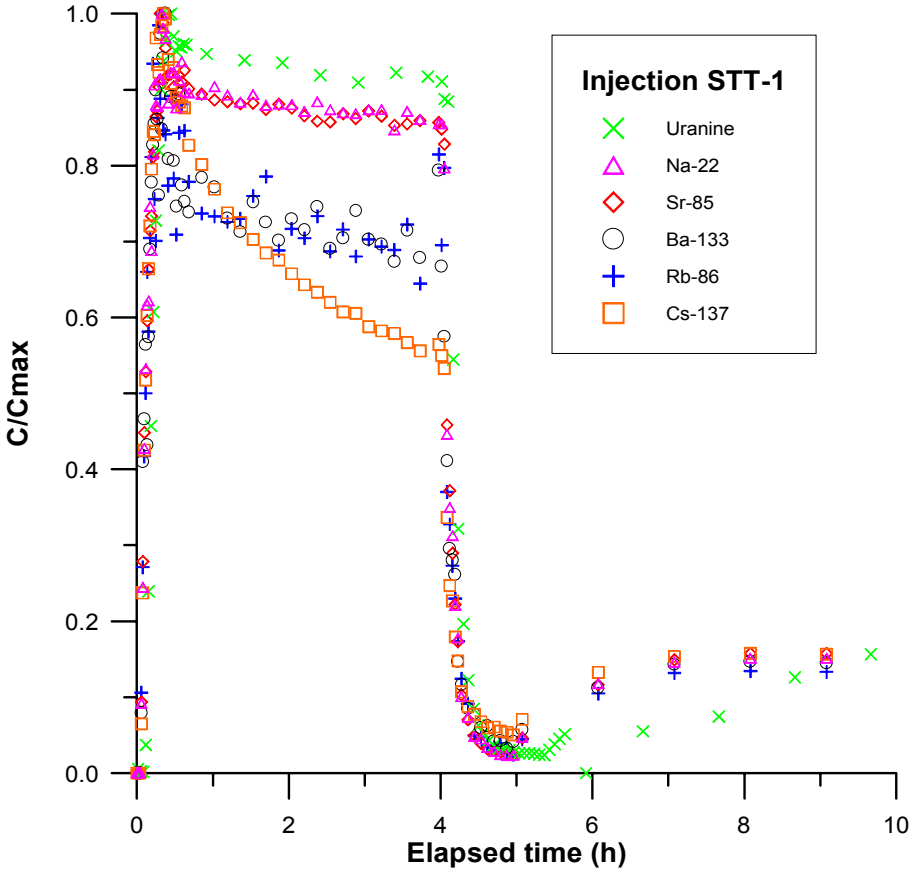

Figure 7-4. *Tracer injection concentrations (activities) normalised to maximum measured concentration (activity) in the injection section KXTT4:R3 during the first 10 hours of injection of STT-1.*

7.4.2 Numerical modelling using a homogeneous approach

The numerical modelling and interpretation of the TRUE-1 tracer experiments have involved several different models and concepts ranging from simple one-dimensional homogeneous models to two-dimensional stochastic continuum approaches. The tests have also been subject to blind predictions and evaluations by the Äspö Task Force on Modelling of Groundwater Flow and Transport of Solutes where a large number of modelling concepts have been applied. Reports describing the analysis of the RC-1 and DP-1 to DP-4 are available, cf. Dershowitz et al. 1996, Tanaka et al. (1997), Gylling et al. (1998), Liedke and Shao (1998), Poteri and Hautojärvi (1998) and Worraker et al. (1998). An evaluation of the above modelling making up Äspö Task Force Tasks 4C and 4D is presented by Elert (1999).

This section describes the "basic" modelling of the tracer tests performed by the project team. A further developed evaluation concept applicable to the evaluation of the tests with sorbing tracers is described in Chapter 8. The breakthrough curves from all radially converging TRUE-1 experiments were first evaluated using the simplest possible approach, namely the one-dimensional advection-dispersion equation. In the

case of sorbing tracers linear sorption was also added (for example Van Genuchten and Alves, 1982):

$$R\frac{\partial C}{\partial t} = -v\frac{\partial C}{\partial l} + D_l\frac{\partial^2 C}{\partial l^2} \qquad (7\text{-}1)$$

Where, t is time (s), l is distance along flow path (m), v is the average water velocity along flow path (m/s), C is the solute concentration, D is the dispersion coefficient (m^2/s), and R is the retardation coefficient (for sorbing tracers).

This "basic" evaluation was also complemented by a similar homogeneous two-dimensional approach for the dipole tests using the hybrid finite difference finite-element code SUTRA (Voss, 1984).

Both these homogeneous approaches simulated variable tracer input concentration by superimposing solutions of the above equations. The measured tracer input concentrations were discretised into time intervals, where each time interval was assigned a constant input concentration. The applied models were used to estimate parameters using an automated parameter estimation program, PAREST (Nordqvist, 1994). The program uses non-linear least squares regression where the best-fit parameters are derived by an iterative procedure.

For the sorbing tracer runs the most interesting parameter to estimate is the retardation factor for the various sorbing tracers. This was accomplished by using two breakthrough curves simultaneously in the regression procedure. One of the tracers was then considered conservative, while the retardation factor for the other tracer relative to the first one could be determined.

The parameters which were estimated in this case were the average velocity (v), dispersion coefficient (D), the retardation factor (R), and two proportionality factors (f and f_c). The factor f represents the dilution caused by the flow field, while the factor f_c simply is the inlet concentration of the retarded solute relative to the conservative one. Whether these factors are estimated or considered known (from measurements) is a subjective choice of the interpreter. In this particular case it was decided to estimate the proportionality factors, and check whether the values appeared reasonable when compared to independent measurements of pumping rates and input concentrations.

Another concern when using multiple data sets for regression is that magnitudes of the dependent variable may differ considerably. In this case, this is handled by using a reliability weight matrix. Each observation was assigned a weight reflecting the analytical uncertainty of the tracer sample. Standard deviations of the laboratory samples of the nuclides were obtained based on the measurement time in the laboratory, while the Uranine measurements were assigned an error of one percent of the value down to the detection limit. All nuclide observations were assigned weights as the inverse of the variance (standard deviation squared), while the weights for the Uranine samples were assumed to be the inverse of the assumed error.

A summary of the main results of the numerical modelling is presented in Section 7.6.

7.4.3 Numerical modelling using stochastic continuum approach

In addition, a two-dimensional stochastic continuum approach was applied (Cvetkovic et al., in prep.) where multiple realisations of the transmissivity field were generated using Monte Carlo simulation. Both unconditioned fields and fields conditioned on measured transmissivity and steady-state heads were used. A mixed hybrid finite element method (Mosé et al., 1994) was used to solve the steady-state flow problem and transport was modelled using particle tracking.

In this concept no pore scale dispersion was included. The only spreading mechanisms incorporated are the spatially variable velocity and the spreading due to the input distribution of tracer.

This approach was used both for scoping and design purposes and for interpretation of the breakthrough curves, cf. Chapter 8.

7.4.4 Simplified analytical interpretation

Besides the parameters determined from the numerical models some additional flow and transport parameters were calculated using simplified analytical expressions. The reason for this was mainly to provide a means of comparing the results between the different tests and also to provide comparison to other similar performed tracer tests where these parameters often are calculated. The assumptions forming the base for deriving parameters like homogeneity, steady-state conditions, etc are often questioned, especially in the case of fracture flow, but they still provide some averaged parameters which can be used for comparisons.

The following parameters were determined for almost all TRUE-1 tracer tests (cf. e.g. Andersson et al, 1999:

- Tracer travel times, t_5, t_{50} and t_{95}, defined as times when 5, 50 and 95% of the recovered mass had arrived, based on injected mass at t_{inj}. The Äspö Task Force modelling teams used these parameters as performance measures.

- Fracture conductivity, K_{fr} (m/s), assuming radial flow and validity of Darcy's law. Calculated based on the mean travel times, t_m, determined from the parameter estimation of the conservative tracers (Gustafsson & Klockars, 1981). See also Winberg, 1996) for derivation.

- Equivalent fracture aperture (transport aperture), $2b$ (m)

- Flow porosity, θ_k (estimated as $\theta_k = K/K_{fr}$), where K is the steady state hydraulic conductivity for the packed-off section containing Feature A. It should be acknowledged that the term flow porosity may be misleading to use for discrete fracture, as it is defined for a porous media. However, it is often used in fractured media as a scaling factor for transport, but then defined over a finite thickness which, in his case, is defined as the length of the packed-off borehole section in the pumping well.

The calculated values for the above parameters are discussed in Section 7.6.

7.4.5 Tracer recovery

The mass recovery of tracer is the best indicator of the level of control of a tracer experiment. Several of the TRUE-1 tracer experiments have shown low mass recovery, indicating mass losses, cf. Section 7.6. If the tracer is truly conservative and the sampling continues long enough such losses must be attributed to the natural gradient and the associated background flow.

Tracer mass recovery was calculated in two different ways for the tracers detected in the pumping section. Common for both methods is that the tracer mass recovered in the pumping borehole was determined by integration of the breakthrough curves for mass flux. The injected mass was determined in the same way but also by weighing and measuring the concentration of the tracer solution removed from the injection section during the exchange procedure and calculating the difference with the known mass added to the stock solution (mass balance).

The mass recovery calculated from integration is in general more accurate than the measured ones. The reason for this is that the injected mass only represents a small portion of the total mass in the stock solution, especially in the tests with a finite pulse injection. Hence, a relatively large uncertainty can be expected in the determination of injected mass from weighing. The uncertainty in the integrated values is dependent on the determination of the injection flow rate, which may be measured quite accurately in the case of a forced injection (dipole). In the case of a radially converging flow, the flow has to be evaluated from the dilution of the tracer in the injection interval. For a finite pulse injection, most of the mass is injected during a short period where relatively few samples can be taken. This generally results in a very uncertain determination of the flow rate for this period. Instead, the period after the finite pulse, when only a minor portion of the total mass is left in the borehole, was used for evaluation, see Figure 7-5.

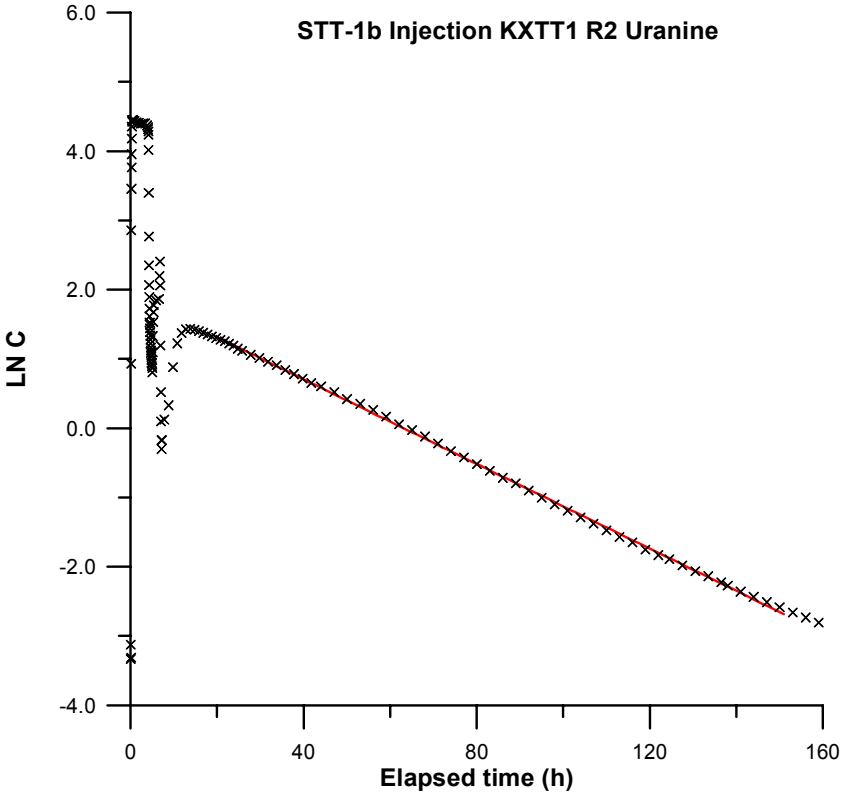

Figure 7-5. *Tracer injection concentration (lnC) versus elapsed time, t (h), for Uranine in the injection section KXTT1:R2 during the first 160 hours of injection in STT-1b.*

7.5 Supporting data

7.5.1 Hydraulic head

The hydraulic head in Feature A has been monitored in all five intersecting boreholes with pressure transducers connected to the Äspö HMS system. The system allows plotting of the hydraulic head and changes in the scanning frequency from a remote position. This has been particularly important for the long-term tracer tests like STT-1, STT-1b and STT-2 where checks of the integrity of the borehole installations as well as indications of other pressure disturbing activities were important to identify.

The measurements have shown that the TRUE-1 site is well connected to the eastern part of the Äspö HRL and that pressure disturbances in this area affects all sections in the TRUE-1 array in a similar way. This implies that the hydraulic gradient within Feature A is relatively constant during each tracer experiment although it may vary somewhat over the years. This is further discussed in Section 5.8.

7.5.2 Water chemistry

The water chemistry at the TRUE-1 site has been checked at several occasions during the project, cf. Table 5-10. Water from Feature A has been sampled within the regular monitoring program at Äspö twice a year and in conjunction with the different tracer tests. In addition a thorough sampling of all boreholes in the TRUE-1 array was performed before the start of the tracer experiments, cf. Section 5.11.1 and Appendix E. In addition samples have been collected from the pumped section att different before the onset of experiments, cf. Table 5-10, to capture changes in water composition over time.

In addition to the sampling, monitoring of electrical conductivity of the water from the sampling borehole has been done during all performed tracer experiments. This has been particularly useful as an indicator of changes in the water chemistry. In most experiments the electrical conductivity has been constant over the pumping period but there is one exception. From the start of PDT-3 until the end of STT-1b (June 1997 to May 1998) a rather dramatic lowering of the electrical conductivity occurred from about 1550 mS/m down to 1150 mS/m (Figure 7-6). In May 1998 the flow rate was changed from 0.4 l/min to 0.2 l/min before start of STT-2. The drop in salinity of the water then seems to stabilise at 1150 mS/m.

This drop in salinity is well correlated to the head drop noted in all boreholes in the TRUE-1 area (cf. Section 5.8) and the lowering of inflow to the tunnel in the TRUE-1 area.

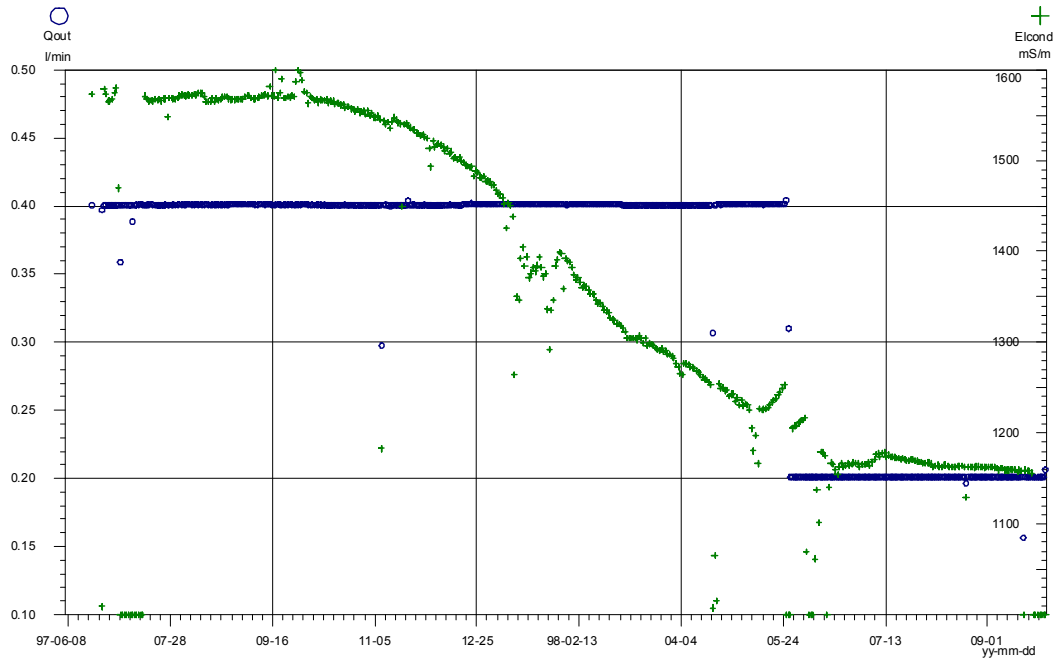

Figure 7-6. *Electrical conductivity (green) and flow rate (blue) of water pumped from KXTT3:R2 during STT-1, STT-1b and STT-2, June 1997 to October 1998.*

7.6 Summary of main results

7.6.1 Flow and non-reactive transport

In total seven different flow paths have been tested within Feature A (cf. Figure 7-1). Tables 7-6 and 7-7 summarise the parameters determined for the two main flow paths tested, KXTT1:R2 → KXTT3:R2 (7 tracer runs) and KXTT4:R3 → KXTT3:R2 (8 tracer runs). The additional five flow paths tested are listed in Table 7-8.

The flow path KXTT1:R2 → KXTT3:R2 has been investigated in seven tracer runs with pumping rates varying between 0.1 to 0.87 l/min. An example set of breakthrough curves from the test STT-1b is shown in Figure 7-7. The results of the tests reveal the following:

Table 7-6. Summary of flow and transport parameters determined for the flow path KXTT1:R2 → KXTT3:R2 (distance 5.03 m).

Test*	Q (l/min)	Δh (m)	R (%)	D/v (m)	K_{fr} (m/s)	$2b$ (m)	θ_k
PTT-1	0.87	24	95	(0.6)***	$3.5\cdot10^{-4}$	$1.4\cdot10^{-3}$	$1.0\cdot10^{-3}$
RC-1	0.2 (0.4)**	2.5 (5.6)**	93	0.24	$5.0\cdot10^{-4}$	$2.2\cdot10^{-3}$	$0.7\cdot10^{-3}$
DP-1	0.1	5.8	88	0.40	$2.8\cdot10^{-4}$	–	$1.2\cdot10^{-3}$
PDT-1	0.1	0.6	44	1.3	$11\cdot10^{-4}$	$2.1\cdot10^{-3}$	$0.4\cdot10^{-3}$
PDT-2	0.2	1.9	52	1.0	$5.6\cdot10^{-4}$	$2.6\cdot10^{-3}$	$0.7\cdot10^{-3}$
PDT-4	0.4	9.3	100	–	–	–	–
STT-1b	0.4	9.3–12.8	100	0.55	$1.8\cdot10^{-4}$	$1.8\cdot10^{-3}$	$1.1\cdot10^{-3}$

* See Tables 7-1, 7-4 and 7-5
** Pumping increased during experiment
*** Uncertain due to transport in equipment

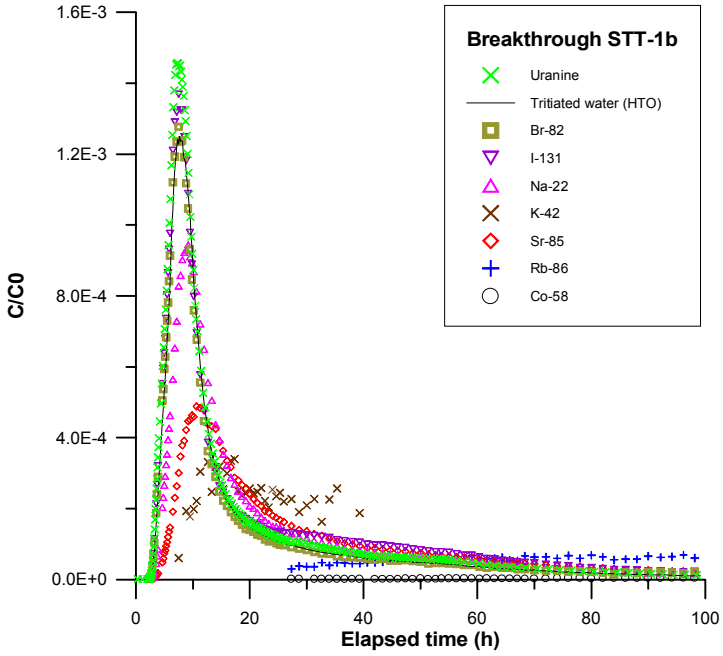

Figure 7-7. *Tracer breakthrough after 100 hours in the pumping section KXTT3:R2 during STT-1b. Concentrations are normalised to concentrations in the injection section at t=2 hours.*

Table 7-7. Summary of flow and transport parameters determined for the flow path KXTT4:R3 → KXTT3:R2 (distance 4.68 m).

Test$^{\Delta}$	Q (l/min)	Δh (m)	R (%)	D/v (m)	K_{fr} (m/s)	b (m)	θ_k
RC-1	0.2 (0.4)$^{++}$	2.8 (6.9)$^{++}$	100	1.6	$7.1\cdot10^{-4}$	$1.4\cdot10^{-3}$	$0.5\cdot10^{-3}$
DP-5	0.1	3.0	28	0.34	$2.0\cdot10^{-4}$	$1.6\cdot10^{-3}$	$0.5\cdot10^{-3}$
DP-6	0.2	3.6	70	0.48	$4.1\cdot10^{-4}$	$2.4\cdot10^{-3}$	$0.4\cdot10^{-3}$
PDT-1	0.1	1.0	74	0.6	$6.4\cdot10^{-4}$	$2.1\cdot10^{-3}$	$0.5\cdot10^{-3}$
PDT-2	0.2	2.3	99	1.1	$5.9\cdot10^{-4}$	$2.0\cdot10^{-3}$	$0.6\cdot10^{-3}$
PDT-3	0.4	6.8	95	1.7	$4.8\cdot10^{-4}$	$1.7\cdot10^{-3}$	$0.7\cdot10^{-3}$
STT-1	0.4	7.2–10.5	100	2.0	$4.2\cdot10^{-4}$	$1.4\cdot10^{-3}$	$0.8\cdot10^{-3}$
STT-2	0.2	5.6–8	88	0.35*	$3.4\cdot10^{-4*}$	$1.3\cdot10^{-3*}$	$1.1\cdot10^{-3*}$
STT-2				0.46**	$1.0\cdot10^{-4**}$	$4.5\cdot10^{-3**}$	$4.0\cdot10^{-3**}$

$^{\Delta}$ See Tables 7-1, 7-4 and 7-5
$^{++}$ Pumping increased during experiment
* Flow path #1
** Flow path #2

- The lowest possible pumping rate to control the flow field in this flow path is around 0.2 l/min as indicated by the tracer mass recovery.

- The influence of the natural gradient has changed over the years as indicated both by hydraulic head measurements and by the difference in mass recovery between RC-1 and PDT-2.

- The dispersivity seems to increase and other calculated parameters deviate when the mass recovery is poor.

- All calculated parameters vary within a factor of 2 to 3 between the different tests if the tests which are showing low mass recovery are omitted.

The flow path KXTT4:R3 → KXTT3:R2 has been investigated in eight tracer runs with pumping rates varying between 0.1 to 0.4 l/min. An example set of breakthrough curves for this flow path is shown in Figure 7-8 from STT-1 (Q=0.4 l/min) and in Figure 7-9 from STT-2 (Q=0.2 l/min). The results of the tests are similar to the ones given for the injection in KXTT1:R2, i.e., low recovery for low pumping rates, lower recovery for dipole flow fields and very similar transport parameters. The one notable exception is that the converging tests show a higher dispersivity. One possible explanation for this observation may be that there are two water conducting fractures in the injection interval with similar transport properties, cf. Figure 7-10. The detailed flow logging, cf. Figure 5-1 and the borehole TV imaging (BIPS) logging also support this conclusion.

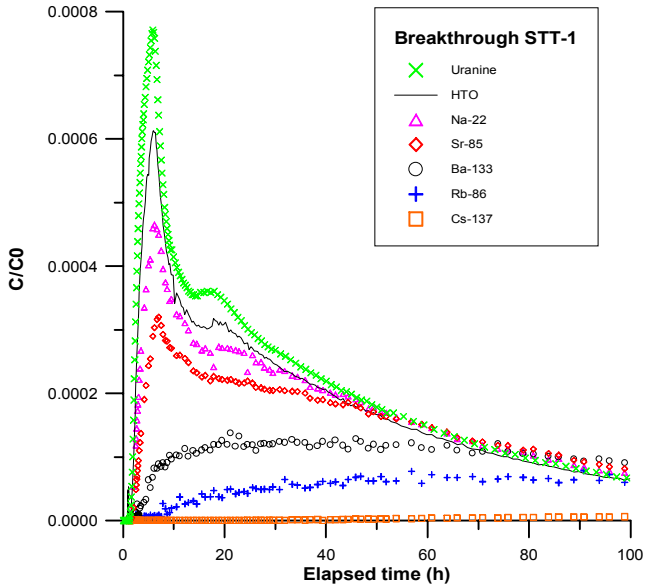

Figure 7-8. *Tracer breakthrough after 100 hours in the pumping section KXTT3:R2 during STT-1. Tracer concentrations are normalised to concentration in injection section at t=4 hours.*

In the case of STT-2 a dual peak breakthrough is observed which is in parity with the previously noted high dispersivity. Transport in the case of STT-1 is assumed to occur in both fractures noted the injection section, both finally connecting to the pumping section, but one of them being the dominating one, and both having the same transport properties. In the case of STT-2, the lowered pump rate in combination with changed boundary conditions, cf. Section 5.8, is assumed to have resulted in a separation of the two flow paths in terms of transport times as reflected in the dual-peak breakthrough curve.

Elert (in prep) analysed the deconvoluted berakthrough curves from STT2 and concluded that the double peak in the response function is not an effect of the injection function. This provide additional support for the hypothesis that the observed double peak can be attributed to a dual flow path.

Table 7-8. Summary of flow and transport parameters determined for the five less tested flow paths (distances varying between 2.59 to 9.57 m).

Test*	Q (l/min)	Δh (m)	R (%)	D/v (m)	K_{fr} (m/s)	$2b$ (m)	θ_k
Flow path	**KXTT2 R2→**	**KXTT3 R2**	**L=6.66 m**				
RC-1	0.2 (0.4)**	0.9 (1.7)**	0 (36)**	–	–	–	–
RC-3	0.4	2.2	13	–	–	–	–
Flow path	**3005A R3→**	**KXTT3 R2**	**L=9.57 m**				
RC-1	0.2 (0.4)**	2.8 (6.4)**	0 (0)***	–	–	–	–
Flow path	**KXTT2 R2→**	**KXTT1 R2**	**L=2.59 m**				
DP-2	0.036	58	56	0.36	$2.2\cdot10^{-4}$	–	$1.1\cdot10^{-3}$
DP-3	0.036	50	45	0.32	$2.5\cdot10^{-4}$	–	$0.9\cdot10^{-3}$
Flow path	**KXTT2 R2→**	**KXTT4 R3**	**L=4.96 m**				
DP-4	0.052	26	30	0.20	$2.2\cdot10^{-4}$	–	$0.8\cdot10^{-3}$
Flow path	**KXTT1 R2→**	**KXTT4 R3**	**L=5.45 m**				
RC-2	0.1	27	5	0.9	$5.0\cdot10^{-6}$	$3.4\cdot10^{-3}$	$4.9\cdot10^{-3}$

* See Tables 7-1 and 7-4
** Pumping increased during experiment
*** Tracer breakthrough detected when KXTT3:R2 was completely opened.

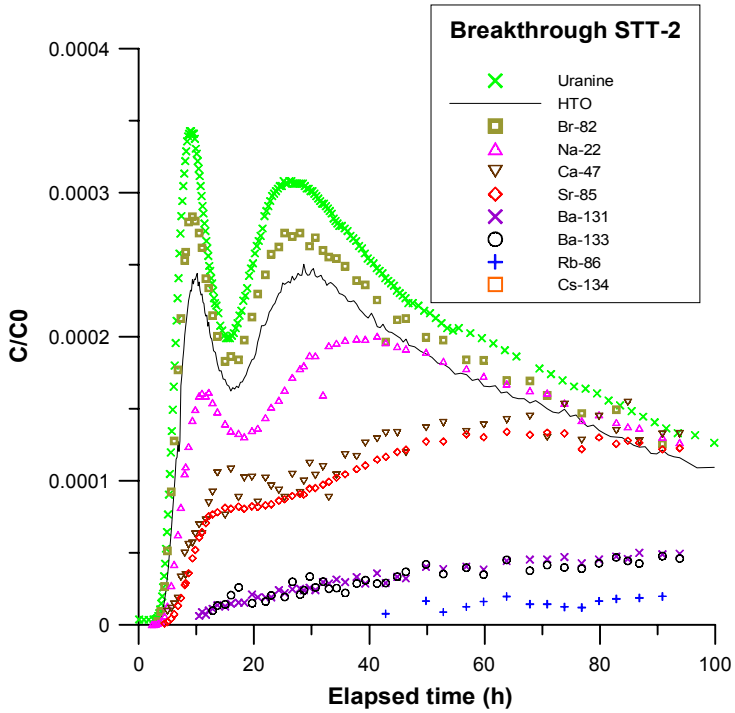

Figure 7-9. *Tracer breakthrough after 100 hours in the pumping section KXTT3:R2 during STT-2. Tracer concentrations are normalised to concentration in injection section at t=2 hrs.*

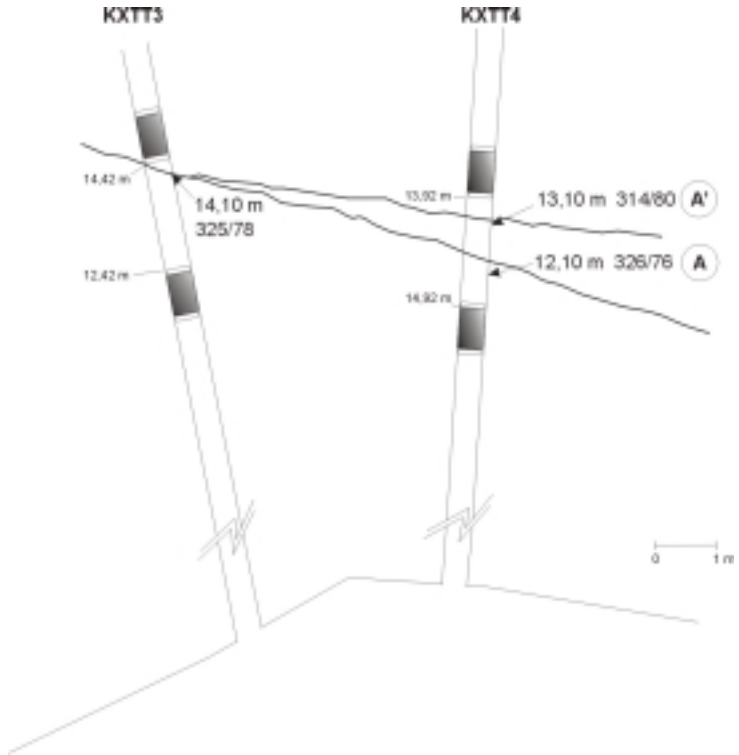

Figure 7-10. *Detailed conceptual model of geometry of flow path between sections KXTT4:R3 and KXTT3:R2.*

The tests performed in other flow paths in Feature A (Table 7-8) generally resulted in low mass recovery, possibly due to less well controlled flow fields. The tests were not fully evaluated due to the low recovery but the parameters determined are still similar to those obtained for the two main flow paths, with the exception of flow path KXTT1:R2 → KXTT4:R3. However, the mass recovery for this flow path was only 5% and the calculated parameters should therefore be considered as uncertain.

Based on the outcome of the tracer tests with conservative tracers the following conclusions may be drawn regarding Feature A:

- The feature is connected over the entire area covered by the boreholes (about 6 m (vertical) x 10 m (lateral))
- The magnitude of the natural gradient in Feature A makes it difficult to perform tests over longer distance than 5 m and with low pumping rates (< 0.2 l/min).
- Dipole flow geometry is difficult to use for the same reason, but also due to the relatively large differences in local transmissivity between the different intercepts.
- Only two flow paths have been identified where high tracer recovery and reasonable tracer travel times can be achieved; KXTT1:R2 → KXTT3:R2 and KXTT4:R3 → KXTT3:R2
- The flow path KXTT4:R3 → KXTT3:R2 has an unnaturally high dispersivity (1.6 m). The reason may be that there are two flowing intercepts with Feature A in KXTT4. The detailed flow log also supports this conclusion, cf. Figure 5-1. The results of STT-2 are interpreted to show a separation of the two flow paths in terms of transport time caused by the reduced flow rate in combination with changes in boundary conditions.
- The measurements of the tracer injection flow rates during the performed radially converging tracer tests show a non-linear dependence to the pumping rate. In general, the portion of flow through the injection sections increases as the pumping rate is increased. This may indicate that the flow path changes in width or is less influenced by the natural gradient as the pumping rate increases.

7.6.2 Reactive transport

The two main flow paths in Feature A have also been tested with radioactive sorbing tracers (STT-1 (STT-1b) and STT-2) at a pumping rate of 0.4 and 0.2 l/min, respectively, in KXTT3:R2. The tests have been evaluated by the project team using both by a simple one-dimensional homogeneous approach and by employing a Lagrangian stochastic advection-reaction framework. The latter is described in Chapter 8. Blind predictions and evaluation of the performed tests with sorbing tests are also being provided by the Äspö Task Force on Modelling of Groundwater Flow and Transport of Solutes (Ström, 1998, Morosini, 1999).

A compliation of breakthrough characteristics related to the performed tests are presented in Table 7-9. Table 7-10 presents calculated tracer recovery for the performed experiments with sorbing tracers.

The results of the qualitative and simplified evaluation of the breakthrough of the sorbing tracers performed by the TRUE project team are:

- Tracer breakthrough has been obtained for eight weakly to moderately sorbing cations namely Na^+, K^+, Rb^+, Cs^+, Ca^{2+}, Co^{2+}, Sr^{2+} and Ba^{2+}.

- High mass recovery (<100%) was obtained for the weakly sorbing tracers Na, Ca and Sr, whereas the most strongly sorbing tracer (Cs) gave a low recovery (<40%).

- No breakthrough was obtained for TcO_4^- indicating reduction to the strongly sorbing TcO_2.

- The attempts to make the injection pulse finite, cf. Section 7.2.2, have not succeeded in full. As a result, the breakthrough curves of the majority of experiment exhibit a tailing associated with the tailing in the injection function, cf. Figure 7-11. This makes identification and quantification of retention processes difficult (eg. McKenna, 1999). Measures will be taken to eliminate this problem for future detailed scale experiments.

- The simple homogeneous model with linear surface sorption can only be made to fit reasonably well for Na and Sr. The linear retardation coefficients were found to be higher than those derived from laboratory values.

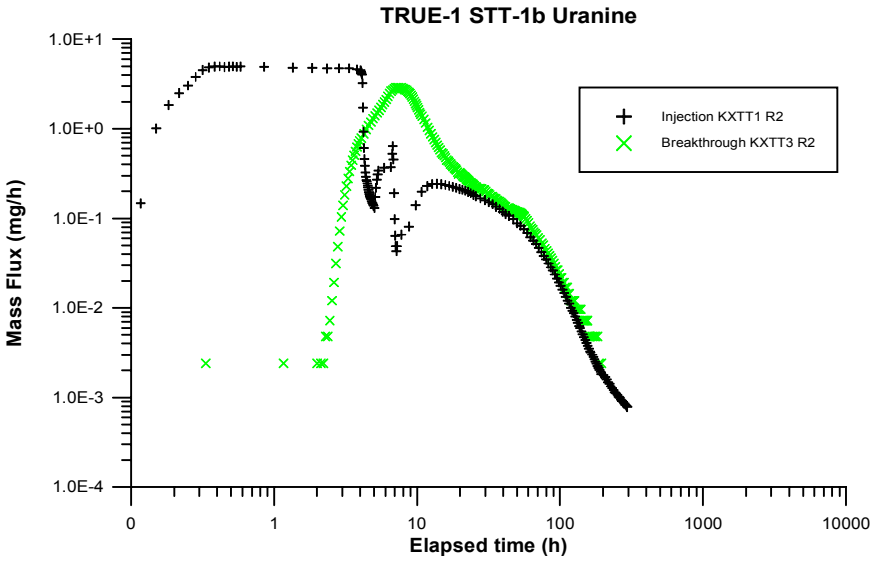

Figure 7-11. *Example from STT-1b showing masking of late time breakthrough by the injection function.*

- The observed drop in salinity, cf. Table 5-10, and especially the drop in Ca^{2+} concentration from ~1700 mg/l at the beginning of STT-1 to ~1000 mg/l at the end of STT-2 may have increased the sorption and thereby the retardation of the sorbing tracers, since ionic strength is an important parameter for ion-exchangeably sorbing tracers (Andersson et al., 1982). For an ideal ion exchange behaviour, K_d for a cation of valence 2+ is inversely proportional to the Ca concentration, whereby at a maximum a 70% increase in K_d could be expected due to the changed water chemistry (Byegård et al.,1995). Alternatively, an increase in retardation in STT-2 may be explained by non-equilibrium in the surface sorption in the preceding experiments, STT-1 and STT-1b, due to the higher flow rate employed.

Table 7-9. Tracer travel times, t_{peak} and $t_{50\%}$, and corresponding retardation ratios, R_{peak} and $R_{50\%}$,, in STT-1 and STT-1b. In STT-2, $t_{5\%}$ was used instead of t_{peak} to calculate the retardation ratio, $R_{5\%}$, due to the double peaks observed in this experiment (from Johansson et al., in press).

	STT-1				***STT-1b***				***STT-2***			
Tracer	t_{peak} (h)	$t_{50\%}$ (h)	R_{peak}	$R_{50\%}$	t_{peak} (h)	$t_{50\%}$ (h)	R_{peak}	$R_{50\%}$	$t_{5\%}$ (h)	$t_{50\%}$ (h)	$R_{5\%}$	$R_{50\%}$
Uranine	5.8	36	1	1	7.3	10.9	1	1	11.2	79	1	1
HTO	6.1	41	1.05	1.1	7.6	11.8	1.04	1.1	13.5	91	1.2	1.15
$^{22}Na^{+}$	6.2	50	1.07	1.4	9.1	16.7	1.2	1.5	18.8	120	1.7	1.5
$^{42}K^{+}$	–	–	–	–	~14	–	1.9	–	–	–	–	–
$^{47}Ca^{2+}$	~7	n.e.	1.2	n.e.	–	–	–	–	26	150	2.3	1.9
$^{58}Co(II)$	–	–	–	–	~260	2300*	36	300*	–	–	–	–
$^{82}Br^{-}$	–	–	–	–	7.5	12	1.03	1.1	12.3	86	1.1	1.1
$^{85}Sr^{2+}$	7.0	64	1.2	1.8	10.7	35	1.5	3.2	31	190	2.7	2.4
$^{86}Rb^{+}$	~60	330	10	9	~75	220	10	20	160	550*	14	15*
$^{99m}TcO_4^{-}$	n.b.o	n.b.o	n.b.o	n.b.o	n.b.o	n.b.o	n.b.o	n.b.o	n.b.o	n.b.o	n.b.o	n.b.o
$^{131}I^{-}$	–	–	–	–	7.5	16	1.03	1.5	–	–	–	–
$^{131}Ba^{2+}$	–	–	–	–	–	–	–	–	84	920	7.5	12
$^{133}Ba^{2+}$	~36	190	6	5	–	–	–	–	82	950	7.4	12
$^{134}Cs^{+}$	–	–	–	–	–	–	–	–	1500	n.e.	130	n.e.
$^{137}Cs^{+}$	~400	3500*	70	230*	–	–	–	–	–	–	–	–

n.b.o. = no breakthrough observed; n.e. = not evaluated; – = not used

t_{peak}: time at which peak concentration was reached.

$t_{5\%}$: time at which 5% of the tracer was recovered.

$t_{50\%}$: time at which 50% of the tracer was recovered.

R_{peak}: peak retardation ratio, i.e. peak travel time ratio between sorbing tracer and uranine.

$R_{50\%}$: "50% retardation ratio", i.e. the ratio of time at which 50% of the tracer was recovered compared with uranine.

* $t_{25\%}$ and $R_{25\%}$ is given for $^{134,137}Cs$, ^{58}Co and ^{86}Rb in STT-2. $t_{25\%}$ for uranine was 15.3h in STT-1, 7.6h in STT-1b and 37h in STT-2.

Table 7-10. Tracer mass recoveries, R_i, in the STT-1, STT-1b and STT-2 experiments, based on integration of injection and breakthrough curves multiplied by injection flow rate and pumping flow rate, respectively. Time given in parenthesis is the integration time (from Johansson et al., in press).

Tracer	STT-1 R_i (%)	STT-1b R_i (%)	STT-2 R_i (%)
Uranine (Na-fluorescein)	100 (360 h)	100 (195 h)	88 (885 h)
HTO (H^3HO, tritiated water)	96 (360 h)	94 (333 h)	83 (640 h)
$^{22}Na^+$	97 (1242 h)	96 (1292 h)	83 (3078 h)
$^{42}K^+$	-	n.e.	-
$^{47}Ca^{2+}$	(97) (132 h)	-	(97) (456 h)
$^{58}Co(II)$	-	29 (3622 h)	-
$^{82}Br^-$	-	88 (82 h)	85 (234 h)
$^{85}Sr^{2+}$	98 (960 h)	82 (505 h)	79 (3078 h)
$^{86}Rb^+$	64 (527 h)	79 (553 h)	49 (1322 h)
$^{99m}TcO_4^-$	-	n.b.o.	n.b.o.
$^{131}I^-$	-	90 (172 h)	-
$^{131}Ba^{2+}$	-	-	56 (1130 h)
$^{133}Ba^{2+}$	87 (1350 h)	-	66 (3078 h)
$^{134}Cs^+$	-	-	11 (3078 h)
$^{137}Cs^+$	33 (7005 h)	-	-

n.b.o. = no breakthrough observed; n.e. = not evaluated; - = not used

8 Evaluation of tests with sorbing tracers

8.1 Introduction

The objective of this evaluation is to provide a consistent interpretation of the measured breakthrough curves (BTC) for all tracers in TRUE-1 tests. A comprehensive description of the theory, evaluation procedure and results is given in Cvetkovic et al. (in prep.). Preliminary results on the STT-1 tracer tests were presented in Cvetkovic et al. (1998b).

Independent model predictions and evaluations of the TRUE-1 experiments using a wide range of model concepts and codes are performed within the context of work performed by the international Äspö Task Force on Modelling of Groundwater Flow and Transport of Solutes (Ström, 1998, Morosini, 1999). The SKB TRUE Project team has in this context provided the available site characterisation data, developed conceptual and geometrical models and experimental premises and breakthrough data.

8.2 Hypotheses and modelling approach

For the purpose of evaluating the TRUE-1 sorbing tracer breakthrough data, we adopt the following hypotheses:

- The Lagrangian Stochastic Advection-Reaction (LaSAR) framework (Cvetkovic et al., 1999) is applicable for evaluating TRUE-1 tracer test data.

- The relationship between the two flow dependent parameters which influence diffusive mass transfer, τ [T] and β [TL^{-1}], cf. Section 8.3, can be approximated as deterministic and *linear.*

- Due to the fact that rock is heterogeneous with respect to mineralogical and physical properties, *in situ* retention parameters for Feature A (e.g., porosity, diffusivity, sorption coefficients) may differ from the "modelling input data set" (abbreviated MIDS and given in Table G-1) used for predictions.

There are essentially two modelling approaches we may take in order to capture the diffusive mass transfer of TRUE-1 tests: (a) viewing the flow path as a *porous medium*; (b) viewing the flow path as an *open fracture*.

In the model type (a), the conceptual picture is one of a porous medium consisting of porous aggregates of different sizes into which the tracer diffuses and sorbs. Thus the mobile water and immobile water (in the porous aggregates) are both assumed present in a Representative Elementary Volume (REV) whereby the mobile and immobile regions of the flow are overlapping continua. The aggregates may be assumed to be of different forms (slabs, spheres, cubes), however, their actual form is not critical for the analysis. The special case of this model is the first-order kinetic sorption model which can be directly related to the models for diffusion into aggregates (e.g., Haggerty and Gorelick, 1995; Carrera et al. 1998). The models of type (a) have been used for transport in aquifers (e.g., Cvetkovic and Dagan 1994; Haggerty and Gorelick, 1995;), soils (Haggerty and Gorelick, 1998), as well as in fractured zones (e.g., Neretnieks and Rasmuson, 1984).

In approach (b), the flow path takes place in an open (heterogeneous) fracture where diffusive mass transfer takes place across the flow path boundary, in particular, across its contact area with the rock matrix. Thus, we have two distinct continua (the mobile phase in the fracture and immobile phase in the rock matrix), whereby one REV is applicable to the fracture and one to the rock matrix; the common assumption is that the rock matrix as unlimited (infinitely large). Models of type (b) have been used extensively for transport in crystalline rock fractures (e.g., Neretnieks, 1980, 1983; Neretnieks et al. 1982; Cvetkovic, 1991).

The modelling approach of the TRUE-modelling team is to utilise essentially both models, however, the *dominant* (or primary) kinetic effects[1)] are to be interpreted with the type (b) model (*open fracture*). This is for several reasons. First, model (b) is intuitive and more consistent with how flow and transport in crystalline fractures is perceived; hence the wide use of this model in earlier studies of transport in rock fractures. Second, model (b) will enable us to assess the effect of fracture aperture variability on the mass transfer; fracture surfaces are known to be highly heterogeneous and the influence of this heterogeneity on tracer retention is an important unresolved issue, in particular for performance and safety assessment (PA/SA). The secondary kinetic effects are interpreted with type (a) model as first-order linear kinetic sorption and are attributed to finer gouge material.

8.3 Evaluation framework

Flow and tracer transport in fractured rock takes place predominantly along distinct conductive features, which in crystalline rocks coincide with fractures, or fracture zones. Feature A is perceived as a planar fracture, i.e., a void bounded by the rock matrix, the surface of which varies in space, cf. Figure 8-1. The opening of the fracture

[1)] In the present context, "kinetic effects" refer to any type of "non-ideal" behaviour of the breakthrough curves in the sense of Brusseau and Rao (1989), where "ideal" behaviour implies transport with pure hydrodynamical dispersion and equilibrium sorption. Thus "kinetic effects" (which in the general case imply enhanced tailing as well as retention) can be due to physical processes (e.g., diffusion) and/or chemical kinetics. Note that "ideal" behaviour cannot be quantified *in situ* due to diffusion.

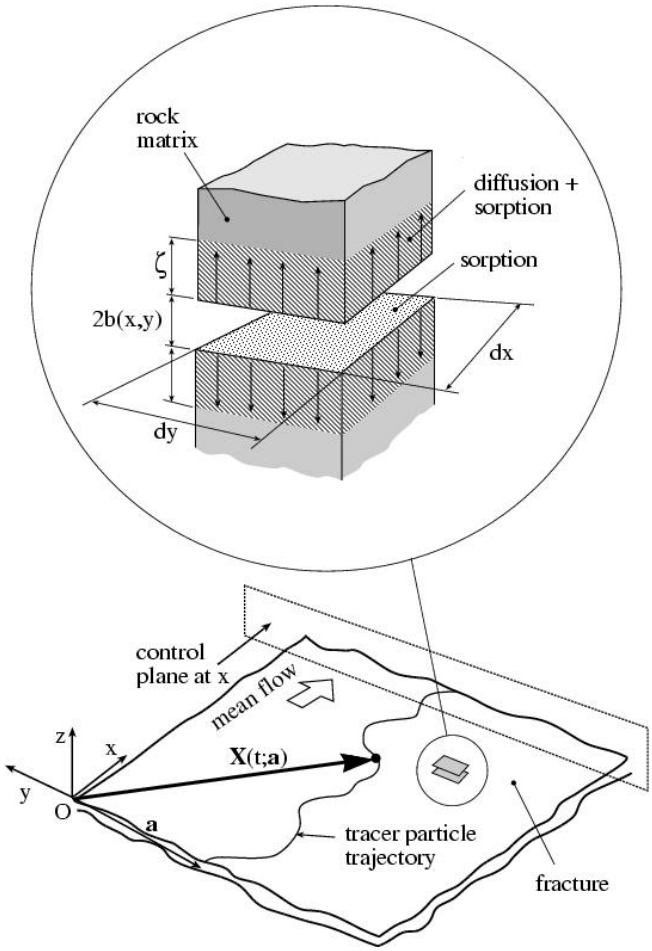

Figure 8-1. *Schematic of a cross section perpendicular to the plane of Feature A.*

(aperture) varies from point to point in the fracture plane, resulting in a two-dimensional heterogeneous flow field, cf. Figure 8-1. A tracer injected in a borehole within Feature A is advected and dispersed, and is subject to various mass transfer reactions. In particular, a tracer diffuses into the rock matrix and (if reactive) sorbs on internal surfaces of the rock; gouge (infilling) material of varying fraction may be present and enhance sorption, i.e. retention.

A Lagrangian stochastic advection-reaction (here abbreviated as LaSAR) framework for reactive transport in rock fractures is presented in Cvetkovic et al. (1999); this framework extends our earlier results (Selroos and Cvetkovic, 1996; Cvetkovic and Dagan, 1994; Cvetkovic et al., 1998a). The LaSAR approach is based on the type (b) model discussed above (*open fracture*) and generalises earlier models of the same type (e.g., Neretnieks, 1980, 1983; Cvetkovic 1991).

The *key assumptions* of the LaSAR model can be summarised as follows:

- All mass transfer reactions are linear.
- The movement of tracers in the rock matrix is assumed to be due to molecular diffusion only, i.e. advection in the matrix is neglected.
- Diffusion is one-dimensional from the fracture into the rock matrix, where transverse fluxes (i.e. diffusive fluxes parallel to the fracture plane) are neglected.
- The mass flux in the fracture is due to advection only.
- Fully mixed conditions prevail in the fracture, in the direction orthogonal to the fracture plane.

Solving the system of coupled transport equations for a single trajectory, a new parameter, β [TL^{-1}], was derived; β is a random quantity integrating the inverse of the velocity-weighted variable aperture along a flow path; we may also refer to β as the "water residence time per unit half-aperture *b*". The parameter β controls surface sorption and diffusion/sorption into the rock matrix, and is related to the flow field. This result enables us to directly account for the effect of flow heterogeneity on the mass transfer reactions. A particular effect that can be accounted for is one of a limited diffusion zone within the rock matrix. In this evaluation stage, however, we simplified the analysis by neglecting the effect of a finite diffusion zone in the rock matrix.

All mass transfer reactions considered in Cvetkovic et al. (1999) are assumed linear whereby the coupled effect is obtained by convolution. In particular, solutions for individual mass transfer processes for pulse injection are convoluted with the input (tracer discharge vs. time) in the injection borehole. To account for dispersive effects, the convoluted result for a single flow path is integrated over different flow paths described by a distribution of τ and β, where τ is the water residence time of a non-reactive (conservative) tracer . The parameters τ and β have been shown to be significantly correlated both for generic conditions (Cvetkovic et al., 1999), and also for the flow conditions of Feature A (Cvetkovic et al., in prep.). Based on these results, we establish an approximate linear (deterministic) relationship between τ and β using Monte Carlo simulations; the coefficient of proportionality for a linear relationship between τ and β corresponds to the "flow-wetted surface per unit volume of water" (Andersson et al., 1998). We note however that generic simulations over a relatively wide range of aperture variability have shown that the relationship between τ and β is non-linear, in form of a power law (Cvetkovic et al., 1999).

The water residence time distribution $g(\tau)$ (that accounts for dispersion effects due to advection variability) is determined from Monte Carlo simulations. However, it is not possible to determine $g(\tau)$ for the single realisation in the field with accuracy sufficient for discriminating mass transfer processes. Hence, $g(\tau)$ will need to be determined from field observations. $g(\tau)$ is contained in the breakthrough curves (abbreviated BTC) of tritiated water (HTO) and Uranine, and is obtained through calibration and deconvolution of the measured HTO breakthrough curves.

8.4 Processes and key parameters

The following five coupled processes have been considered in the evaluation:

1) **Advection along random flow paths** – The key parameters are the mean and variance of the water residence time distribution ($\bar{\tau}$ [T], σ_τ^2 [T^2]), both of which are calibrated using the non-reactive (conservative) tracer breakthrough curve (HTO). An additional flow-dependent parameter k [L^{-1}] in the relationship $\beta=k\tau$, is determined through a combination of calibration of conservative tracer breakthrough with Monte Carlo simulations[2)] of particle transport in equi-probable realisations of Feature A. Note that the quantities τ (water residence time) and β [$L^{-1}T$] are dependent on the *in situ* flow conditions and by definition cannot be determined in the laboratory.

The Monte Carlo simulations of particle transport in Feature A indicate an approximate relationship between τ and β as $\beta = k_0 \tau$ (reflected in the second hypothesis) where $k_0 \approx 3400$ m^{-1} . The value $k_0 \approx 3400$ m^{-1} was obtained by correlating τ and β over all streamlines (from the injection to the detection boreholes) from (almost) all 100 realisations; we defined this as a "representative" value of k (denoted as k_0). Note that $k_0 \approx 3400$ m^{-1} has not been obtained solely on the basis of the hydraulic test data; $k_0 \approx 3400$ m^{-1} incorporates the "transport" aperture which was calibrated using the non-reactive tracer test data. The deviations in k between different (equi-probable) realisations are significant and $k_0 \approx 3400$ m^{-1} is one of the possible mean values. In other words, due to the spatial variability in fracture transmissivity (aperture), the geometry of the flow path is uncertain and can vary significantly from realisation to realisation, implying that larger or smaller values of k relative to k_0, may, from the hydraulic point of view, be applicable for Feature A.

2) **Surface sorption** is assumed linear and equilibrium. The key parameter is the surface sorption distribution coefficient K_a [L].

K_a is the distribution coefficient for the fracture surface. Using $\beta = k_0 \tau$, we can write the parameter group for surface sorption as $K_a k_o \tau$ (Cvetkovic et al., 1999). Since

---

[2)] A self-calibrating simulation algorithm (Gomez-Hernandez et al., 1997) was used to generate 2D transmissivity fields conditional to both transmissivity and head measurements. The method was previously used for predictions of non-reactive tracer tests RC-1 and DP1-DP4 (Selroos and Cvetkovic, 1998). A Total of 100 equally probable transmissivity fields were generated with $T=10^Y$ where $\langle Y \rangle = -6.9$ and $\sigma_Y^2 = 0.66$ (T is obtained in unit [m^2 /s]). The "cubic law" then yields an arithmetic mean "hydraulic" aperture of 0.06 mm, under the assumption that both T and aperture 2b are log-normally distributed. Transmissivity values were multiplied by a factor 3000 in order for the simulated "ensemble" mean advective travel times to be consistent with observed HTO mean residence time; this yields a calibrated mean aperture of 0.9 mm (factor $14.4 \approx 3000^{1/3}$), which is referred to as the "transport" aperture. Dirichlet boundary conditions are postulated as the constant, steady-state head value which is an average of the linear hear variation prior to pumping. The domain is 20x20m with discretisation of 0.4 m in both directions. The flow is solved using MODFLOW (1994), and non-reactive transport using a particle tracking algorithm as proposed by Mose et al. (1994). The cubic law is assumed to be valid locally (i.e., over each element). The parameters β and τ are obtained by integration along particle trajectories, following definitions presented in Appendix G.

measured BTCs indicate strong kinetic effects attributed to diffusion, we anticipate a comparatively small effect of surface sorption.

3) **Diffusion/sorption into the "matrix"** (rim zone) where sorption is assumed linear and equilibrium. The key parameter group following Cvetkovic et al. (1999) is $\beta\kappa$ for diffusion/sorption in the rock matrix. The diffusion parameter $\kappa = \theta[D(1+\rho K_d^m/\theta)]^{1/2} = \theta(DR_m)^{1/2}$ where θ [–] is the porosity of the rock matrix (note that we do not distinguish the "total porosity" from the "diffusion porosity"), D [L^2T^{-1}] is the pore diffusivity in the rock matrix ($D_e=\theta D$) is the effective diffusion coefficient in the rock matrix; the "formation factor" F is defined as $F = D_e/D_w$, where D_w is the diffusivity in water) and K_d^m [L^3M^{-1}] is the sorption coefficient in the rock matrix.

In Table G-1 of Appendix G we summarise the "Modelling Input Data Set" (MIDS) for K_a and κ determined in the laboratory, cf. Section 6.4.4, on intact (unaltered) Äspö diorite using through-diffusion tests, for all tracers which have been used in the evaluation.

4) **Diffusion into stagnant water zones** – Here we approximate all water adjacent to the flow path as stagnant (which is an exaggeration), while neglecting the possibility of "stagnant islands" within the flow path. The controlling parameter is $\kappa_w=(D_w)^{1/2}$. Values of D_w for all tracers are given in Table G-1.

5) **Sorption in gouge material** – The additional parameters to be considered in the evaluation are the dimensionless distribution coefficient for the gouge material K_d^g [–] (once equilibrium is reached) and the kinetic rate (i.e. backward rate coefficient) α [T^{-1}], cf. Appendix G. The parameters K_d^g and α both need to be calibrated from the measured *in situ* breakthrough data since relevant laboratory values are not available at present.

8.5 Calibration parameters and evaluation steps

The consequence of the third hypothesis in section 8.2 is that κ and K_a, as given in Appendix G, cf. Table G-1 (MIDS), may not be applicable for *in situ* conditions. Furthermore, the "representative" slope $k_0 \approx 3400$ m^{-1} is uncertain, hence the *in situ* value may be larger or smaller. In other words, calibration will generally be required for *all* parameters which depend on *in situ* conditions.

The controlling parameter group for diffusion/sorption is $\kappa k_o = k_o\theta[D(1+\rho K_d^m/\theta)]^{1/2} = k_o(\theta D_e R_m)^{1/2} = k_o(\theta F D_w R_m)^{1/2}$. We now introduce a calibration parameter referred to as the *enhancement factor*, f, and calibrate the controlling parameter group as $f\kappa k_0$, where $f \neq 1$ will account for the discrepancy between the *in situ* retention parameters and the "representative" data set (MIDS and $k_0 \approx 3400$ m^{-1}) used for model predictions. The factor f is calibrated for 6 tracers (HTO, Na, Sr, Ba, Rb and Cs) and 3 test configurations, a total of 18 values (see Table 8-1).

In addition to diffusion/sorption in the rim zone, we account for the effect of tracer retention by finer gouge fractions, described as a first-order kinetic sorption process; the two calibration parameters are K_d^g and α . This effect is anticipated relatively small (see first hypothesis of 8.2). Although K_d^g and α are tracer-dependent and may differ between test configurations, we shall assume that α is constant for all tracers and configurations (since kinetic effects are anticipated mainly due to diffusional resistance). The total number of parameters for first-order kinetic sorption is then 16 (K_d^g for 5 reactive tracers in 3 configurations, plus one value of α).

The evaluation procedure consists essentially of two steps:

1) We determine the water residence time distribution $g(\tau)$ by deconvoluting breakthrough curves for tritiated water (HTO), accounting for diffusion into the matrix; the actual form of $g(\tau)$ is assumed as inverse-Gaussian, and the first two water residence time moments are calibrated.

2) We use $g(\tau)$ to model the reactive tracer breakthrough curves by accounting for mass transfer processes, with parameters determined in the laboratory. If the modelled BTCs deviate from the observed BTCs, we enhance mass transfer by increasing the factor f (where $f\ k_o\ \kappa$ is the calibrated value), and also incorporate sorption in finer gouge fractions as a first-order kinetic process.

The group $k_o \kappa f$ with f >1 implies larger *in situ* values of some or all of the parameters θ, F, K_d^m and k, compared to values of the "representative" MIDS data set for predictive modelling (Table G-1, and $k_0 \approx 3400\ m^{-1}$). If f >1 is due to larger values of θ, F and $k > k_o$, then its impact has to be accounted for in the modelling of the conservative HTO breakthrough curves. In other words, the above two steps become an iterative procedure, by which the moments of $g(\tau)$ are calibrated.

For each tracer and test we can write $k_o f \kappa = k^* (\theta^* F^* D_w R^*_m)^{1/2}$ where $R^*_m = 1 + \rho K_d^{m*}/\theta^*$ and the asterix "*" denotes *in situ* (unknown) values of respective parameters. Parameters k^*, θ^* and F^* are independent of the tracer, and $K_d^{m*} = 0$ for HTO; thus we have an undetermined system, with two unknowns more than independent equations. We introduce an additional constraint in form of "Archie's law" $F^* = 0.71 (\theta^*)^{1.58}$ (e.g., Valkiainen, 1992). With this constraint we have only one degree of freedom for the *in situ* retention parameters; in other words, by specifying one *in situ* parameter (say θ^*), all other parameters (i.e., k^*, F^* and K_d^{m*} for the 5 sorptive tracers) can be computed. Detailed steps of these computations are described in Cvetkovic et al. (in prep). In this manner we can estimate ranges of *in situ* retention parameters for each test configuration in Feature A.

8.6 Evaluation results

The breakthrough data for the TRUE-1 tests normalised with the total injected mass indicate that the sorbing tracers can be roughly classified into three groups; the weakly sorbing tracers Na and Sr, moderately sorbing tracers Ba and Rb, and the strongly sorbing tracer Cs. The modelled BTCs for Na and Sr are more strongly influenced by the detailed form of the HTO BTC in comparison to the modelled BTCs for Ba, Rb and Cs.

In Figures 8-2 through 8-4 we exemplify the mass transfer effects for three tracers that represent each group, chosen from one of the tests; Cs from the STT-2, Ba from STT-1 and Sr from STT-1B test. The measured BTCs are compared with the modelled BTCs and the key evaluation steps are exemplified and explained in the figure caption of Figure 8-2. The calibrated temporal moments for HTO are mean =7 h and variance = 49 h^2 for STT-1 and mean =5 h and variance =1.5 h^2 for STT-1B. For the STT-2 test, a bimodal $g(\tau)$ was used reflecting the likely two distinct pathways. The moments for the two modes in the latter case are: 35% of area with mean =8 h and variance =10 h^2 , and 65% area with mean =21 h and variance=30 h^2.

Table 8-1. Calibrated parameters for tritiated water (HTO) and the sorbing tracers used in the TRUE-1 tracer tests. Note that only the tracers for which laboratory data are available within the TRUE programme are included. The representative slope of the linear relationship $\beta = k_o \tau$, is $k_0 \approx 3400$ m^{-1} .

Tracer	Enhanced diffusion factor f			K_d^g [–] for gouge (α=0.3h^{-1})		
	STT-1	STT-2	STT-1B	STT-1	STT-2	STT-1B
HTO	40	35	32	0.0	0.0	0.0
Na-22	40	40	32	1.0	1.0	0.5
Sr-85	40	50	32	2.0	2.0	1.6
Ba-131	–	40	–	–	4.0	–
Ba-133	40	40	–	4.0	4.0	–
Rb-86	45	32	34	5.0	5.0	4.0
Cs-134	–	96	–	–	10.0	–
Cs-137	137	–	–	10.0	–	–

Curve 1 of Figure 8-2 is obtained for pure surface sorption, where β is assumed constant and equal to the ensemble mean value from Monte Carlo simulations. Accounting for aperture variability, (through the variability in β and its correlation with τ) increases the spreading of the BTC significantly and yields a BTC (Curve 2 in Figure 8-2) which is consistent in shape with data. Accounting for matrix diffusion, using

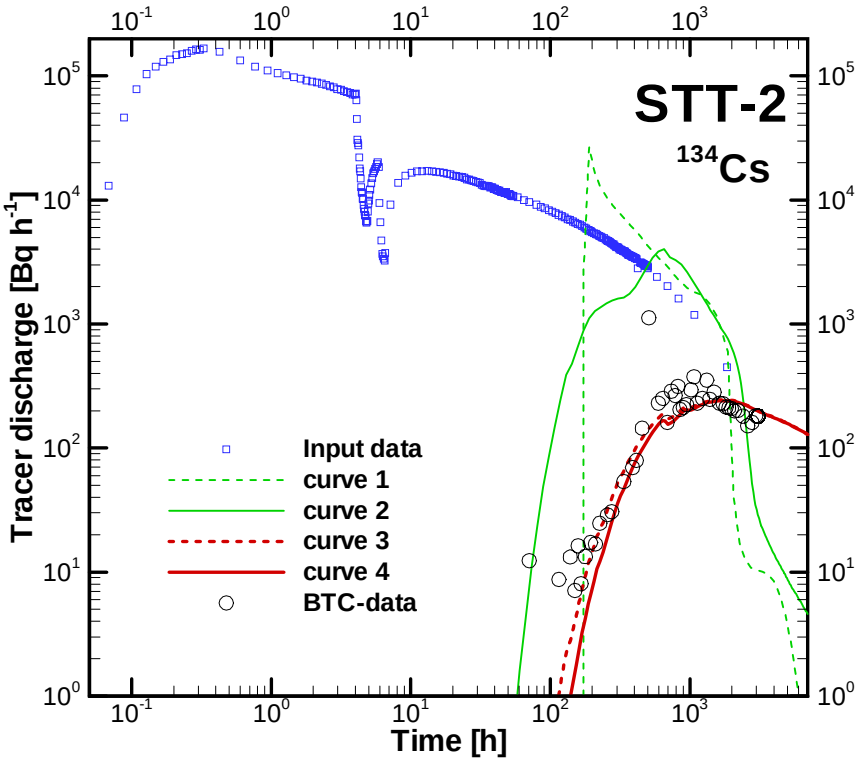

Figure 8-2. *Example of evaluation graph for Cs obtained from test STT-2. Curves 1,2,3 and 4 are obtained using the LaSAR model (all equations are given in the Appendix G); Curve 1 is obtained by assuming that surface (equilibrium) sorption with constant (effective) β is the only retention mechanism, Curve 2 is obtained by assuming that surface (equilibrium) sorption with variable β (accounting for aperture variability) is the only retention mechanism, Curve 3 is obtained by assuming that surface (equilibrium) sorption, matrix diffusion and matrix sorption with variable β are the retention mechanisms, and Curve 4 is the same as Curve 3 where in addition non-equilibrium sorption in the gouge is accounted for.*

MIDS, yields a BTC that is close to Curve 2. Thus, *Curve 2 is in effect the breakthrough for Cs that can be predicted using the selected MIDS data set.* Since Curve 2 deviates from the measured BTC, it is apparent that the "representative" data set do not accurately represent *in situ* retention properties. Enhancement with f=96, yields a BTC that is close to the measured data (Curve 3). Accounting for sorption in gouge material has a small effect on the Cs breakthrough (compare Curves 3 & 4). The factor f=96 was calibrated with the factor f=35 for HTO. A change of f=35 for HTO within say 30% does not affect the calibrated factor f for Cs significantly, indicating that the iterative calibration procedure is robust. However, the actual form of the modelled Cs BTC is sensitive to changes in f that are larger than 10–20%.

Ba sorbs moderately and the kinetic effects are less dominated by matrix diffusion in comparison to those of Cs. Curves 1 and 2 of Figure 8-3 result from a pure surface sorption model. Curve 1 disregards aperture variability where we use an effective β, whereas Curve 2 accounts for aperture variability. Curves 1 and 2 differ somewhat in the initial part, however, the difference is significantly smaller than for Cs; Cs sorbs more strongly, hence the effect of β variability on surface sorption is amplified. Adding matrix diffusion using MIDS yields a BTC that is very close to Curve 2. Enhanced diffusion/sorption with f=40, yields a BTC close to the data, with some deviation in the peak (Curve 3 in Figure 8-3). Accounting further for sorption in gouge material closely reproduces the measured data (Curve 4). In comparison to Cs, the modelled BTC for Ba (Curve 4 in Figure 8-3) is less sensitive to the factor f and more sensitive to K_d^g.

The measured BTCs for weakly sorbing tracers exhibit considerably smaller kinetic effects in comparison to Cs. Curve 2 of Figure 8-4 accounts for surface sorption only. Since Sr sorbs weakly, the effect of β variability on surface sorption is negligible. Accounting for matrix diffusion with f=32 (consistent with the HTO value f=32 for STT-1B), has a relatively small effect (Curve 3 in Figure 8-4). Accounting for kinetic sorption in gouge yields a BTC that is close to the data. The most significant kinetic effect appears to be due to finer gouge fractions, thus the modelled BTC (Curve 4) is sensitive to the calibrated value K_d^g.

Table 8-1 shows that the calibrated K_d^g is correlated to K_d^m (or K_a), for all TRUE-1 tests. There is also a consistent increase of the factor f with increasing K_a (Table G-1 in Appendix G), however, this increase is comparatively small. If the entire kinetic effects are inter-preted as diffusion/sorption in the rock matrix, the "enhancement factor" f required for closely modelling measured BTCs, is larger than the values given in Table 8-1. For example, f=70 is required for Ba, f=90 for Na and f=140 for Sr in STT-1.

Aperture variability in the fracture (incorporated through the variability in β) influences both diffusion into the matrix, and surface sorption since the two parameter groups are K_a β and κβ (see Appendix G). The incorporation of the variability in fracture aperture affects the diffusive mass transfer significantly for strongly sorbing tracers (see Figure 11-1). In fact, the observed spreading of, for instance, the Cs breakthrough, cannot be explained with the current model if the effect of aperture (or β) variability on mass transfer processes is neglected. The variability in β was incorporated using an approximate deterministic relationship between β and τ obtained from Monte Carlo simulations. A modification of this relationship would imply changes in the calibrated values of f.

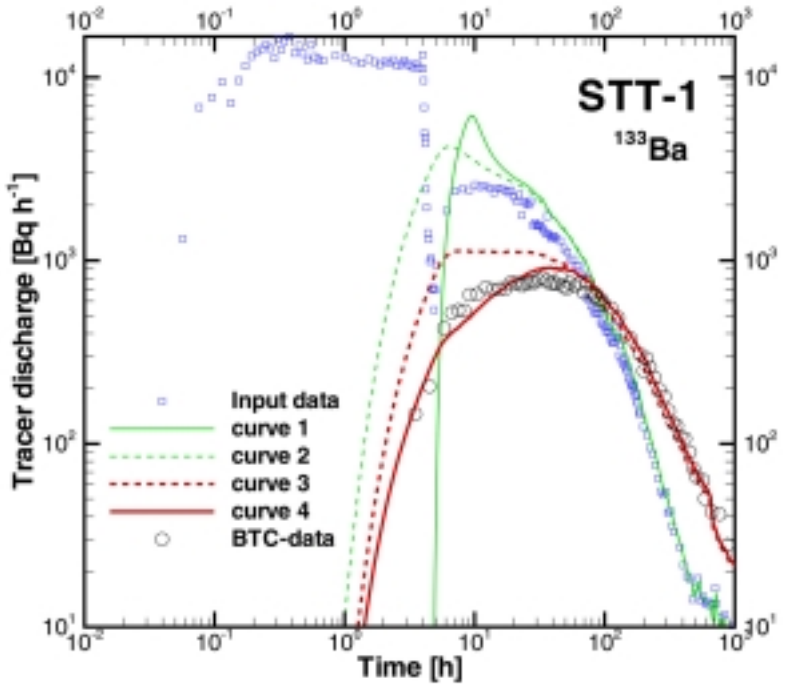

Figure 8-3. *Example of evaluation graph for Ba obtained from test STT-1. The various curves are explained in the figure caption of Figure 8-2.*

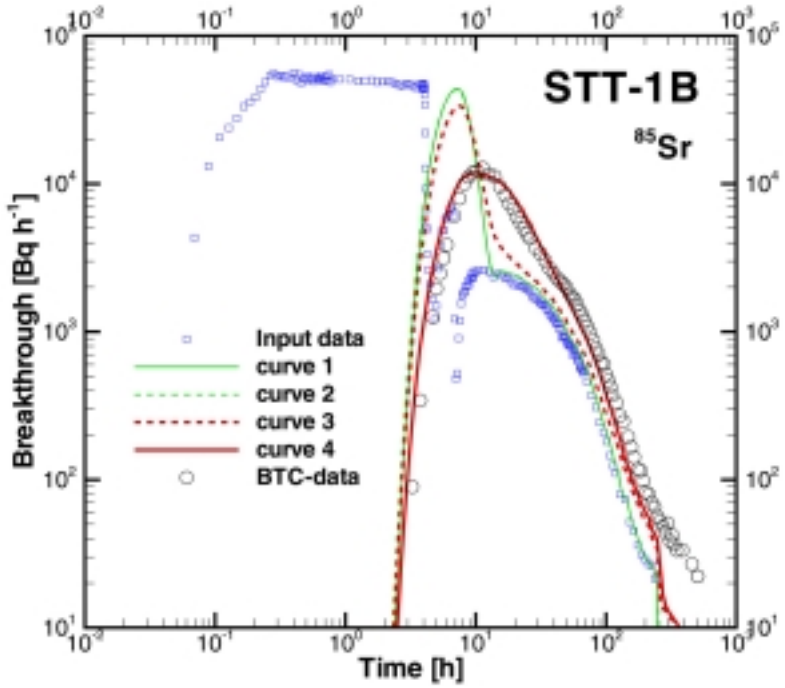

Figure 8-4. *Example of evaluation graph for Sr obtained from test STT-1b. The various curves are explained in the figure caption of Figure 8-2.*

8.7 Discussion of results

We evaluated and interpreted the breakthrough data for the sorbing tracers within the TRUE-1 tests using the LaSAR framework (Cvetkovic et al. 1999). All the equations used in the evaluation are summarised in the Appendix G; all calibrated parameters are summarised in Table 8-1, and the "Modelling Input Data Set" (MIDS) for the retention parameters is given for all tracers in Table G-1, cf. Appendix G.

The observed BTCs for more strongly sorbing tracers exhibit significant retention and tailing; these are attributed primarily to diffusive mass transfer and sorption in the rock matrix. The retention observed *in situ* cannot be fully reproduced based on the "representative" data set (MIDS of Table G-1 for κ and $k_0 \approx 3400$ m^{-1}). Calibration with a factor f is required for obtaining a close fit between the modelled and observed BTCs. We also included sorption in gouge as reversible first-order kinetic sorption and calibrated parameters K_d^g and α. The calibration parameters f and K_d^g vary only moderately between different tracers, and for the different TRUE-1 tests. If we incorporate the entire effect of gouge as part of diffusion/sorption into the rock "matrix" (setting $K_d^g = 0$), we can still obtain a close fit but then the factor f is larger, 2–3 times for Na and Sr, only slightly larger for Ba and Rb, and unchanged for Cs.

In spite of the fact that the factor f and its interpretation may not be unique, it is interesting that a relatively narrow range of f was sufficient for interpreting measured BTCs for all tracers and in all TRUE-1 tests: f = 32–50 (excluding Cs), where almost 85% of the f values fall in the interval 32–40, cf. Table 8-1. Since K_d^g and α are moderately important for Ba and Rb, and somewhat important for Cs, one can argue that *two* calibration parameter f are required for interpreting the more sorbing tracers of the TRUE-1 tracer tests (say f = 50 for Ba and Rb, and f = 137 for Cs).

In the following, we briefly discuss a few important issues:

Heterogeneity and uncertainty

Data available within the TRUE-1 programme indicate that Feature A is heterogeneous with respect to both flow and mass transfer properties. In particular, the aperture varies spatially which determines the variable flow field and consequently the distribution of the transport parameters τ and β along flow paths. Furthermore, mineralogical analysis indicates that in the area covered by the experiment, Feature A consists of both mylonite and altered Äspö diorite. However, the exact proportion and distribution along the flow paths activated by the TRUE-1 experiments is unknown. Presumably the flow paths of all tests are in contact with both rock types. The *in situ* sample that has been subject to through-diffusion in the laboratory represents predominantly mylonite which has lower porosity and diffusivity than the generic material (see Table G-1 in Appendix G), and is also assumed to have a lower diffusivity and porosity than the altered Äspö diorite. However, no (*in situ*) data are currently available on the altered diorite. The uncertainty in the exact mineralogy adjacent to the flow path implies uncertainty in the mass transfer parameters K_a and κ. The observed heterogeneity in the flow and mass transfer properties

implies that the selected "representative" data set used for predictions (Table G-1 in Appendix G and $k_0 \approx 3400$ m^{-1}) may not be applicable to *in situ* conditions.

Hydraulic parameters

The modelled BTCs are sensitive to the actual form of the water residence time distribution, $g(\tau)$. Hence it is important to have an accurate form of $g(\tau)$ for process discrimination and evaluation.

In the LaSAR framework, $g(\tau)$ depends on variable advection, which in turn is dependent on the heterogeneous flow field. Thus hydraulic parameters provide the principle basis for obtaining $g(\tau)$. However, the accuracy with which $g(\tau)$ can be obtained from stochastic simulations of water flow in Feature A using available transmissivity data is insufficient for evaluating reactive tracer breakthroughs. The hydraulic information alone (i.e. transmissivities estimated from hydraulic tests) underestimates the fracture aperture such that modelled water residence times are considerably shorter in comparison to those measured (e.g. 0.5 h modelled vs. 6–7 h measured for STT-1, Andersson (1996)).

When the hydraulic information is complemented with (non-reactive) tracer test data, and mean aperture calibrated appropriately, $g(\tau)$ can be "predicted" sufficiently well to capture first-order effects. However, flow simulations also underestimate hydrodynamic dispersion mainly because the support scale for the available transmissivity data is relatively large. Since the prime objective here is to evaluate retention parameters, we have used the most accurate means for obtaining $g(\tau)$, i.e., by *calibrating* $g(\tau)$ on the measured HTO breakthrough data for the particular test in question. Note that the measured HTO or Uranine breakthroughs for the same flow path and flow rate can differ if the tests were performed at different times, due to changes in boundary conditions, cf. Sections 5.8 and 7.6.

In summary, we have obtained $g(\tau)$ by calibration on HTO data, rather than from independent predictions using available hydraulic information. The hydraulic information, including boundary conditions, was used in the simulations for obtaining the β–τ relationship. However, even in these simulations it was necessary to use the mean calibrated aperture as obtained from the (non-reactive) tracer tests.

Diffusive mass transfer

We found that an "enhancement factor" $f > 1$ is required for explaining measured breakthroughs; f varies in a relatively narrow range (40–137 for STT-1, 32–34 for STT-1B and 32–96 for STT-2), cf. Table 8-1, and its dependence on sorption properties is weak.

We emphasise that all the kinetic effects can in principle be interpreted as diffusion/sorption in rock matrix, however, in that case the factor f attains higher values in particular for weakly sorbing tracers. Evaluation results indicate that diffusion is more enhanced along the STT-1 flow path, than along the STT-1B flow path by approximately 25–30% (see Table 8-1). The factor f reflects an effective value along a

given flow path and its variation between the two flow paths can be due to larger scale heterogeneity. The difference in f between STT-1 and STT-2 tests (which were carried out between the same borehole sections but with different flow rates), is likely to be due to the fact that the flow paths in the two tests are activated in different ways due to changes in natural boundary conditions (cf. Sections 5.8 and 7.6), as indicated by the bimodal form of $g(\tau)$ for the STT-2 test and unimodal for the STT-1 test.

Diffusion into stagnant water zones has been accounted for following the expressions given in Appendix G. These expressions are approximate and yield maximum effect (since all water adjacent to the flow path is treated as stagnant). The model for diffusion into stagnant water is thus equivalent to the model for diffusion into the rock matrix, except that the "flow-wetted surface" is interpreted as adjacent to the stagnant water in the fracture plane, rather than the contact area with the rock matrix.

The controlling parameter group for diffusion into stagnant water is $\kappa_w\beta_w$ (see Appendix G). The flow-dependent parameter β_w [TL^{-1}] is corresponding to β, where we assume $\beta_w = k_w \bar{\tau}$. The parameter $\bar{\tau}$ is the mean water residence time, and k_w is computed as $k_w = 2/W$, where W [L] is the estimated width of the flow path. To obtain W, we use the average relationship $\bar{\tau} = 2LWb/Q_{IB}$, where Q_{IB} [L^3T^{-1}] is the evaluated flow rate in the injection borehole; note that the factor 2 appears since b is the "half-aperture" which we estimate as $b = 1/k = 0.3$ mm. For STT-1, $Q_{IB} = 42 \cdot 10^{-6}$ m^3h^{-1}, L=5 m, $\bar{\tau}$ =7 h, and we obtain W = 0.1 m, whereby $\beta_w = 2\bar{\tau}/0.1 = 20\ \bar{\tau}$ =140 h m^{-1}. Note that W=0.1 m is an approximation based on an idealized geometry of a flow path, and is not necessarily "physical". In fact, numerical simulations summarized in Cvetkovic et al (in prep.) indicate that the average flow path width is less than 0.1 m. Nevertheless, this approximate value has been used for all tracers and tests.

Since the parameters for matrix diffusion and diffusion into stagnant water zones appear as a single parameter group, we could in principle have attributed the enhancement factor f as given in Table 8-1, to $\kappa_w\beta_w$ rather than $\kappa\beta$, i.e., enhanced diffusion into stagnant water zones rather than into the rock matrix. The physical interpretation would then be that the flow path consists of multiple "channels" with mobile water adjacent to multiple "islands" of stagnant water (in a sandwich-like configuration) into which tracer diffuses. The estimated flow path width of W=0.1 m would then be divided by the assumed number of "channels"/"islands" (say N_i), which would increase β_w by a factor N_i and thus enhance diffusion. To obtain a close comparison between data and modelled breakthrough curves with this interpretation, we, for instance, require N_i = 17 for Ba in STT-1 (to compensate for f=40) and N_i = 663 for Cs in STT-1 (to compensate for f=137). In other words, the "appropriate" (calibrated) number N_i would *vary* considerably between different tracers, which is incompatible with its physical interpretation.

Attributing dominant kinetic effects to diffusion into stagnant water (as a single flow path, as we have done, or as multiple "channels"/"islands") implies that *all* tracers have to be subject to mass transfer by approximately the *same rate* (see Table G-1 in Appendix G). This would contradict our results which clearly indicate that the mass transfer rate is strongly dependent (or, is a function of) the sorption coefficient, i.e. stronger diffusion is exhibited by more strongly sorbing tracers. Hence, in our view the

kinetic effect can only be explained as integrated diffusion *and* sorption, and not diffusion alone.

Interpretation of *f*

The slope *k*, and the "enhancement factor" *f* control diffusion as a product. In view of the uncertainty of k_0, one could consider the product $k_0 f$ to be a *single* calibration parameter. For instance, the value for Cs in the STT-1 test is $k_0 f$=466 000 m^{-1} (see Table 8-1). Thus if the slope was 466 000 m^{-1} rather than 3400 m^{-1}, then f=1, implying that the MIDS data set accurately represent *in situ* retention properties. However, the value of the slope would also influence surface sorption since the parameter group for surface sorption is $k_0 K_a$. Our analysis shows that if K_a is as given in Table G-1, then the slope k_0 for Cs should be roughly 3400 m^{-1}. However, K_a in Table G-1 has been determined from K_d^m assuming spherical particles, and it varies considerably depending on the method for its estimation, cf. Section 6.4 and Byegård et al., 1998). In view of the complexity of the Feature A surface, *in situ* K_a should be considered highly uncertain.

Table 8-2. Estimated *in situ* parameter range for an assumed porosity of the accessible part of the altered rim zone $\theta^* = 2–2.4\%$, with/without explicitly accounting for sorption in gouge. These are compared to MIDS values, as well as to results from TRUE-1 batch tests on 1–2 mm fractions and tests on all fractions combined. The estimated range of *in situ k* for $\theta = 2–2.4\%$ is 8 800–11 000 m^{-1}.

Tracer	$D_e \times 10^9$ [m^2 h^{-1}]		$K_d^m \times 10^3$ [m^3 kg^{-1}]	
	In situ **STT-1**	**MIDS**	***In situ*** **STT-1**	**MIDS (batch)**
HTO	13 – 17	0.42	0	0
Na	7.2 – 9.6	0.24	0.007 – 0.06	0.0014 (0.0044 – 0.0068)[1] (0.007 – 0.01)[3]
Sr	4.2 – 5.6	0.14	0.024 – 0.32	0.0047 (0.01 – 0.09)[1] (0.03 – 0.1)[3]
Ba	4.5 – 6	0.15	1 – 3.2	0.2 (0.4 – 1.8)[1] (0.74 – 4.3)[3]
Rb	11 – 15	0.37	1.7 – 4.5	0.4 (2.8)[2] (1.4 – 8)[3]
Cs	11 – 15	0.37	30 – 56	0.8 (53)[2] (8 – 290)[3]

[1] Feature A rock, 9-day batch tests, 1–2 mm fraction, Byegård et al, (1998), cf. Table 6-13.
[2] Generic rock (ÄD), 36-day batch tests, 1–2 mm fraction, Byegård et al, (1998).
[3] Generic rock (ÄD), 14-day batch tests, from all fractions, Byegård et al, (1998), cf Table 6-1.

In equations $k_0 f\kappa = k^* [\theta^* F^* D_w(1+\rho K_d^{m*}/\theta^*)]^{1/2}$, which can be written for each tracer and test configuration, the left-hand side is known (calibrated), and k^*, θ^* and F^* for each test configuration, as well as K_d^{m*} for each sorptive tracer and test configuration, are unknown values. Using "Archie's law" that relates *in situ* F^* and θ^* (e.g., Valkiainen, 1992), we have obtained an estimated range for *in situ* retention parameters for Na, Sr, Ba, Rb and Cs, summarised in Table 8-2. For these values, we have assumed that the *in situ* porosity of the accessible part of the Feature A rim zone is in the range 2–2.4% (Cvetkovic, et al., in prep). This value is consistent with the measured rim zone porosity of a natural fracture at Äspö (1.34%, see Landström et al., in prep), once the effect of the sample size is accounted for. If the *in situ* porosity of Feature A rim zone is larger or smaller than 2.4%, respectively, then the values of Table 8-2 have to be modified accordingly; tables with inferred (estimated) retention parameters for all tracers and tests, covering a porosity range between 0.1% and 4%, are given in Cvetkovic et al. (in prep). Based on the *in situ* estimates given in Table 8-2, we can distinguish different "contributions" to the "enhancement", i.e., we can estimate an "enhancement" factor for k, for K_d^m as well as for F and θ (details are given in Cvetkovic et al., in prep), cf. Section 8.8.5.

Sorption in the matrix (rim zone)

The sorption coefficients obtained within the TRUE-1 laboratory program varied over a relatively wide range, depending on the test method (batch or through-diffusion tests), tests duration (from 1–36 days), fraction size for batch tests (0.045 mm – 2 mm) (Byegård et al., 1998). For instance, the range of K_d^m values for batch tests of duration 1–36 days on 1–2 mm fractions varied between 0.0012–0.054 $m^3\ kg^{-1}$ for Cs. Considering a wider range of fractions, the range of K_d^m values is even greater, 0.008–0.29 $m^3\ kg^{-1}$. The dependence of K_d^m on the test duration was strongest for Cs, however, it has been observed also for other tracers, in particular Ba and Rb.

K_d^m selected for predictions for different tracers ("Modelling Input Data Set" or MIDS in Table G-1 of Appendix G) was obtained from through-diffusion tests. This value was considered as the most representative for diffusion/sorption under idealised conditions (homogeneous fracture and matrix). However, under natural conditions, where both the mineralogy and aperture vary along the flow path, the fracture surface and the accessible part of the matrix of the rim zone constitute a more complex physical/chemical setting than that seen in the laboratory. Hence, K_d^m obtained from through-diffusion experiments using unaltered rock samples, does not necessarily represent the sorption properties applicable *in situ* for Feature A.

Based on the calibrated f, and using "Archie's law" as described above, we estimated K_d^m for all sorptive tracers, assuming the *in situ* porosity in the range 2–2.4% (with a corresponding formation factor in the range 0.0015–0.002). Estimated ranges of K_d^m are given in Table 8-2 and compared to parameter intervals as determined within the TRUE-1 laboratory program. The most interesting is K_d^m values for more sorbing tracers Bs, Rb, and in particular Cs. We estimate for Ba *in situ* K_d^m = 0.001–0.0032 $m^3\ kg^{-1}$ which can be compared to 0.0004–0.0018 $m^3\ kg^{-1}$ for Feature A rock (9-day batch tests on 1–2 mm fraction, cf. Table 6-13), and 0.00074–0.0043 $m^3\ kg^{-1}$ for generic rock, cf. Table 6-1. We estimate for Rb *in situ* 0.0017–0.0045 $m^3\ kg^{-1}$ which

can be compared to 0.0028 m^3 kg^{-1} for Feature A rock (36-day batch tests on 1–2 mm fraction, Byegård et al., (1998)), and 0.0014–0.008 m^3 kg^{-1} for generic rock, cf. Table 6-1. We estimate for Cs *in situ* K_d^m = 0.03–0.056 m^3 kg^{-1} which can be compared to 0.053 m^3 kg^{-1} for generic rock (36-day batch tests on 1–2 mm fraction, Byegård et al., (1998), and 0.008–0.29 m^3 kg^{-1} for generic rock, cf. Table 6-1. The estimated *in situ* K_d^m can be compared to the MIDS values: 0.0002 m^3 kg^{-1} for Ba, 0.0004 m^3 kg^{-1} for Rb, and 0.0008 m^3 kg^{-1} for Cs, cf. Table G-1 in Appendix G.

"Effective" apertures

The slope k is primarily controlled by the variability of the Feature A aperture, as well as by the injection conditions. Statistics of Feature A aperture have not been obtained directly. However, based on the estimated spreading of the water residence time (see the calibrated travel time moments in Table 8-1), the variability of the Feature A aperture appears to be significant. From the hydraulic tests we estimated an effective ("hydraulic") aperture of 0.06 mm. The effective ("transport") aperture has been estimated based on the water residence time moments for STT-1, cf. Section 8.6, as 0.9 mm. We have introduced another effective aperture referred to as the "β-aperture" defined as $2/k$ (see definition of β in Appendix G). The "β-aperture" obtained from the "representative" data set is $2/k_0 = 2/3400 = 0.6$ mm. Calibrated values of k (assuming an *in situ* porosity range of 2–2.4%) are in the range 8 800–11 000 m^{-1}; this yields the range for the calibrated effective "β-aperture" in the range 0.18–0.23 mm, which is closest to the "hydraulic" aperture. Details of this analysis are given in Cvetkovic et al. (in prep).

We found that the effect of aperture variability on diffusive mass transfer is more significant for more strongly sorbing tracers, simply because for those tracers diffusion/sorption has strongest effect (see Table G-1 in Appendix G). Accounting for this variability was crucial for obtaining a consistent interpretation for all TRUE-1 tests.

β-τ relationship and "flow-wetted surface"

The β–τ relationship was here assumed as linear for two reasons. First, the performed Monte Carlo simulations indicate that a linear relationship is not unreasonable for the considered scale and range of aperture variability. Second, the linear relationship is relatively simple for implementation. However, a non-linear (power-law) relationship is more consistent with simulation data as also shown by Cvetkovic et al. (1999).

It is of interest to compare our values of k and β with estimates that can be made using either the injection or the pumping flow rate. For instance, in the STT-1 tests, the pumping flow rate is Q = 0.024 m^3h^{-1} whereas the evaluated injection rate is Q_{IB} = $42 \cdot 10^{-6}$ m^3h^{-1}. The crudest estimate of β is obtained by assuming pumping in a uniform fracture. Then $\beta = 2\pi L^2/Q = 6545$ hm^{-1}, where L = 5 m is the distance between the pumping and injection boreholes. If we divide $\beta = 6545$ hm^{-1} with the mean water residence time of 7 h, we get an estimate of $k = 935$ m^{-1}, which yields an effective "β-aperture" estimate of $2b = 2/k = 2.1$ mm. A finer estimate, which to some extent

accounts for the heterogeneity in the flow, is $\beta = 2dL/Q_{IB} = 13\ 300\ hm^{-1}$, where d = 0.056 m is the diameter of the borehole. Thus, there is more than one order of magnitude difference in the two estimates. Dividing $\beta = 13\ 000\ hm^{-1}$ by 7 h, we get an estimate of $k = 1900\ m^{-1}$ and the effective "β-aperture" would be $2/k \approx 1$ mm. Note that both of these estimates of k are lower than the calibrated range $k = 8\ 800–11\ 000\ m^{-1}$.

The sensitivity to the assumed β-τ relationship (linear or non-linear) clearly depends on the extent to which a tracer is subject to sorption/matrix diffusion. For the tracers in question, one could expect Cs to be more sensitive to the τ-β relationship. A power-law β-τ relationship would imply stronger diffusion for larger τ in comparison to a linear one. Further study is required for a more conclusive statement on the impact of the β-τ relationship on the evaluation of TRUE-1 tests. Note that a non-linear β-τ relationship implies that the notion of a "flow-wetted surface per unit volume of water" as currently applied in performance assessment (Andersson et al., 1998) is not applicable.

Sorption in gouge

We evaluated the measured breakthrough curves by incorporating first-order, kinetically controlled, reversible sorption, assumed taking place in smaller fractions of the gouge material. The retention effect of larger fractions (e.g., altered rock fragments), is indistinguishable from diffusion/sorption in the rock "matrix" of the rim zone. Thus reference to "sorption in gouge" essentially implies sorption into smaller gouge fractions. The kinetic effects from gouge material are small for Cs and dominant for Na and Sr; for Ba and Rb the kinetic effects due to matrix diffusion/sorption are comparable to those of sorption in gouge.

Laboratory transport data for gouge material from Feature A are not available at present, and the two parameters K_d^g and α are instead obtained by calibration. We found the rate coefficient $\alpha = 0.3\ h^{-1}$ in all cases, which indicates that the kinetic effects are presumably due to intra-particle diffusion. If these effects where due to chemical kinetics, a larger difference would be expected between the different tracers. The weakly sorbing tracers are more sensitive to the actual values of K_d^g and α than the moderately and strongly sorbing tracers. The results are less sensitive to the values of α than to the values of K_d^g, indicating that α captures the additional kinetic effects in a robust manner. The calibrated values of K_d^g are relatively low, where log K_d^g is proportional to log K_a (i.e. to log K_d^m).

Predictive capability

As discussed above, hydraulic data combined with numerical simulations are insufficient for predicting the water residence times in Feature A. Thus we require a calibration of the water residence time distribution g(τ). The issue we discuss here is: given an accurate (calibrated) g(τ), how well can we predict the breakthrough curves of sorbing tracers using the "representative" MIDS data set?

Given the MIDS data in Table G-1 of Appendix G, with $k_0 \approx 3400\ m^{-1}$, matrix diffusion combined with diffusion into stagnant zones has a relatively small impact, and the modelled BTCs are close to the curves for pure surface sorption. Hence, Curve 2 in Figures 8-2 through 8-4 essentially exemplify the extent to which the breakthrough of sorbing tracers *can be predicted*, given the water residence time distribution $g(\tau)$, the MIDS data set and a "representative" slope $k_0 \approx 3400\ m^{-1}$. Clearly, Curve 2 typically underestimates the retention effects, in particular for the more strongly sorbing tracers.

The relatively strong diffusion effects observed in the TRUE-1 tests with sorbing tracers are attributed to the fact that the parts of the altered rock of the rim zone adjacent to the flow paths of TRUE-1 tests which are accessible over the time frames of the experiments have stronger retention properties than the unaltered rock on which the selected "representative" MIDS data set was based. However, this zone is, by definition, of finite extent. Thus experiments that would be carried out on longer time scales, would eventually experience the effect of limited diffusion. Once the altered rock zone is saturated, matrix diffusion could be well represented by MIDS obtained on generic (unaltered) rock samples.

8.8 Main results and conclusions

The main results and conclusions of this chapter may be summarised as follows:

8.8.1 Evaluation framework (LaSAR)

For the purpose of predicting and evaluating tracer tests within the TRUE programme, a modelling framework (LaSAR) was developed (Cvetkovic et al., 1999). In the LaSAR model, we can account for essentially 3 types of linear mass transfer processes: (i) *equilibrium (surface) sorption* on instantly available sites, (ii) *unlimited diffusion/ sorption* in the "rock matrix" which on the scale of TRUE-1 experiments implies a limited domain of the rim zone adjacent to the fracture, possibly integrated with larger gouge particles (e.g., altered rock fragments); (iii) *limited diffusion/sorption* into smaller gouge fractions, quantified as a first-order kinetic sorption-desorption process. We conceptualise Feature A as an open fracture, and account for diffusion/sorption into the (unlimited) rock matrix as a one-dimensional, linear process; this is in line with previous models for comparable conditions (e.g., Neretnieks, 1980). The novelty of the employed modelling approach is the parameter β [TL^{-1}] which in a general manner accounts for the effect of aperture/flow variability on diffusive mass transfer.

8.8.2 Controlling retention mechanisms and parameters

The dominant mass transfer (retention) process in Feature A on the time scales of the TRUE-1 experiments is *unlimited diffusion/sorption* into the "rock matrix". The parameters which control this process are summarised by the parameter group $\beta\kappa \equiv \beta\sqrt{\theta F D_w R_m}$, cf. Appendix G. The group $\beta\kappa$ conveniently separates the two major (and independent) effects on tracer retention: β accounts for the effect of spatially variable aperture and flow (i.e. geometry and boundary conditions), whereas the group κ accounts for physical properties such as porosity θ and formation factor F of the rim zone, and chemical/sorption properties summarised by the retardation coefficient $R_m = 1+K_d^m\rho/\theta$ where K_d^m is the volumetric sorption (distribution) coefficient. For the conditions of the TRUE-1 experiments in Feature A, we hypothesize (assume) that β can be approximated as a linear function of the water residence time τ, as $\beta = k\tau$; k [L^{-1}] then corresponds to what is referred to as the "flow-wetted surface per unit volume of water" in a PA/SA context (Andersson et al., 1998).

8.8.3 Calibration parameters

We calibrated the parameter group $\kappa\sqrt{\theta F D_w R_m}$ as $f\kappa\sqrt{\theta F D_w R_m}$ where f is referred to as the "enhancement" factor, and where $\kappa\sqrt{\theta F D_w R_m}$ is determined based on the "modelling input data set" (MIDS) and we used $k_0 \approx 3400$ m^{-1}; f was calibrated for each tracer and test configuration, a total of 18 (all given in Table 8-1). In addition to diffusion/sorption in "matrix" rock, we accounted for first-order kinetic sorption-desorption in gouge material; for this process we have one dimensionless distribution coefficient (K_d^g) for each reactive tracer for the 3 tests, and one rate $\alpha = 0.3$ h^{-1} for all tracers and test configurations, a total of 16 (all given in Table 8-1). Thus the total number of calibrated parameters for a close fit is 18+16=34. However, f varied comparatively little between different tracers and tests: 40–137 for STT-1, 32–34 for STT-1B and 32–96 for STT-2). The range for K_d^g is 0.5–2 for Na and Sr, 4–5 for Rb and Ba, and 10 for Cs. Since the dominant retention mechanism is unlimited diffusion/sorption in "matrix" rock, sorption in (small fraction) gouge particles (described as first-order kinetic sorption-desorption with K_d^g and α) can be conveniently *integrated* with diffusion/sorption in matrix, which reduces the calibrated parameters to 18. When "re-calibrating" $f\kappa\sqrt{\theta F D_w R_m}$ with $K_d^g = 0$, we get f values that are larger by a factor 2–3 for Na and Sr, but only slightly larger for Ba (e.g., f = 65 for STT-1), Rb (f = 55 for STT-1), and unaffected for Cs.

8.8.4 Role of the Feature A rim zone

On the time scale of the TRUE-1 experiments, the physical and mineralogical/sorption properties of a narrow part the Feature A altered rim zone which is accessible over the time frames of the *in situ* experiments control tracer retention. These properties are quantified by three parameters: F, θ and K_d^m. A relatively accurate knowledge of these

three parameters is required for accurate predictions of the tracer BTCs. The altered rock of the rim zone is generally characterised by distinct, albeit variable, physical and mineralogical properties, relative to unaltered rock. In particular, the porosity θ and the formation factor *F* are generally higher in the rim zone, due to chemical alteration and mechanically induced micro-fissures (e.g., Eliasson, 1993, Valkiainen, 1992). The change of the porosity and formation factor in the vicinity of the rim zone is over relatively short distances, implying the existence of an *in situ* "gradient" in these parameters away from the fracture surface. The "modelling input data set" (MIDS), cf. Table G-1 in Appendix G, was obtained on generic (unaltered) rock samples from through-diffusion tests. Thus applying MIDS for predicting tracer transport in the altered rim zone, is subject to uncertainty.

8.8.5 Interpretation of *f* and K_d^m, α

A typical value for the calibrated "enhancement" factor *f* of the most sorbing tracer Cs is 137. We have estimated that approximately a factor 3 is to be attributed to the slope *k*, and 46 to κ, in the product kκ, (Cvetkovic et al, in prep). In other words, the *in situ* slope *k* is 3 times larger relative to the "representative" value $k_0 \approx 3400$ m^{-1}, whereas the group $\kappa = \sqrt{\theta F D_w R_m}$ is 46 times larger relative to the MIDS value. Since D_w is fixed, we thus have an "enhancement" of $46^2 = 2116$ for the product $\theta F R_m$. We have estimated that *in situ* θ is around 6 times, and *F* around 40 times, larger than θ and *F* of the intact (generic) rock, and approximately a factor 8 is related to the retardation factor R_m. Note that R_m is almost identical for the rim zone and generic rock for all tracers except Cs, since both θ and K_d^m are enhanced by approximately the same factor. Thus 1/3 of the "enhancement" factor squared (i.e., $(f/3)^2 = 46^2 = 2116$) may be interpreted as the "gradient" of θF between the rim zone and intact rock. If we account explicitly for first-order kinetic sorption-desorption, K_d^g and α presumably account for sorption into gouge material (e.g., altered rock fragments) of such a (relatively small) amount that diffusion limitations are observable (in particular for Na and Sr for which unlimited diffusion/sorption in "matrix" is weak), but equilibrium is nevertheless reached quickly (implied by a relatively large Damkohler number $\bar{\tau}\alpha = 7 \times 0.3 = 2.1$).

8.8.6 *In situ* porosity θ and formation factor *F*

We hypothesise the *in situ* porosity θ of the accessible part of the Feature A rim zone as 2–2.4%, which, after accounting for sample size, is consistent with the value of 1.34% found by Landström et al. (in prep) for the rim zone of a natural fracture at Äspö. The *in situ* formation factor *F* was then determined using an empirical relationship ("Archie's law", e.g., Valkiainen, 1992), as F=0.0015–0.002. Based on these *in situ* estimates of θ and *F* we could determine the *in situ* K_d^m for all tracers, using the calibrated "enhancement" factors, cf. Table 8-2 and Section 8.8.8.

Currently available independent site-specific information (i.e., independent from the *in situ* tracer tests), on the *in situ* values of θ and F of Feature A are limited: F and θ are available for one sample dominated by mylonite from the intercept with Feature A in the KXTT1 borehole. The obtained values from the sample ($\theta = 0.001$ and $F = 1.7\times10^{-5}$) are relatively low and are not considered representative, for instance, of altered Äspö diorite, with which a large part of the flow path is expected to be in contact.

8.8.7 *In situ* slope *k*

Our estimated range of the *in situ* slope k for Feature A, as given by the TRUE-1 tests, is 8 800–11 000 m^{-1}, for an *in situ* porosity 2–2.4%. The probability for $k > 8800$ m^{-1} based on 89 equi-probable realizations of Feature A is 5–10%. If the *in situ* porosity would be say 3.2%, then the slope k would be around 6000 m^{-1} which is more probable, at least based on simulations. The slope k depends on the aperture distribution and flow/injection conditions, and hence cannot, even in principle, be determined in the laboratory. Numerical (Monte Carlo) simulations constitute a suitable means of determining β (and hence k) statistically, provided that the fracture aperture statistics are known. The hydraulic tests conducted in Feature A, however, do not provide a sufficient data base for inferring aperture statistics accurately; the 100 realizations are known to under-estimate aperture variability. Hence our "representative" average value $k_0 \approx 3400$ m^{-1} should be considered not more than an "order-of-magnitude estimate". Following the defintion of β, the slope k may be interpreted as the inverse of an "effective" half-aperture; we refer to $2/k$ as an effective "β-aperture". We find that the calibrated range 8 800–11 000 m^{-1} yields an *in situ* range of the "β-aperture" as 0.18–0.23 mm, which can be compared to the "hydraulic" aperture of 0.06 mm and the "transport" aperture of 0.9 mm. Thus we find that the calibrated *in situ* "β-aperture" is in magnitude closest to the "hydraulic" aperture. If this result can be generalized, then new possibilities may become available for utilizing hydraulic tests for *in situ* determination the bounds for the slope k (corresponding to the "flow-wetted surface per unit volume of water"). We emphasize that accounting for the variability in β (here using the approximate relationship $\beta = k_0\tau$) was crucial for obtaining a consistent interpretation for all tracers and tests.

8.8.8 *In situ* sorption coefficients K_d^m

Five *in situ* K_d^m values for 5 reactive tracers in each test configuration, were determined based on an assumed *in situ* porosity range of θ=2–2.4% and formation factor of F=0.0015–0.002. The obtained parameter ranges are summarised in Table 8-2, cf. Section 8.7, and compared to parameter intervals as determined within the TRUE-1 laboratory programme. K_d^m values obtained from longer batch tests on crushed material (in particular 1–2 mm fractions), appear to be more representative of the sorption properties of the rim zone, than K_d^m obtained from through-diffusion tests on compact cores. This suggests that the size fraction and time scale used for the above batch

sorption experiments in an average sense have captured the variability in sorption (and in mineralogy/geochemistry) along the *in situ* flow paths over the time scales of the *in situ* experiments. The reported estimated *in situ* diffusivities in Table 8-2 indicate that the *in situ* diffusivity is in the order of a factor 30 higher that the diffusivites for the various tracers of the MIDS data set of Table G-1, cf. Appendix G.

8.8.9 Uniqueness and verification

We have obtained unique estimates of *in situ* parameters for Feature A by *assuming in situ* average porosity of the accessible part of the Feature A rim zone as 2–2.4%, supported by independent results by Landström et al. (in prep). If future investigations would find that a representative *in situ* porosity for Feature A is say 3.2%, then our current estimates can be corrected (updated) according to expressions/tables provided in Cvetkovic et al. (in prep). *In situ F* would in this case be estimated as 0.0031, k as 6100 m^{-1} and K_d^m for Cs as 0.075 $m^3\ kg^{-1}$; thus a larger *in situ* porosity than 2–2.4% would imply smaller k, but larger F and K_d^m . If on the other hand, future investigations find that a smaller average porosity, say 1.2%, is representative for the Feature A rim zone (almost identical to the porosity found by Landström et al. (in prep), our estimates would be corrected as follows: F = 0.00066, k=22 000 m^{-1} and K_d^m =0.028 $m^3\ kg^{-1}$ for Cs. Thus a smaller *in situ* porosity than 2–2.4% would imply larger k, but smaller F and K_d^m than our current estimates. Independent information on any of the parameters can therefore be used for *verification* of our estimates, and/or for their correction. All values in Table 8-2 are valid under the condition that the calibrated temporal moments e.g. for STT-1 are 7 h (mean, consistent with independently obtained estimate by Andersson (1996)) and 49 h^2 (variance). If the temporal moments are also treated as unknowns, then the values of Table 8-2 need to be modified accordingly. We have shown the sensitivity of f to the temporal moments, as well as the type of modification which would be required, in Cvetkovic et al. (in prep). The provided estimates onf *in situ* parameters are also based on Archie's law, cf. Section 8.5, which has been established on core rock samples which generally do not represent the porosity/diffusivity of the rim zone. It is plausible that for the accessible part of the narrow rim zone, the exponent in "Archie's law" needs to be somewhat decreased, which would yield lower (and more realistic) estimates of the slope k. The sensitivity of the estimated k on the exponent in "Archies law" is given in Cvetkovic et al. (in prep.). We emphasize that the estimated values of Table 8-2 can be obtained *without any* reference to the "representative" data set (MIDS) and $k_0 \approx 3400\ m^{-1}$.

8.8.10 Model limitations and extensions

The comparison between evaluated and measured BTC for Cs in the case of STT-1 shows a deviation in the peak part of the BTC where the model overestimates the measured peak height by about 80%, cf. Figure 11-1. We could not account for this deviation (and obtain a consistent comparison for all other tracers and tests) with the current version of our model. Model simplifications potentially contributing to noted deviation are: (i) linear mass transfer: Cs has been found to be subject to non-linear

sorption e.g., on Grimsel rock (e.g., Aksoyoglu, 1990); (ii) linearisation of the β-τ relationship: this relationship is both statistical and non-linear which may have a strongest impact on Cs being the most sorbing tracer; (iii) equilibrium sorption in the "matrix"; generally Cs exhibits slower desorption (Byegård et al., 1998) implying that a kinetic model for sorption in the "matrix" may be more appropriate (a very low reversible rate would imply essentially irreversible sorption). The model can be extended to account for effects (ii) and (iii) (Cvetkovic et al., 1999). Currently available breakthrough data for Cs are insufficient for providing conclusive evidence of irreversible sorption in the matrix. However, we believe that incorporating sorption kinetics in the *matrix* with a slow desorption rate, could account for the deviation between the modelled and measured Cs breakthrough curves. An additional limitation is related to the flow model used in the Monte Carlo simulations for determining the statistics of β. Detailed studies have shown that the Reynold's equation which is based on the "cubic law" may not be applicable, in particular, for larger variations of the aperture (e.g., Zimmerman and Bodvarsson, 1996). A comprehensive study would be required for developing an alternative and more appropriate flow model for Feature A.

8.8.11 Implications for future TRUE tests

The rim zones of estimated 90% of fractures at Äspö are lined with partially altered rock. Thus the rim zones of fractures in which tracer tests of future detailed scale experiments and the ongoing TRUE Block Scale are to be carried out, are likely to exhibit physical properties (porosity, formation factor) and even mineralogical properties (combined mylonite and altered Äspö diorite), resembling those of Feature A. As with the TRUE-1 tests, the retention on the time scales of the planned detailed scale TRUE-2 and ongoing TRUE Block Scale tracer tests will be dominated by the properties of the rim zone, which is generally hard to characterise in full. Samples from at most a few points in a given fracture/structure may be available. Our estimates of the *in situ* parameters for Feature A may complement the laboratory data to provide a basis for reasonably accurate predictions. Ongoing complementary laboratory investigations focused on the rim zone of Feature A and future injections of epoxy resin in the investigated fracture with subsequent excavation and laboratory analyses are expected to add further to this knowledge.

8.8.12 Implications for PA/SA

For reactive transport on TRUE-1 experimental time scales, the retention properties in the immediate vicinity of a fracture are dominant. However, for increasing time scales of transport, such as those that would be relevant for performance assessment (PA) and/or safety analysis (SA), the effect of the narrow rim zone would diminish, whereby the parameters such as θ and F obtained on generic intact matrix rock samples, could well represent radionuclide retention even for the far-field. With increasing transport scale, we may therefore anticipate a "convergence" toward *more accurate* predictions over longer times using MIDS, than what we find in the TRUE-1 tests. This of course presupposes that the distributions of the flow-dependent parameters τ and β are known

with reasonable accuracy. In other words, we may consider retention parameters, such as sorption coefficient, porosity and effective diffusivity obtained from unaltered rock samples using through-diffusion tests, to provide conservative estimates for PA. Whereas an increasing transport scale may result in *improved* accuracy regarding the diffusion/sorption parameters, the *opposite* is anticipated for τ and β : An increasing transport scale is likely to *increase* the uncertainty. We have shown that accounting for variability in β is critical, in particular for providing accurate estimates of the tracer *first arrival*. Our results indicate that until a more general β-τ relationship is established for single fractures and fracture networks in granitic rock, the linear relationship $\beta=k\tau$ may provide a reasonable approximation. Also, the results show that the slope k estimated from the "hydraulic" aperture (obtained from hydraulic tests) provides an *upper bound* for k (2/0.06 mm = 33 000 m^{-1}), whereas k estimated using the injection flow rate and a simple flow path geometry, cf. Section 8.7, provides a *lower bound* (1 900 m^{-1}); thus the *hydraulic information* and *flow rate estimates* (either from dilution tests or direct flow measurements) may provide bounds for k for site investigation, where the lower bound from the assessment made using flow rates would represent a conservative estimate.

An important aspect of our evaluation results is that all model parameters are intuitive and consistent with properties commonly associated with discrete fracture-matrix systems: θ, F, K_d^m and random aperture fields. Moreover, all the parameters used in the modelling/evaluation can in principle be *verified*, either by laboratory experimentation on rock materials (θ, F and K_d^m) or simulation (β or k).

An important aspect of the developed LaSAR modelling framework used in the TRUE-1 evaluation, is its generality. The LaSAR approach can be applied for quantifying reactive transport in granular porous media (e.g., Cvetkovic and Dagan, 1994; Cvetkovic et al., 1998), in single fractures (Cvetkovic et al., 1999) as well as discrete fracture networks (Painter et al., 1998). The probabilistic framework of LaSAR enables the analysis of transport problems on a variety of scales, which makes it suitable for PA/SA. Thus using the LaSAR approach, the parameters estimated within TRUE-1 can in a consistent manner be incorporated within PA/SA analysis. Evaluation results of TRUE-1 tracer tests indicate that one of the most difficult challenges for PA/SA applications is *up-scaling* of β, and quantifying the corresponding uncertainty. In this context, we require a better understanding of the β-τ correlation, and its predictive potential. Also, we need to better understand the possibilities and limitations of using simple estimates, such as those provided by estimates of aperture, or by direct *in situ* measurement of flow rates in boreholes (flow meter data and/or tracer dilution test data), and constructing their statistics, combined with estimated source injection and transport problem length scales. Combining simulations of advective transport in single fractures, as well as in network of fractures, with experimental data from future detailed scale experiments and the ongoing TRUE Block Scale experiments, will provide a unique opportunity for further improving our predictive capability of retention processes in crystalline rocks.

9 Pore space from epoxy resin injection

One component of the First TRUE Stage is characterisation of the connected pore space of the target volume using resin injection and subsequent excavation. The purpose of the characterisation using resin is both qualitative and quantitative. On the one hand, resin may reveal the geometry of the flow pattern, thereby improving our understanding of the flow path geometry. On the other hand, resin may be used for estimation of physical fracture aperture, which could possibly be related in a quantitative manner to tracer advection and mass transfer. The detailed pore space data may also be used to provide insight into the validity of the assumptions made in the evaluation and modelling of tracer tests conducted in the same fracture plane and in fracture planes in general.

Prior to application of the resin impregnation technology in the TRUE-1 target structure, it has to be developed and tested in a pilot scale experiment in an easy accessible (near-drift) fracture. The objective of the Pilot Resin Experiment is to develop a proper resin injection technique, determine the rheologic properties of the selected resin under the field conditions that exist at Äspö and to assess that acceptable penetration of the resin into the fracture plane(s) can be obtained, and finally to analyse resin thickness from excavated core samples.

The technology development and planned field application of the pore space characterisation technology at the TRUE-1 site is designed to generate techniques that can be applied during subsequent experimental phases of TRUE.

This section describes the results of the performed Pilot Resin Experiment (PRE). A comprehensive account of the experiment and results is proveded by Birgersson et al. (2000a,b) and Hakami and Gale (1999).

9.1 Experimental procedure

The Pilot Resin Experiment has included the following main steps:

- Identification and characterisation of the test site
- Instrumentation with packer systems
- Resin injection
- Exploratory drilling (Ø 56 mm)
- Quantifiable drilling (Ø 200 mm and Ø 146 mm)
- Sample preparation
- Analysis of the pore space
- Conceptual modelling

9.2 Site description

A well defined, more or less isolated, structure located in the F-tunnel at the 450 m level in the Äspö Hard Rock Laboratory was chosen for the PRE, cf. Figure 1-3.

9.2.1 Main results from the site characterisation

The site was characterised using 9 cored boreholes, Ø 56 mm, each about 3–4 m in length. The characterisation programme included:

- Surveying
  - Collar coordinates
  - Deviation
- Geology
  - Core logging
  - Borehole TV (Pearpoint)
- Hydrogeology
  - Flow logging (resolution 0.05 m)
  - Measurement of hydraulic pressure
  - Interference tests
  - Tracer tests

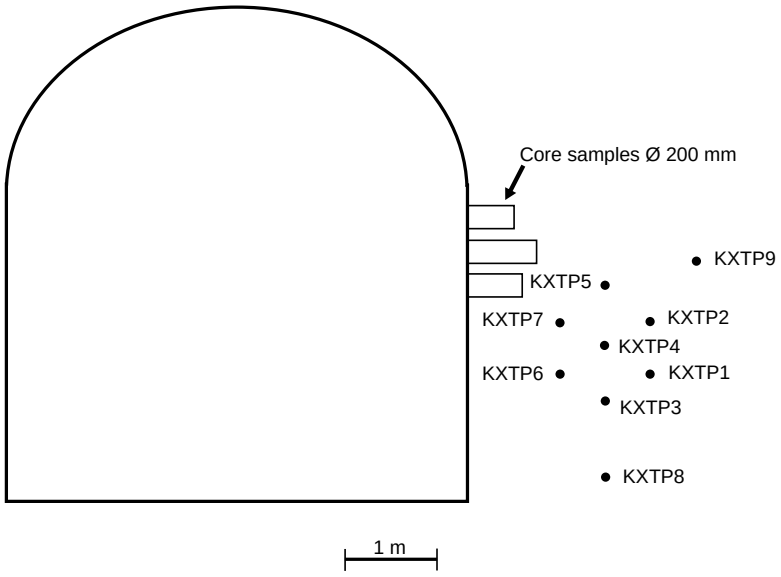

Figure 9-1. *Cross-section of the Pilot Resin site seen from the east. The intersection with the target structure for the nine KXTP-boreholes used for the site characterisation and three larger holes drilled prior to provide material for laboratory tests are illustrated.*

9.2.2 Drilling programme

All holes drilled at the site have been core drilled. All cores have been logged. A compilation of the boreholes is given in Table 9-1.

Table 9-1. Boreholes drilled at the Pilot Resin site.

Borehole	Number of boreholes	Diameter [mm]	Pilot hole [mm]	Comment
KXTP	9	56	–	Used to characterise the site
KXTRI	10 + 2	56	–	Used to characterise the resin spread
KXTE	3 + 3	200 / 146	36	Sampled the structures for resin

The KXTP1 through KXTP9 boreholes were drilled in order to characterise the site. These boreholes were drilled prior to the resin injection. The remaining boreholes were drilled after the resin injection. The KXTP boreholes are intersecting the target structure about 1–2 m from the drift wall.

The KXTRI1 through KXTRI10 boreholes were drilled in order to characterise the resin spread. The information from these boreholes were incorporated in a 3D CAD-model in order to guide the drilling of the large diameter boreholes.

The KXTE1 through KXTE6 holes were drilled in order to sample the structures at the site for resin. The core samples which were eventually used for the resin thickness analysis originated from these cores.

9.2.3 Core loggings and borehole TV inspection

The core logging and borehole TV inspections were carried out to characterise the fractures intersecting the cores with regard to fracture filling, fracture location (x, y, z) and absolute orientation (dip, strike). This information was combined for the nine cores to obtain a description of the structures at the site. The core logging, together with the hydraulic testing and the tracer tests, formed the basis for the descriptive model of the structures at the site, cf. Figure 9-2. Apart from providing the basis for the structural description, the core logging showed that:

- The dominating rock type is Äspö diorite, which is found in about 90–95% of the core length. The remaining 5–10% consists of red fine-grained granite.
- The fracture frequency is about 3–4 fractures per metre. The fractures are rather evenly distributed along the core length.
- The dominating fracture coating material is chlorite, followed by calcite. Both these coating materials are found in a large number of fractures. Epidote and quartz is found in a few fractures.

9.2.4 Hydraulic testing

Hydraulic testing was carried out in the KXTP boreholes in order to identify structures with high water inflow rates. The results from the hydraulic testing, together with the findings from the core loggings and the tracer tests, formed the basis for the descriptive model of structures at the site, see Figure 9-2. The hydraulic testing programme included:

- High resolution flow logging (0.05 m increments).
- Measurement of hydraulic pressure (in packed off sections).
- Interference tests.

It is quite obvious from the hydraulic testing programme that there are at least two important hydraulic structures at the site. These structures have been given a blue colour in Figure 9-2.

Flow logging

The flow logging was carried out using a single packer in such a way that it was possible to differentiate the water inflow into 0.05 m sections. The total inflow rates, pressure drops and calculated specific capacities are given in Table 9-2. On the average, about 50% of the total inflow into the entire borehole was found in a single 0.05 m section. The flow logging clearly showed that the water inflow into the boreholes can be associated with one or a few intersecting structures.

Flow logging was not carried out in boreholes KXTP5, KXTP6 and KXTP7 due to the very low water inflow rates observed in these boreholes.

Table 9-2. Water inflow rates and calculated specific capacities (Q/dH).

Borehole(s)	Inflow rate (Q) [ml/min]	Pressure drop dH (m)	Capacity (Q/dH) [m^2/s]
KXTP 1, 2 and 9	~ 70	~ 210	$\sim 6 \cdot 10^{-9}$
KXTP 3 and 4	~ 20	~ 110	$\sim 3 \cdot 10^{-9}$
KXTP 8	~ 10	185	$\sim 9 \cdot 10^{-10}$

Hydraulic pressure

The boreholes were equipped with mechanical packers packing off the interior of the borehole. The length of the sections varied between 0.6 and 2.9 m. The pressure in the sections were logged using individual pressure transducers and portable data loggers. It was found that the pressure generally increase with increasing distance from the drift. The gradient was found to be in the order of 100 m/m.

Boreholes KXTP1, KXTP2 and KXTP9 (and possibly also KXTP8) were found to have about the same hydraulic pressure, 20 bars. The hydraulic pressure in boreholes KXTP3 and 4 was about 10 bars. No reliable pressure data could be obtained from boreholes KXTP5, KXTP6 and KXTP7 due to very low water inflow rates into these borehole sections.

Interference tests

In the interference tests, one borehole was opened to atmospheric pressure and the pressure responses were monitored in the remaining eight boreholes. A change in pressure indicates a hydraulic connection between boreholes.

It is obvious from the results of the interference tests that there are at least two important flow systems at the site. The flow situation is in many ways similar in boreholes KXTP1, -2 and -9. Boreholes KXTP3 and KXTP4 exhibit a similar flow situation. These observations support the findings from the measurement of the hydraulic pressure and the flow logging, see above.

The structures of main hydraulic importance are illustrated in Figure 9-2.

9.2.5 Tracer tests

The purpose of the tracer test carried out at the site was to obtain estimates of transport properties. The tracer test was performed in a converging flow geometry by using the tunnel as sink. Two tracer injections were made in the packed off sections in KXTP2 and KXTP3, respectively. This correspond to one injection in each of the hydraulic important structures, see Figure 9-2. The injections were made as decaying pulse injection without applying any excess pressure. The tracers used were Uranine (sodium flourescein) and Rhodamine WT. Samples for tracer breakthrough were also taken in the packed off sections in KXTP1, KXTP3, KXTP4 and KXTP9. Occasional samples were also taken from seepage points in the tunnel.

Tracer injection in borehole KXTP2 gave a fast breakthrough in KXTP1 (<0.5 h) and a relatively high recovery (37%). The breakthrough in KXTP9 is much slower (first arrival = 5.5 h) and show a low mass recovery (0.1%) indicating a minor flow path.

The injection of Rhodamine WT in KXTP3 gave no breakthrough other than in the tunnel.

9.3 Descriptive model of the site

The objectives of the model building were to develop a geometrical model showing the boreholes and fractures in 3D as well as identifying the fractures that are associated with the most of the observed water inflow.

The descriptive model in 3D of the PRE site has mainly been constructed from the data and observations related to geology/geometry from the logging and results from the hydraulic tests and the tracer tests presented in the previous sections. The borehole TV was one important tool in the determination of the absolute orientation of the involved structures

The compilation of the information led to the interpretation that there are four main structures within the site. Two structures are intersected in boreholes KXTP1, KXTP2 and KXTP9. Another structure is intersected in KXTP3 and KXTP4. These three structures were found to be hydraulically active. Boreholes KXTP3 and KXTP8 are connected by another structure. The hydraulic importance of this structure was however found to be minor.

The target structure for the drilling campaign of the KXTP-boreholes can be found in all boreholes. The characterisation programme was initially focused upon this structure, but none of the boreholes, except for KXTP8, show any significant water inflow at the intersection with this structure. This structure was as a consequence found not suitable as the main target for the PRE. This finding was quite surprising.

The interpretation of the most hydraulic important structures at the Pilot Resin site is given in Figure 9-2.

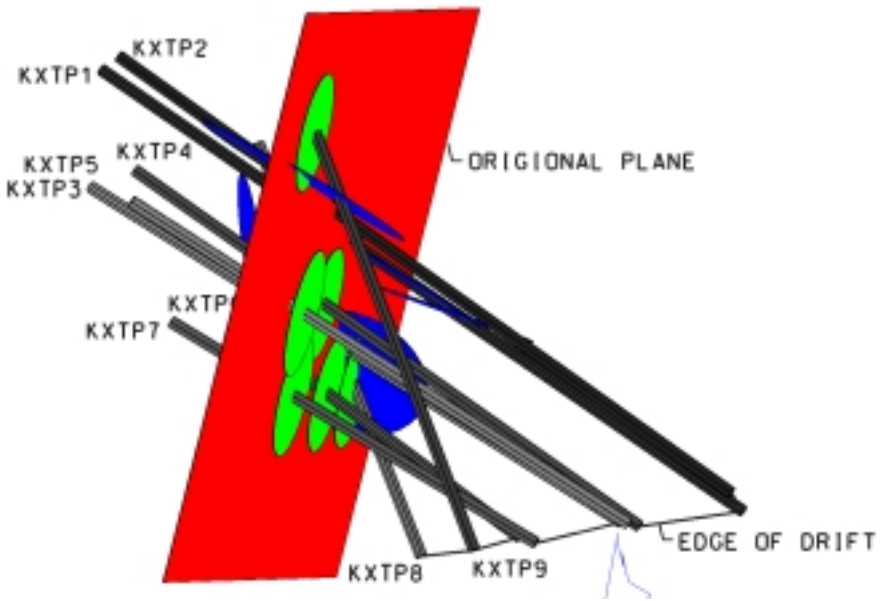

Figure 9-2. *View of the pilot resin site showing the KXTP-boreholes, fracture planes of main hydraulic importance (blue) and the initial target structure (green discs and red plane).*

9.4 Dye and resin injections

Laboratory experiments have shown that water in a fracture has to be removed or exchanged with another liquid, using i.e. alcohol, before resin is injected in order to obtain a good resin impregnation without any "fingering" effects. This was achieved in the field using injection of iso-propanol. Apart from being tested in the laboratory, this procedure has been tested during *in situ* epoxy resin tests at the Grimsel test site in Switzerland (Dollinger et al., 1995).

It is important to ensure that water and resin flow in the same flow paths. Therefore, all fluid injections prior to the actual resin injection were labelled with a slightly sorbing dye (Rhodamine B) which should not be washed away during subsequent excavation and drilling activities.

These considerations resulted in the following injection sequence:

- Dye-labelled water.
- Dye-labelled iso-propanol.
- Dye-labelled epoxy resin.

The resin injection sequence started with injection of water labelled with a slightly sorbing dye, Rhodamine B. Subsequently iso-propanol was injected, also labelled with Rhodamine B. Finally, epoxy resin labelled with uranine and a dye was injected. The resin injection was carried out using a specially designed injection pump. The two resin components (resin + hardener) were continuously mixed in line in proper proportions (4:1).

9.4.1 Resin injection strategy

Once the two resin components are mixed, the curing process starts and the viscosity will increase with time. It will take a few hours before the resin have cured so much that it no longer is possible, using moderate injection pressures, to inject it further into the fractures.

The strategy of the resin injection was to:

1. Get the resin "far" into the target structure intersecting the injection section.

2. Create a boundary "far" away from the injection hole as the resin cures, against which the pressure could build up.

3. Continue to inject against this boundary "as long as possible" in order to get a good resin impregnation of the structure(s).

At the time of the resin injections, a total of nine boreholes (the KXTP-holes) were available. To start with, all boreholes were packed off and closed. The injection took place in one hole at the time. When the injection was started, one or a few of the other

boreholes were opened in order to speed up the resin spread. During some of the injections, a resin breakthrough was observed in sections which were kept under atmospheric pressure. Resin was allowed to bleed from these holes for a couple of minutes before the section was shut in, in order to increase the pressure and create a boundary.

9.4.2 Resin injections

Resin was injected in boreholes KXTP1, KXTP2, KXTP3 and KXTP7. The injections in KXTP1, KXTP3 and KXTP7 were successful, while the injection in KXTP2 did not succeed due to a packer failure, cf. Table 9-3. The injection pressure was at all times kept between 30–55 bars.

The injected resin was labelled with different dyes (blue, red and green) for the different injections in order to allow identification of origin. A fluorescent dye, uranine, was in addition added to all resin mixtures in order to facilitate the subsequent analysis of the resin thickness. The hardener was not labelled.

Resin injection in borehole KXTP7

Resin labelled blue was injected in borehole KXTP7. A total resin volume of a few 100's of ml's was injected during about 9 hours. Boreholes KXTP5 and KXTP6 were kept open and used as drainage holes. Resin breakthrough was seen in the inner part of the lowest of the large diameter sampling holes (200 mm hole) drilled into the target fracture, cf. Figure 9-1.

Resin injection in borehole KXTP3

Resin labelled red was injected in borehole KXTP3 while borehole KXTP4 was kept open and used as drainage hole. A total of resin volume of about 2000 ml was injected during about 4 hours. Resin breakthrough was seen in borehole KXTP4.

Resin injection in borehole KXTP1

Resin labelled green was injected in borehole KXTP1 while boreholes KXTP2 and KXTP9 were kept open and used as draining holes. A total resin volume of 1500 ml was injected during about 6.5 hours. Resin breakthrough was observed in borehole KXTP2.

Resin injection in borehole KXTP2

Injection had to be stopped after about 15 minutes due to packer failure.

9.4.3 Outcome of the resin injections

It was possible to inject resin for several hours during the injections. This was a very positive outcome, since it prior to the injections was estimated that it should only be possible to inject resin for about one hour.

It was possible to inject relatively large volumes of resin into the structure. The injected volume in the structures should cover an area of square metre(-s) assuming a fracture aperture of 0.1–1 mm. This was a positive result compared to what was expected.

The injection pressures were up to about 50 bar above the natural pressures, but no significant pressure increases were observed in the adjacent boreholes. This indicates that the pressure drop was located in the vicinity of the injection hole.

The mixing of the two components that constitute the injected resin was carried out continuously by mixing the two fluids emerging from the cylinders using a common mixing head. It was however not possible to maintain the constant mixing ratio (4:1) during the entire duration of the injections.

Table 9-3. Summary of performed resin injections at the Pilot Resin Experiment site.

Injection hole	Hydraulic conductivity	Injection time	Injected volume	Injection pressure	Resin breakthrough	Pressures
KXTP7	Low	9 hours	A few 100´s ml´s	Up to 55 bars (natural pressure 6 bar).	In the lower sampling hole in the target structure after about 1 h. Distance ≈ 0.5 m.	No pressure increase in the other boreholes
KXTP3	Medium	4 hours	One or a few 1000´s ml´s.	Up to 55 bars (natural pressure 10 bar).	Resin breakthrough in KXTP4. Distance ≈ 0.5 m. No resin breakthrough in the drift.	Pressure increase in borehole KXTP4 (expected). No pressure increase in the other holes.
KXTP1	High	6.5 hours	About 1500 ml´s.	Up to 45 bars (natural pressure 20 bar).	Resin breakthrough in hole KXTP2.	No observed pressure increase.
KXTP2	High	Injection had to be stopped after about 15 minutes due to packer breakdown.				

9.5 Sampling procedure

The sampling of the site for resin impregnated fractures started with drilling of the twelve (10+2) Ø 56 mm exploration boreholes (the KXTRI boreholes), each with a length of about 4 m to assess the resin spread. These drill cores were inspected for resin occurrence. This information was incorporated in a CAD-model in order to guide the subsequent sampling using large diameter core holes.

The sampling of the resin impregnated fractures was carried out using large diameter core holes. The drilling arrangement was changed from a Ø 200 mm single tube drilling with a small diameter pilot hole which was used to bolt the core (KXTE1 through KXTE3) to Ø 146 mm triple tube drilling (KXTE4 through KXTE6). This change was imposed by the large number of unwanted core breaks when handling the cores of the essentially subhorizontal boreholes. Most core breaks took place in resin filled fractures. This observation initiated laboratory experiments regarding resin bonding, cf. Section 9.7.

A summary of the resin findings in the six KXTE cores is given in Table 9-4.

Table 9-4. Compilation of resin occurrence in the KXTE cores.

Core	Core section [m]	Section length [m]	Comment
KXTE1	1.95–2.83	0.88	Probably resin.
KXTE2	1.5–1.9	0.4	Probably resin.
KXTE3	0.86–1.55	0.69	Contains resin.
KXTE4	–	–	No candidates
KXTE5	1.7–1.9	0.2	Might contain resin.
KXTE6	1.7–2.0	0.3	Contain resin. Core destroyed.

It can be seen from Table 9-4 that about 2.5 m of the KXTE cores contain, or may contain, fractures which have been impregnated with resin. The core sections used for analysis of the resin thickness were taken from KXTE1 and KXTE3, see Figure 9-3.

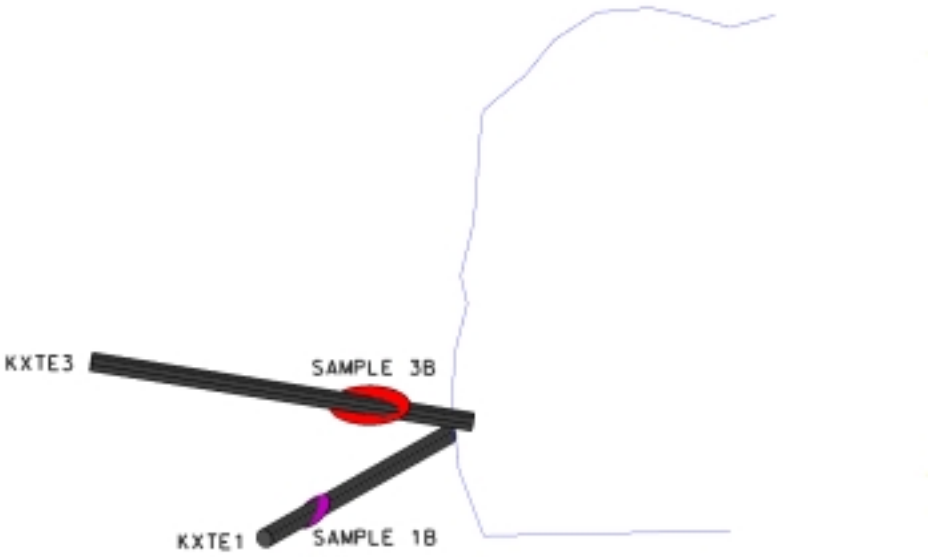

Figure 9-3. *Resin sampling holes KXTE1 and KXTE3 (vertical section seen from west) The indicated discs illustrate the location of the fracture planes used for resin thickness analysis.*

It can be seen in the figure that the two fracture planes have quite different dips and strikes and that they are located quite close to the drift wall. The fracture making up Sample 3B (012/88) is located about 1.2 m from the drift and the fracture making up Sample 1B (251/58) about 2.4 m from the drift.

9.6 Analysis of pore space

The main objective of the Pilot Resin Experiment is to develop and test methodologies which can be used to describe the aperture distribution of a selected fracture, and characterise the fracture pore space at *in situ* fracture conditions.

One objective with the pore space data analysis was to perform the analysis of the collected data using two slightly different techniques.

Samples of the two different resin impregnated fracture planes, Samples 1b and 3b, were collected and mapped for the thickness of the resin filled fracture pore space, the observed (non-filled) voids, and contact areas (between fracture surfaces). For this purpose, a series of sections were cut on which the above entities were mapped.

Two techniques where employed in the analysis, 1) based on an *image analysis* system developed by Royal Institute of Technology, Stockholm (KTH) and 2) based on a *photo-microscope* technique developed by Fracflow Consultants Inc., S:t Johns, Canada, have been applied to measure the fracture apertures in the resin filled fractures. The two techniques are quite similar in principle. They both imply measurement of fracture resin layer thickness in sections cut orthogonal to the fracture surface. The main difference is that the photo-microscope technique is based on continuous traces (manual digitising) of the fracture surface profiles on a series of overlapping photographs, whereas the image analysis technique is based on individual measurements at a given separation on continuous digital binary images along the section profile. The distance between the measurement points in both cases is 0.07 mm.

9.6.1 The analysed samples

Sample 1b

This fracture belongs to a group of tension fractures which have fracture infillings consisting of idiomorphic calcite crystals. The main part of the fracture consists of one single fracture with a fairly constant aperture. The surfaces of the fracture are generally fairly rough, suggesting that no movement has occurred along the fracture. The resin impregnation of the fracture is complete and there is very little contact noted between the fracture surfaces.

Sample 3b

Sample 3b is from another group of fractures that has been observed at Äspö, which are generally characterised by hydrothermal alteration of the adjacent wall rock. Generally, the fracture surfaces of Sample 3b are smooth and the aperture is fairly constant, except in areas with infilling material, suggesting that a movement has occurred along the fracture. Portions of Sample 3b consists of void spaces or areas not filled with resin.

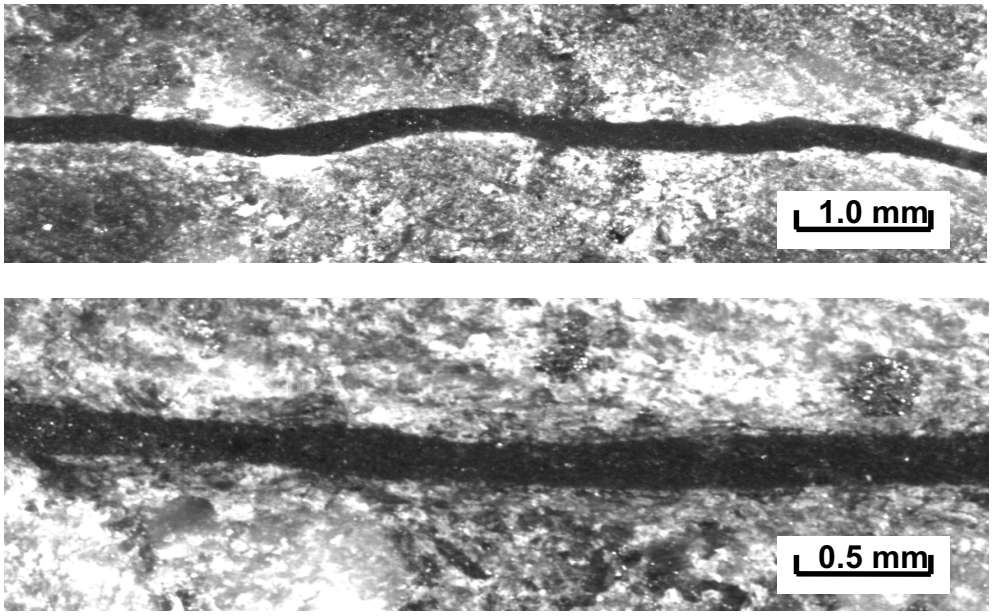

Figure 9-4. *Image examples. a) Typical section from Sample 1b. Fairly constant aperture. Fairly rough fracture surfaces. b) Typical section from sample 3b in area without contacts. Fairly constant aperture between contacts. Smooth surfaces.*

9.6.2 Pore space statistics

Both fracture planes that were analysed were cut into four equal size quadrants. The resin thickness in quadrants I, II and III were measured using the "image analysis technique" (KTH). Quadrant IV was measured using the "photo-microscope technique" (Fracflow). Table 9-5 summarises, for both samples, the statistics for each quadrant and the total sample. For each quadrant and for the total sample, the data from the profiles are lumped together and the statistics calculated on all data. It can be seen from the table that the mean aperture is fairly stable between quadrants in both samples. No major differences can be seen between results obtained using the different methods.

The mean aperture in the resin impregnated areas is in the same order for both samples, 281 μm and 295 μm, respectively. Also the coefficient of variation of the aperture is in the same order for both fractures, 37 % and 39 %, respectively. The difference in character between the two samples is revealed in the larger percentage of contact areas for Sample 3b, and also in a larger percentage void area for this sample.

Table 9-5. Summary statistics of data from complete samples and sample quadrants.

Fracture Sample	Mean Aperture Resin	Coefficient of variation	Contact Area	Void area	Mean Aperture All data
	[μm]	[%]	[%]	[%]	[μm]
1bI	308	33	0.5	0	284
1bII	280	32	1.6	0	260
1bIII	240	41	2.3	0	221
1bIV	290	39	0.02	0	289
1bTotal	281	37	1.0	0	266
3bI	310	27	31	18	218
3bII	327	31	21	9	258
3bIII	282	39	37	17	179
3bIV	278	46	13	27	268
3bTotal	295	39	22	20	239

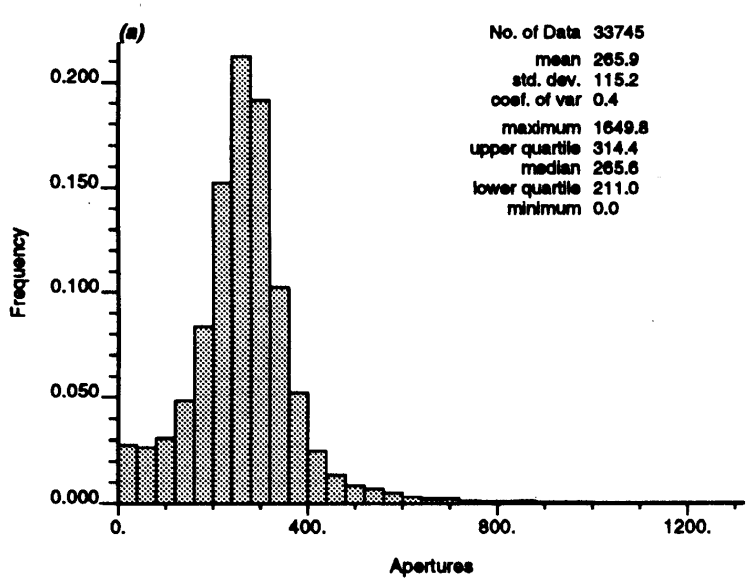

Figure 9-5. *Example of a histograms showing aperture (μm) distribution of Sample 1b (integration of all four quadrants). Contact areas are included in the analysis.*

9.6.3 Aperture distribution

An example of a frequency histogram of aperture is given in Figure 9-5. For each histogram, the mean aperture, median, standard deviation, coefficient of variation, maximum and minimum, and the upper and lower quartile of resin thickness (in micrometers) are calculated and plotted along with the histograms. The histogram presented in Figure 9-5, relevant to Sample 1b is based on more than 33 000 data points (aperture measurements).

9.6.4 Analysis of spatial variability

The spatial continuity of the aperture was determined by carrying out semi-variogram analyses on both samples using the complete aperture data sets (resin + voids + contacts).

Figure 9-6 shows an example of variograms and fitted models in the X and Y directions for analysed data from Sample 3b. The experimental variograms rise from the origin (no nugget effect) and more or less level off at distances of about 3 to 5 mm, suggesting a practical range of about 3-5 mm. The value at which they level off, i.e. the initial sill, varies with direction and the quadrant analysed.

It can be seen that the presented variograms in both the X and Y direction show a fairly constant sill, suggesting strong continuity with distance. For both Sample 1b and 3b, the fitted models in both directions can be closely described by a nested model comprising of two exponential models.

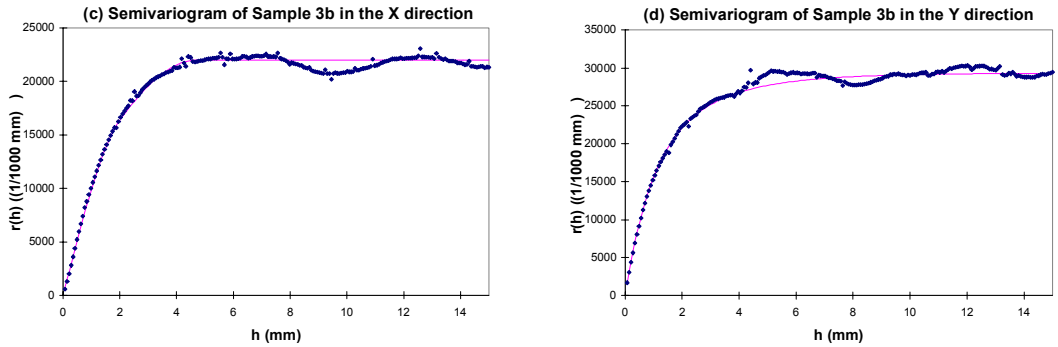

Figure 9-6. *Sample 3b. Semivariograms for X- and Y-directions based on all four quadrants.*

9.7 Discussion and conclusions

In situ resin injection followed by excavation and aperture measurements has been demonstrated in the Pilot Resin Experiment. The results show that a workable method is available which can be used to obtain valuable information on the connected pore space to be used for conceptual modelling.

Site

The site selected for the Pilot Resin Experiment was quite suitable with regard to the overall purposes of the experiment. The site was however more structurally and hydraulically complex than first assumed.

One drawback with the PRE site the near-drift location. The use of ordinary drill and blast schemes makes it likely that site is damaged close to the tunnel periphery and disturbed due to stress rearrangement. This implies that the obtained results are not necessarily valid for undisturbed rock further away from the drift. It should however be remembered that the main objective with the performed Pilot Resin Experiment was to develop techniques to be applied at other locations.

Resin and resin injection

The curing time for the resin as well as the resin spreading was found to be good. This is a very positive outcome, since one of the concerns prior to the experiment was that the curing time might be too short to allow acceptable penetration.

Rhodamine B has not been found to be a good agent to tag the water flow paths within the injected fractures. Rhodamine B may have affected the colour of the resin and may therefore have complicated the evaluation of resin origin. The water and iso-propanol injected prior to the resin should therefore be labelled with other types of dyes in future experiments. Performed post experiment resin bonding experiments in the laboratory have shown that water chemistry, iso-propanol and the addition of uranine have little effect on the resin bonding. Rather it appears that the apparent separation of resin from the rock that was observed in some samples is related to stress relief when the static load is removed from the fracture plane, or destressed by over coring drilling.

Excavation/sampling procedure

The arrangement with drilling exploratory sampling boreholes, Ø 56 mm, prior to the sampling of the site using large diameter drillings was found necessary. It was not possible to predict the resin spread prior to the drilling of the Ø 56 mm holes except for some “qualified guesses” that could be made based on resin breakthroughs in adjacent boreholes during the resin injections.

Pore space analysis

Both the image analysis and photo-microscopic methods show the same magnitude of aperture, and similar standard deviations. Both methods have sufficient accuracy for fractures with a mean aperture larger than about 100 μm.

Both measurement techniques can be improved with increased colour contrast between the epoxy resin and the natural materials of the rock.

The photo-microscope technique has been the fastest technique employed in this project. The time needed for the image analysis technique is more dependent on the particular image contrast conditions of a specific fracture sample. The possibilities for automatisation, and higher analysis speed, increase with good image contrast between the resin and the rock.

Pore space analysis in Detailed Scale experiments

The transmissivity of injected features at the PRE site is considerably lower (one to two orders of magnitude) compared to that of Feature A at the TRUE-1 site and other potential target structures. This implies that it may be harder to obtain a good resin spread, but also less problem with the "natural" water flow and water pressure at the TRUE-1 site.

The bonding of the resin to the fracture surfaces was at several locations found to be very weak. The observed bonding problems might become even larger at the TRUE-1 site, or at other potential target structures, compared to the PRE site due to even larger stress releases.

One factor that complicated the injections at the PRE site was the large hydraulic gradient, > 100 m/m. The hydraulic gradient at the TRUE-1 site, and possibly at other potential target structures, is significantly lower which will facilitate the spreading of the resin.

The target structure at the TRUE-1 site is located about 10–15 m away from any drift. This will make the sampling of the target structure quite complicated and expensive. One way to sample the target structure is to drill large diameter (Ø 96–146 mm) triple tube boreholes subparallel to the investigated feature and study the resin thickness/aperture in those parts of the fracture plane that are recovered in these cores. Alternatively, the target structure can be accessed by excavating a drift to the vicinity of the target structure and sample the structure by short large diameter triple tube boreholes.

Both techniques for measuring the fracture aperture can be used in future experiments. The photo-microscope method may be preferred when extensive profiles are to be measured and the fracture geometry or information is not very complex. The image analysis technique may be preferred when there is a need to attach different information to each separate data point, for example if the geometrical pattern is complex or if information about filling materials is also to be recorded.

10 Integrated main results

This chapter sets out to integrate the results from the characterisation and tracer tests performed at the TRUE-1 site. What do we know about the geological, mineralogical and structural character of Feature A? How does the feature behave hydraulically, and how does it connect hydraulically to its immediate environment? What controls groundwater flow in the studied block, and in Feature A in particular? Further, what processes control transport of solutes in Feature A?, and in particular the transport of sorbing tracers?

10.1 Geological and structural model

The developed geological and structural model describes the conductive geometry of the investigated site and the target feature for the performed tracer tests. The investigated site is bounded by a series of major structures. These structures include Fracture zones NNW-4, NW-2, NW-3, cf. Figure 4-2. Another structure, NW-2', bounds the investigated block in the immediate vicinity of the investigated target feature, Feature A. The latter structure is interpreted to be in hydraulic contact with Feature A, cf. Section 10.2.

Four structures have been identified in the studied block, Features A, B, C and D. Of these, Features B and D show multiple intercepts in each borehole, interpreted to be complex and made up of multiple fractures, and are represented in Figures 4-2 and 4-3 in a simplified way. Feature C is interpreted as a subhorizontal feature, known in two boreholes. The feature is regarded as uncertain, but can potentially establish connection between Features A and B.

Feature A, intersected by five boreholes, is a reactivated mylonite which has been exposed to brittle deformation, the latter which has formed the main fault plane. This fault is interpreted to constitute the main conductive element of Feature A. This type of conductor is typical of the investigated block, and also to Äspö in general. A conceptual breakdown of the structural and conductive elements in the TRUE-1 block is shown in Figure 10-1. Feature A shows different geometries at its five intercepts but can be interpreted either as one undulating structure, or alternatively, as a structure made up of several interconnected fractures. The extent of Feature A is estimated at 10–20 m. No intercept is interpreted in the tunnel.

Feature A which essentially follows the mylonite, is interpreted to be bounded by a rim zone consisting of altered Äspö diorite which constitutes a band of disturbed rock along the studied feature. The main difference between the two lithological units is found in mineralogical composition, grain size and porosity, where the porosity of the mylonite is lower than the altered Äspö diorite. The total thickness of the feature including

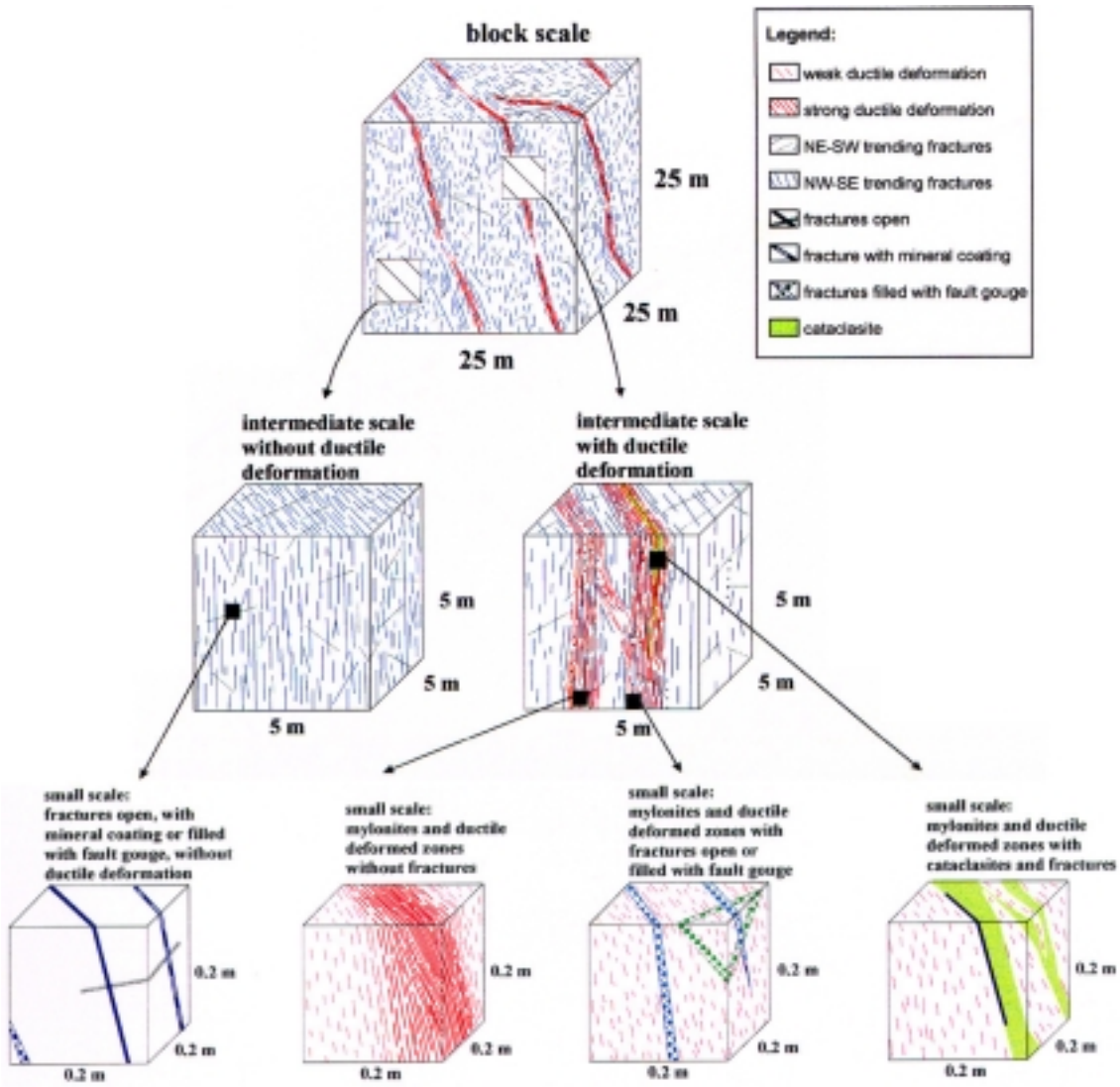

Figure 10-1. *Schematic conceptual breakdown of structures and conductive elements at different scales in the TRUE-1 block (from Bossart et al., in prep.).*

altered Äspö diorite is varying between 0.05 and 0.09 m. The physical aperture of the fracture is assumed variable and is estimated to be in the order of 1–3 mm.The fault plane is not centred on the mylonite along its extent, cf. Figure 10-2. As a consequence, water is assumed to be interchangeably in direct contact either with mylonite or altered Äspö diorite.

The main fracture minerals in Feature A are calcite, fluorite, quartz, k-feldspar and pyrite, found as idiomorphic crystals. SEM/EDS analyses also show the presence of clay minerals as an outer rim of the fracture mineral coating. This suggests that gouge material may be present in Feature A, but this has not been substantiated by the performed core drilling. Subsequent drilling with triple tube techniques within the framework of other projects at Äspö has shown hard evidence of fault gouge in structures similar to Feature A (Puigdomenech, et al., 1999). It is assumed that the

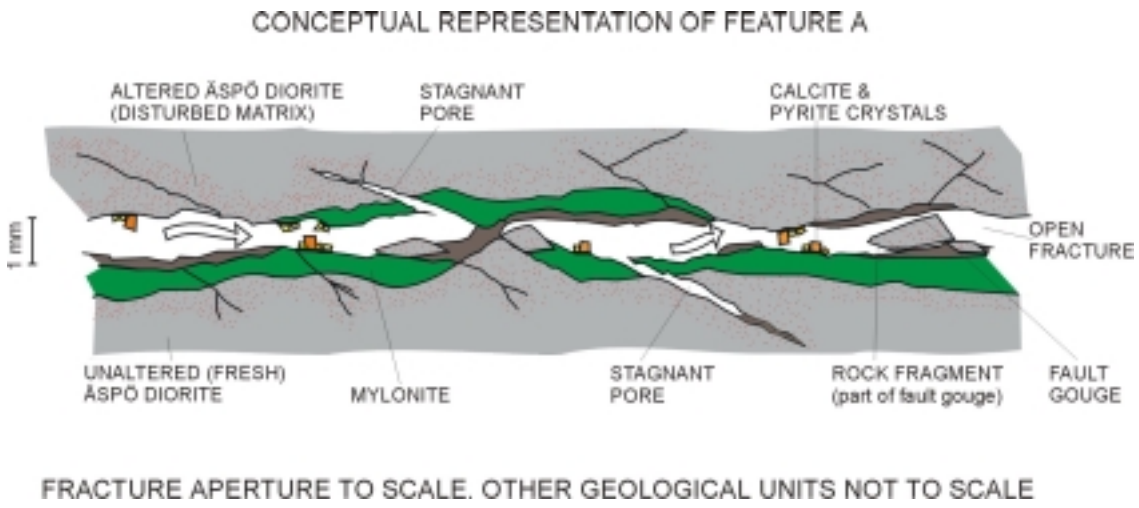

Figure 10-2. *Schematic conceptual representation of Feature A in cross section. Note that the fracture aperture is to approximate scale. The thickness of the remainder of the constituents is not to scale. The total thickness of Feature A including altered Äspö diorite is varying between 0.05 and 0.09 m.*

gouge material apart from a fine clay fraction, consists of macro-sized fragments of primarily altered Äspö diorite.

10.2 Hydraulic model

With the hydraulic model we understand a description of the entities which control groundwater flow in the TRUE-1 block and in the target Feature A. The understanding of groundwater flow is the base for designing discriminating and quantifying tracer tests in the studied Feature A, which ultimately will increase our understanding of transport of conservative and sorbing tracers.

Hydraulic tests show flow dimensions greater than two, and sometimes higher than three, indicating that Feature A can be regarded as a leaky aquifer, possibly affected by a constant head boundary. In some cases constant head boundaries are evident which can be attributed to the structures bounding the investigated block, cf. Section 10.1. The hydraulic tests have eg. shown effects of Zone NW-2. An additional constant head boundary in the vicinity of the experimental site is the tunnel itself which constitutes an atmospheric boundary.

The measurements of hydraulic head clearly indicate that there exists a hydraulic gradient towards the tunnel with a higher head in the interior of the borehole array than that observed in the borehole sections closest to the tunnel wall. The hydraulic gradient across the block has increased from about 0.6 m/m to about 1.0 m/m during the course of the project.

The hydraulic head evaluated from pressure measurements in packed off sections containing individual structures also indicate groundwater flow directed towards the tunnel. The hydraulic gradient in the investigated Feature A has been found to be relatively stable at 10% over the duration of the project.

Performed interference tests show that sections containing identified structures within the TRUE-1 block, Features A, B, and D, all respond in unison to disturbances outside the investigated block. Indirect evidence in support of this response pattern, other than the responses themselves, are the flow dimensions inferred from interpretation of hydraulic tests which yield flow dimensions varying between 2–4. High values on the flow dimension indicate pseudo-spherical flow, or an effect of a leaky aquifer system, possibly in combination with a constant pressure boundary.

With regards to the structures bounding the investigated area, Feature A is interpreted to be in hydraulic contact with Zone NW-2', as evidenced by the similar hydraulic head in the two structures and a similar chemical signature. In fact, when we apply pumping in Feature A, in the preferred pumping section KXTT3:R2, we may to some extent stimulate Structure NW-2', given the close proximity of this section to the interpreted intersection between the two structures, cf. Figure 4-2. Likewise, the relatively high transmissivity of Feature A evaluated for its KXTT3 intercept may reflect this close proximity intersection between NW-2' and Feature A.

Hydraulic head data support a relative separation between Feature A (and NW-2') on the one hand and Features B and D. The latter group which shows a 10 metre lower hydraulic head. In addition, Feature A responds in a more isolated way (single section response) compared to Structure B and D when a section in a given structure is allowed to flow, cf. Appendix D. It should also be noted that a three-dimensional flow situation, as suggested by the noted pressure responses and evaluated flow dimensions, should manifest itself in an equilibrated pressure distribution within the studied block. However, this is not what is seen in the hydraulic head data. Consequently the view of Feature A as a leaky aquifer model is assumed to hold.

The transmissivity of Feature A ranges from about $8 \cdot 10^{-9}$ to $4 \cdot 10^{-7}$ m^2/s. A typical specific storage for Feature A based on the evaluation using General Radial Flow theory is in the range $1 \cdot 10^{-6}$ to $2 \cdot 10^{-5}$ s^{-1}.

Hydrogeochemical analyses show that the groundwater sampled in Feature A is saline with a chloride concentration in excess of 5000 mg/l. The chemical data support the interpretation of the relative isolation of Feature A in relation to adjacent structures. Stable isotope data indicate that the sampled waters are derived from post-glacial environments.

Groundwater flow in the TRUE-1 block is directed towards the tunnel. A possible drainage route for the block is a sequence; NW-2 → NW-2'→ Feature A (possibly Feature C) → Features B and D → the tunnel by way of NNW-4, where the main sink is exerted by NNW-4's intersection with the TBM Assembly Hall, cf. Figures 4-2 and 3-1. The drainage of Feature A to Structure B is substantiated by pressure registrations in KA3005A .

The flow in Feature A is directed from the extreme upstream section KXTT3:R2 towards KA3005A and the tunnel. It should be emphasised that Feature A has no interpreted intersection, nor any visible outflow at the point of projected intersection with the tunnel. However, a reactivated mylonite does occur at the projected location of the intersection with the tunnel, but with a much more gentle inclination. The latter structure shows no visible indications of water seepage. It cannot be ruled out that the observed feature constitutes a splay of the investigated Feature A.

No significant changes in natural flow rate has been observed in repeated tracer dilution tests in packed-off borehole sections over the period October 1995 through April 1997. Values of natural groundwater flow in Feature A range from 0.1 ml/min (KXTT1) to about 1.4 ml/min (KXTT3). The observation of a stable background flow is also supported by a stable hydraulic gradient in the order of 10%. Minor deviations from this stable gradient is observed in conjunction with the PDT-1 and PDT-2 tests, cf. Section 7.1.

10.3 Transport of conservative tracers

Connectivity in terms of solute transport breakthrough has been established throughout the investigated portion of Feature A. A subtle balance exists for overcoming the background flow and obtaining breakthrough for a given flow path over longer distances, and at low flow rates. The minimum flow rate at which acceptable mass recoveries have been obtained is about 0.2 l/min.

Transport parameters (fracture conductivity, flow porosity and dispersivity) interpreted from the initial evaluation are generally, with a few exceptions, in good agreement, indicating a relative homogeneity in transport properties for different source-sink pairs (flow paths). The fracture conductivity K_{fr} obtained from the evaluation vary from $2.8 \cdot 10^{-4}$ to $7.1 \cdot 10^{-4}$ m/s, if the flow paths with low mass recovery are discarded. Likewise, the evaluated flow porosity θ_k vary from $0.4 \cdot 10^{-3}$ to $2.4 \cdot 10^{-3}$.

The dispersivity inferred for the flow path KXTT4→ KXTT3 is about 7 times higher than for the path KXTT1 → KXTT3. The latter observation provided early indication of the possible existence of two fractures forming the inlet for tracer to Feature A in KXTT4. During STT-2, cf. Section 10.4, where the flow rate is 50% of that employed during STT-1, performed in the same flow path, the breakthrough shows a distinct dual peak, with the peaks separated by approximately 17 hours. This effect is attributed to the reduced flow rate in combination with a subtle change in boundary conditions. The anomalous high dispersivity interpreted for the preceding conservative tracer tests, has hence been shown to be an indicator of the presence of dual merging flow paths, with similar properties, masking one another in the tests preceding STT-2. The hypothesis of dual flow paths being responsible for the observed double peak is supported by an observed double peak in the response function obtained from deconvolution of the experimental data.

10.4 Mass transfer

Cation exchange is the major sorption process relevant to Äspö conditions for the weakly to moderately sorbing tracers Na^+, Ca^{2+}, Sr^{2+}, Rb^+, Ba^{2+}, Cs^+ used in the laboratory experiments. These tracers were also used in the performed field experiments. In addition, K^+, Co^{2+}, and the anion TcO_4^- were used in the *in situ* experiments.

Laboratory results show that the sorbtivity of the geological material is depending on the amount of biotite available. The higher the biotite content the higher the sorbtivity. These high-capacity minerals are aligned with the fracture surfaces and are short-circuited by micro-cracks.

The sorbtivity of the tracers used in the laboratory experiments on geological material from Äspö, show the following relative order; $Na^+ < Ca^{2+} \approx Sr^{2+} < Rb^+ \approx Ba^{2+} < Cs^+$, ranging from $(4–30)\cdot10^{-6}$ m^3/kg for Na^+ to $(10–300)\cdot10^{-3}$ m^3/kg for Cs^+ (Byegård, et al., 1998). The observed relative sorbtivity is also consistent with the results of the *in situ* tests using the above tracers. Diffusivities for the site-specific material from Feature A are in the order of $1.3–3 \cdot10^{-14}$ m^2/s.

The average porosity of the generic matrix Äspö diorite is estimated to 0.4%. The diffusion porosity of the single diffusion cell with site-specific Feature A material, dominated by mylonite, is estimated to 0.1% . The porosity of the mylonite is generally lower than in the altered Äspö diorite.

Laboratory results show indications of extremely slow reversible processes, or alternatively irreversible sorption, for Cs, Rb and Ba. Experimental results from the *in situ* experiments with sorbing tracers (STT-1, STT-1b and STT-2) show indications of very slow reversible sorption of Cs, but also of Co and Ba. At the time when the pumping for STT-2 was discontinued in October 1998, approximately 63% of the Cs mass initially injected still remained sorbed on the rock faces of the injection section and the fracture after some 15 months.

Tracer breakthrough was observed for all sorbing tracers previously employed in the laboratory. No breakthrough was observed for TcO_4^-, indicating reduction to the strongly sorbing TcO_2, which was expected, and to be demonstrated. However, none of the sorbing tracers could be fully recovered, partly due to the duration of the sampling, and in part because of the short half-lives of some of the isotopes.

The preliminary evaluation using a simple homogeneous model with linear surface sorption could only be made to fit for the weakly sorbing species Na and Sr.

Enhanced diffusion/sorption relative to the Modelling Input Data Set (MIDS) derived from laboratory through-diffusion tests has been interpreted from the performed evaluation of the tests with sorbing tracers. The evaluated *f*-factor, cf. Chapter 8, varies in a narrow interval (40–137 (STT-1), 32–34 (STT-1b) and 32–96 (STT-2)). This enhancement may be partly attributed to sorption (stronger sorption in the field than in

the laboratory), but the main reason for the enhanced diffusion is attributed to physical effects (higher matrix porosity/diffusivity than observed in the laboratory). The observed enhanced diffusion in the tests with sorbing tracers is in a physical sense attributed to an altered rim zone along fracture surface, featured by increased porosity through hydrothermal alteration and increased micro-fracturing.

The effect of diffusion into stagnant zones has been included in the evaluation and is most evident for transport of tritiated water (HTO), although being comparatively small.

Evidence of gouge material in Feature A exists in the form of remnants of clay particles on fracture surfaces (chlorite and clay minerals on fracture rims), cf. Section 3.4. No gouge material has actually been recovered in the TRUE-1 cores but results from borehole KA3065A01 as part of the REX project (Puigdomenech, et al., 1999) indicate that the amount of unconsolidated gouge material is in the order of 1.1 kg/m^2. Sorption in gouge material is included in the evaluation framework of the TRUE-1 sorbing tests, but is not critical to evaluation of strongly sorbing tracers, eg. Cs, this since the kinetic effects are small. However, kinetic effects are dominant for the weakly sorbing species Na and Sr, attributed to sorption in the gouge material. In the case of Ba and Rb the kinetic effects due to matrix diffusion and sorption are comparable to those of sorption in the gouge material.

10.5 Heterogeneity within Feature A

Feature A is intercepted by five boreholes. It is clear that five data points are not sufficient for a rigorous analysis of heterogeneity and spatial correlation of eg. transmissivity. Attempts made to infer two-point statistical estimates using the obtained transmissivity data are presented by Winberg (1996). These inferences regarding spatial variability of transmissivity indicate a correlation length for transmissivity of about 0.3–0.4 m (Winberg, 1996).

Likewise, compilations of two point statistics related to (hydraulic or physical) aperture relevant to Äspö and Stripa conditions show a span of reported practical ranges for aperture of approximately 0.005–0.1 m (Hakami, 1995) and 0.05–0.2 m (Abelin, 1990), for Äspö and Stripa conditions, respectively. Subsequent analysis by Hakami and Larsson (1996) on a specimen from Äspö HRL, indicate practical ranges of 0.005–0.02 m. The lower bounds reported by Hakami (1995) and Hakami and Larsson (1996) fit with the practical ranges observed for the analysed samples from the Pilot Resin Injection experiment, 0.003–0.005 m, cf. Section 11.4.

The preliminary evaluation of the performed transport experiments show, with a few exceptions, very similar transport parameters (dispersivity (accounting for all small scale heterogeneity), hydraulic aperture and flow porosity). This finding indicates, at least from a transport perspective, that the studied Feature A shows a relative homogeneity as inferred from the investigated flow paths, cf. Figure 7-1 and Table 7-1.

The results of the evaluation indicates that the diffusion is about 25–30% more enhanced in the flow path KXTT4→KXTT3 compared to the path KXTT1→ KXTT3. The factor *f* should be viewed as an effective value along a given flow path. The observed variability between the two flow paths can thus be due to larger scale heterogeneity. In principle there should not be a difference in *f* as evaluated from the STT-1 and STT-2 tests which have been run in the same flow path. The observed difference in *f* suggests the two tests have seen different flow paths. This is also substantiated by the dual peak breakthrough observed in STT-2, cf. Section 10.3.

11 Discussion and conclusions

11.1 Site characterisation

The investigation methodology employed in the characterisation of the TRUE-1 site has emphasised use of hydraulic pressure responses obtained during drilling and interference tests to arrive at the conductive geometry of the investigated block. The pressure interference data has also been used in the selection of the prime target feature from the initial three candidates identified in the investigated block. An important additional component from the geological characterisation is the borehole imaging tool (BIPS), which has provided a visualisation of the structures identified by pressure interference testing. Combining the results of the BIPS with the results of the single packer flow logging with a 0.5 m resolution enabled ample identification of the conductive structures.

In the TRUE Block Scale Project (Winberg, 1997, Winberg, 1999) the flow logging tool developed by POSIVA has been applied with great success. The tool builds on a measurement of the dilution of a thermal pulse. A single point resistivity sensor which is part of the probe allows identification of a single conductive feature with a resolution of 0.1 m. The high resolution identification of a conductive features in combination with the BIPS visualisation constitute an effective package for future characterisation work.

The methodology for detailed geological structural characterisation used as part of the collaboration with the FCC project (Bossart et al., in prep.) has proven to be an important contribution to the conceptualisation of the TRUE-1 block.

11.2 Tracer test methodology

The tracer test methodology employed has overall proved to work effectively. The radially converging flow test geometry has been found to be the most efficient flow geometry to test the system. For future tests, weak dipole test configuration (monopoles) may become an alternative for certain applications, with due considerations to foreseen mass losses associated with the dipole geometry.

Differences in hydraulic head, the hydraulic gradient, constitutes the driving force for the background groundwater flow in the investigated feature. In our transport experiments we have had to take the natural background flow, directed towards the tunnel system, into account in our test design at all times. If the natural gradient is not superseded, there is a high risk of loosing tracer mass in an uncontrolled way during a

tracer experiment. Such an uncontrolled loss of mass cannot be accepted for the tests with radioactive sorbing tracers. A significant loss of tracer also entails ambiguity in the interpretation of the performed tests. The flow paths used for tests with radioactive sorbing tracers show mass recoveries close to 100% for the flow rates employed.

For the tracer tests with radioactive sorbing tracers there is a need for a balance act between obtaining as a high a recovery as possible, and allowing a sufficiently low flow rate to allow mass transfer processes to become measurable.

In general, the results of our tests show low recovery for low pumping rates and lower recovery for dipole flow fields. Out of the seven flow paths tested, only two showed high enough mass recovery at low flow rates to make them candidates for tests with sorbing tracers.

The injection scheme and the existing downhole instrumentation was initially constructed to administer decaying tracer pulses without disturbing the pressure field. When a demand for a tracer pulse with a distinct termination (finite pulse) was posed, this request was resolved by exchanging the tracer solution in the injection circulation loop with non-traced formation water. It was shown during STT-1 that a single exchange was not sufficient. Even with a repeated second exchange, employed during STT-2, resulting in an initial 99% efficiency, the occurrence of a second tracer pulse is visible in the injection signal after a few minutes. This secondary pulse is attributed to an insufficient penetration of the exchange, whereby stagnant pockets of tracer solution remaining in the bottom of the test section diffuse back into the circulation loop over time. The problem of inadequate downhole homogenisation during the tracer solution exchange will be resolved for future phases of TRUE.

Over the duration of the TRUE-1 tracer test programme, a successively more elaborate instrumentation, including on-line measurement using a HPGe detector monitoring the injection signal of the radioactive sorbing tracers, has been employed. During STT-2 also the output concentration has been monitored on-line on a continuous basis. Likewise, the output concentration of the fluorescent dyes (mainly Uranine) has been monitored in-line using a portable fluorometer. For future phases of TRUE the use of downhole monitoring of the tracer concentration will be evaluated, at least for the dye tracers.

11.3 Understanding of transport in a single fracture

This section provides a discussion of the level of understanding of transport of sorbing tracers in a single fracture in crystalline bedrock. This with special emphasis on the dominant mass transfer processes, the extent to which parameters needed in the evaluation can be obtained from laboratory and *in situ* data. In addition the predictive capability of the developed model of the Feature A fracture is discussed, as well as its extrapolation to larger transport scales. Finally the effect of (aperture) variability is discussed. Where applicable, the findings are discussed in relation to results of relevant experiments and results, eg. the Grimsel MI experiment (Switzerland), the Palmottu

Analogue Project (Finland) and studies of hydrothermal weathering and associated migration at Äspö.

The studied migration zone in the Grimsel MI experiments constitutes a fractured shear zone represented by a confined planar aquifer. The corresponding transport model is based on the dual porosity concept where the migration zone is made up of a mixture of fault gouge and wall rock. Matrix diffusion in the water of the porous rock is modelled perpendicular to the flow direction, and is assumed limited to the migration zone. Surface sorption is neglected and sorption on the pore surfaces is assumed equilibrium (Haderman and Heer, 1996).

The Palmottu example pertains to assessment of the altered zone around a fracture in a granite using helium gas measurements of porosity and diffusivity and α-autoradiography of natural uranium activity (Hartikainen et al., 1996).

It should in this context be pointed out that independent model predictions and evaluations of the TRUE-1 tracer test data is provided by the modelling groups of the international Äspö Task Force on Modelling of Ground-water Flow and Solute Transport using a wide variety of model concepts and codes (Ström, 1998, Morosini, 1999).

11.3.1 Dominant mass transfer processes

Unlimited diffusion/sorption in the matrix rock is the dominant retention mechanism identified for the time scales of the TRUE-1 *in situ* experiments in Feature A. This is particularly true for the more strongly sorbing tracers, eg. Cs. The effects on tracer retention by equilibrium surface sorption and rate-limited sorption into (small fraction) gouge material are observable, but of secondary importance, cf. Sections 8.4 and 8.8. and 8.8.2. Similarly, the effect of sorption into stagnant water zones is small, and consistent with the fact that observed mass transfer rates are proportional to the parameter governing diffusion/sorption.

Reported analysis results by the Paul Scherrer Institute (PSI) of the Grimsel MI experiments (Haderman and Heer, 1996) include analysis of tests with Na, Sr and Cs. A comparison between the results from the TRUE-1 and Grimsel MI tests has to take into account the difference between the studied geological structures. The Grimsel MI structure is a well defined zone, 0.05 m wide, with about four fractures, each with an approximate physical aperture of 0.04 mm (from resin impregnation). In addition the MI zone contains significant amounts of gouge. This should be compared with Feature A which is assumed to be a singular open fracture with a interpreted physical aperture is in the order of 1–3 mm and an interpreted "transport aperture" of about 0.9 mm, possibly partly filled with gouge material. In addition the test configurations differ, (unequal) dipoles in the case of Grimsel MI, and radially converging flow geometry in the case of TRUE-1.

Tracer transport in the Grimsel MI zone is assumed to take place within the shear zone in a number of planar, parallel-walled open conduits, representing open channels within

the fault gouge in sub-fractures of the shear zone. Matrix diffusion into connected diffusion-accessible porosity is considered perpendicular to the advection direction. Reversible sorption on the surfaces of the open channels and on the surfaces of diffusion-accessible pores is calculated with the assumption of instantaneous equilibrium between the sorbed tracer and the tracer in the solution (Heer and Smith, 1998). Further, according to the PSI concept (Heer, pers. comm) fault gouge in the Grimsel MI zone represents predominantly diffusion accessible porosity, but is not generating increased surface sorption. This implies that sorption is predominantly coupled to matrix diffusion.

The dominant retention processes at the Grimsel MI and TRUE-1 sites, are consequently principally the same. The main difference lies in the fact that at Grimsel, the combined diffusion/sorption process takes place in the gouge material, and being limited as seen in the experimental data, whereas our interpretation attributes the main retention mechanism in the TRUE-1 tests to unlimited diffusion/sorption in the matrix rock, including the altered rim zone associated with the studied fracture.

11.3.2 Model parameters and model calibration

The evaluation framework used in our evaluation, cf. Sections 8.4 and 8.8.3, requires retention parameters which define the diffusion/sorption in the matrix (κ), surface sorption on readily accessible sites (K_a), and a volumetric distribution coefficient (K_d^g) and a rate coefficient (α) associated with gouge material. The former two of these parameters are obtained from a selected "Modelling Input Data Set" (MIDS) based on laboratory through-diffusion data, cf. Table G-1 in Appendix G. The parameters related to sorption in gouge are presently not available from the laboratory, and are calibrated using *in situ* tracer test results. Further, a statistical relation between β and τ is required, obtained from a combination of a residence time distribution calibrated using conservative tracer (HTO) breakthrough and Monte Carlo simulations of particle transport in the modelled feature, cf. Section 8.4.

In order to obtain an almost exact match between the modelled and measured breakthrough curves (assuming water residence time and β-τ relationship known), only one single calibration parameter is required (assuming sorption in gouge second-order and integrated with diffusion/sorption in the matrix), with essentially one single value for all tracers and all tests performed at the TRUE-1 site. The introduced factor f ,with a typical value of 137 for the most sorbing tracer Cs accounts for an enhanced diffusion as $f\kappa\beta$, is primarily attributed to physical effects associated with increased porosity/diffusivity in a finite rim zone immediately adjacent to the studied fracture. In a physical sense, $f > 1$ implies that either β, as obtained from Monte Carlo simulations, is underestimated (implying k, in $\beta = k\tau$ is too small), or that the parameter κ as determined in the laboratory is underestimated relative to *in situ* values, or a combination of both. Our analysis, cf. Section 8.8.5, indicates that a factor 3 of the typical value of f can be attributed to enhancement in k, whereas the remaining component of enhancement, a factor 46, is attributed to enhancement in the parameter κ.

11.3.3 Role of the rim zone and estimation of *in situ* parameters

On the time scale of TRUE-1 experiments, the physical and mineralogical/sorption properties of a narrow layer the Feature A altered rim zone control tracer retention. These properties are quantified by three parameters: F, θ and K_d^m required for accurate predictions of tracer breakthrough. The altered rock of the rim zone is generally characterised by distinct physical and mineralogical properties, relative to unaltered rock. In particular, the porosity and the formation factor are generally higher in the rim zone, due to chemical alteration and mechanically induced micro-fissures (e.g., Eliasson, 1993, Valkiainen, 1992).

It should be acknowledged that limited amount of laboratory derived transport parameters are available for certain Feature A specific geological materials which are part of our conceptual model (The present proportions are : gouge < mylonite < altered Äspö diorite < generic Äspö material). In this context it should be noted that experimental work within the TRUE programme is under way which will improve the knowledge of diffusion and sorption characteristics of the rim zone of fractures with mylonitic precursors, as well as that of gouge material. However, information of the properties and transport characteristics of the altered rim zone are available from other sources.

Hartikainen et al. (1996) observed an exponential drop in porosity away from a natural fracture surface in a specimen from the Palmottu site investigated in slices. The diffusivity remains stable and enhanced relative to the diffusivity of the intact matrix rock over some 50 mm, after which a rapid drop in diffusivity amounting to about a factor 25 occurs. In the case of the Palmottu fracture, the zone of enhanced diffusivity extended some 25 mm beyond the chemically altered rim zone with an estimated width of about 24 mm.

Unpublished results from studies at Äspö also indicate an increased porosity/diffusivity in the proximity of a natural fracture surface. Landström et al. (in prep) in their study of a natural fracture surface at a depth of 170 m identify an hydrothermal weathering zone (25 mm) featured by dominant loss of Ca due to alteration of plagioclase, the latter associated with increased porosity. The porosity decreases almost exponentially from about 1.3% at the surface to a background value of 0.4% in unaltered rock some 13–17 cm into the rock. Increased values in Br in the pore water and Cs sorbed on secondary minerals are interpreted as evidence of matrix diffusion and subsequent sorption in the altered zone. In addition increased $^{234}U/^{238}U$ activity ratios in the altered zone indicate accumulation of uranium by recent diffusion from the groundwater (<1.25 Ma).

Using the results accounted for above Cvetkovic et al. (in prep) hypothesise that the *in situ* porosity θ of the part of the Feature A rim zone accessible over the time frames of the *in situ* experiments is 2–2.4%. Using Archie's law, an *in situ* formation factor was estimated at F=0.0015–0.002. Using a fixed value of a selected parameter, say the porosity θ, a calibrated parameter group $k_0 f\kappa$ (describing the calibrated *in situ* diffusion/sorption in the matrix rock), estimates valid for *in situ* conditions of all other transport parameters (ie. *in situ* k, F and K_d^m) for the 5 analysed sorbing tracers can be computed, cf. Section 8.5 and Table 8-2. Comparison of results with performed

laboratory data shows that K_d^m values from batch tests performed on the 1–2 mm size fraction over longer time compare best with estimated values of *in situ* K_d^m. This suggests that the time aspects and the size fraction used in these batch tests capture the mineralogical/geochemical variability seen along the *in situ* flow paths over the time scales of the TRUE-1 *in situ* experiments.

The framework for deriving *in situ* estimates of the important transport parameters provides a means to generate updated estimates when new data become available, say more representative estimates of the porosity θ. Typically, the amount of laboratory data will always be limited and associated with uncertainty. It should be remembered that the actual flow path between a source and sink section which a tracer subject to retention experiences, is very difficult to characterise and sample directly. Hence, the presented estimation of *in situ* values of important parameters can be used to provide prior estimates for (predictive) modelling of future and ongoing TRUE experiments.

It should in this context be mentioned that new unpublished results presented by Byegård et al. (in prep) from water saturation porosity measurements and C-14 metamethyl-acrylate (PMMA) impregnation (eg. Sittari-Kauppi et al., 1998, Hellmuth et al., 1999) on site-specific Feature A material support the notion of an increased porosity in the rim zone. The PMMA impregantions (sample from KXTT3) map porosities up to 2.5% very close to the rime zone, whereas water saturation porosities on centimetre-sized sectioned samples from KXTT2 consisting of mylonite and altered Äspö diorite vary between 0.3 and 1%, in a direction towards the fracture surface. Interpretation of through-diffusion experiments on the KXTT2 samples require a log-normal distribution of porosity to obtain a good fit with the concentration data.

11.3.4 Predictive capability and accounting for aperture variability

Laboratory data of diffusion/sorption parameters constitute a basis for robust and relatively accurate predictions of reactive tracer breakthrough. This provided that the water residence time distribution $g(\tau)$ is known and that variability in the β parameter is accounted for. Using laboratory data for diffusion/sorption (κ) the first arrival is predicted accurately (in particular that of the strongly sorbing Cs), or is somewhat underestimated. The peak concentration of Cs is however overestimated with up to one order of magnitude, and somewhat less for the other tracers. The latter deviations can be considered conservative from a performance assessment perspective.

It should be emphasised that the residence time is significantly underestimated by transmissivity data and the cubic law. Further, the statistically limited hydraulic data set from the five borehole intercepts with associated large support volumes (radii of influence) result in transmissivity/aperture random fields that underestimate the spreading (dispersion) process, the latter captured by the variance of the residence time distribution, cf. Section 8.4.

Aperture variability has a significant impact on diffusion/sorption and ultimately on retention. This is evident in Figure 11-1 exemplified by Rb and Cs breakthrough curves from STT-1, where all modelled curves include surface sorption and diffusion/sorption

only; the "best fit" curve includes also kinetic sorption into gouge material. It is seen that incorporating β variability is critical in capturing the correct shape of the breakthrough as well as the first arrival. The cases with constant β would range between the red and the blue dashed lines in Figure 11-1, significantly deviating from observations. Thus calibrating with the factor f would not provide a close and consistent comparison for all tracers and tests had the variability in β not been included.

The effect of aperture (or β) variability is increasingly more apparent for tracers with stronger sorbtivity. For a fixed residence time τ the variability in β can be considerable; hence the linear β-τ model is only an approximation. If the transport scale increases it is anticipated that the uncertainty in diffusion/sorption parameters will decrease, mainly through averaging effects. However, the opposite is expected for β and τ. In this context a neglect to account for β variability (say by assuming a constant β) will entail a non-conservative overestimation in the first arrival, cf. Figure 11-1.

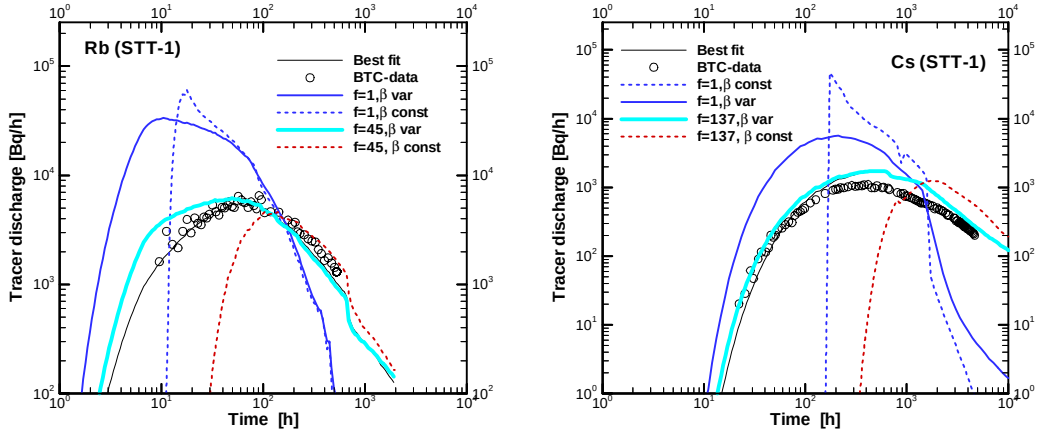

Figure 11-1. *Predictive capability and effect of variability in β exemplified using a) Rb and b) Cs breakthrough in the STT-1 test. Only matrix diffusion/sorption and surface sorption are considered except in the "best fit" curve where sorption in gouge is added.*

11.4 Pore space data from resin injection

The methodology for obtaining pore space data from epoxy resin injection and subsequent excavation and analysis as applied in the Pilot Resin Experiment has shown to be workable. However, the use of large diameter coring (200 mm) has been shown to be associated with problems related to ability to keep the collected samples bonded during the drilling and subsequent extraction process. This problem has been associated with a) stress relief when the static load acting on the injected fracture planes is removed b) the handling of the large massive of the cores in combination with essentially horizontal boreholes.

The results from the Pilot Resin Injection Experiment show mean apertures of 239–266 μm (contact areas and voids included), with coefficients of variation in the order of 40%. Variograms calculated along the analysed profiles show practical ranges of about 3–5 mm. It should in this context be emphasised that the transmissivity of the structure investigated by the Pilot Resin Injection Experiment is about one order of magnitude lower that that of Feature A.

For application of the developed methodology at the TRUE-1 site we plan to take advantage of the lower hydraulic gradient at the TRUE-1 site which is about 1% of that faced at the Pilot Resin Site, which is expected to entail an improved resin spread. The fact that the transmissivity of Feature A is about one order of magnitude higher than that faced in the Pilot Resin Injection experiment may counteract the benevolent aspects of the gradient since the background flow is given by the product of the two entities.

For application at the TRUE-1 site, the foreseen injected parts of Feature A will be located some 10–15 m into the rock with a focus on the triangle formed by the KXTT3, KXTT1 and KXTT4 intersections. The plans are to explore the possibility to drill targeted large diameter holes (ϕ=96–146 mm) oblique, and along to the plane of the feature over the target area. An alternative is to drive a tunnel up from behind, against the face of Feature A and drill short large diameter core holes on a dense grid.

Before starting epoxy resin injection at the TRUE-1 site, it should be demonstrated that a equally good site a next detailed scale experiment has been identified.

11.5 Implications for repository development

The inferences which can be made in relation to repository development are at this point mostly related to techniques and methodologies. Most of the techniques developed as part of TRUE can be applied at selected stages in the development of a repository. This applies to the characterisation methods which are useful in eg. positioning storage tunnels and deposition holes. In the case of TRUE-1, the application of the borehole imaging system (BIPS) combined with detailed flow logging has been a valuable set of tools in the identification and interpretation of conductive fractures. Likewise the developed tracer test methodology and procedures can be applied for obtaining site-specific *in situ* transport and retention parameters at any given site.

The results from the evaluation of the TRUE-1 tests with sorbing tracers indicate that the TRUE project eventually can provide useful predictive tools whereby site-specific laboratory data in combination with conservative (non-sorbing) tracer test results can be used to predict transport of sorbing tracers at practical experimental time scales and length scales ranging from approximately 5–50 m.

11.6 Implications for performance assessment

The performance assessment implications can be divided in two categories. One demonstrative and one quantitative.

The semi-analytical evaluation framework (LaSAR) applied to the TRUE-1 experiments is in principle also directly applicable in performance assessment calculations. Hence, the data reduction going from evaluation of *in situ* test data to performance assessment calculations can be made more easily and using essentially one analysis environment. By retaining the same modelling tool for experimental evaluation and performance assessments, overall credibility in performance assessment is improved.

The results from the TRUE-1 experiments includes an *in situ* demonstration of strong retention of Cs in crystalline bedrock. The results are in parity with the laboratory-based indication that Cs shows slow reversibility in sorption, or is even irreversible sorption. At the time of discontinuing the STT-2 experiment, the total recovery of Cs is 36.6% after 10 870 hours (15 months) of pumping since injection during STT-1, implying that approximately 63% is sorbed in the injection section and in the fracture. The above number is in agreement with the recovery observed for a 4.9 m flow path in the Grimsel MI fracture, where after 14 000 hours a recovery of 32% had been obtained for Cs (Heer, pers. comm.). It should be pointed out that available breakthrough data for Cs from the TRUE-1 *in situ* experiments are insufficient for providing conclusive evidence of irreversible sorption in the matrix.

For reactive transport on TRUE-1 experimental time scales, retention is dominated by the characteristics of the rim zone in the immediate proximity of the fracture. However, for long term performance assessments, the laboratory derived diffusivities and porosites are assumed to be representative. In the context of performance assessment we may regard retention parameters obtained from unaltered rock samples using through-diffusion tests as conservative.

The representative proportionality constant $k \approx 3400$ m^{-1}, evaluated for the assumed linear β-τ relationship of the TRUE-1 tests, is similar to the "flow wetted surface" per volume of water a_w, under the strict assumption of a linear relationship $\beta = k \cdot \tau$. Bounding values for k in the range 1 900–33 000 m^{-1} can be obtained using the tracer injection flow rate and the "hydraulic" aperture, respectively, cf. Section 8.7 and 8.8.12. For the purpose of PA and repository site evaluation, bounding values of k are thus possible to obtain from site investigation data, where the lower bound corresponds to a conservative estimate.

Glynn and Voss (1999) evaluated an average effective value of $a_w = 3100$ m^{-1} derived from concentrations of ^{222}Rn in Äspö groundwaters and a ^{222}Rn flux from fracture surfaces derived based on uranium content of the Äspö rock and measured fluxes for Stripa granite ($F = 125$ atoms s^{-1} m^{-2}). Similarly, using the radon flux presented by Glynn and Voss and the average radon concentration measured in Feature A at the TRUE-1 site, [^{222}Rn] = 328 Bq/l, a value $a_w = 2600$ m^{-1} is estimated, ie. close to the value of k reported above. No estimate of radon flux relevant to Äspö conditions is

available at present, but it should be lower given the higher Th and U content in the Stripa granite, which would entail a higher value on the estimate of a_w.

In the most recent SKB performance and safety analysis SR 97 (SKB, 1999) it is shown that the F parameter governs the flow-related transport of sorbing species. The F parameter is defined in Equations 11-1 and 11-2.

$$F = t \cdot a_w \quad (11\text{-}1)$$

or

$$F = a_r \cdot L/q \quad (11\text{-}2)$$

where

F = parameter which govern the geometry- and flow-related transport.
t = $L\varepsilon/q$ = advective travel time of a non-sorbing tracer (T)
a_w = "flow wetted surface" per volume of water (L^{-1})
a_r = "flow wetted surface" per volume of rock (L^{-1})
L = average length of pathway (L)
Q = Darcy flux (L/T)
ε = flow porosity (–) = a_r/a_w

When a singe fracture is considered, the F and β parameters are similar if a linear relationship between β and τ is assumed. The concept of a "flow-wetted surface" in a performance assessment context is discussed in detail by Andersson et al. (1998).

Andersson et al. (1998) report estimates of a_r for crystalline rock varying between 0.01–10 m^{-1}, recommended as a typical range of values for use in the SKB safety assessment study SR 97 (SKB, 1999). Estimates of a_w, equitable to the value of *k* reported in the present study, are reported to vary between 1100–8700 m^{-1}. Andersson et al. (1998) further stress that neither a_w nor a_r are material properties. Any estimation of a_w needs to be consistent with an assessment of the flow porosity. Likewise, an estimate of a_r, needs to be combined with estimates of the Darcy flux along the flow path.

Andersson et al. (1998) also describe methods which can be used to estimate a_r using the conductive fracture frequency (P_{10c}), ie. number of fracture intersections per metre, and the conductive fracture intensity (P_{32}), ie. the fracture surface per cubic metre;

$$\langle a_r \rangle = 4 \cdot P_{10c} \quad (11\text{-}4)$$

$$\langle a_r \rangle = 2 \cdot P_{32} \quad (11\text{-}5)$$

Using the values of the two intensity entities presented in Section 3.5.3, estimates of a_r amounting to 6.2 m^{-1} and 6.3 m^{-1}, respectively, are obtained. The equivalence between the two estimates is consistent with existing theory. In addition the estimated value is within bounds of the range of a_r presented above.

One of the major challenges in relation to PA is the upscaling of the β parameter, and quantifying the corresponding uncertainty. Better understanding of the β-τ correlation (non-linearity) and its predictive power.

11.7 Implications for future stages of TRUE

The combined use of borehole imaging (BIPS) and high resolution flow logging (eg. POSIVA flow log) will prove to be powerful set of tools for assessing the conductive geometry of a new detailed scale experimental site. The use of tracer dilution tests have been shown to be an effective means to identify suitable injection points for tracer.

The results of the First TRUE Stage entail that we are well equipped with experiences, methodologies and instrumentation applicable for future detailed scale experiments. A challenge will be to successively introduce tracers which are highly relevant to making the safety case of a repository.

Having tested different types of test configurations and flow geometries in TRUE-1 we should be in a position to take the step from basic characterisation and conservative tracer tests to a direct address of mass transfer in a shorter time.

Future detailed scale experiments will be more directed towards process identification and discrimination. With the developed evaluation framework and other alternative model approaches we are well equipped to perform realistic model predictions using available estimates of water residence time distributions and relevant laboratory data on distribution coefficients, diffusivities and porosities.

A challenge for future work will be to successfully sample fault gouge from target features using triple-tube drilling techniques. In TRUE-1 only integrated diffusivity and porosity estimates have been obtained for the package of mylonite and altered Äspö diorite. An additional challenge is to obtain laboratory estimates of the above parameters also for the minute constituents of the altered rim zone of an investigated target feature. The estimates of in situ values for important transport parameters provided in Sections 8.8.6 through 8.8.8 provides means for prior estimates for input to modelling, where the estimates can be updated as new data, say porosity data, become available.

Future modelling work will focus on improving the understanding of the β-τ relationship, and the foundation for a linear relationship between the two parameters. Further, the effect of diffusion enhancement over different time scales, given the limitation in the extent of the altered zone around a given fracture, will be studied. Finally, efforts will be directed towards relating the calibrated entities for diffusion enhancement (f) and volume distribution coefficients for the rim zone (K_d^m) and gouge material (K_d^g) to independent laboratory data (mineralogy, porosity, diffusivity etc.).

12 Summary conclusions

The following summary conclusions can be drawn from the results of the First Stage of the Tracer Retention Understanding Experiments (TRUE-1) in relation to set up objectives and stated hypotheses;

- Available **tracer test methodology** has been successfully adapted and applied in the detailed scale at the prevailing conditions (high hydraulic pressures (P >30 bars) and high salinity ([Cl] > 5000 mg/l).
  - Feature A is found to be connected in a transport sense over its investigated area.
  - The use of tracer dilution tests in combination with pumping has proven to be a good tool for identification of workable injection sections and subsequent tracer test design.
  - The existing natural gradient in the investigated Feature A (10%) controls the background flow and makes it difficult to perform high-recovery tracer tests over longer distances (> 5 m) and at low pump flow rates (< 0.2 l/min).
  - Two flow paths in Feature A qualified for tests with radioactive sorbing tracers have been successfully used.

- **Cationic sorbing tracers** featured by sorption by cation exchange have been successfully applied in laboratory experiments and in *in situ* experiments.
  - The sorbtivity of the exposed geological material is shown to depend on the concentration of biotite.
  - The sorption in the batch laboratory experiments is observed to be time dependent, ie. the evaluated K_d increase with increasing contact time. This finding is attributed to chemical kinetics, mass transfer (intra-particle diffusion) or geochemical changes in the solid phase, or combinations thereof.
  - Breakthrough in the *in situ* experiments has been observed for the sorbing tracers Na^+, Ca^{2+}, Sr^{2+}, Rb^+, Ba^{2+}, Cs^+, K^+ and Co^{2+}. Uranine, tritiated water (HTO), $^{131}I^-$ and $^{82}Br^-$ were used as conservative tracers.
  - The sorbtivity of the tracers used in the laboratory experiments on geological material from Äspö, show the following relative order; $Na^+ < Ca^{2+} \approx Sr^{2+} <$ $<Rb^+ \approx Ba^{2+} < Cs^+$. The observed relationship is also consistently observed in the *in situ* test results.

– Laboratory results indicate that the sorption of the more sorbing species, Rb, Ba and Cs, are affected by slowly reversible processes. Similarly, the performed *in situ* experiments show a similar behaviour for Co, Ba and Cs. At the time of termination of STT-2 in October 1998, after some 10 870 hours of pumping, approximately 63% of the ^{137}Cs mass injected as part of STT-1 still remained sorbed in the injection section and the fracture. With the data presently available, no distinction is possible between reversible and irreversible contributions to the sorption of Cs.

- The developed Lagrangian **evaluation framework** (LaSAR) has been found suitable for modelling the dominant effects of reactive transport in a single fracture.

  – Unlimited diffusion/sorption in the rock matrix is the **dominant retention mechanism** in Feature A over the time scales of the TRUE-1 *in situ* experiments, particularly so for the more strongly sorbing tracers, eg. Cs. The effects of equilibrium surface sorption, limited sorption in gouge material and diffusion into stagnant zones are observable, but less important.

  – The relative importance of the processes included in the evaluation of the TRUE-1 *in situ* experiments are also assumed valid over time scales relevant to performance assessment.

  – A key result is the derivation of the parameter β which integrates the inverse velocity-weighted aperture along the flow path. It controls surface sorption and diffusion/sorption into the matrix, accounting for the effect of aperture variability on retention. A linear relationship $\beta = k \cdot \tau$ was found suitable for modelling retention in Feature A. A representative estimate of k obtained from simulations is $k_0 \approx 3400$ m^{-1}.

  – Assuming a strict linear relation between β and τ, the proportionality factor k is equivalent to the "flow wetted surface" per volume of water (a_w). The value k is within bounds of a_w reported in the literature.

- Values of **parameters for the main retention processes** included in evaluation concept (LaSAR) have been obtained either from laboratory data, or through estimation using *in situ* data and the calibrated parameter group ($\kappa = \theta[D(1+\rho K_d^m/\theta)]^{1/2}$) which controls diffusion/sorption in the matrix rock.

  – The parameter values for diffusion/sorption estimated for *in situ* conditions have been shown to be enhanced compared to those measured in the laboratory. Enhanced diffusion/sorption in the order of a factor $f = 32–50$ (excluding Cs) and $f = 137$ for Cs have been evaluated for the different tracers and experiments. The enhancement is mainly attributed to higher values on matrix porosity and/or diffusivity, and matrix sorption applicable to *in situ* conditions compared to values measured in the laboratory. A minor contribution to the enhancement is also attributed to the flow-dependent parameter k in the $\beta = k \cdot \tau$ relationship, hence being higher in the field than what has been interpreted from performed Monte Carlo simulations.

– The parameters related to sorption in gouge material have been calibrated using *in situ* breakthrough data. Effects of sorption onto gouge material have been found to be most evident for the weakly sorbing tracers Na and Sr, since for these tracers, matrix diffusion/sorption is relatively small.

- The **representative laboratory data set (MIDS) and $k_0 \approx 3400$ m^{-1}** constitute a basis for robust predictions of reactive tracer breakthrough in the TRUE-1 experiments. Relatively accurate *first arrival* is obtained while the *peaks* are overestimated by approximately one order of magnitude.

  – This provided that the water residence time distribution (conservative breakthrough) is known (can be assessed) and that variability in the β parameter is accounted for.

- The **altered rim zone** along the studied feature is interpreted to show enhanced, albeit variable, porosity/diffusivity in relation to the unaltered matrix rock, and is important for the tracer retention over the time scales of the TRUE-1 experiments.

  – The rim zone is interpreted to be made up of primarily of altered Äspö diorite and mylonite, the latter with a lower porosity/diffusivity.

  – The average range of porosity of the parts of the rim zone of Feature A which is accessible over the time scales of the *in situ* experiments is estimated to be 2–3%. Independent information and new site-specific data indicate that this estimate is realistic.

  – Analysis eg. indicate that performed 36 day batch sorption tests on 1–2 mm size fractions of generic Äspö diorite material capture, in an average sense, the variability in sorption along the studied flow paths, over the time scales of the *in situ* experiments.

  – The tested flow path is only known at its respective intercepts in the injection and pumping borehole. The actual distribution of transport properties along the flow path can only be analysed in detail when the fracture excavated, preceded by injection of epoxy resin.

  – Over time scales relevant to performance assessment, the role of altered rim zone of fractures is assumed second order. Over the PA time scales the diffusivities from the through-diffusion experiments on unaltered geological material (cf. MIDS data set) are assumed applicable for predictions.

- The **performance assessment** related conclusions based on the results of the TRUE-1 experiments can be summarised as follows;

  – The important processes and their realtive importance, identified at the experimental time scales are assumed valid also over PA time scales

  – Laboratory data on unaltered rock, not associated with fracture rim zones, are assumed applicable over performance assessment time scales.

  – A value on "flow wetted surface per volume of water" $a_w = k_0 \approx 3400\ m^{-1}$ has been estimated based on *in situ* experiments and associated modelling. This value is in parity with previous estimates found in the literature.

  – Bounding values of the "flow wetted surface per volume of water" can be estimated using the tracer injection flow rate and the hydraulic aperture. The former estimate is in this context regarded as conservative.

- A workable technology and procedure for obtaining **pore space/aperture data** from *in situ* epoxy resin injection and subsequent excavation and analysis has been developed and applied in a Pilot Resin Injection Experiment (at a different location than the TRUE-1 experiment).

  – A fracture system with a one order of magnitude lower transmissivity than Feature A has been subject to resin injection.

  – The average aperture of the analysed samples are 239 and 266 μm, respectively with a coefficient of variation of about 40%.

  – Evaluated variograms of the aperture mapped by the epoxy indicate practical ranges varying between 3 to 5 mm.

- The performed characterisation provides a powerful set of tools for assessment of conductive geometry and connectivity in future preliminary **site characterisation**, and in particular during future detailed site characterisation.

  – The use of borehole TV imaging in combination with detailed flow logging identifies the conductive features in a borehole.

  – Cross-hole pressure interfere testing, including observations during drilling of a new borehole, provide information on how the conductive features connect.

  – The tracer test methodology developed and used in this work is applicable to characterisation work in various phases of repository development.

- The performed transport experiments in the laboratory combined with detailed mineralogical and geochemical characterisation provide a platform for **export of estimated *in situ* values of transport parameters** and generic transport characteristics to sites with similar geological and chemical conditions.

- The close interaction with the Äspö Task Force on Modelling of Groundwater Flow and Transport of Solutes has provided important support in initial experimental design. Further, by performing **blind model predictions**, a basis for a scientific test of our understanding and predictive capability is obtained. The ongoing evaluation of the predictions of tests with sorbing tracers will provide further insight in our understanding of flow and retention in a single feature.

13 References

Abelin, H., Neretnieks, I., Tunbrant, S. and Moreno, L. 1985 : Final report of the migration in a single fracture – Experimental results and evaluation. OECD/NEA International Stripa Project. Stripa Technical Report TR 85-03.

Abelin, H., Birgersson, L., Gidlund, J., Moreno, L., Neretnieks, I., Widen, H., and Ågren. T. 1987 : 3-D migration experiment – report 3, part 1 performed experiments, results and evaluation. Stripa Project Technical Report TR 87-21.

Abelin, H., L. Birgersson, H. Widen, Ågren, T., Moreno, L., and Neretnieks, I. 1990 : Channelling experiment. OECD/NEA International Stripa Project. Stripa Technical Report TR 90-13.

Alley W M, 1993. Regional groundwater quality. ISBN 0-442-00937-2. Van Nostrand Reinhold, New York, USA.

Almén, K-E., and Stenberg, L. (in prep.) : Äspö hard Rock Laboratory. Characterisation methods and instruments. Experiences from the Construction Phase. Swedish Nuclear Fuel and Waste Management Company. Technical Report in prep.

Andersson, J., Elert, M., Hermanson, J., Moreno, L., Gylling, B. and Selroos, J.O., 1998 : Derivation and treatment of the flow wetted surface and other geosphere parameters in the transport models FARF31 and COMP23 for use in safety assessment. Swedish Nuclear Fuel and Waste Management Company. SKB Report R-98-60.

Andersson, K., Torstenfelt, B. and Allard, B. 1982 : Sorption behaviour of long-lived radionuclides in igneous rock, Environ. Migr. Long-Lived Radionuclides, Proc. Int. Symp. IAEA, Vienna, Austria.

Andersson, P. and Klockars, C-E. 1985 : Hydrogeological investigations and tracer tests in a well-defined rock mass in the Stripa mine. SKB Technical Report TR 85-12.

Andersson, P., Gustafsson, E., and Sellgren, A. 1992 : Flow pattern investigations in an isolated rock mass in the Stripa mine. Swedish Nuclear Fuel and Waste Management Company. SKB Progress Report AR 92-66.

Andersson, P., Nordqvist, R., Persson, T., Eriksson, C-O., Gustafsson, E. and Ittner, T., 1993: Dipole tracer experiment in a low-angle fracture zone at Finnsjön – Results and interpretation. The Fracture Zone Project – Phase 3. Swedish Nuclear Fuel and Waste Management Company. SKB Technical Report TR 93-26.

Andersson, P., 1995 : Compilation of tracer tests in fractured rock. Swedish Nuclear Fuel and Waste Management Company. Äspö Hard Rock Laboratory Progress Report PR 25-95-05.

Andersson, P. 1996 : TRUE 1st stage tracer test programme. Experimental data and preliminary evaluation of the TRUE-1 radially converging tracer test (RC-1). Swedish Nuclear Fuel and Waste Management Company. Äspö Hard Rock Laboratory Progress Report HRL-96-24.

Andersson, P. and Jönsson, S. 1997 : TRUE 1st stage tracer test programme. Complementary Tracer Tests (RC-2, DP-5, DP-6). Experimental description and preliminary evaluation. Swedish Nuclear Fuel and Waste Management Company. Äspö Hard Rock Laboratory Progress Report HRL-97-23.

Andersson, P., Nordqvist, R., Jönsson, S., 1997: TRUE 1st stage tracer test programme. Experimental data and preliminary evaluation of the TRUE-1 dipole tracer tests DP-1–DP-4. Swedish Nuclear Fuel and Waste Management Company. Äspö Hard Rock Laboratory Progress Report HRL-97-13.

Andersson, P. and Wass, E. 1998 : TRUE 1st stage tracer test programme. Preliminary Design Tests for tests with radioactive sorbing tracers (PDT-1, PDT-2, PDT-3). Experimental description and preliminary evaluation. Äspö Hard Rock Laboratory Progress Report HRL-98-13.

Andersson, P., Johansson, H., Nordqvist, R., Skarnemark, G., Skålberg, M., Wass, E. (in prep) : TRUE 1st stage tracer test programme. Tracer tests with sorbing tracers STT-1. Experimental description and preliminary evaluation. Swedish Nuclear Fuel and Waste Management Company. Äspö Hard Rock Laboratory International Progress Report IPR-00-XX.

Andersson, P., Johansson, H., Skarnemark, G., Skålberg, M. and Wass, E. 1999 : TRUE 1st stage tracer test programme. Tracer tests with sorbing tracers STT-1b. Experimental description and preliminary evaluation. Swedish Nuclear Fuel and Waste Management Company. Äspö Hard Rock Laboratory International Progress Report IPR-99-12.

Andersson, P., Byegård, J., Johansson, H., Skarnemark, G., Wass, E., 1999: TRUE 1st stage tracer test programme. Tracer tests with sorbing tracers STT-2. Experimental description and preliminary evaluation. Swedish Nuclear Fuel and Waste Management Company. Äspö Hard Rock Laboratory International Progress Report IPR-99-15.

Aksoyoglu, S. 1990, Cesium sorption on mylonite, J. Radioanal. Nucl. Chem., v. 140, pp. 301-313.

Beauheim, R.L. , Meigs, L.C., and Davies, P.B. 1996 : Rationale for the H-19 and H-11 tracer tests at the WIPP site. In Proc. of OECD/NEA GEOTRAP workshop on Field Tracer Experiments – Role in the prediction of radionuclide migration. Cologne, Germany, August 28-30, 1996, pp. 107-118.

Birgersson, L., Widen, H., Ågren, T., Neretnieks, I., and Moreno, L. 1992 : Site characterization and validation – Tracer migration experiment in the Validation drift, Report 2, Parts 1 and 2. OECD/NEA International Stripa Project. Stripa Project Technical Report TR 92-03.

Bossart, P., Hermanson, J., and Mazurek, M. (in prep) : Fracture Characterisation and Classification Project, Final Report – Analysis of fracture networks based on the integration of structural and hydrogeological observations on different scales. Swedish Nuclear Fuel and Waste Management Company. SKB Technical Report TR-00-XX.

Brusseau, M.L., and P.S.C. Rao, Sorption nonideality during organic contaminant transport in porous media, CRC Crit. Rev. Environ. Control 19, 33-99, 1989.

Byegård, J. 1993 : The possibility of using slightly sorbing cations in tracer experiments in the Äspö Hard Rock Laboratory. Swedish Nuclear Fuel and Waste Management Company. Äspö Hard Rock Laboratory Progress Report PR 95-93-14.

Byegård, J., Skarnemark, G. and Skålberg, M. 1995 : The use of some ion-exchange sorbing tracer cations in in-situ experiments in high saline groundwaters. Mat. Res. Soc. Symp. Proc., vol. 353, pp. 1077-1084.

Byegård, J., Johansson, H., Skålberg, M, and Tullborg, E-L. 1998 : The interaction of sorbing and non-sorbing tracers with different Äspö rock types – Sorption and diffusion experiments in the laboratory scale. Swedish Nuclear Fuel and Waste Management Company. SKB Technical Report TR-98-18.

Byegård, J, Siitari-Kauppi, M. and Johansson, H. (in prep) : Compementary laboratory investigateions of site-specific material from Feature A. Swedish Nuclear Fuel and Waste Management Company. Äspö Hard Rock Laboratory Progress Report IPR-00-XX.

Cady, C.C., Silliman, S.E., and Shaffren, E. 1993 : Variation in aperture estimate ratios from hydraulic and tracer tests in a single fracture. Water Resources Research, vol. 29, no. 9, pp. 2975-2982.

Carrera, J., Sanchez-Vila, X., Inmaculada, B., Medina, A., Galarza, G., and Guimera, J. 1998 : On matrix diffusion: formulations, solution methods and qualitative effects, Hydrogeology J., 6, 178-190, 1998.

Crank, J. 1975 : The mathematics of diffusion, pp. 50-51, 2nd edition. Oxford University Press, New York.

Cvetkovic, V. 1991 : Mass arrival of reactive solute in single fractures, Water Resour. Res., 27, 177-183.

Cvetkovic, V., and Dagan, G. 1994 : Transport of kinetically sorbing solute by steady random velocity in heterogeneous porous formations, *J. Fluid Mech.*, **265**, 189-215.

Cvetkovic, V., Dagan, G. and Cheng, H. 1998a : Contaminant transport in aquifers with spatially variable flow and sorption properties, *Proc. R. Soc. Lond. A*, **454**, 2173-2207.

Cvetkovic, V., Cheng, H. and Selroos, J-O. 1998b : Lagrangian modelling of TRUE-1 reactive tracer tests at the Äspö Hard Rock Laboratory, Sweden, *GQ'98 Groundwater Quality: Remediation and protection*, IAHS Publication no. 250, pp. 375-379.

Cvetkovic, V., Selroos, J-O. and Cheng, H. 1999 : Transport of reactive solute in single fractures, *J. Fluid Mech.*, **318**, 335-356.

Cvetkovic, V., Cheng, H. and Selroos, J-O. (in prep) : Evaluation of TRUE-1 sorbing tracer experiments at Äspö: Theory and applications, SKB Äspö Hard Rock Laboratory International Cooperation Report ICR in preparation.

Dershowitz, W. and Herda, H.H. 1992 : Interpretation of Fracture Spacing and Intensity. Proceedings of the 33rd U.S. Symposium on Rock Mechanics, Santa Fe, NM. AA Balkema Publishers, Rotterdam. p. 757.

Dershowitz, W., Lee, G., Geier, J., Foxford, P., LaPointe, P., and Thomas, A. 1995 : Fracman interactive discrete feature data analysis, geometric modeling, and exploration simulation : User documentation version 2.5. Golder Associates Inc., Redmond, WA.

Dershowitz, W., Thomas, A. and Busse, R. 1996 : Discrete fracture network analysis in support of the Äspö Tracer Retention Understanding Experiment (TRUE-1), Swedish Nuclear Fuel and Waste Management Company, International Cooperation Report ICR 96-05.

Doe, T. and Geier, J. 1991 : Interpretation of fracture system geometry using well test data. OECD/NEA International Stripa Project. Stripa Technical Report TR-91-03.

Dollinger, H., Bulher, C., Frieg, B., and Bossart, P. 1995 : GTS Excavation Project : Dipole epoxy resin experiments. NAGRA Interner Bericht 95-91E.

Elert, M. 1999 : Evaluation of the TRUE-1 radially converging and dipole tests with conservative tracers. The Äspö Task Force on modelling of groundwater flow and transport of solutes. Tasks 4C and 4D. Swedish Nuclear Fuel and Waste Management Company. SKB Technical Report TR-99-04.

Elert, M. (in prep) : Deconvolution of breakthrough curves STT-2 (Task 4F). The Äspö Task Force on modelling of groundwater flow and transport of solutes. Tasks 4F. Swedish Nuclear Fuel and Waste Management Company. Äspö Hard Rock Laboratory. International Progress Report IPR-00-XX.

Eliasson, T. 1993 : Mineralogy, geochemistry and petrophysics of red coloured granite adjacent to fractures. Swedish Nuclear Fuel and Waste Management Company. Technical Report TR 93-06.

Frape, S.K., Fritz, P., 1987 : Geochemical trends for groundwaters from the Canadian shield. *In*: Fritz, P. and Frape, S.K., Saline water and gases in crystalline rocks. Geol. Assoc. of Canada Spec. Pap., no. 33, pp. 19-38.

Frape, S.K., Fritz, P. and McNutt, R.H., 1984. The role of water-rock interaction in the chemical evolution of groundwaters from the Canadian shield. Geochim. et Cosmochim. Acta, vol. 48, pp. 1617-1627.

Frick, U., Alexander, W.R., Bayens, B., Bossart, P., Bradbury, M.H., Bühler, C., Eikenberg, J., Fierz, T., Heer, W., Hoehn, E., McKinley, I.G. and Smith, P.A. 1992 : Grimsel Test Site : The radionuclide migration Experiment – Overview of investigations 1985-1990. NAGRA Technical Report NTB 91-04. NAGRA Wettingen, Schweiz.

Glynn, P. and Voss, C. 1999 : *Site-94* – Geochemical characterization of Simpevarp groundwaters near the Äspö Hard Rock Laboratory. Swedish Nuclear Power Inspectorate. SKI Technical Report 96:29.

Gómez-Hernández, J.J., Sahuquillo, A. and Capilla, J.E. 1997 : Stochastic simulation of transmissivity fields conditional to both transmissivity and piezometric data, 1, Theory, J. Hydrology, vol. 203, pp. 158-170.

Gustafsson, E. and Klockars, C-E., 1981: Studies of groundwater transport in fractured crystalline rock under controlled conditions using non-radioactive tracers. Swedish Nuclear Fuel and Waste Management Company. SKBF/KBS Technical Report TR 81-07.

Gustafsson, E. and Andersson, P. 1991 : Groudwater flow conditions in a low-angle fracture zone at Finnsjön, Sweden. J. of Hydrology, vol. 126, pp. 79-111.

Gylling, B., Khademi, B. and Moreno, L. 1998 : Modelling of the Tracer Retention Understanding Experiment Task 4C-D. Swedish Nuclear Fuel and Waste Management Company. Äspö Hard Rock Laboratory. International Cooperation Report ICR 98-01.

Haderman, J. and Heer, W. 1996 : The Grimsel (Switzerland) migration experiment : integrating field experiments, laboratory investigations and modelling. J. of Contaminant Hydrol., vol. 21, pp. 87-100.

Haggerty, R., and Gorelick, S.M. 1995 : Multiple-rate mass transfer for modeling diffusion and surface reactions in media with pore-scale heterogeneity, Water Resour. Res., 31, 2383-2400.

Haggerty, R., and Gorelick, S.M. 1998 : Modeling masss transfer processes in soil columns with pore scale heterogeneity, Soil Sci. Soc. Am. J., vol. 62, pp.62-74.

Hakami, E. 1995 : Aperture distribution of rock fractures. PhD-thesis TRITA-AMI PHD1003. Royal Institute of Technology (KTH), Stockholm, Sweden.

Hakami, E. and Larsson, E. 1996 : Aperture measurements and flow experiments on a single natural fracture. Int. J. of Rock Mech. and Mining Sciences & Geomech. Abstr., vol. 33, no. 4, pp. 395-404.

Hantush, M. S. 1967 : Flow to wells in aquifers separated by a semipervious layer. J. Geophys. Res., vol. 72, no. 6, pp. 1709-1720.

Hartikainen, K., Pietarila, A. Rasilainen, K., Nordman, H., Ruskeeniemi, T., Hölttä, P., Siitari-Kauppi, M. and Timonen, J. 1996 : Characterization of the altered zone around a fracture in Palmottu natural analogue. Mat. Res. Soc. Symp. Proc., vol. 412, pp. 839-846.

Heer, W. and Smith, P.A. 1998 : Modelling the radionuclide migration experiments at Grimsel. What have we learned? Mat. Res. Soc. Proc., vol. 506, pp. 663-670.

Hellmuth, K-H., Siitari-Kauppi, M., Klobes, P., Meyer, K., and Goebbels, J. 1999 : Imaging and Analyzing Rock porosity by Autoradiography and Hg-Porosimetry/X-ray Computertomography-Applications, Phys. Chem. Earth (A), Vol. 24, No. 7, pp. 569-573.

Hoehn, E., Eikenberg, J., Fierz, T., Drost, W. and Rechlmayr, E. 1998 : The Grimsel Migration Experiment : Field injection-withdrawal experiments in fractured rock with sorbing tracers. J. of Contaminant Hydrol., vol. 34, pp. 85-106.

Ittner, T., and Byegård, J., 1997 : Äspö Hard Rock Laboratory First TRUE Stage. Test of tracer sorption on equipment. Swedish Nuclear Fuel and Waste Management Company. Äspö Hard Rock Laboratory Progress Report HRL-97-28.

Johansson, H., Siitari-Kauppi, M., Skålberg, M., and Tullborg, E-L. 1997 : Diffusion pathways in crystalline rocks – Examples from Äspö-diorite and fine-grained granite. J. of Contaminant Hydrol., vol. 35, no. 1-3, pp. 41-53.

Johansson, H., Byegård, J., Skarnemark, G., Skålberg, M. Andersson, P. and Wass, E. (in press) : *In-situ* migration experiments at Äspö Hard Rock Laboratory, Sweden : Results of radioctive tracer migration studies in a single fracture. Paper submitted to Radiochimica Acta.

Laaksoharju, M., Skårman, C., 1995 : Groundwater sampling and chemical characterisation of the HRL tunnel at Äspö, Sweden. Swedish Nuclear Fuel and Waste Management Company. Äspö Hard Rock Laboratory Progress Report PR 25-95-29.

Laaksoharju, M., Smellie, J.A.T., Nilsson, A-C. and Skårman, C. 1995 : Groundwater sampling and chemical characterisation of the Laxemar deep borehole KLX02. Swedish Nuclear Fuel and Waste Management Company. SKB Technical Report TR 95-05.

Landström, O., Klockars, C-E., Persson, O., Tullborg, E-L., Larsson, S-Å., Andersson, K., Allard, B., and Torstenfeldt, B. 1983 : Migration Experiments in Studsvik. SKBF/SKB Technical Report TR 83-18.

Landström, O., Tullborg, E-L., Eriksson, G. and Sandell, Y. (in prep) : Effects of post- glacial weathering compared with hydrothermal alteration – Implications for matrix diffusion. Results from drillcore studies in porphyritic quartz monzodiorite from Äspö, SE Sweden. (Manuscript being prepared for scientific publication).

La Pointe, P., Wallmann, P., and Follin, S. 1995 : Estimation of effective block conductivities based on discrete network analyses using data from the Äspö site, Swedish Nuclear Fuel and Waste Management Company. Technical Report TR 95-15.

Liedke, L. and Shao, H. 1998 : Modelling of the tracer experiments in Feature A at Äspö HRL. Swedish Nuclear Fuel and Waste Management Company. Äspö Hard Rock Laboratory. International Cooperation Report ICR 98-02.

Ljunggren, C. and Bergsten, K-Å. 1998 : Rock stress measurements in KA3579G. Swedish Nuclear Fuel and Waste Management Company. Äspö Hard Rock Laboratory Progress Report HRL-98-09.

McKenna, S.A. 1999 : Solute transport modelling of the Äspö STT-1b tracer tests with multiple rates of mass transfer. Task 4E. Äspö Task Force on Modelling of Groundwater Flow and Transport of Solutes. Swedish Nuclear Fuel and Waste Management Company. Äspö Hard Rock Laboratory. International Cooperation Report ICR-99-02.

Meigs, L.C., Beauheim, R.L., McCord, J.T., Tsang, Y.W., and Haggerty, R. 1996 : Design, modelling and current interpretation of the H-19 and H-11 tracer tests at the WIPP site. *In* Proc. of OECD/NEA GEOTRAP workshop on Field Tracer Experiments – Role in the prediction of radionuclide migration. Cologne, Germany, August 28-30, 1996, pp. 157-169.

Mishra, S. 1992 : Part II : Methods for analyzing single- and multi-well hydraulic test data. *In* Vomvoris, S. and Frieg, B (eds) Interpretation of crosshole hydralic tests and a pilot fluid logging test for selected boreholes within the BK-site. Grimsel Test Site. NAGRA Technical Report 91-09.

MODFLOW/EM, The USGS Three Dimensional Ground Water Flow Model, Maximal Engineering Software, Inc, 1994.

Moreno, L. and Neretnieks, I. 1993 : Flow and nuclide transport in fractured rock : The importance of flow-wetted surface for radionuclide migration. J. Contaminant Hydrol., vol. 13, pp. 49-71.

Morosini, M. 1999 : Äspö Task Force on Modelling of Groundwater Flow and Transport of Solutes. Proceedings from the 11th task force meeting at Äspö, Sweden, September 1-3, 1998. Swedish Nuclear Fuel and Waste Management Company. Äspö Hard Rock Laboratory International Progress Report IPR-99-02.

Mosé, R., Siegel, P. and Ackerer, P. 1994: Application of the mixed hybrid finite element approximation in a groundwater flow model: Luxury or necessity? Water Resources Research, 30, 3001-3012.

Moye, D.G. 1967 : Diamond drilling for foundation exploration. Civil Engineering Transactions, April 1967, pp. 95-100.

Myrvang, A.M. 1997 : Evaluation of in-situ rock stress measurements at the ZEDEX test area. Swedish Nuclear Fuel and Waste Management Company. Äspö Hard Rock Laboratory Progress Report HRL-97-22.

Möri, A. and Bossart, P. 1997 : Conceptual model for PICNIC modeling (PSI). GI-Nr. 131.2946, Geotechnishes Institut, Bern.

Neretnieks, I. 1980 : Diffusion in the rock matrix : An important factor in radionuclide migration? J. Of Geophysical Res., vol. 85, no. 8, pp. 4379-4397.

Neretnieks, I. 1983 : A note on fracture flow dispersion mechanisms in the ground, Water Resour. Res, 19, 364-370.

Neretnieks, I., Eriksen, T. and Tähtinen, P. 1982 : Tracer movement in a single fissure in granitic rock: Some experimental results and their interpretation, Water Resour. Res., 18, 849-858.

Neretnieks, I., and Rasmuson, A. 1984 : An approach to modelling radionuclide migration in a medium with strongly varying velocity and block sizes along the flow path, Water Resour. Res., 20, 1823-1836.

Nordqvist, R.1994 : Documentation of some analytical flow and transport models implemented for use with PAREST – Users manual. GEOSIGMA GRAP 94 006, Uppsala.

Osnes, J.D., Winberg, A., Andersson, J-E. and Larsson, N-Å. 1991 : Analysis of well test data – Application of probabilistic models to infer hydraulic properties of fractures. US DOE Report DOE/CH/10378-9.

Painter, S., Cvetkovic, V. and Selroos, J-O. 1998 : Transport and retention in fractured rock : Consequences of a power-law distribution for fracture lengths. Physical Review, vol. 57, no. 6, pp. 6917-6922.

Pickens, J.F., Grisak, J.D., Avis, D.W., Belanger, D.W. and Thury, M. 1987 : Analysis and interpretation of borehole hydraulic tests in deep boreholes : Principles, model development, and applications. Water Res. Research, vol. 23, no. 7, pp. 1341-1375.

Poteri, A. and Hautojärvi, A. 1998 : Modelling of the tracer tests in radially converging and dipole flow fields in the first phase of the TRUE project. Swedish Nuclear Fuel and Waste Management Company. Äspö Hard Rock Laboratory. International Cooperation Report ICR 98-03.

Puigdomenech, I. et al (1999) : Redox experiment in detailed scale, First project status report. Swedish Nuclear Fuel and Waste Management Company. Äspö Hard Rock Laboratory International Cooperation Report ICR-99-01.

Rhén, I., Gustafsson, G., Stanfors, R., Wikberg, P., 1997. Äspö HRL-Geoscientific evaluation 1997/5. Models based on site characterisation 1986-1995. Swedish Nuclear Fuel and Waste Management Company. SKB Technical Report TR 97-06.

Roberts, R. 1998 : Data analyses using GTFM for selected floe and pressure buildup tests in the TRUE-1 borehole array. Swedish Nuclear Fuel and Waste Management Company. Äspö Hard Rock Laboratory Progress Report HRL-98-06.

Selroos, J.O. and Cvetkovic, V. 1996 : On the characterisation of retention mechanisms in rock fractures. Swedish Nuclear Fuel and Waste Management Company. SKB Technical Report 96-20.

Selroos, J-O. and Cvetkovic, V. 1998 : Prediction of the TRUE-1 radially and converging and dipole tracer tests, Äspö Task Force, Tasks 4C and 4D. Swedish Nuclear Fuel and Waste Management Company. Äspö Hard Rock Laboratory International Cooperation Report ICR-98-07.

Sibson, R.H. 1977 : Fault rocks and fault mechanisms. *J. Geol. Soc. Lond*. **133,** 191-213.

Siitari-Kauppi, M., Flitsiyan, E.S., Klobes, P., Meyer, K. and Hellmuth, K-H. 1998 : Progress in physical rock matrix characterization: Structure of the pore space. In: I.G. McKinley, C. McCombie (ed:s.), Scientific Basis for Nuclear Waste Management XXI, Mat. Res. Soc. Symp. Proc. v. 506, pp. 671-678.

SKB 1999 : Deep repository for nuclear fuel; SR 97 – Post-closure safety. Swedish Nuclear Fuel and Waste Management Company, SKB, Stockholm, Sweden.

Stanfors, R., Liedholm, M., Munier, R., Olsson, P. and Stille, H. 1993a : Geological – structural evaluation of data from section 700-1475 m. Swedish Nuclear Fuel and Waste Management Company. Äspö Hard Rock Laboratory Progress Report PR 25-93-05.

Stanfors, R., Liedholm, M., Munier, R., Olsson, P. and Stille, H. 1993b : Geological – structural evaluation of data from section 1475-2265 m. Swedish Nuclear Fuel and Waste Management Company. Äspö Hard Rock Laboratory Progress Report PR 25-93-10.

Stanfors, R., Olsson, P., Stille H., 1997. Äspö HRL – Geoscientific Evaluation 1997/3, Results from pre-investigations and detailed site characterization. Comparison and observations. Geology and mechanical stability. Swedish Nuclear Fuel and Waste Management Company. SKB Technical Report TR 97-04.

Ström, A. : Äspö Task Force on Modelling of Groundwater Flow and Transport of Solutes. Proceedings from the 10th meeting in Kamaishi, Japan, November 11-13, 1997. Swedish Nuclear Fuel and Waste Management Company. Äspö Hard Rock Laboratory Progress Report HRL-98-01.

Sävestad, A. and Nilsson, A-C. 1999 : Compilation of groundwater chemistry data. January 1995 to April 1998. Swedish Nuclear Fuel and Waste Management Company. Äspö Hard Rock Laboratory International Progress Report IPR-99-13.

Tanaka, Y., Hasegawa, T. and Kawanishi, M. 1997 : Numerical analysis with FEGM/FERM for TRUE-1 non-sorbing tracer tests. Swedish Nuclear Fuel and Waste Management Company. Äspö Hard Rock Laboratory. International Cooperation Report ICR 97-07.

Valkiainen, M. 1992 : Diffusion in the rock matrix – A review of laboratory tests and field studies. Nuclear Waste Commission of Finnish Power Companies. Report YJT-92-04.

Van Genuchten M. Th, and Alves W. J, 1982 : Analytical solutions of the one-dimensional convective-dispersive solute transport equation. U.S. Dep. Agric. Tech. Bull., 1661.

Wikberg, P. (ed), Gustafson, G., Rhén, I. And Stanfors, R. 1991 : Äspö Hard Rock Laboratory. Evaluation and conceptual modelling based on the pre-investigations. Swedish Nuclear Fuel and Waste Management Company. SKB Technical Report TR 91-22.

Winberg, A. 1994 : Tracer retention Understanding Experiments (TRUE) – Test plan for the First TRUE Stage. Swedish Nuclear Fuel and Waste Management Company. Äspö Hard Rock Laboratory Progress Report PR 25-94-35.

Winberg, A., Andersson, P., Hermanson, J. and Stenberg, L. 1996 : Results of the SELECT Project - Investigation Programme for Selection of Experimental Sites for the Operational Phase. Swedish Nuclear Fuel and Waste Management Company. Äspö Hard Rock Laboratory Progress Report PR HRL-96-01.

Winberg, A. (ed) 1996 : First TRUE Stage – Tracer Retention Understanding Experiments: Descriptive structural-hydraulic models on block and detailed scales on the TRUE-1 site. Swedish Nuclear Fuel and Waste Management Company. Äspö Hard Rock Laboratory. International Cooperation Report ICR 96-04.

Winberg, A. (ed) 1999 : TRUE Block Scale Project scientific and technical status. Position report prepared for the 2nd TRUE Block Scale Review Meeting, Stockholm, Nov 17, 1998. Swedish Nuclear Fuel and Waste Management Company. Äspö Hard Rock Laboratory International Progress Report IPR 99-07.

Worraker, W., Holton, D. and Cliffe, K.A. 1998 : Modelling TRUE-1 (RC-1) tracer tests using a heterogeneous variable aperture approach. Swedish Nuclear Fuel and Waste Management Company. Äspö Hard Rock Laboratory. International Cooperation Report ICR 98-06.

Voss, C. 1984 : SUTRA – A finite-element simulation model for saturated-unsaturated, fluid-density-dependent groundwater flow with energy transport or chemically-reactive single-species solute transport. Version V06902D. U.S. Geological Survey Water Resources Investigation Report 84-4369.

Zimmerman, R.W. and Bodvarsson, G.S. 1996 : Hydraulic conductivity of rock fractures, Transport in Porous Media, vol. 23, pp. 1-30.

14 Appendices

Appendix A

Tabulation of structural data related to interpreted features in the TRUE-1 Block. Coordinates given in metres in local Äspö coordinate system. Strike given in relation to local Äspö north. Dip given in relation to horizontal plane.

Table A-1. Feature A – Coordinates and structural characteristics of intercepts (Winberg, 1996).

Borehole	Length	Eastings	Northings	Z	Strike	Dip	Form	Condition
KXTT1	15.79	2323.26	7435.27	–403.41	319	79	Undulating	Oxidised
KXTT2	15.04	2323.80	7432.78	–402.95	344	74	Network	Dull
KXTT3	14.10	2321.43	7438.02	–399.54	325	78	Undulating	Open
KXTT4	12.10	2322.29	7433.66	–398.28	326	76	Planar	Open
KA3005A	44.97	2324.72	7430.02	–403.43	340	88	Planar	Cavities

Table A-1. Feature B – Coordinates and structural characteristics of intercepts (Winberg, 1996).

Borehole	Length	Eastings	Northings	Z	Strike	Dip	Form	Condition
KXTT1	8.27	2318.63	7432.76	–398.03	321	83	Network	Oxidised
	10.0	2319.69	7433.53	–399.26	329	77	Planar	Cavities
KXTT2	9.18	2320.13	7430.77	–398.85	320	81	Planar	Open
	12.22	2322.03	7431.81	–400.98	148	72	Planar	Cavities
	13.1	2322.58	7432.11	–401.60	144	65	Planar	Cavities
KXTT3	9.20	2318.69	7435.21	–396.60	329	68	Flow struct.	Oxidised
	9.36	2318.78	7435.30	–396.69	315	75	Planar	Cavities
KXTT4	8.74	2319.95	7432.31	–396.29	112	86	Planar	Cavities
	9.71	2320.63	7432.70	–396.86	300	69	Undulating	Open
KA3005A	48.24	2321.89	7431.63	–403.68	149	68	Planar	Oxidised
	48.45	2321.71	7431.74	–403.69	143	73	Planar	Open

Table A-3. Feature C – Coordinates and structural characteristics of intercepts (Winberg, 1996).

Borehole	Length	Y	X	Z	Strike	Dip	Form	Condition
KXTT1	15.70	2323.20	7435.24	–403.34	80	40	Crushed	Open
KXTT2	14.29	2323.33	7432.52	–402.43	74	38	Crushed	Open

Table A-4. Feature D – Coordinates and structural characteristics of intercepts (Winberg, 1996).

Borehole	Length	Y	X	Z	Strike	Dip	Form	Condition
KXTT1	4.11	2316.08	7431.37	–395.06	114	77	Planar	Open
	4.18	2316.13	7431.39	–395.11	63	51	Planar	Open
	6.10	2317.30	7432.03	–396.48	292	86	Undulating	Open
	7.26	2318.02	7432.42	–397.31	107	69	Planar	Open
KXTT2	5.51	2317.83	7429.52	–396.28	46	67	Undulating	Open
	6.42	2318.40	7429.83	–396.92	110	72	Planar	Open
	9.18	2320.13	7430.77	–398.85	320	81	Planar	Open
KXTT3	4.08	2315.83	7432.28	–393.52	154	9	Planar	Cavities
KXTT4	5.44	2317.65	7430.99	–394.33	98	65	Undulating	Cavities

Appendix B

Location of packed-off section used in the characterisation of the TRUE-1 Block (OLD,P). In addition for the revised sections used in TRUE-1 RC-1 are presented (NEW,R) (**C** means section equipped for tracer sampling/injection.

Borehole	Sec	OLD INSTALLATION Borehole length (m)	Sec	NEW INSTALLATION Borehole length (m)	Feature
KXTT1	P1	17.00 – 28.76	R1	17.00 – 28.76	NW-2N
	P2	15.00 – 16.00 **C**	R2	15.50 – 16.00 **C**	A
	P3	8.50 – 10.50 **C**	R3	7.50 – 11.50 **C**	B
	P4	3.00 – 7.50	R4	3.00 – 6.50	D
KXTT2	P1	14.30 – 18.30	R1	16.55 – 18.30	?
	P2	11.30 –13.30 **C**	R2	14.55 – 15.55 **C**	A
	P3	8.80 – 10.30 **C**	R3	11.55 – 13.55 **C**	B
	P4	3.05 – 7.80	R4	7.55 – 10.55	B
		–	R5	3.05 – 6.55	D
KXTT3	P1	15.42 – 17.43	R1	15.42 – 17.43	NW-2N
	P2	10.92 – 14.42 **C**	R2	12.42 – 14.42 **C**	A
	P3	8.92 – 9.92 **C**	R3	8.92 – 11.42 **C**	B
	P4	3.17 – 7.92	R4	3.17 – 7.92	B+D
KXTT4	P1	24.42 – 49.31	R1	24.42 – 49.31	NW-2
	P2	14.92 – 23.42 **C**	R2	14.92 – 23.42	NW-2N
	P3	11.42 – 13.92	R3	11.92 – 13.92 **C**	A
	P4	8.42 – 10.42 **C**	R4	8.42 – 10.42 **C**	B
	P5	3.17 – 7.42	R5	3.17 – 7.42	B+D
KA3005A	P1	46.43 – 58.11	R1	51.03 – 58.11	B?
	P2	44.43 – 45.43 **C**	R2	46.93 – 50.03 **C**	B
	P3	38.93 – 43.43	R3	44.78 – 45.78 **C**	A
	P4	36.93 – 37.93 **C**	R4	39.03 – 43.78	A?
	P5	6.53 – 35.93	R5	6.53 – 38.03	?

Appendix C

Defined response measures and their indexing

I) normalised response time ratio; $t_r(s=0.1m)/R^2$
II) normalised drawdown ratio; $\log(s/Q)$

where:

$t_r(s=0.1m)$ = time (min) at which drawdown s in a given observation section is 0.1m
s = drawdown in a given observation section due to pumping (m)
Q = measured flow from source section during interference test
R = Straight line distance between source and receiver section mid points

Table C-1. Indexing used for the normalised response time ratio $t_r(s=0.1m)/R^2$.

$t_r(s=0.1m)/R^2$	Index I	Comment
<0.005	7	Excellent
0.005 – 0.01	6	Almost excellent
0.01 – 0.05	5	Very good
0.05 – 0.10	4	Good
0.10 – 0.50	3	Rather good
0.50 – 1.0	2	Rather poor
> 1.0	1	Poor
no response	0	None

Table C-2. Indexing of the normalised drawdown ratio log(s/Q).

log(s/Q)	Index II	Comment
> 3.0	7	Excellent
2.5 – 3.0	6	Almost excellent
2.0 – 2.5	5	Very good
1.5 – 2.0	4	Good
1.0 – 1.5	3	Rather good
0.5 – 1.0	2	Rather poor
0.0 – 0.5	1	Poor
< 0	0	None

Appendix D

Responce matrices based on defined response measures

Appendix D-1. TRUE-1 Interference tests – Connectivity matrix of indexed response measure I $t_r(s=0.1\ m)/R^2$.

SOURCE		RECEIVER	KXTT1 P1	P2	P3	P4	KXTT2 P1	P2	P3	P4	KXTT3 P1	P2	P3	P4	KXTT4 P1	P2	P3	P4	P5	KA2858A P2	KA2862A P1	KA3005A P1	P2	P3	P4	KA3010A P2	KA3067A P1	P2	P3	P4	KA3105A P1	P2	P3	P4	KA3110A P1	P2	SA2880A P1	SA3045A P1	KA2050A P1	P2	P3	HA1960A P1
KXTT1	P1-4						5	5	7	3	2	5	5	3	5	4	5	5	5	7	7	4	2	2	3	5	5	5	5	5	5	3	4	3	5	4	5	5	5	5	4	5
	P2		1		0	0	1	0	0	0	3	4	0	0	0	1	3	0	0			1	1	1	1	0	0	0	0	0	0	0	0	0	0	0	0	0	0	0	0	0
	P3		5	5		5	5	5	4	3	1	3	4	3	3	4	1	4	3			3	1	1	1	0	0	0	0	0	0	0	0	0	0	0	0	0	0	0	0	0
KXTT2	P1		3	1	3	3		2	2	3	1	3	2	3	4	0	3?	2	3			1	1	1	1	0	0	0	0	0	0	0	0	0	0	0	0	0	0	0	0	0
	P2		0	0	5	5	1		1	1	0	1	3	4	0	0	1	3	4	0	3	1	1	1	1	0	0	0	0	0	0	0	0	0	0	0	0	0	0	0	0
	P3		3	1	4	5	5	4		5	1	1	3	5	1	0	1	3	7			3	1	1	1	0	0	0	0	0	0	0	0	0	0	0	0	0	0	0	0	0
KXTT3	P2		7	5	5	5	5	5	5	6	5		4	5	4	5	5	5	4	0	4	4	4	3	3	3	3	3	4	3	0	0	0	0	0	0	3	3	3	3	0	0
	P3		0	0	4	5	3	3	4	3	0	1		3	0	0	1	4	3	0	0	2	1	1	1	0	0	0	0	0	0	0	0	0	0	0	0	0	0	0	0	0
KXTT4	P2		5	4	5	5	5	4	5	5	5	5	6	5	5		4	4	5	7	4	5	2	2	3	3	5	4	5	4	0?	0	0	0	0	0	4	5	4	4	3	0
	P3		2	3	1	1	3	1	0	1	1	3	1	1	0	1		1	3	0	0	1	3	3	3	0	0	0	0	0	0	0	0	0	0	0	0	0	0	0	0	0
	P4		0	0	4	5	3	3	3	3	0	1	7	3	0	0	1		2	0?	0	2	1	1	1	2	0	0	0	0	0	0	0	0	0	0	0	0	0	0	0	0
KA3005A	P2		1	1	1	1	2	1	1	1	1	3	1	1	1	1	5	1	1	0	0	2		5	2	0	0?	0	0	0	0	0	0	0	0	0	0	0	0	0	0	0	0
	P4		3	3	1	1	2	1	1	1	3	4	1	7	0	2	3	1	1	0	0	1	3	5		0	0	0	0	0	0	0	0	0	0	0	0	0	0	0	0	0
KA3010A	P1-2		5	4	3	2	5	3	2	2	5	5	3	3	5	5	5	3	3	4	5	3	4	4	5		5	5	6	7	5	4	3	3	3	3	5	6	4	5	5	0

Note : Light shade (yellow) = Interpreted primary responses induced by tests in Feature A Dark shade (green) = Interpreted primary responses induced by tests in Feature B

Appendix D-2. TRUE-1 Interference tests – Connectivity matrix of indexed response measure II (log (s/Q).

SOURCE		RECEIVER	KXTT1 P1	P2	P3	P4	KXTT2 P1	P2	P3	P4	KXTT3 P1	P2	P3	P4	KXTT4 P1	P2	P3	P4	P5	KA2858A P2	KA2862A P1	KA3005A P1	P2	P3	P4	KA3010A P2	KA3067A P1	P2	P3	P4	KA3105A P1	P2	P3	P4	KA3110A P1	P2	SA2880A P1	SA3045A P1	KA2050A P1	P2	P3	HA1960A P1
KXTT1	P1-4						3	4	4	4	3	2	4	4	1	4	2	4	4	0	0	3	2	2	2	0	0	0	0	0	0	0	0	0	0	0	0	0	0	0	0
	P2		1		0	0	1	0	0	0	3	4	0	0	0	1	3	0	0			1	1	1	1	0	0	0	0	0	0	0	0	0	0	0	0	0	0	0	0
	P3		1	1		7	3	7	7	7	1	1	7	7	0	1	2	7	7			5	4	4	3	0	0	0	0	0	0	0	0	0	0	0	0	0	0	0	0
KXTT2	P1		2	3	3	3		3	2	3	3	4	3	5	2	0	3	3	2			5	5	5	4	0	0	0	0	0	0	0	0	0	0	0	0	0	0	0	0
	P2		1	2	7	6	3		6	6	0	2	6	6	0	1	3	6	6	0	1	5	4	4	3	1	0	1	1	0	0	0	0	1	0	1	0	0	0	0	0
	P3		1	0	6	7	3	7		7	1	1	6	7	1	0	2	6	7			5	4	4	3	0	0	0	0	0	0	0	0	0	0	0	0	0	0	0	0
KXTT3	P2		2	4	1	1	6	2	1	1	2		2	2	1	2	3	2	1	0	0	2	3	3	3	0	0	0	0	0	0	0	0	0	0	0	0	0	0	0	0
	P3		0	1	6	6	3	6	6	6	0	1		6	0	0	1	7	6	0	0	5	3	3	2	0	0	0	0	0	0	0	0	0	0	0	0	0	0	0	0
KXTT4	P2		3	2	0	0	2	0	0	0	3	2	0	0	1		2	0	0	0	0	1	2	2	2	0	0	0	0	0	0	0	0	0	0	0	0	0	0	0	0
	P3		2	2	2	1	3	2	0	1	2	3	2	1	0	2		1	2	0	0	2	4	4	4	0	0	0	0	0	0	0	0	0	0	0	0	0	0	0	0
	P4		0	1	6	6	3	6	6	6	1	2	7	6	1	1	2		6	1	0	5	3	3	2	1	0	1	1	1	0	1	0	0	0	0	0	0	0	0	0
KA3005A	P2		2	2	4	4	5	5	4	4	2	3	4	4	1	2	5	4	4	0	0	5		7	6	0	1	0	0	0	0	0	0	0	0	0	0	0	0	0	0	0
	P4		1	2	3	3	4	3	3	3	2	3	2	3	0	2	4	3	3	0	0	3	6	7		0	0	0	0	0	0	0	0	0	0	0	0	0	0	0	0	0
KA3010A	P1-2		0	0	0	0	0	0	0	0	0	0	0	0	1	0	0	0	0	0	0	0	0	0	0		1	1	1	1	1	0	0	0	0	0	0	1	1	1	1	0

Note : Light shade (yellow) = Interpreted primary responses induced by tests in Feature A Dark shade (green) = Interpreted primary responses induced by tests in Feature B

Appendix E

TRUE-1 – Water composition in Feature A – Major elements and trace elements, and a selection of stable isotopes and radioactive isotopes, Samples collected in April 1996.

Bh Section	Secup	Seclow	#	Na (mg/l)	K (mg/l)	Ca (mg/l)	Mg (mg/l)	HCO3 (mg/l)	Cl (mg/l)	SO4 (mg/l)	SO4_S (mg/l)	Br (mg/l)	Si (mg/l)	Fe (mg/l)	Fetot (mg/l)
KXTT1:R2	15.00	16.00	2341	1769.0	14.1	1286.0	81.4	91.0	5084.0	343.0	108.9	22.6	5.27	0.681	0.713
KXTT2:R2	14.55	15.55	2348	1754.0	13.8	1263.0	80.8	91.0	5119.0	358.0	107.4	27.0	5.31	0.667	0.713
KXTT3:R2	12.42	14.42	2343	1776.0	14.3	1301.0	82.3	92.0	5091.0	347.0	108.7	23.5	5.22	0.701	0.732
KXTT4:R3	11.92	13.92	2345	1764.0	14.2	1254.0	81.5	98.0	5013.0	343.0	109.6	25.0	5.20	0.674	0.717
KA3005:R3	44.78	45.78	2344	1730.0	13.6	1191.0	82.5	93.0	4878.0	351.0	106.2	20.8	5.52	0.640	0.679

Bh Section	Secup	Seclow	#	Fe-II (mg/l)	Mn (mg/l)	Li (mg/l)	Sr (mg/l)	pH	Cond mS/m)	D (o/oo)		O18 (o/oo)	DOC (mg/l)	U (ug/l)	Th (ug/l)
KXTT1:R2	15.00	16.00	2341	0.646	0.498	0.795	20.5	7.5	1410.0	–76.9		–10.2	4.4	0.1	0.0919
KXTT2:R2	14.55	15.55	2348	0.629	0.503	0.768	20.2	7.5	1410.0	–78.4		–10.2	4.1	0.38	0.0609
KXTT3:R2	12.42	14.42	2343	0.646	0.481	0.795	20.7	7.5	1410.0	–78.4		–10.2	4.1	0.64	0.0698
KXTT4:R3	11.92	13.92	2345	0.629	0.489	0.752	19.8	7.6	1390.0	–78.6		–10.1	4.4	0.71	0.0585
KA3005:R3	44.78	45.78	2344	0.61	0.517	0.719	18.8	7.4	1360.0	–75.5		–10.0	4.3	0.33	0.0639

Bh Section	Secup	Seclow	#	Sc (ug/l)	Cr (ug/l)	Co (ug/l)	Ni (ug/l)	Zn (ug/l)	Rb (ug/l)	Y (ug/l)	Zr (ug/l)	Mo (ug/l)	In (ug/l)	Sb (ug/l)	Cs (ug/l)
KXTT1:R2	15.00	16.00	2341	0.0074	1.94	0.233	<40	<22,0	42.4	0.357	<44	40.0	0.082	0.144	3.63
KXTT2:R2	14.55	15.55	2348	0.0021	1.30	0.07	<40	6.8	41.1	0.25	<19	21.0	0.097	0.018	3.57
KXTT3:R2	12.42	14.42	2343	0.0232	20.6	4.17	<40	233.0	41.0	0.427	<40	31.0	0.079	0.157	3.76
KXTT4:R3	11.92	13.92	2345	0.0023	<4,5	0.085	<40	11.4	40.0	0.374	<41	29.0	0.102	0.040	3.63
KA3005:R3	44.78	45.78	2344	0.0015	<1,5	0.0419	<40	9.9	39.4	0.332	<18	32.0	0.074	0.086	3.47

Bh Section	Secup	Seclow	#	Ba (ug/l)	La (ug/l)	Hf (ug/l)	Tl (ug/l)	Ce (ug/l)	Pr (ug/l)	Nd (ug/l)	Sm (ug/l)	Eu (ug/l)	Gd (ug/l)	Tb (ug/l)	Dy (ug/l)
KXTT1:R2	15.00	16.00	2341	56.0	0.35	<0,16	0.022	0.348	0.055	0.489	0.074	<0,016	0.369	0.01	0.05
KXTT2:R2	14.55	15.55	2348	54.0	0.102	<0,068	<0,02	0.106	0.027	0.401	0.079	1.30	0.154	0.464	0.063
KXTT3:R2	12.42	14.42	2343	57.0	0.357	<0,13	<0,02	0.379	0.048	0.428	0.071	<0,05	0.134	0.012	0.068
KXTT4:R3	11.92	13.92	2345	54.0	0.336	<0,18	<0,02	0.361	0.048	0.521	0.073	0.037	0.147	0.012	0.054
KA3005:R3	44.78	45.78	2344	51.0	0.328	<0,063	<0,02	0.335	0.046	0.438	0.088	0.05	0.115	0.347	0.068

Bh Section	Secup	Seclow	#	Ho (ug/l)	Er (ug/l)	Tm (ug/l)	Yb (ug/l)	Lu (ug/l)	Ra226 (B/l)	Ra228 (B/l)	Rn222 (B/l)	U238 (Bq/kg)	U235 (Bq/kg)	U234(Bq/kg)	Th228(Bq/kg)
KXTT1:R2	15.00	16.00	2341	0.064	0.054	<0,014	0.140	0.011	6.98E-01	1.19E+00	3.82E+02	6.29E-03	2.06E-04	2.41E-02	6.76E-02
KXTT2:R2	14.55	15.55	2348	0.193	0.047	<0,014	0.088	0.025	6.83E-01	1.13E+00	3.74E+02	4.67E-03		2.32E-02	1.42E-01
KXTT3:R2	12.42	14.42	2343	0.109	0.047	<0,014	0.118	0.013	6.66E-01	1.17E+00	3.33E+02	7.94E-03		3.18E-02	8.66E-02
KXTT4:R3	11.92	13.92	2345	0.573	0.064	<0,014	0.112	0.014	7.01E-01	1.09E+00	3.22E+02	8.75E-03	5.22E-04	3.24E-02	6.82E-02
KA3005:R3	44.78	45.78	2344	0.149	0.056	<0,014	0.107	0.018	5.70E-01	9.99E-01	3.46E+02	4.08E-03		1.64E-02	7.12E-02

Appendix F

Borehole equipment including packers, dummy and infiltration tubes.

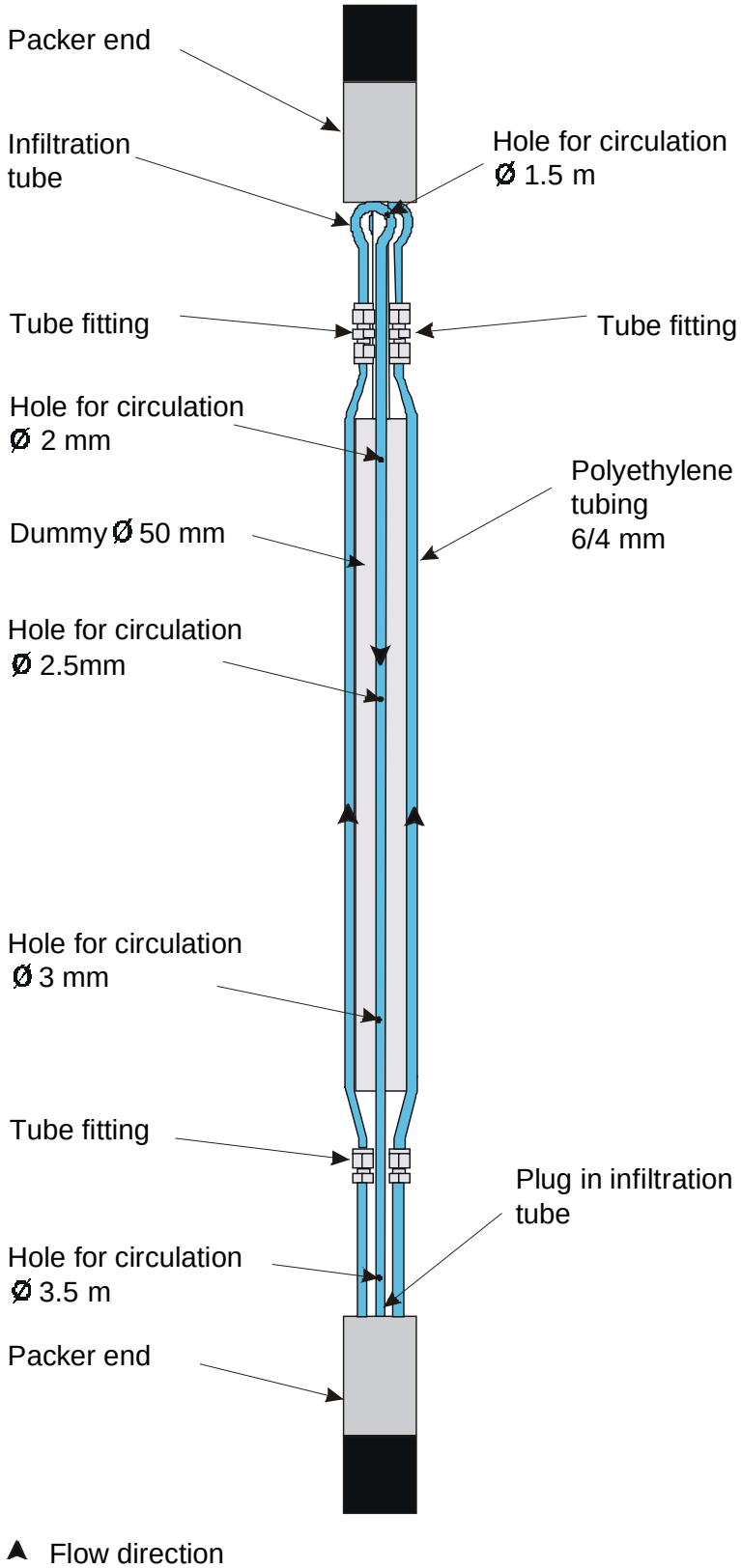

Appendix G

Summary of equations used in the LaSAR framework

The breakthrough curve, s(t) [M/T], for the reactive tracers is computed as

$$s(t) = \int (\phi * \gamma) g(\tau) d\tau$$

where ϕ [M/T] is the input function, * denotes the convolution operator and g(τ) is the water residence time distribution. The function γ is referred to as the reaction function and is computed as $\gamma = \gamma_1 * \gamma_2 * \gamma_3$, where γ_1 , γ_2 and γ_3 account for the matrix diffusion/sorption, surface sorption and sorption in gouge material, respectively.

The reaction function for diffusion into the rock matrix and stagnant water is

$$\gamma(t,\tau;\beta) = \frac{H(t-\tau)\,(\kappa\beta + \kappa_w \beta_w)}{2\sqrt{\pi}\,(t-\tau)^{3/2}} \exp\left[\frac{-(\kappa\beta + \kappa_w \beta_w)^2}{4(t-\tau)}\right]$$

where H is the Heaviside function and

$$\tau(l) = \int_0^l \frac{dl'}{v(l')}$$

$$\beta = \int_0^l \frac{dl'}{v(l')b(l')}$$

$$\kappa = \theta\sqrt{DR_m}$$

$$\beta_w(l) = \int_0^l \frac{dl'}{v(l')w(l')}$$

$$\kappa_w = \sqrt{D_w}$$

$$R_m = 1 + K_d^m \rho(1-\theta)/\theta$$

are the flow path integrated parameters: τ is the water residence time which depends on variable advection only, β is the velocity-weighted aperture integrated along the flow path, and β_w is the integrated velocity-weighted width of the flow path. β controls diffusion into the rock matrix whereas β_w controls the diffusion into stagnant water.

The parameter group $\kappa\beta = \kappa\beta + \kappa_w\beta_w$ controls the entire diffusive mass transfer, where $\kappa = \theta(R_m D)^{1/2}$ and $\kappa_w = (D_w)^{1/2}$, with $R_m = 1 + K_d^m \rho(1-\theta)/\theta$ being the retardation factor in the matrix, D the diffusion coefficient in the rock matrix, and D_w the diffusion coefficient of

a given tracer in water. Linear relationship is assumed as $\beta = 3400\tau$ [h m^{-1}] where 3400 m^{-1} was obtained as the average value from Monte Carlo simulations (see footnote 2 in Section 8.6), and $\beta_w = 20 \times 7 = 140$ [h m^{-1}] where 20 m^{-1} =2/0.1 m, and 0.1 m is the estimated width of the flow path, cf. Section 8.7.

The reaction function for equilibrium sorption on the fracture surface is

$$\gamma_2(t,\tau;\beta) = \delta(t-\tau-K_a\,\beta)$$

The reaction function for linear kinetic (reversible) sorption in gouge material is

$$\gamma_3(t,\tau) = e^{-\alpha K_d{}^g\,\tau}\,\delta(t-\tau) + \alpha^2\,K_d{}^g\tau \exp\left\{-\alpha\left[K_d{}^g\tau + (t-\tau)\right]\right\}\tilde{I}_1\left[\alpha^2\,K_d{}^g\tau\,(t-\tau)\right]$$

$K_d{}^g$ is the distribution coefficient and α the mass transfer rate in the gouge, and $\tilde{I}_1(Z) = I_1(2\sqrt{Z})/\sqrt{Z}$ with I_1 being a Bessel function of the first kind of order one (see e.g., Cvetkovic and Dagan (1994)).

The values of the relevant parameters used in the evaluations are listed in Table G-1 below.

Table G-1. The "Modelling Input Data Set" (MIDS) representing average values obtained from through-diffusion tests on generic (unaltered) rock samples. Additional laboratory values used in the evaluation are θ=0.004, cf. Section 6.4.3, and ρ=2700 kg m^{-3}.

Tracer	K_a [m] *)	$K_d{}^m$ [m^3 kg^{-1}] **)	D [m^{2}h^{-1}]	D_w [m^{2}h^{-1}]	$\kappa=\theta(DR_m)^{1/2}$ [mh$^{-1/2}$]
HTO	0.0	0.0	1.1E-7	8.4E-6	0.130E-5
Na	7.0E-7	1.4E-6	5.8E-8	4.8E-6	0.134E-5
Sr	8.0E-6	4.7E-6	3.6E-8	2.8E-6	0.155E-5
Ba	2.0E-4	2.0E-4	3.6E-8	3.0E-6	0.883E-5
Rb	5.0E-4	4.0E-4	9.0E-8	7.3E-6	1.968E-5
Cs	8.0E-3	8.0E-4	9.0E-8	7.3E-6	7.622E-5

*) from Table 6-12
**) from Table 6-11

ISSN 1404-0344

CM Digitaltryck AB, Bromma, 2000